Water Cycling under Climate Change

Interactions between the water cycle, vegetation and a changing (sub)tropical climate

ISBN: 978-90-6266-306-4

Figures: Geomedia, Faculty of Geosciences, Utrecht University

Cover image of the 'Blue Marble': NASA

Printed by CPI Koninklijke Wöhrmann, Zutphen

Water Cycling under Climate Change

Interactions between the water cycle, vegetation and a changing (sub)tropical climate

De waterkringloop tijdens klimaatverandering

Interacties tussen de waterkringloop, vegetatie en een veranderend (sub)tropisch klimaat

(met een samenvatting in het Nederlands)

Proefschrift

ter verkrijging van de graad van doctor aan de Universiteit Utrecht op gezag van de rector magnificus, prof.dr. G.J. van der Zwaan, ingevolge het besluit van het college voor promoties in het openbaar te verdedigen op vrijdag 14 september 2012 des middags 4.15 uur

door

Hugo Jan de Boer

geboren op 3 december 1981
te Purmerend

Promotor:	Prof.dr. M.J. Wassen
Co-promotor:	Dr. S.C. Dekker

Contents

Chapter 1

Overview

Introduction

From space the Earth is easily identified by the blues of the oceans, the whites of the clouds and the glaciers, and the greens of the terrestrial vegetation. Even from such a distant perspective, the central role that water and plants play in the functioning of the Earth system is evident. Taking a closer look learns that the recycling of water is essential to our planet's ability to support life. The physical properties of water in its liquid, solid and gaseous phases allow for a continuous redistribution of energy and water in the oceans and atmosphere keeping climate conditions in a life-sustaining range. A brief overview of the fundamental processes comprising the water cycle is presented in Box 1. At the scale of individual organisms, water and energy are also essential for the biochemical reactions required for life to develop and reproduce. Especially plant life is an important part of the global water and energy cycles because it captures light from the sun and exchanges carbon dioxide (CO_2) for water vapor and oxygen via photosynthesis. This gas exchange occurs dominantly through microscopically small pores (called stomata) that cover the leaf surfaces. Interactions between the vegetation and the water and energy cycles may change with the ability of individual plants to adapt to environmental changes or, at longer timescales, with changes in the plant community through competition and evolution at the scale of entire ecosystems. For a climate scientist, these adaptive responses of the vegetation are interesting for two main reasons. First, alterations in water use and carbon sequestration may act to amplify or counteract climatic changes via feedbacks with the water and carbon cycles. Second, fossilized plant remains that are stored in sedimentary archives provide so-called proxy evidence for climatic changes that occurred prior to the start of instrumental measurements.

In this thesis we focus on this dual role plants play in the climate system by altering and documenting changes in the water and carbon cycles. The aim is to gain understanding about interactions between the various components of the climate system during time periods in which (relatively) rapid fluctuations in the water and carbon cycles occurred. As the main study site we focus on the Florida peninsula and its surrounding ocean basins. This region is interesting from both ecological and climatological perspectives because it is situated on the boundary between the humid tropics and the subtropics. Due to the moist climate, peat deposits and lake sediments allow for the storage of (sub)fossil plant remains which can be used to study ecosystem responses to past climate changes. Moreover, as the Florida peninsula is surrounded by the Atlantic Ocean and Gulf of Mexico, changes in the Florida plant community can be used to infer climate changes related to alterations in ocean circulation through these basins. The research is presented in 6 chapters that make up this thesis. The first chapter presents an overview of the general context of this research, a discussion of the key results, and a general conclusion (synthesis). The research papers are presented in the chapters 2 through 6. We note that a reference list is included at the end of each chapter and abbreviations are defined in each chapter individually.

Box 1: The global water cycle and plants

Water is continuously redistributed between the oceans, the atmosphere, and the land (Figure 1.1). Throughout this cycle, water may change between its liquid, solid and gaseous phases, and by doing so alters its role in the climate system. The circulations of water in the atmosphere and oceans thereby help to spread energy from the equator towards the poles. Oceans store approximately 97% of the water on Earth while the remainder is distributed between icecaps and glaciers, the groundwater, the fresh surface water and the atmosphere. The water cycle starts with the ocean surfaces supplying the atmosphere with water vapor by evaporation. After evaporation, atmospheric water vapor is redistributed with the atmospheric circulation and condenses to form clouds. Precipitation then falls over the oceans and the land. Over water, this cycle may begin again. Over land, the water cycle involves many more steps such as storage in snow and glaciers, runoff and infiltration, storage in deep groundwater and lakes, river flow and evaporation and transpiration (called evapotranspiration combined). The terrestrial biosphere affects (evapo)transpiration because plants can actively control the rate at which they lose water to the atmosphere by closing the microscopically small pores that cover the surfaces of their leaves (the cuticle). These pores are called stomata (Greek for *mouths*) and allow plants to take up CO_2 from the atmosphere and limit water loss through the cuticle. Plants thereby constitute a biological link between the water and carbon cycles in the climate system.

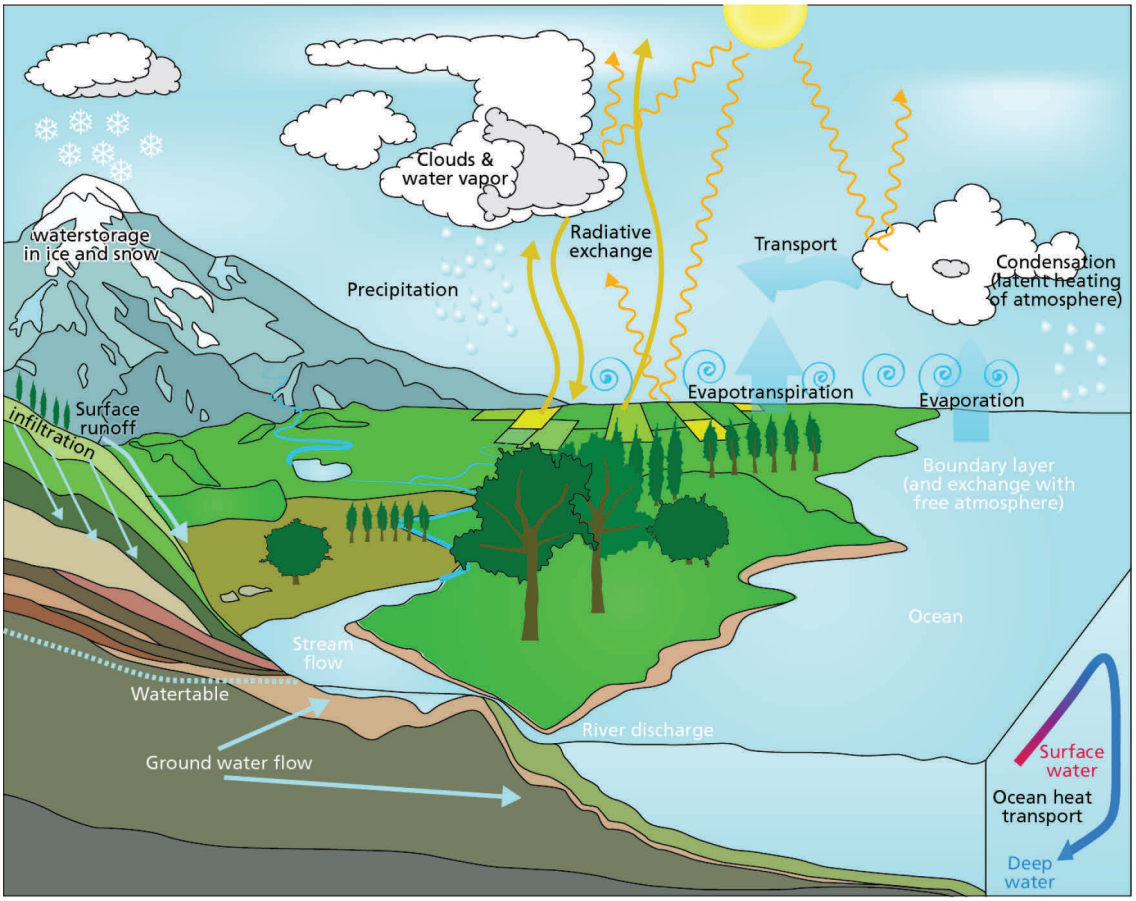

Figure 1.1 Overview of the key processes that comprise the global water cycle.

Feedbacks in the climate system

The Earth's climate has been able to support life over the past 3.5-3.9 billion years (Schopf, 1993; Mojzsis et al., 1996). Over this timeframe the climate has ranged from (near) global ice cover producing a so-called "snowball Earth" (Hoffman and Schrag, 2002) to an extreme greenhouse allowing for example the growth of palms in the Arctic (Sluijs et al., 2009). Considering that global temperatures have returned from either extreme suggests that stabilizing (negative) feedbacks dominate over destabilizing (positive) feedbacks in the climate system. Two key feedbacks that stabilize the climate are indicated in Figure 1.2 (Kiehl and Ramanathan, 2006). The first and most important stabilizing feedback links the Earth's surface temperature to the amount of infrared radiation (IR) emitted back to space. This feedback stabilizes temperature changes at relatively short timescales (~annual) (Jarvis, 2011). The second feedback links changes in the atmospheric CO_2 concentration (C_a) to the carbonate-silicate cycle which stabilizes temperature changes at geological timescales (millions to billions of years) (Walker et al., 1981). This feedback entails a positive relationship between C_a and temperature due to the greenhouse effect, and a positive relation between temperature and rainfall. A stabilizing mechanism emerges because the rate at which atmospheric CO_2 is dissolved in rainwater to form carbonic acid increases with higher surface temperatures. In turn, carbonic acid weathers continental silicate rocks and provides marine organisms with a source of bicarbonate to form their tests. After their death these organisms accumulate on the ocean floor and are eventually buried in deep sediments to form a carbon sink at geological timescales. This carbonate-silicate feedback provides a link with the biosphere as plants enhance silicate weathering by their roots (Berner, 1993) and they may enhance precipitation through the recycling of atmospheric moisture (Boyce and Lee, 2010).

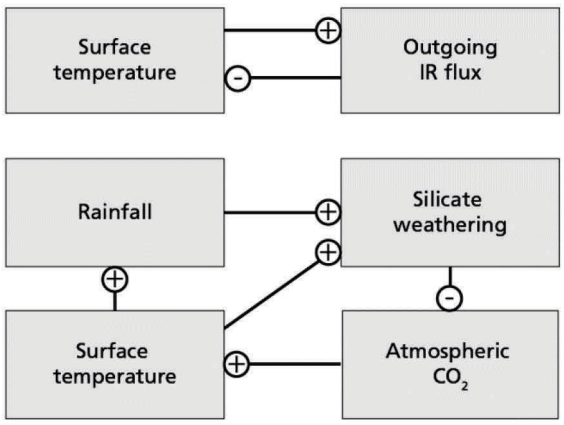

Figure 1.2 Two key stabilizing (negative) feedbacks in the Earth's climate system. The feedback between surface temperature and Infrared Radiation (IR) emitted to space (Top) and the feedback from chemical weathering (Bottom) are shown. Lines with a (+) signed head between system components denote a positive effect, lines with a (-) signed head denote a negative effect. A stabilizing feedback emerges from a combination of effects that are interlinked and have an overall negative sign. As a result, a perturbation in one of the system components results in changes in the other connected components that counteract and stabilize the initial change. Figure is based on Kiehl and Ramanathan (2006).

Despite that those stabilizing feedbacks appear to dominate the climate system, destabilizing (positive) feedbacks may still play a role during periods in which the climate undergoes (relatively) rapid fluctuations. Two key destabilizing feedbacks in the climate system are indicated in Figure 1.3 (Kiehl and Ramanathan, 2006). The first destabilizing feedback links the property of atmospheric water vapor to trap outgoing long-wave radiation to the property of air to increase its water holding capacity according to the Clausius-Clapeyron relationship. As a result, atmospheric water vapor is the largest absorber of outgoing long-wave radiation (Schmidt et al., 2010) and thereby enhances the heat trapping effect of atmospheric CO_2 and the other greenhouse gasses. The second feedback links the planetary albedo (a measure for reflectivity) with the surface temperature. If global temperatures decrease, the snow and ice cover increases which enhances the planetary albedo. Increased albedo then further decreases the surface temperature by reflecting more energy from the sun back to space. This destabilizing feedback has been proposed to have led to the "snowball Earth" (Hoffman and Schrag, 2002), but may also be responsible for amplification of global warming via decreased polar ice cover (Notz, 2009).

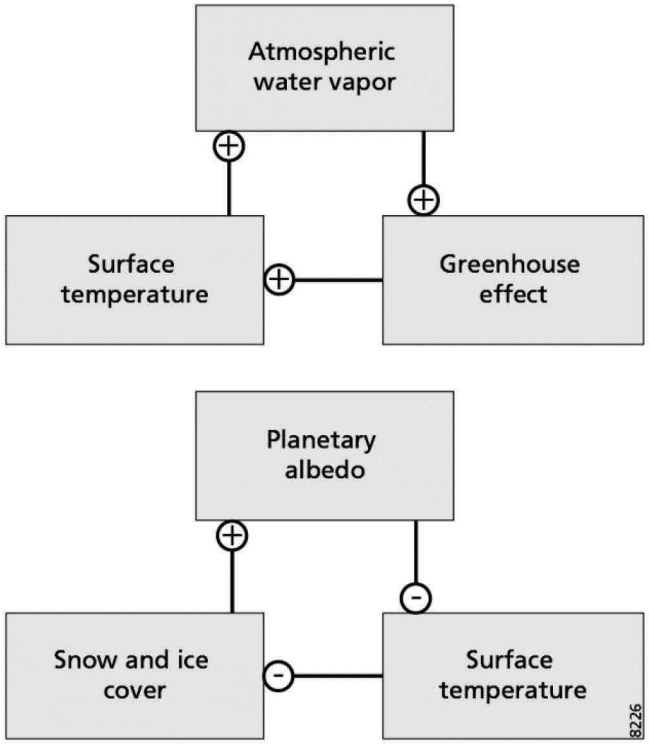

Figure 1.3 Two key destabilizing (positive) feedbacks in the Earth's climate system. The water vapor feedback (Top) and the ice-albedo feedback (Bottom) are shown. Lines with a (+) signed head between system components denote a positive effect, lines with a (-) signed head denote a negative effect. A destabilizing feedback emerges from a combination of effects that are interlinked and have an overall positive sign. As a result, a perturbation in one of the system components results in changes in the other connected components that amplify the initial change. Figure is based on Kiehl and Ramanathan (2006).

Climate change and plants

Watson and Lovelock (1983) demonstrated that biological feedbacks related to the Earth's albedo may, in theory, stabilize the climate system. Using a conceptual model involving black and white daisies with different temperature responses, Watson and Lovelock showed that differences in reflectivity of these two species may compensate for a gradual increase in solar output and thereby keep the surface temperature near stable. Although their model provides an elegant mathematical formulation to demonstrate the underlying Gaia hypothesis, the idea that biological processes act intentionally and in concert to stabilize the climate globally may be criticized based on its scientific merit (Kirchner, 1989). Despite criticism on the concept, even Kirchner (1989) could not deny that biological processes create feedbacks that are relevant in the functioning of the climate system. When considering those processes related to terrestrial plant life, climate feedbacks emerge via interactions between the surface energy balance, and the water and carbon cycles (Bonan, 2008). Changes in energy fluxes are related to the albedo of vegetation and the partitioning of the incoming energy between outgoing latent and sensible heat fluxes and the heat flux into the soil. Interactions between vegetation and the carbon cycle exist because plants take up CO_2 from the atmosphere via photosynthesis and enhance the weathering of silicate rocks at geological timescales (cf. Figure 1.2). A general response of plants is that rising C_a stimulates photosynthesis and growth. These responses enhance CO_2 uptake from the atmosphere and may, in turn, compensate for the initial C_a increase (Figure 1.4A) (Woodwell et al., 1998). Moreover, enhanced weathering of silicate rocks during the evolutionary rise of vascular plants may have contributed to falling atmospheric CO_2 concentrations over the course of the Phanerozoic (the last ~540 million years) (Berner, 1998). The water cycle is affected by the ability of plants to capture and intercept water that would have been lost to runoff or deep groundwater in the absence of vegetation (Bonan, 2008).

An intricate feedback exists between the water and carbon cycles involving the biosphere. At first order, transpiration increases with decreasing humidity. However, plants can actively prevent excess transpiration by closing their stomata when water loss exceeds the water transport capacity of the plant (Nobel, 1999). This response also affects the carbon cycle because, due to the comparable diffusive properties of water vapor and CO_2, carbon uptake and transpiration are intrinsically linked (Figure 1.4A). As a result, photosynthesis is reduced when plants close their stomata to reduce the (diffusive) stomatal conductance of their leaves during drought. Moreover, changes in C_a evoke inverse changes in stomatal conductance which may then alter transpiration and affect the water cycle (Ainsworth and Rogers, 2007). These stomatal adaptations can occur at relatively short timescales (~minutes) via opening and closing responses but also at decadal and longer timescales because plants may develop leaves with altered stomatal densities (D) and sizes of fully opened stomata (a_{max}) (Figure 1.4B). The structural adaptation of these stomatal properties may alter the maximal stomatal conductance (g_{smax}) of plant leaves and thereby constrain the short-term stomatal opening and closing responses (Franks and Farquhar, 2007; Franks and Beerling, 2009b).

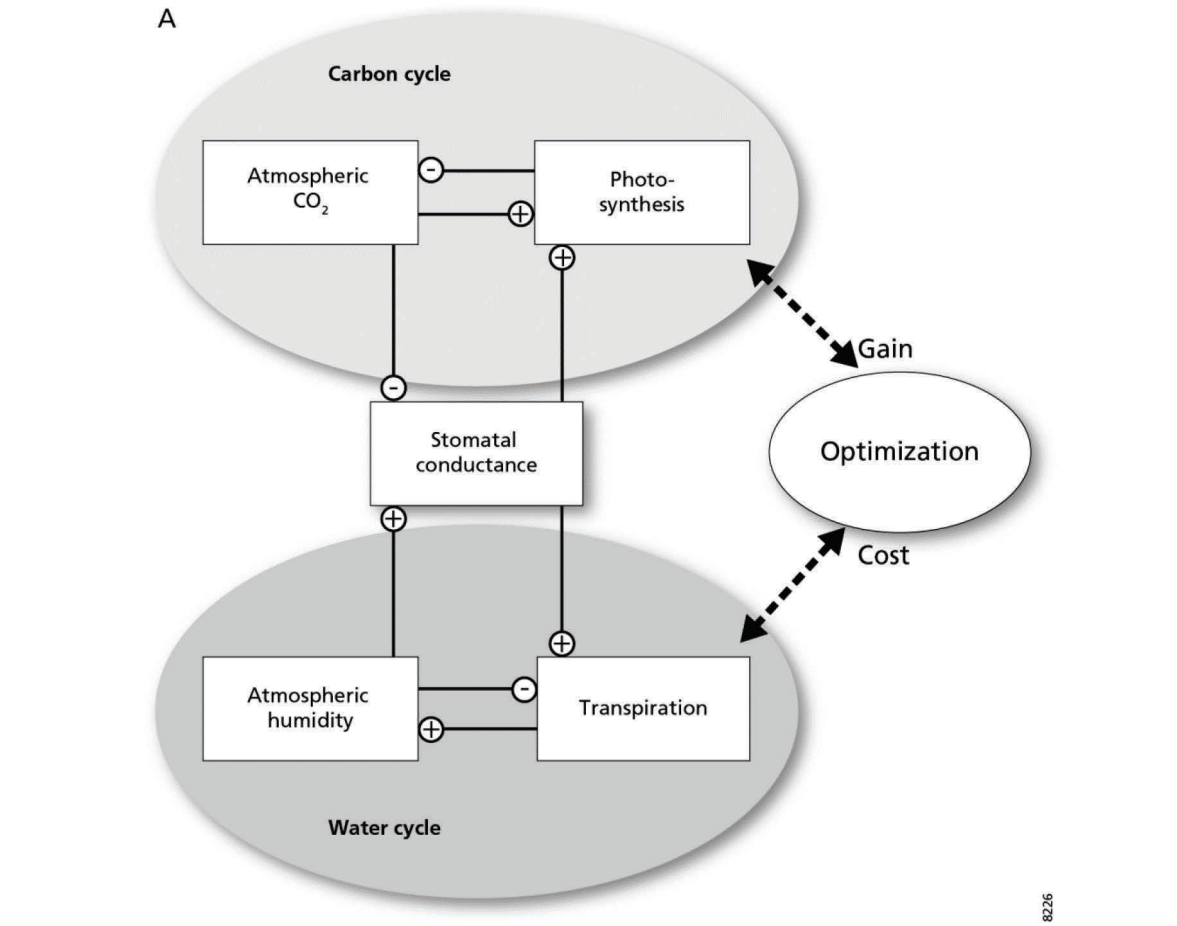

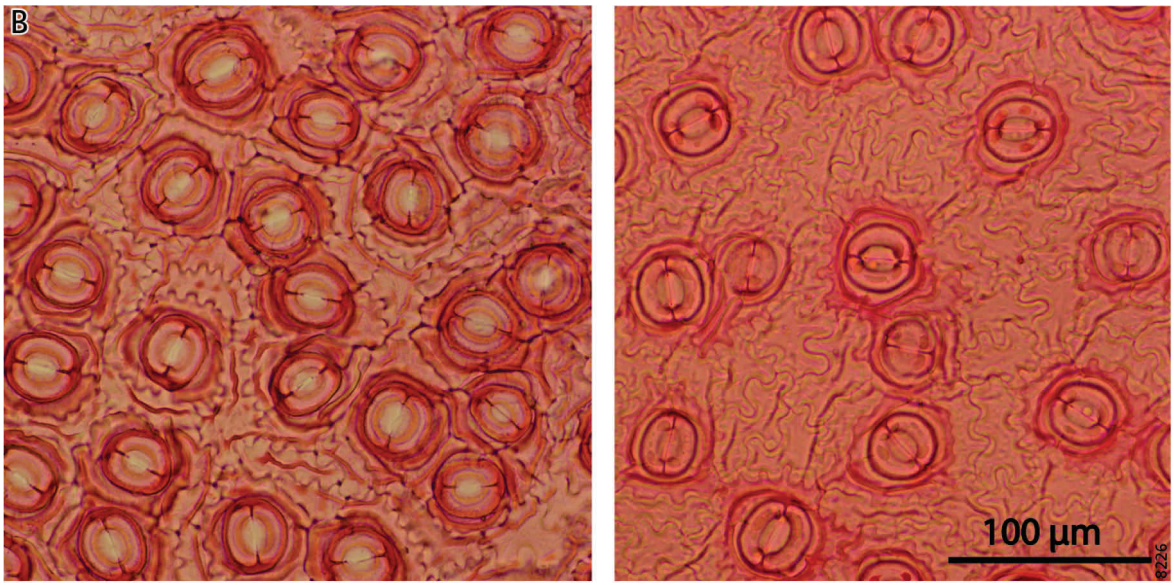

Figure 1.4 Links between the carbon and water cycles via stomatal responses. (A) Feedbacks between the water and carbon cycles via stomatal optimization. Lines with (+) and (-) signed heads denote positive and negative effects between system components, respectively. Changes in stomatal conductance allow for an (optimal) tradeoff between carbon gain by photosynthesis and water loss by transpiration. (B) Microscope photographs using equal magnification of the cuticle and stomata of Dahoon Holly (*Ilex cassine*). The left image shows a leaf from 1877 grown under a C_a of approx. 290 parts per million (ppm) and the right image shows a leaf from 2009 grown under a C_a of approx. 387 ppm. A change in stomatal density is visible.

Stomatal responses to the combined effects of C_a, water availability and atmospheric humidity may be described mathematically via the principle of optimization (Cowan and Farquhar, 1977; Mäkelä et al., 1996; Katul et al., 2010; Manzoni et al., 2011). The optimization principle entails that carbon gained by photosynthesis is maximized under the constraint of water lost to transpiration. This principle stools on the idea that, even when water is ample, water loss presents a cost to plants. The resulting tradeoff likely emerged from evolutionary adaptation because the water transport capacity of a plant is finite (Tyree and Sperry, 1988) and increasing water transport requires additional carbon investments in water transport tissue (Blonder et al., 2011). Hence, depending on environmental conditions, different stomatal properties may allow for an optimal tradeoff between water loss and carbon gain. Changes in environmental conditions can therefore drive plastic adaptations in individual plants or, at longer timescales, changes in the plant community through competition and evolution (Franks and Beerling, 2009a; Walther, 2010). Subsequent changes in coupling between the vegetation and their environment may initiate feedbacks that propagate to scales relevant to the functioning of the climate system as a whole (Rietkerk et al., 2011).

Apart from interacting with the climate system at various spatial and temporal scales, individual and community level adaptations of plants can also be used as so-called paleoecological proxy evidence to study and reconstruct climate changes that occurred in the past (Bradley, 1999). Adaptive responses of individual plants to changes in water availability and C_a may be reconstructed by measuring the stomatal properties D and a_{max} on the cuticles of (sub)fossil leaves (Royer, 2001; Wagner-Cremer et al., 2010). Vegetation changes at the community level can be reconstructed from fossil evidence such as pollen assemblages and plant remains. As pollen can be transported by wind and water they typically reflect the community composition at regional scales whereas macrofossils usually reflect the vegetation at smaller spatial scales. Besides interpreting these community-level responses in a qualitative manner, a quantitative interpretation may be obtained by using (statistical) pollen-climate inference models. Such models are often based on calibration data from modern pollen assemblages containing the relevant species in the relevant climate zone (Webb and Bryson, 1972; Finsinger et al., 2007). Under the assumption that plant communities have responded equally to climate change in the past, pollen-climate inference models allow to quantitatively reconstruct historic climate variables such as precipitation and temperature.

Focus on the (sub)tropical Florida region

The research presented in this thesis is for a large part based on data obtained from terrestrial and marine sedimentary archives in Florida and the surrounding ocean basins. The Florida peninsula is located in the southeastern USA (between 24-31˚N and 79-87˚W) and is bordered by the Atlantic Ocean to the east and the Gulf of Mexico to the west (Figure 1.5). This region is climatically interesting because it is located on the border of the tropics and the subtropics. The tropics are defined as the geographic region between Tropic of Cancer and the Tropic of Capricorn (23˚N-S) while the subtropics are defined as the climatic zone adjacent to the tropics according to the Köppen climate classification (Köppen and Geiger, 1936). Typically, the subtropics extend up to 40˚N-S. According to the Köppen climate classification, Florida has a humid subtropical climate except for the southernmost tip which is considered tropical. A central feature in the (sub)tropical climate is the atmospheric circulation consisting of convective regions around the equator with rising air in the Inter-Tropical Convergence Zone (ITCZ) and non-convective regions in the subtropics with subsiding air (Figure 1.5A) (Seidel et al., 2007). Intense precipitation occurs in the ITCZ due to the rising air while the subtropics are typically dry due to the descending air (Figure 1.5B). Geographic and seasonal differences in maximum precipitation are related to the centers of heating on and near the continental land masses and the zonal temperature gradients in the Pacific and Atlantic basins. The position of the ITCZ thereby displaces towards the warmer hemisphere at seasonal and longer timescales (Chiang et al., 2002; Broccoli et al., 2006). Due to the steep gradient in precipitation between the convective and non-convective regions, (sub)tropical climate change is often reflected by changes in the water cycle (Seidel et al., 2007). For example, a cooling of the North Atlantic leads to drying in the northern parts of South America (Peterson et al., 2000) and the African Sahel region (Shanahan et al., 2009), whereas increased precipitation occurs on the southern margin of the ITCZ (Jaeschke et al., 2007).

The climate of Florida is strongly influenced by the North Atlantic and the Gulf of Mexico owing to its vicinity to these water masses. A dominant ocean feature in this region is the Atlantic Warm Pool (AWP), which is defined as the region of the Atlantic with Sea Surface Temperatures (SSTs) above 28.5˚C. At present, the AWP extends from the tropical Northwest Atlantic through the Caribbean Sea up to the Gulf of Mexico during boreal summer and fall. The AWP thereby constitutes a northward expansion of warm (tropical) waters and is partly responsible for the balmy climate in the southern tip of Florida. Changes in the spatial extent of the AWP affect precipitation throughout the region (Wang et al., 2006). Expansion of the AWP during summer is influenced by changes in low-latitude summer insolation (Ziegler et al., 2008) and North Atlantic temperatures as well as global climate variability (Wang et al., 2008a). Proxy-based climate reconstructions from sites in or near Florida are therefore specifically suited to study changes in the (sub)tropical water cycle in relation to regional and global climate changes.

We investigate three coupling pathways that interlink the water and carbon cycles with the climate system in the Florida region (Figure 1.5C): (1) land-atmosphere coupling reflected by changes in leaf gas exchange of plants responding to changes in C_a, (2) ocean-atmosphere-land coupling reflected by changes in the plant community responding to precipitation and temperature anomalies linked to changes in ocean circulation, and (3) ocean-atmosphere-ocean coupling between the Atlantic and Pacific basins via atmospheric moisture transport across the Central American isthmus. The coupling between these system components is investigated using a combination of proxy data and numerical models. The rationale for using models in addition to proxy data to infer climate signals is that models allow for the representation of processes that may not be directly documented in the data. Models thereby help to explore mechanisms and sharpen hypotheses to explain observations that may, potentially, be linked.

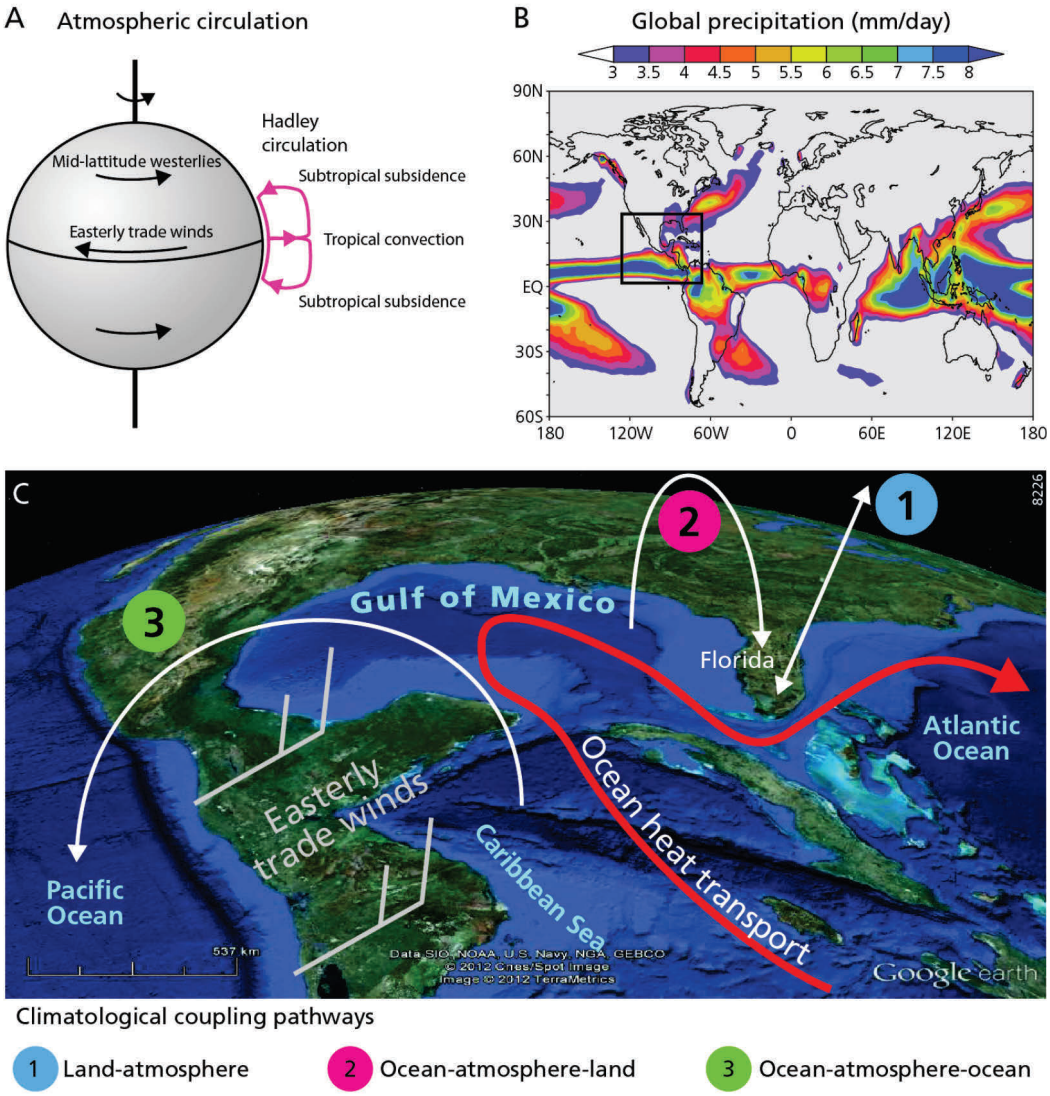

Figure 1.5 Key determinants for the humid (sub)tropical climate of the Florida region and the climate system components analyzed in this thesis. (A) Global atmospheric circulation. (B) Global (annual average) precipitation patterns with most intense precipitation occurring in the convective (sub)tropical regions. The box indicates the Florida region. (C) Focus area of this thesis with the three coupling pathways indicated.

Aims and research questions

The research presented in this thesis focuses on the dual role plants play in the climate system by altering and documenting changes in the water and carbon cycles. This approach provides crucial information about the functioning of plants under climate change and allows for the reconstruction of climate fluctuations that occurred in the past. We thereby consider three distinct periods in the Earth's history during which (relatively) rapid changes in the climate system occurred and plants either played an active role in altering the water and carbon cycles, or they are indicative of changes in these elemental cycles. These geological time frames are briefly introduced in Box 2.

In chapters 2 and 3 of this thesis we focus on the climate of the last 150 years to study the effect of the anthropogenic rise in C_a on stomatal gas exchange of common C3 plant species from Florida. During this period, C_a increased from approximately 280 to 385 parts per million (ppm) while precipitation and temperature showed no trend in Florida. Measurements of stomatal properties on leaves stored in peat deposits and herbaria therefore provide potential evidence for adaptive stomatal responses to rising C_a at decadal to centennial timescales. The key research question addressed in these chapters is: **How do C3 plant species from Florida adapt their maximal stomatal gas exchange capacity to the anthropogenic rise in atmospheric CO_2 and how may this response alter transpiration fluxes?**

In chapters 4 and 5 we focus on a part of the last glacial period (between approximately 114 and 11.7 thousand years ago) during which climate fluctuations occurred at millennial timescales. These climate shifts were related to the slowdown and restart of ocean heat transport in the North Atlantic. The imprints of these climate fluctuations are documented by shifts in pollen composition in a lake sediment record from Florida. Moreover, the reconstructed changes in the (sub)tropical hydrological cycle may constitute feedbacks with ocean circulation by altering the freshwater budget of the North Atlantic. The key research question addressed in these chapters is: **What climate signals are reflected in a lake sediment pollen record from Florida and how may these climatic changes be interlinked with reorganizations of North Atlantic circulation during the last glacial?**

In chapter 6 we focus on a fundamental question in ecology which addresses the period of rapid diversification of broad-leaved and flowering (angiosperm) plant species during the Cretaceous (between 145 and 66 million years ago). During this period, C_a declined from approximately 2000 ppm to 800 ppm (Berner and Kothavala, 2001) and at the same time terrestrial plant life evolved relatively rapid towards modern biodiversity. Although a role for falling C_a in driving angiosperm evolution has been suggested before, the mechanisms involved remain debated. The key research question addressed in this last chapter is: **How could falling atmospheric CO_2 concentrations trigger the sudden evolutionary success of broad-leaved (flowering) angiosperms at the expense of conifers during the Cretaceous?**

Box 2: Geological timescale and periods considered in this thesis

Chapters 2 and 3 consider the industrial period starting approximately in 1850. A key change that occurred in the climate system over this timeframe is the rise of atmospheric CO_2 concentrations from 280 ppm in 1850 to 393 ppm in 2012 due to anthropogenic CO_2 emissions (IPCC, 2007). This recent rise in atmospheric CO_2 in relation to CO_2 and climate changes that occurred at geological timescales is shown in Figure 1.6.

Chapters 4 and 5 consider the last part of the Pleistocene (or Quaternary) glaciation, an epoch which started 2.58 million years ago and ended 11.7 thousand ago at the start of the Holocene. During the Pleistocene, the climate was typically in a glacial state with massive continental ice cover. These glacial conditions were intermittently disrupted by warmer interglacial conditions comparable to the present climate. During glacial conditions, rapid climate fluctuations occurred at shorter (millennial) timescales (NGRIP-Members, 2004). Our focus is on these rapid (millennial-scale) climate fluctuations that occurred during the last glacial, between approximately 114 to 11.7 thousand years ago.

Chapter 6 considers the Cretaceous period which lasted from 146 to 66 million years ago and is part of the Mesozoic era. During the Cretaceous, CO_2 concentrations declined strongly (Veizer et al., 1999; Berner and Kothavala, 2001). Although some geological evidence exists for continental ice cover during the early Cretaceous, the Cretaceous climate is typically believed to have been in a warm and ice-free greenhouse state (Moriya, 2011). The Cretaceous period ended with a mass extinction that could have been caused by the impact of a massive asteroid (Alvarez et al., 1980).

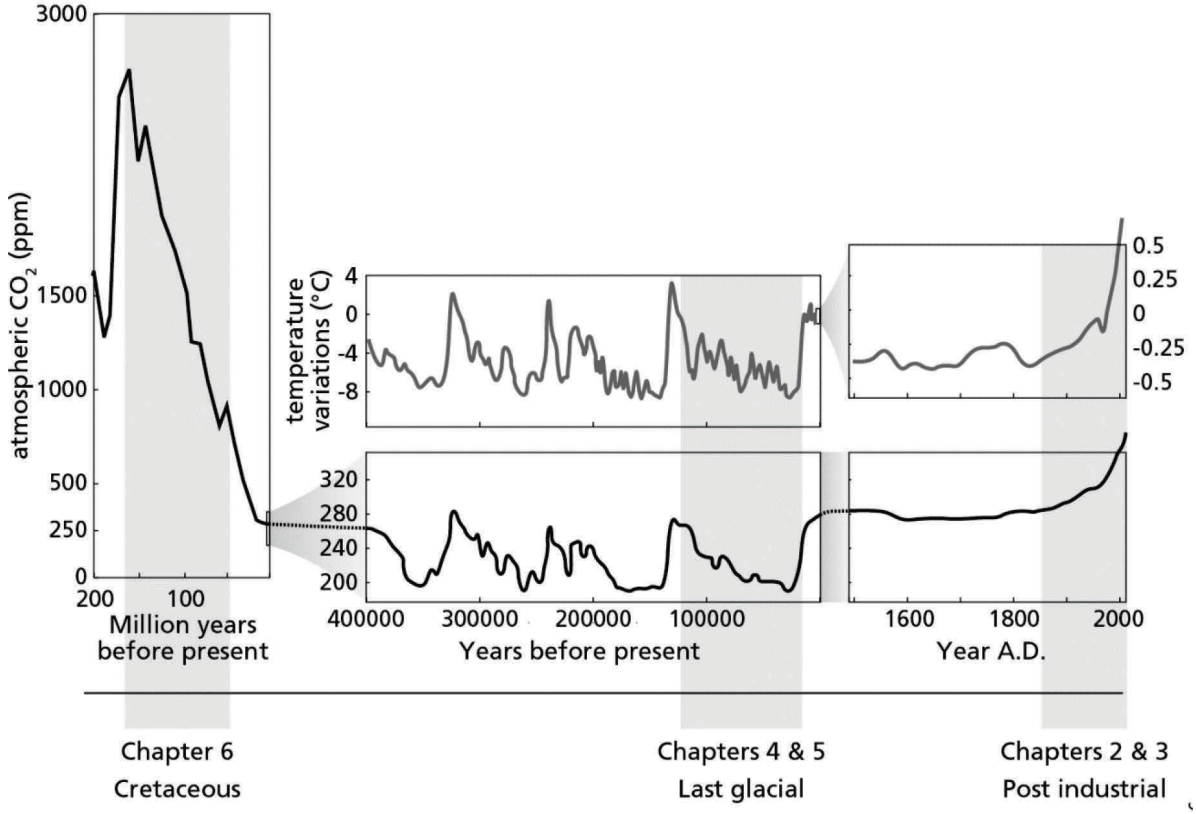

Figure 1.6 Geological timescale with climate fluctuations considered by the chapters in this thesis.

Results and discussion

Optimization of maximal stomatal conductance observed in Florida C3 plant species

The diffusion of CO_2 and water vapor through the stomatal pores on plant leaves is at the basis of the interactions between the biosphere and the atmosphere. Adaptive responses in the diffusive properties of stomata under rising C_a may thereby affect the water cycle and alter the surface energy balance by changing transpiration (Boucher et al., 2009). Structural stomatal adaptations of D and a_{max} have been observed under changes in C_a at geological timescales (Royer, 2001; Franks and Beerling, 2009b). However, the question remains if these adaptations also occur at decadal to centennial timescales. In chapter 2 we present measurements of D and a_{max} on the leaves of nine common C3 species from Florida. These leaves were stored in terrestrial organic sediments and herbaria over the last 150 years and subsequently span a CO_2 range between approximately 280 and 390 ppm. The species studied include 5 angiosperms, 3 conifers and one fern. With these data we calculate g_{smax} for the leaves studied, which is a generic measure for the upper limit of stomatal gas exchange capacity (Franks and Farquhar, 2007). The results show a 34% (±12%) reduction in g_{smax} expressed per 100 ppm C_a increase. This response is comparable among the conifers and angiosperm species. We do observe differences in species-specific g_{smax} values, whereby the angiosperms sampled attain high g_{smax} by developing leaves with numerous small stomata and the conifers and fern attain lower g_{smax} with fewer and larger stomata. These different stomatal properties are explained from the different evolutionary backgrounds of angiosperms, conifers and ferns.

To explain the common decline in g_{smax} observed in the Florida C3 species we hypothesize that structural stomatal adaptations are aimed at optimizing photosynthesis with minimal transpiration in response to rising C_a. In chapter 3.1 we use a stomatal optimization model based on the approach of Konrad et al. (2008) to investigate if the observed changes in g_{smax} can be explained by optimization at decadal and longer timescales. The optimization model reproduces the observed changes in g_{smax} under the anthropogenic C_a rise and thereby provides support for the hypothesis that plants optimize the gas exchange capacity of their leaves by altering D and a_{max}. A potential unrealistic result of the optimization model is the prediction that g_{smax} will continue to decrease under rising C_a without considering the potential constraints posed by the phenotypic plasticity of individual plants. As structural stomatal adaptation may take decades or longer (Royer, 2001), limits to phenotypic responses in stomatal traits cannot be observed in short running experiments (Kürschner et al., 1997). We therefore use ranges in phenotypic plasticity observed at geological timescales (Franks and Beerling, 2009b) to estimate the potential limits to stomatal trait plasticity. This approach suggests that the angiosperm species may reach the limit of their phenotypic plasticity before the conifer species. Yet, both groups will likely not reach their response limits during the C_a rise projected for the 21st century (IPCC, 2007). The optimization model revealed that a doubling of present atmospheric CO_2 concentrations may reduce transpiration fluxes by approximately 50%. Our results therefore suggest that stomatal adaptations to rising C_a are altering the freshwater cycle by reducing transpiration.

The publication of these results (de Boer et al., 2011a; Lammertsma et al., 2011) sparked a debate about the stomatal control on transpiration and the potential feedbacks with the hydrological cycle (Miglietta et al., 2011). The comment by Miglietta et al. (2011) and our reply (de Boer et al., 2011b) are included in chapter 3.2 of this thesis. The key points of discussion involved the scaling between leaf-level responses to rising C_a and the subsequent effects on transpiration at larger spatial scales. Following this argument, changes in transpiration at the leaf level do not necessarily result in changes in evapotranspiration at larger spatial scales. Potentially compensating mechanisms are changes in Leaf Area Index (LAI), the more efficient use of available water during drought, and feedbacks in the boundary layer. We agree with these arguments, however, we also note that plants eventually determine the maximum rates of transpiration by their dynamic stomatal responses. Changes in g_{smax} may thereby crucially constrain the maximum transpiration rates of individual leaves. When changes in diffusive properties of stomata occur in regions with dense and extensive vegetation cover, such as (sub)tropical forests, decreased transpiration may still result from leaf level responses. The effects of stomatal responses may be different in other ecosystems where increases in LAI can occur due to the effect of carbon 'fertilization' and the more efficient use of water. Additional observations are therefore required to unravel if (and how) plants adjust the properties of their stomata in other climate zones and environments.

Rapid glacial climate fluctuations reflected by the Florida plant community

In chapters 4 and 5 of this thesis we focus on the last glacial period. During this time frame rapid climate shifts occurred at millennial timescales due to disruptions in the northward heat transport by the Atlantic Meridional Overturning Circulation (AMOC) (Broecker, 1994; Alley et al., 1999). These climate fluctuations are termed Dansgaard-Oeschger (D-O) oscillations and appear organized in so-called Bond cycles (Alley, 1998; Bond et al., 1993; Dansgaard et al., 1993). Heinrich events occurred towards the end of Bond cycles during the coldest D-O stadials and are recognized by sediment deposits from massive iceberg surges from a decaying Laurentide ice sheet (Heinrich, 1988; Bond et al., 1992). Melting of these icebergs in the North Atlantic is identified as a key mechanism in disrupting northward heat transport by the density-driven AMOC (Broecker, 1994; Rahmstorf, 1996). The additional freshwater flux thereby hinders the sinking of cold and high salinity (dense) surface waters in the North Atlantic at high latitudes. This so-called deep water formation is a key driver for the AMOC. Apart from the freshwater input from ice sheet decay, also changes in the (sub)tropical hydrological cycle may affect the AMOC by altering the freshwater budget of the North Atlantic (Broecker, 2003; Chiang, 2009). Changes in the atmospheric moisture flow from the Atlantic across the low-lying Central American isthmus towards the Pacific provide a mechanism for constituting feedbacks with the glacial AMOC (Leduc et al., 2007; Rahmstorf, 1996). Although much progress has been made in unraveling the mechanisms responsible for these enigmatic climate fluctuations, the role of the (sub)tropical freshwater cycle in a potential feedback with the glacial AMOC remains to be resolved.

In chapter 4 we use a pollen–climate inference model to quantify the climatic significance of pine phases coeval with Heinrich events that were documented in a lake sediment record from Florida (Grimm et al., 2006). Our results indicate an increase in summer precipitation of 0.5–0.9 mm/day and an increase in mean November temperature of 2.0–3.0°C during the Heinrich events. These results appear at odds with the cooling observed in the extra-tropical North Atlantic region during these periods with disrupted AMOC (Hemming, 2004). However, warming is observed in proxy-based SST reconstructions from the Gulf of Mexico and the western tropical Atlantic (e.g. Rühlemann et al., 1999; Schmidt et al., 2004; Ziegler et al., 2008) during periods with disrupted AMOC. This low-latitude warming suggests a potential link with the heat and moisture anomalies observed in Florida. We hypothesize that the climate changes in Florida are related to these temperature changes in the area of the modern day AWP. This hypothesis is explored with a climate model sensitivity analysis considering different sea surface temperature boundary conditions. Our modeling results reveal that a positive heat anomaly in the Gulf of Mexico and equatorial Atlantic best approximates the pollen-inferred climate reconstruction from Lake Tulane during the Heinrich events. These results indicate that intensification of the (sub)tropical freshwater cycle may have occurred during the last glacial at times when heat accumulated in the (sub)tropical North Atlantic.

Such changes in the (sub)tropical climate may constitute feedbacks with the climate system by changing atmospheric and oceanic circulation patterns globally (Chiang, 2009). From observations and modeling studies focused on the modern climate, the idea is emerging that heat anomalies in the AWP region evoke inverse pressure changes in the North Atlantic subtropical (Azores) high pressure system (Wang et al., 2008a, 2008b) via the Gill-type atmosphere response (Gill, 1980). These atmospheric pressure changes alter the strength of the easterly trade winds and thereby affect atmospheric moisture transport from the Atlantic across the Central American isthmus to the Pacific (Wang, 2007; Muñoz et al., 2008). Changes in cross-isthmus moisture transport may affect the freshwater budget of the Atlantic and thereby evoke changes in the density driven AMOC (Rahmstorf, 1996). In chapter 5 we put forward the hypothesis that atmospheric (Gill-type) responses to changes in expansion of the glacial AWP may alter atmospheric moisture transport across the Central American isthmus. This hypothesis is explored with coupled and uncoupled ocean-atmosphere models used to perform simulations based on paleoclimate SST reconstructions. Our model results indicate that, comparable to the present, variations in glacial AWP expansion evoke inverse surface pressure changes in the Azores high pressure system. These pressure changes affect the easterly trade winds and associated low-level atmospheric moisture transport from the Atlantic across the Central American isthmus towards the Pacific. Our model results are discussed in relation to proxy-based evidence on changes in cross-isthmus moisture transport which imply that stabilizing (negative) and destabilizing (positive) feedbacks may exist with the millennial-scale glacial climate fluctuations.

Falling atmospheric CO_2 and the sudden success of Cretaceous angiosperms

In the final chapter of this thesis (chapter 6) we focus on the Cretaceous period (145-66 million years ago) during which broad-leaved flowering (angiosperm) rapidly rose to ecological dominance at the expense of needle-leaved (conifer) species (Lidgard and Crane, 1988; Frohlich and Chase, 2007). As the rise of angiosperms occurred under falling C_a (Berner, 2006; Royer, 2006), this study was motivated by the question if the present rise in C_a may provide a competitive advantage to conifers via the stomatal adjustments discussed in chapters 2 and 3. Although no direct answer was found to this question, we did find evidence to support a novel hypothesis that may explain why angiosperms could suddenly outcompete conifers under the Cretaceous C_a decline. The proposed hypothesis is relevant in an evolutionary context, especially as no satisfactory explanation has yet been provided for the sudden success of angiosperms (Crepet and Niklas, 2009; Friedman, 2009). Also in a climate context this hypothesis is relevant because the rise of angiosperms may have enhanced carbon sequestration (Berner, 1998) and hydrological cycling in moist (sub)tropical forests (Boyce et al., 2010).

Central to our hypothesis are the basic morphological differences between planar shaped (angiosperm) broad leaves and tubular shaped (conifer) needle leaves, and the consequence of these leaf morphologies for the leaf interior transport path lengths for water and CO_2. Our results show that the period of rapid angiosperm evolution started when a gradual rise in leaf vein density rendered the leaf interior transport distance for water shorter than for CO_2. Our hypothesis entails that, due to the nonlinearity of diffusive transport inside leaves (Parkhurst, 1994), surpassing this critical vein density may have provided a "tipping point" in angiosperm evolution by suddenly rewarding the development of leaves with higher D and lower a_{max} with higher carbon returns from equal water loss. Based on the idea that structural stomatal adaptations are aimed at optimizing photosynthesis with minimal water loss, we suggest that surpassing the critical leaf vein density allowed evolving angiosperms to develop leaves with more and smaller stomata. The proposed competitive advantage of angiosperms emerges from Stefan's diameter law (Stefan, 1882) which describes that the rate of evaporation expressed per unit of pore area increases with smaller pores. This mechanism also applies to stomatal gas exchange (Parlange and Waggoner, 1970) and requires plants to develop leaves with more and smaller stomata to reach highest g_{smax} (Franks and Beerling, 2009b). The same adaptation was required to increase g_{smax} to prevent carbon starvation under the Cretaceous C_a decline (Franks and Beerling, 2009a). Our results also suggest that, due to their tubular leaf morphology, needle-leaved conifers could not profit similarly from developing leaves with more and smaller stomata. Surpassing the critical leaf vein density by evolving angiosperms may therefore have initiated a sudden carbon uptake advantage over conifers. We suggest that the resulting competitive advantage of angiosperms over conifers may have sparked their rapid evolutionary development at the expense of conifers during the Cretaceous C_a decline. As evolving angiosperms increased their leaf gas exchange capacities to unprecedented levels (Feild et al., 2011), their radiation may have altered the water and carbon cycles globally (Berner, 1998; Boyce et al., 2010).

Conclusions

The results presented in this thesis underline that the terrestrial biosphere links the global water and carbon cycles and that stabilizing (negative) and destabilizing (positive) feedbacks emerge within the climate system at various spatial and temporal scales. In chapters 2 and 3 we have shown that (sub)tropical canopy species from Florida adjust the diffusive properties of their stomata to optimize leaf gas exchange under falling C_a at decadal to centennial timescales. These stomatal adaptations reduce transpiration at the leaf level and may initiate changes in the hydrological cycles at larger spatial scales. However, further analysis is required to understand the consequences of these leaf-level responses for ecosystem scale fluxes of water. In chapters 4 and 5 we have shown that the rapid climatic shifts that occurred at millennial time scales during the last glacial were documented by shifts in species composition of Florida ecosystems. These community level responses reflected changes in the (sub)tropical water cycle related to changes in heat transport in the Atlantic Ocean. The changes in the water cycle were interpreted to constitute a potential feedback with the rapid climate fluctuations by altering the freshwater budget of the North Atlantic. Key uncertainties regarding the quantitative interpretation of plant responses in terms of climate variables arise from the potential of plants to adapt their phenotypes and genotypes to environmental changes, as shown in chapters 2, 3 and 6 of this thesis. Stomatal responses may therefore not only reflect changes in environmental conditions such as C_a and water availability, they could also be indicative of evolutionary advances in the plants water transport system. We therefore argue that climatic interpretation of paleoecological proxy-evidence should be embedded in multi-disciplinary approaches including plant physiology climate modeling.

The results presented in this thesis also provide new insights in the consequences of continued anthropogenic CO_2 emissions for the climate system. Besides that the enhanced greenhouse effect alters the climate by global warming and intensification of the freshwater cycle, rising C_a also directly influences the biosphere by enhancing photosynthesis and reducing leaf-level transpiration. A key question for ongoing research is how the combined effects of global warming and carbon 'fertilization' will alter the interactions between the biosphere and atmosphere due to stomatal responses. Also we tentatively suggest that differences in stomatal trait plasticity may influence competition between different species. The results presented in chapter 6 suggest that, at geological timescales, global scale shifts in species composition may occur due to changes in C_a and thereby affect water and carbon cycles in return. Yet, additional information on the responses of tropical, temperate and (semi-)arid ecosystems to rising C_a is required to understand the potential of the biosphere to affect climate through physiological adaptations at decadal to centennial timescales. As ecosystem responses to climate change require decades or longer to manifest themselves, the consequences of the ongoing rise in C_a cannot be fully appreciated yet. We therefore advocate further research on plant responses to rising C_a at these timescales. Such research may not only increase our understanding of ecosystem responses to ongoing climate change, it may also aid our interpretation of historic climate changes derived from paleoecological proxy.

References

Ainsworth, E. A. and Rogers, A.: The response of photosynthesis and stomatal conductance to rising CO2: mechanisms and environmental interactions, Plant, Cell and Environment, 30(3), 258–270, doi:10.1111/j.1365-3040.2007.01641.x, 2007.

Alley, R. B.: Palaeoclimatology: Icing the North Atlantic, Nature, 392(6674), 335–337, doi:10.1038/32781, 1998.

Alley, R., Clark, P. U., Keigwin, L. D., Webb, R. S. and Al, E.: Making sense of millennial-scale climate change, AGU AMERICAN GEOPHYSICAL UNION, 112(2003), 385–394, doi:10.1126/science.1081056, 1999.

Alvarez, L. W., Alvarez, W., Asaro, F. and Michel, H. V.: Extraterrestrial Cause for the Cretaceous-Tertiary Extinction, Science, 208(4448), 1095–1108, doi:10.1126/science.208.4448.1095, 1980.

Berner, R. A.: Paleozoic Atmospheric CO2: Importance of Solar Radiation and Plant Evolution, Science, 261(5117), 68–70, doi:10.1126/science.261.5117.68, 1993.

Berner, R. A.: The carbon cycle and CO2 over Phanerozoic time: the role of land plants, Phil.Trans. R. Soc. Lond., 353, 75–82, 1998.

Berner, R. A.: GEOCARBSULF: A combined model for Phanerozoic atmospheric O2 and CO2, Geochimica et Cosmochimica Acta, 70(23), 5653–5664, doi:10.1016/j.gca.2005.11.032, 2006.

Berner, R. A. and Kothavala, Z.: Geocarb III: A Revised Model of Atmospheric CO2 over Phanerozoic Time, Am J Sci, 301(2), 182–204, doi: 10.2475/ajs.301.2.182 , 2001.

Blonder, B., Violle, C., Bentley, L. P. and Enquist, B. J.: Venation networks and the origin of the leaf economics spectrum, Ecology Letters, 14(2), 91–100, doi:10.1111/j.1461-0248.2010.01554.x, 2011.

de Boer, H. J., Lammertsma, E. I., Wagner-Cremer, F., Dilcher, D. L., Wassen, M. J. and Dekker, S. C.: Climate forcing due to optimization of maximal leaf conductance in subtropical vegetation under rising CO2, Proc Natl Acad Sci USA, 108(10), 4041 –4046, doi:10.1073/pnas.1100555108, 2011a.

de Boer, H. J., Lammertsma, E. I., Wagner-Cremer, F., Dilcher, D. L., Wassen, M. J. and Dekker, S. C.: Reply to Miglietta Et Al.: Maximal Transpiration Controlled by Plants, Proc Natl Acad Sci USA, 108(28), E276–E276, doi:10.1073/pnas.1107648108, 2011b.

Bonan, G. B.: Forests and Climate Change: Forcings, Feedbacks, and the Climate Benefits of Forests, Science, 320(5882), 1444–1449, doi:10.1126/science.1155121, 2008.

Bond, G., Broecker, W., Johnsen, S., McManus, J., Labeyrie, L., Jouzel, J., Bonani, G. and Ivy, S.: Correlations between climate records from North Atlantic sediments and Greenland ice, Nature, 365(6442), 143–147, doi:10.1038/365143a0, 1993.

Bond, G., Heinrich, H., Broecker, W., Labeyrie, L., McManus, J., Andrews, J., Huon, S., Jantschik, R., Clasen, S., Simet, C., Tedesco, K., et al.: Evidence for massive discharges of icebergs into the North Atlantic ocean during the last glacial period, Nature, 360(6401), 245–249, 1992.

Boucher, O., Jones, A. and Betts, R.: Climate response to the physiological impact of carbon dioxide on plants in the Met Office Unified Model HadCM3, Climate Dynamics, 32(2), 237–249, doi:10.1007/s00382-008-0459-6, 2009.

Boyce, C. K. and Lee, J.-E.: An exceptional role for flowering plant physiology in the expansion of tropical rainforests and biodiversity, Proceedings of the Royal Society B: Biological Sciences, 277(1699), 3437–3443, doi:10.1098/rspb.2010.0485, 2010.

Boyce, C. K., Lee, J.-E., Feild, T. S., Brodribb, T. J. and Zwieniecki, M. A.: Angiosperms Helped Put the Rain in the Rainforests: The Impact of Plant Physiological Evolution on Tropical Biodiversity, Annals of the Missouri Botanical Garden, 97(4), 527–540, doi:10.3417/2009143, 2010.

Bradley, R. S.: Paleoclimatology: reconstructing climates of the Quaternary, Academic Press., 1999.

Broccoli, A. J., Dahl, K. A. and Stouffer, R. J.: Response of the ITCZ to Northern Hemisphere cooling, Geophys. Res. Lett., 33, 4 PP., doi:200610.1029/2005GL024546, 2006.

Broecker, W. S.: Massive iceberg discharges as triggers for global climate change, Nature, 372(6505), 421–424, doi:10.1038/372421a0, 1994.

Broecker, W. S.: Does the Trigger for Abrupt Climate Change Reside in the Ocean or in the Atmosphere?, Science, 300(5625), 1519 –1522, doi:10.1126/science.1083797, 2003.
Chiang, J. C. H.: The Tropics in Paleoclimate, Annu. Rev. Earth Planet. Sci., 37(1), 263–297, doi:10.1146/annurev.earth.031208.100217, 2009.
Chiang, J. C. H., Kushnir, Y. and Giannini, A.: Deconstructing Atlantic Intertropical Convergence Zone variability: Influence of the local cross-equatorial sea surface temperature gradient and remote forcing from the eastern equatorial Pacific, J. Geophys. Res., 107, 19 PP., doi:200210.1029/2000JD000307, 2002.
Cowan, I. R. and Farquhar, G. D.: Stomatal function in relation to leaf metabolism and environment, Symp. Soc. Exp. Biol, 31, 471–505, 1977.
Crepet, W. L. and Niklas, K. J.: Darwin's second "abominable mystery": Why are there so many angiosperm species?, Am J Bot, 96(1), 366 –381, doi:10.3732/ajb.0800126, 2009.
Dansgaard, W., Johnsen, S. J., Clausen, H. B., Dahl-Jensen, D., Gundestrup, N. S., Hammer, C. U., Hvidberg, C. S., Steffensen, J. P., Sveinbjornsdottir, A. E., Jouzel, J. and Bond, G.: Evidence for general instability of past climate from a 250-kyr ice-core record, Nature, 364(6434), 218–220, doi:10.1038/364218a0, 1993.
Feild, T. S., Brodribb, T. J., Iglesias, A., Chatelet, D. S., Baresch, A., Upchurch, G. R., Gomez, B., Mohr, B. A. R., Coiffard, C., Kvacek, J. and Jaramillo, C.: Fossil evidence for Cretaceous escalation in angiosperm leaf vein evolution, Proc Natl Acad Sci USA, 108(20), 8363–8366, 2011.
Finsinger, W., Heiri, O., Valsecchi, V., Tinner, W. and Lotter, A. F.: Modern pollen assemblages as climate indicators in southern Europe, Global Ecology and Biogeography, 16(5), 567–582, doi:10.1111/j.1466-8238.2007.00313.x, 2007.
Franks, P. J. and Beerling, D. J.: CO2-forced evolution of plant gas exchange capacity and water-use efficiency over the Phanerozoic, Geobiology, 7(2), 227–236, doi:10.1111/j.1472-4669.2009.00193.x, 2009a.
Franks, P. J. and Beerling, D. J.: Maximum leaf conductance driven by CO2 effects on stomatal size and density over geologic time, Proc Natl Acad Sci USA, 106(25), 10343–10347, doi:10.1073/pnas.0904209106, 2009b.
Franks, P. J. and Farquhar, G. D.: The Mechanical Diversity of Stomata and Its Significance in Gas-Exchange Control, Plant Physiol., 143(1), 78–87, doi:10.1104/pp.106.089367, 2007.
Friedman, W. E.: The meaning of Darwin's "abominable mystery," Am. J. Bot., 96(1), 5–21, doi: 10.3732/ajb.0800150 , 2009.
Frohlich, M. W. and Chase, M. W.: After a dozen years of progress the origin of angiosperms is still a great mystery, Nature, 450(7173), 1184–1189, doi:10.1038/nature06393, 2007.
Gill, A. E.: Some simple solutions for heat-induced tropical circulation, Quarterly Journal of the Royal Meteorological Society, 106(449), 447–462, doi:10.1002/qj.49710644905, 1980.
Grimm, E. C., Watts, W. A., Jacobson Jr., G. L., Hansen, B. C. S., Almquist, H. R. and Dieffenbacher-Krall, A. C.: Evidence for warm wet Heinrich events in Florida, Quaternary Science Reviews, 25(17-18), 2197–2211, doi:10.1016/j.quascirev.2006.04.008, 2006.
Heinrich, H.: Origin and consequences of cyclic ice rafting in the Northeast Atlantic Ocean during the past 130,000 years, Quaternary Research, 29, 142–152, doi:10.1016/0033-5894(88)90057-9, 1988.
Hemming, S. R.: Heinrich events: Massive late Pleistocene detritus layers of the North Atlantic and their global climate imprint, Rev. Geophys., 42, 43 PP., doi:10.1029/2003RG000128, 2004.
Hoffman, P. F. and Schrag, D. P.: The snowball Earth hypothesis: testing the limits of global change, Terra Nova, 14(3), 129–155, doi:10.1046/j.1365-3121.2002.00408.x, 2002.
IPCC: Climate Change 2007: The Physical Science Basis. Contribution of Working Group I to the Fourth Assessment Report of the Intergovernmental Panel on Climate Change, edited by Solomon, Manning, Chen, Marquis, Averty, Tignor, and Miller,, 2007.
Jaeschke, A., Rühlemann, C., Arz, H., Heil, G. and Lohmann, G.: Coupling of millennial-scale changes in sea surface temperature and precipitation off northeastern Brazil with high-latitude climate shifts during the last glacial period, Paleoceanography, 22, 10 PP., doi:200710.1029/2006PA001391, 2007.

Jarvis, A.: The magnitudes and timescales of global mean surface temperature feedbacks in climate models, Earth System Dynamics, 2(2), 213–221, doi:10.5194/esd-2-213-2011, 2011.
Katul, G., Manzoni, S., Palmroth, S. and Oren, R.: A stomatal optimization theory to describe the effects of atmospheric CO2 on leaf photosynthesis and transpiration, Ann Bot, 105(3), 431–442, doi:10.1093/aob/mcp292, 2010.
Kiehl, J. T. and Ramanathan, V.: Frontiers of Climate Modeling, Cambridge University Press. [online] Available from: http://dx.doi.org/10.1017/CBO9780511535857, 2006.
Kirchner, J. W.: The Gaia hypothesis: Can it be tested?, Rev. Geophys., 27(2), 223–235, doi:198910.1029/RG027i002p00223, 1989.
Konrad, W., Roth-Nebelsick, A. and Grein, M.: Modelling of stomatal density response to atmospheric CO2, J Theor Biol, 253(4), 638–658, doi:10.1016/j.jtbi.2008.03.032, 2008.
Köppen, W. and Geiger, G.: Das geographisca System der Klimate, in Handbuch der Klimatologie, pp. 1–44, Gebr, Borntraeger., 1936.
Kürschner, F. Wagner, E. H. Visscher and H. Visscher: Predicting the response of leaf stomatal frequency to a future CO2-enriched atmosphere: constraints from historical observations, Geologische Rundschau, 86(2), 512–517, doi:10.1007/s005310050158, 1997.
Lammertsma, E. I., Boer, H. J. de, Dekker, S. C., Dilcher, D. L., Lotter, A. F. and Wagner-Cremer, F.: Global CO2 rise leads to reduced maximum stomatal conductance in Florida vegetation, Proc Natl Acad Sci USA, 108(10), 4035 –4040, doi:10.1073/pnas.1100371108, 2011.
Leduc, G., Vidal, L., Tachikawa, K., Rostek, F., Sonzogni, C., Beaufort, L. and Bard, E.: Moisture transport across Central America as a positive feedback on abrupt climatic changes, Nature, 445(7130), 908–911, doi:10.1038/nature05578, 2007.
Lidgard, S. and Crane, P. R.: Quantitative analyses of the early angiosperm radiation, Nature, 331(6154), 344–346, doi:10.1038/331344a0, 1988.
Mäkelä, A., Berninger, F. and Hari, P.: Optimal Control of Gas Exchange during Drought: Theoretical Analysis, Ann Bot, 77(5), 461 –468, doi:10.1006/anbo.1996.0056, 1996.
Manzoni, S., Vico, G., Katul, G., Fay, P. A., Polley, W., Palmroth, S. and Porporato, A.: Optimizing stomatal conductance for maximum carbon gain under water stress: a meta-analysis across plant functional types and climates, Funct Ecol, 25(3), 456–467, doi:10.1111/j.1365-2435.2010.01822.x, 2011.
Miglietta, F., Peressotti, A., Viola, R., Körner, C. and Amthor, J. S.: Stomatal Numbers, Leaf and Canopy Conductance, and the Control of Transpiration, PNAS, 108(28), E275–E275, doi:10.1073/pnas.1105831108, 2011.
Mojzsis, S. J., Arrhenius, G., McKeegan, K. D., Harrison, T. M., Nutman, A. P. and Friend, C. R. L.: Evidence for life on Earth before 3,800 million years ago, Nature, 384(6604), 55–59, doi:10.1038/384055a0, 1996.
Moriya, K.: Development of the Cretaceous Greenhouse Climate and the Oceanic Thermal Structure, Paleontological Research, 15(2), 77–88, doi:10.2517/1342-8144-15.2.077, 2011.
Muñoz, E., Busalacchi, A. J., Nigam, S. and Ruiz-Barradas, A.: Winter and Summer Structure of the Caribbean Low-Level Jet, J. Climate, 21(6), 1260–1276, doi:10.1175/2007JCLI1855.1, 2008.
NGRIP-Members: High-resolution record of Northern Hemisphere climate extending into the last interglacial period, Nature, 431(7005), 147–151, doi:10.1038/nature02805, 2004.
Nobel, P. S.: Physicochemical and environmental plant physiology, Academic Press., 1999.
Notz, D.: The future of ice sheets and sea ice: Between reversible retreat and unstoppable loss, Proc Natl Acad Sci USA, 106(49), 20590–20595, doi:10.1073/pnas.0902356106, 2009.
Nurnberg, D., Ziegler, M., Karas, C., Tiedemann, R. and Schmidt, M.: Interacting Loop Current variability and Mississippi River discharge over the past 400 kyr, Earth and Planetary Science Letters, 272(1-2), 278–289, doi:10.1016/j.epsl.2008.04.051, 2008.
Parkhurst, D. F.: Tansley Review No. 65. Diffusion of CO2 and Other Gases Inside Leaves, New Phytol, 126(3), 449–479, 1994.
Parlange, J.-Y. and Waggoner, P. E.: Stomatal Dimensions and Resistance to Diffusion, Plant Physiol, 46(2), 337–342, 1970.

Peterson, L. C., Haug, G. H., Hughen, K. A. and Rohl, U.: Rapid Changes in the Hydrologic Cycle of the Tropical Atlantic During the Last Glacial, Science, 290(5498), 1947–1951, doi:10.1126/science.290.5498.1947, 2000.

Rahmstorf, S.: On the freshwater forcing and transport of the Atlantic thermohaline circulation, Climate Dynamics, 12(12), 799–811, doi:10.1007/s003820050144, 1996.

Rietkerk, M., Brovkin, V., van Bodegom, P. M., Claussen, M., Dekker, S. C., Dijkstra, H. A., Goryachkin, S. V., Kabat, P., van Nes, E. H., Neutel, A.-M., Nicholson, S. E., et al.: Local ecosystem feedbacks and critical transitions in the climate, Ecological Complexity, 8(3), 223–228, doi:10.1016/j.ecocom.2011.03.001, 2011.

Royer, D.: CO2-forced climate thresholds during the Phanerozoic, Geochimica et Cosmochimica Acta, 70(23), 5665–5675, doi:10.1016/j.gca.2005.11.031, 2006.

Royer, D. L.: Stomatal density and stomatal index as indicators of paleoatmospheric CO2 concentration, Review of Palaeobotany and Palynology, 114(1-2), 1–28, doi:10.1016/S0034-6667(00)00074-9, 2001.

Rühlemann, C., Mulitza, S., Muller, P. J., Wefer, G. and Zahn, R.: Warming of the tropical Atlantic Ocean and slowdown of thermohaline circulation during the last deglaciation, Nature, 402(6761), 511–514, doi:10.1038/990069, 1999.

Schmidt, G. A., Ruedy, R. A., Miller, R. L. and Lacis, A. A.: Attribution of the present-day total greenhouse effect, J. Geophys. Res., 115, 6 PP., doi:201010.1029/2010JD014287, 2010.

Schmidt, M. W., Spero, H. J. and Lea, D. W.: Links between salinity variation in the Caribbean and North Atlantic thermohaline circulation, Nature, 428(6979), 160–163, doi:10.1038/nature02346, 2004.

Schopf, J. W.: Microfossils of the Early Archean Apex Chert: New Evidence of the Antiquity of Life, Science, 260(5108), 640–646, doi:10.1126/science.260.5108.640, 1993.

Seidel, D. J., Fu, Q., Randel, W. J. and Reichler, T. J.: Widening of the tropical belt in a changing climate, Nature Geoscience, 1(1), 21–24, doi:10.1038/ngeo.2007.38, 2007.

Shanahan, T. M., Overpeck, J. T., Anchukaitis, K. J., Beck, J. W., Cole, J. E., Dettman, D. L., Peck, J. A., Scholz, C. A. and King, J. W.: Atlantic Forcing of Persistent Drought in West Africa, Science, 324(5925), 377–380, doi:10.1126/science.1166352, 2009.

Sluijs, A., Schouten, S., Donders, T. H., Schoon, P. L., Rohl, U., Reichart, G.-J., Sangiorgi, F., Kim, J.-H., Sinninghe Damste, J. S. and Brinkhuis, H.: Warm and wet conditions in the Arctic region during Eocene Thermal Maximum 2, Nature Geosci, 2(11), 777–780, doi:10.1038/ngeo668, 2009.

Stefan, J.: Ueber die Verdampfung aus einem kreisförmig oder elliptisch begrenzten Becken, Annalen der Physik, 253(11), 550–560, doi:10.1002/andp.18822531108, 1882.

Tyree, M. T. and Sperry, J. S.: Do Woody Plants Operate Near the Point of Catastrophic Xylem Dysfunction Caused by Dynamic Water Stress? : Answers from a Model, Plant Physiol., 88(3), 574–580, doi:10.1104/pp.88.3.574, 1988.

Veizer, J., Ala, D., Azmy, K., Bruckschen, P., Buhl, D., Bruhn, F., Garden, G. A. F., Diener, A., Ebneth, S., Godderis, Y., Jasper, T., et al.: 87Sr/ 86Sr, δ 13C and δ 18O evolution of Phanerozoic seawater, Chemical Geology, 161(1), 59–88, 1999.

Wagner-Cremer, F., Donders, T. H. and Visscher, H.: Drought stress signals in modern and subfossil Quercus laurifolia (Fagaceae) leaves reflect winter precipitation in southern Florida tied to El Nino-Southern Oscillation activity, Am. J. Bot., 97(5), 753–759, doi:10.3732/ajb.0900196, 2010.

Walker, J. C. G., Hays, P. B. and Kasting, J. F.: A negative feedback mechanism for the long-term stabilization of Earth's surface temperature, J. Geophys. Res., 86(C10), PP. 9776–9782, doi:198110.1029/JC086iC10p09776, 1981.

Walther, G.-R.: Community and ecosystem responses to recent climate change, Phil. Trans. R. Soc. B, 365(1549), 2019–2024, doi:10.1098/rstb.2010.0021, 2010.

Wang, C.: Variability of the Caribbean Low-Level Jet and its relations to climate, Clim Dyn, 29(4), 411–422, doi:10.1007/s00382-007-0243-z, 2007.

Wang, C., Enfield, D. B., Lee, S. and Landsea, C. W.: Influences of the Atlantic Warm Pool on Western Hemisphere Summer Rainfall and Atlantic Hurricanes, J. Climate, 19(12), 3011–3028, doi:10.1175/JCLI3770.1, 2006.

Wang, C., Lee, S.-K. and Enfield, D. B.: Atlantic Warm Pool acting as a link between Atlantic Multidecadal Oscillation and Atlantic tropical cyclone activity, Geochem. Geophys. Geosyst., 9, 16 PP., doi:10.1029/2007GC001809, 2008a.

Wang, C., Lee, S.-K. and Enfield, D. B.: Climate Response to Anomalously Large and Small Atlantic Warm Pools during the Summer, J. Climate, 21(11), 2437–2450, doi:10.1175/2007JCLI2029.1, 2008b.

Watson, A. J. and Lovelock, J. E.: Biological homeostasis of the global environment: the parable of Daisyworld, Tellus B, 35B(4), 284–289, doi:10.1111/j.1600-0889.1983.tb00031.x, 1983.

Webb, T. and Bryson, R. A.: Late-and postglacial climatic change in the northern Midwest, USA: Quantitative estimates derived from fossil pollen spectra by multivariate statistical analysis, Quaternary Research, 2(1), 70–115, doi:10.1016/0033-5894(72)90005-1, 1972.

Woodwell, G. M., MacKenzie, F. T., Houghton, R. A., Apps, M., Gorham, E. and Davidson, E.: Biotic feedbacks in the warming of the earth, Climatic Change, 40(3-4), 495–518, 1998.

Ziegler, M., Nurnberg, D., Karas, C., Tiedemann, R. and Lourens, L. J.: Persistent summer expansion of the Atlantic Warm Pool during glacial abrupt cold events, Nature Geosci, 1(9), 601–605, doi:10.1038/ngeo277, 2008.

Chapter 2

Global CO_2 rise leads to reduced maximum stomatal conductance in Florida vegetation

Published as: Lammertsma, E. I., Boer, H. J. de, Dekker, S. C., Dilcher, D. L., Lotter, A. F. and Wagner-Cremer, F.: Global CO2 rise leads to reduced maximum stomatal conductance in Florida vegetation, Proc Natl Acad Sci USA (*PNAS*), 108(10), 4035 –4040, 2011.

Abstract

A principle response of C3 plants to increasing concentrations of atmospheric CO_2 (CO_2) is to reduce transpirational water loss by decreasing stomatal conductance (g_s) and simultaneously increase assimilation rates. Via this adaptation, vegetation has the ability to alter hydrology and climate. Therefore, it is important to determine the adaptation of vegetation to the expected anthropogenic rise in CO_2. Short-term stomatal opening–closing responses of vegetation to increasing CO_2 are described by free-air carbon enrichment growth experiments, and evolutionary adaptations are known from the geological record. However, the effects of CO_2 perturbations at decadal to centennial timescales on stomatal conductance are still largely unknown. Here we reconstruct a 34% (±12%) reduction in maximum stomatal conductance (g_{smax}) per 100 ppm CO_2 increase as a result of the adaptation in stomatal density (D) and pore size at maximal stomatal opening (a_{max}) of nine common species from Florida over the past 150 y. The species-specific g_{smax} values are determined by different evolutionary development, whereby the angiosperms sampled generally have numerous small stomata and high g_{smax}, and the conifers and fern have few large stomata and lower g_{smax}. Although angiosperms and conifers use different D and a_{max} adaptation strategies, our data show a coherent response in g_{smax} to the CO_2 rise of the past century. Understanding these phenotypic adaptations of C3 plants to rising CO_2 at decadal to centennial time scales is essential for quantification of plant physiological forcing in the context of global warming.

Introduction

Land plants play a crucial role in regulating our planet's hydrological and energy balance by transpiring water through the stomatal pores on their leaf surfaces. A fundamental response of C3 plants to increasing atmospheric CO_2 concentration (CO_2) is to minimize transpirational water loss by reducing diffusive stomatal conductance (g_s) and simultaneously increasing assimilation rates (1). The resulting increased intrinsic water-use efficiency (*iWUE*: the ratio of assimilation to g_s) improves the vegetation's drought resistance and reduces the cost associated with the leaf's water transport system like leaf venation (2, 3). On a regional to global scale, decreasing rates of transpiration concurrently affect climate through reduced cloud formation and precipitation (4) and with this exert a physiological feedback on climate and hydrology on top of the radiative forcing of increasing CO_2 (5–7). In the light of continuing anthropogenic climate change, it is therefore imperative to determine how plants adapt to rising atmospheric CO_2.

During their 400 million year history, land plants have been exposed to large variations in environmental conditions that prompted genetic adaptations toward mechanisms that optimize individual fitness. Over this period, plant adaptation to CO_2 is apparent as periods with high CO_2 favored species with few relatively large stomata and low g_s, whereas periods with low CO_2 (as at present) favored species with many relatively small stomata and higher g_s (8). Moreover, decreasing CO_2 after ~100million years likely triggered the evolutionary development of a more extensive leaf vein network in angiosperms, giving them the advantage of potentially higher g_s than gymnosperms with low vein density (9). At shorter timescales, plants have the ability to adjust their phenotype to optimize gas exchange. In response to short (seconds to hours) perturbations in CO_2, plants open and close their stomata (10, 11), whereas in response to CO_2 changes at decadal to centennial timescales, plants adjust leaf stomatal density (D) and/or maximum stomatal dimensions (a_{max}) (12–15). This process of epidermal structural adaptation is in part controlled by a signaling mechanism from mature to developing leaves, optimizing stomatal density and size to the changed environmental conditions (16). These epidermal characteristics determine the anatomical maximum stomatal conductance to water vapor (g_{smax}, $mol \cdot m^{-2} \cdot s^{-1}$) of fully opened stomata and can be calculated as (8, 17):

$$g_{s\max} = \frac{\frac{d_w}{v} \cdot D \cdot a_{\max}}{l + \frac{\pi}{2}\sqrt{a_{\max}/\pi}} \qquad (2.1)$$

in which stomatal density [D (number of stomata$\cdot m^{-2}$)], the size of the fully opened stomata a_{max} (m^2), and depth of the stomatal tube l (m) are the determining variables. The diffusivity of water vapor d_w ($m^2 \cdot s^{-1}$) and the molar volume of air v ($m^3 \cdot mol^{-1}$) are constants. Values of a_{max} and l are derived from the stomatal pore length L (m). Maximum stomatal conductance to CO_2 is $g_{smax}/1.6$ (18).

The most comprehensive analyses of plant adaptation to elevated CO_2 in (semi)natural environments are available from free-air carbon enrichments (FACE) growth experiments (19). Although decreases in D of C3 plants did occur in some studies (20), the observed reduction in g_s was found to be caused by instantaneous adaptation only (21). Apparently, the run-time of these growth experiments of < 5 y might be too short to trigger statistically significant epidermal structural adaptation (22). Consequently, the subtle adaptation of vegetation to continuously increasing CO_2 can only be elucidated from material covering periods long enough to deduce quantifiable structural adaptation. Because CO_2 has already increased by ~100 ppm over the past 150 y, historical leaves preserved in sediments and stored in herbarium collections offer an excellent opportunity to study the adaptation of g_{smax} to the gradual rise in CO_2.

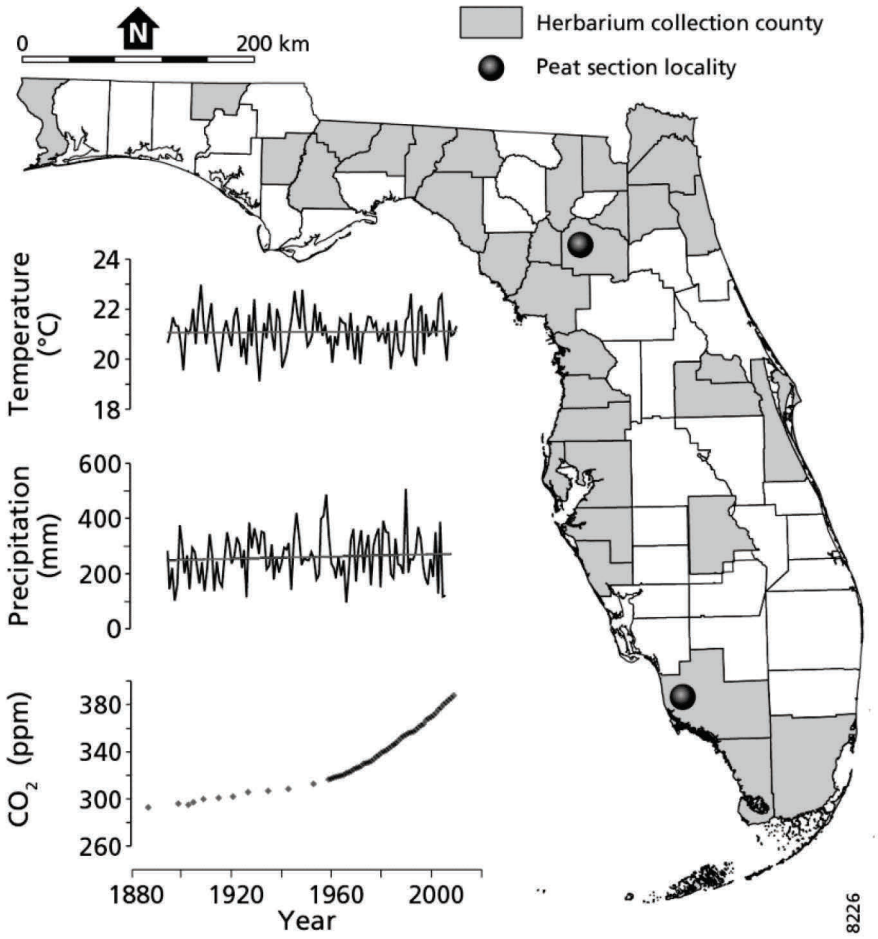

Figure 2.1 Locations of leaf material collection sites in Florida: state counties covered by herbarium material (gray) and subfossil leaf fragment sites (black stars). Florida averaged spring (March, April, and May) temperature and cumulative precipitation (http://www.ncdc.noaa.gov) and global atmospheric CO_2 concentration (ppm) [Siple station (26); Mauna Loa (27)] from 1880 A.D. to present are given. The various sites are situated approximately at sea level. Black lines in the temperature and precipitation graphs are long-term means of approximately 21 °C and 260 mm, respectively.

Because the leaf epidermal properties D and a_{max} are also influenced by other environmental factors such as light, temperature, and water availability (23–25), it is necessary to use leaf material from plants that grew under conditions in which the global CO_2 rise is the dominant variable factor. This prerequisite is met in Florida, where the vegetation has been exposed to the global ~100 ppm CO_2 increase under near constant average growth season temperatures and precipitation rates over the past 150 y (Figure 2.1). Moreover, structural adaptation to increasing CO_2 by decreasing D has already been demonstrated for a number of Florida forest taxa (28, 29).

Here we present a high-resolution historical record of nine C3 species that adapted g_{smax} to the 100 ppm rise in CO_2 since approximately 1880 A.D. Species studied are the woody angiosperms *Acer rubrum* (Aceraceae), *Myrica cerifera* (Myricaceae), *Ilex cassine* (Aquifoliaceae), *Quercus laurifolia* (Fagaceae), and *Quercus nigra* (Fagaceae), the conifers *Pinus elliottii* (Pinaceae), *Pinus taeda* (Pinaceae), and *Taxodium distichum* (Cupressaceae), and the fern *Osmunda regalis* (Osmundaceae). This selection embraces species with deciduous and evergreen leaf types, growing in wet to well-drained sites in upper to lower canopy layers (see Appendix A, Table A1). The cuticle material analyzed originates from subfossil leaf fragments retrieved from well-dated young peat deposits (26, 30) as well as herbarium and modern material collected from various sites in Florida (Figure 2.1).

In the present study we aim to quantify how these species have adapted g_{smax} in response to the industrial rise in CO_2. Moreover, the present selection includes multiple angiosperm and coniferous species, of which the leaves are characterized by a high and low leaf vein density, respectively. Because angiosperms have invested more in an elaborate leaf hydraulic system (31), we raise the hypothesis that they will benefit more by reducing g_{smax} stronger to rising CO_2. The data we present here allow for quantification of plant physiological adaptation at timescales relevant for anthropogenic climate change and provide much needed data for parameterization and validation of climate models that include these physiological feedbacks.

Results

A consistent decrease in g_{smax} over the anthropogenic rise in CO_2 is observed in all species studied ($P < 0.05$) (Figure 2.2). The inferred g_{smax} values of these nine species range between ~0.4 ($mol \cdot m^{-2} \cdot s^{-1}$) to ~4 ($mol \cdot m^{-2} \cdot s^{-1}$), with the highest values for the angiosperm canopy species *Q. nigra*, *Q. laurifolia*, and *A. rubrum* and the lowest values for the fern *O. regalis*. Despite the large differences in absolute values of g_{smax} between species, relative sensitivities in g_{smax} over ~100 ppm CO_2 rise are highly comparable, with a mean slope of −34% (±12%) per 100 ppm (Table 2.1). The weakest responses occur in *P. elliottii* and *Q. laurifolia*, with a relative sensitivity of only −17% and −18% per 100 ppm, whereas *P. taeda* shows the strongest sensitivity in g_{smax}, with −55% per 100 ppm. Despite these differences in CO_2 response, the total change exceeds the maximum intrinsic variability quantified as the root mean square error (RMSE) in all species (see

Appendix A, Table A2). The CO_2-induced phenotypic decrease in g_{smax} on decadal timescales resembles evolutionary g_{smax} adaptation over geological timescales (32), reflecting the permanent attempt of plants to optimize individual fitness.

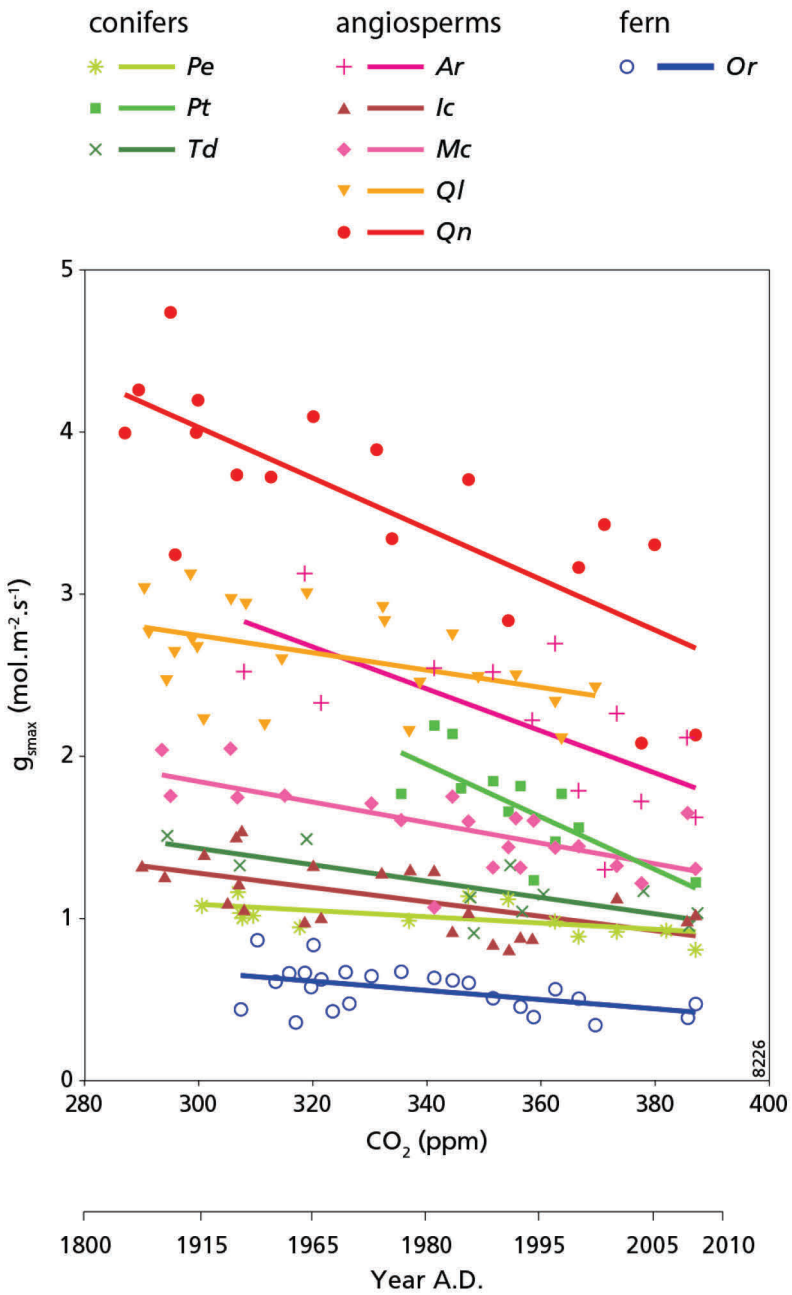

Figure 2.2 Species-specific relation between g_{smax} and CO_2 over the past 150 y. Symbols are average g_{smax} (mol·m^{-2}·s^{-1}) for each species per CO_2 level (ppm) studied (n = 160), and accompanying year A.D. (species names and abbreviations are given in Table 2.1). Solid lines show linear regressions between CO_2 and g_{smax} for each species, r^2 and relative sensitivity are given in Table 2.1. The functions and RMSE for each species are provided in Table A2, in Appendix A.

As on geological timescales (8), combined values of D and a_{max} on which the calculation of g_{smax} is based here are negatively correlated and follow a power law relationship in which high values of D are accompanied by low a_{max} values, and vice versa (Figure 2.3). For individual species, however, D and a_{max} are confined to specific ranges forming clusters distributed along this power law, where significant negative correlations are also apparent in five out of nine individual clusters (*P. elliottii*, *T. distichum*, *Q. laurifolia*, *M. cerifera*, and *O. regalis*; Table A3, Appendix A). This implies that the clusters represent the phenotypic plasticity of the various species, showing adjustments of both D and a_{max} that occurred in response to the complex of environmental perturbations to which the sampled vegetation was exposed, including CO_2. Within the total dataset, the most prominent difference exists between the angiosperm clusters with many small stomata that display large diversity in D and the conifers and fern clusters with few large stomata that display large diversity in a_{max}. The position of individual species on this power law curve likely represents their different evolutionary history (33, 34), with an earlier design for conifers and ferns and a more innovative design for angiosperms. Nevertheless, different combinations of D and a_{max} can lead to the same g_{smax} (Figure 2.3) and the same decrease in g_{smax} in response to rising CO_2 (Table 2.1).

Testing the CO_2 sensitivity of D and a_{max} individually, we observe that the plastic response of D is always negative and more pronounced than in a_{max} (Table 2.1). This consistent decrease of D under rising CO_2 has already been reported for the angiosperm and fern species in our dataset (26, 27). We now complement the range of species known to reduce D in response to rising CO_2 by including the conifers *P. elliottii*, *P. taeda*, and *T. distichum*. Over the sampled CO_2 rise, the relative sensitivity in D varies from maximal −42% per 100 ppm in *P. taeda* to minimal −9% per 100 ppm in *Q. laurifolia* (Table 2.1) ($P < 0.05$ for all but *O. regalis* and *Q. laurifolia*, with $P = 0.12$ and $P = 0.10$, respectively). The total change in D exceeds the maximum intrinsic variability quantified as the RMSE in all species except *O. regalis* and *Q. laurifolia* (see Appendix A, Table A4). These rates are broadly consistent with decreases in D reported for European tree species grown under anthropogenic CO_2 increase (12, 13, 15, 35).

Table 2.1 Relative response sensitivities (%·ppm^{-1}) of g_{smax}, D and a_{max} to CO_2 changes for the species sampled. The intercept for 100% is taken at 280 ppm CO_2. The r^2 is based on linear regressions. Numbers of observations are indicated in Table A1 in Appendix A.

Species names and abbreviations		g_{smax}	r^2	D	r^2	a_{max}	r^2
Acer rubrum	Ar	-0.41*	0.45	-0.29*	0.30	-0.27*	0.40
Ilex cassine	Ic	-0.30*	0.36	-0.26*	0.38	-0.13	0.04
Myrica cerifera	Mc	-0.36*	0.49	-0.31*	0.40	0.01	<0.001
Osmunda regalis	Or	-0.42*	0.24	-0.27	0.09	-0.31*	0.31
Pinus elliottii	Pe	-0.17*	0.36	-0.23*	0.55	0.13	0.15
Pinus taeda	Pt	-0.55*	0.54	-0.42*	0.56	-0.25	0.25
Quercus laurifolia	Ql	-0.18*	0.21	-0.09	0.13	-0.14	0.07
Quercus nigra	Qn	-0.37*	0.61	-0.28*	0.44	-0.21	0.18
Taxodium distichum	Td	-0.33*	0.58	-0.35*	0.52	0.06	0.06

Focusing on the changes in a_{max} over the sampled CO_2 increase, weak and unidirectional relations are observed. Significant relations were only found for *A. rubrum* and *O. regalis*, which show reductions in a_{max} of −27% and −31% per 100 ppm, respectively (Table 2.1). Moreover, the changes in our a_{max} data series only exceed the RMSE for five of the species studied (see Appendix A, Table A5). This variable response is different from changes in a_{max} to anthropogenic CO_2 rise reported earlier for two European tree species, for which a weak increase was observed (13, 36). From these observations it is apparent that D is highly sensitive to rising CO_2, whereas changes in a_{max} are variable between species and seem to be governed independently.

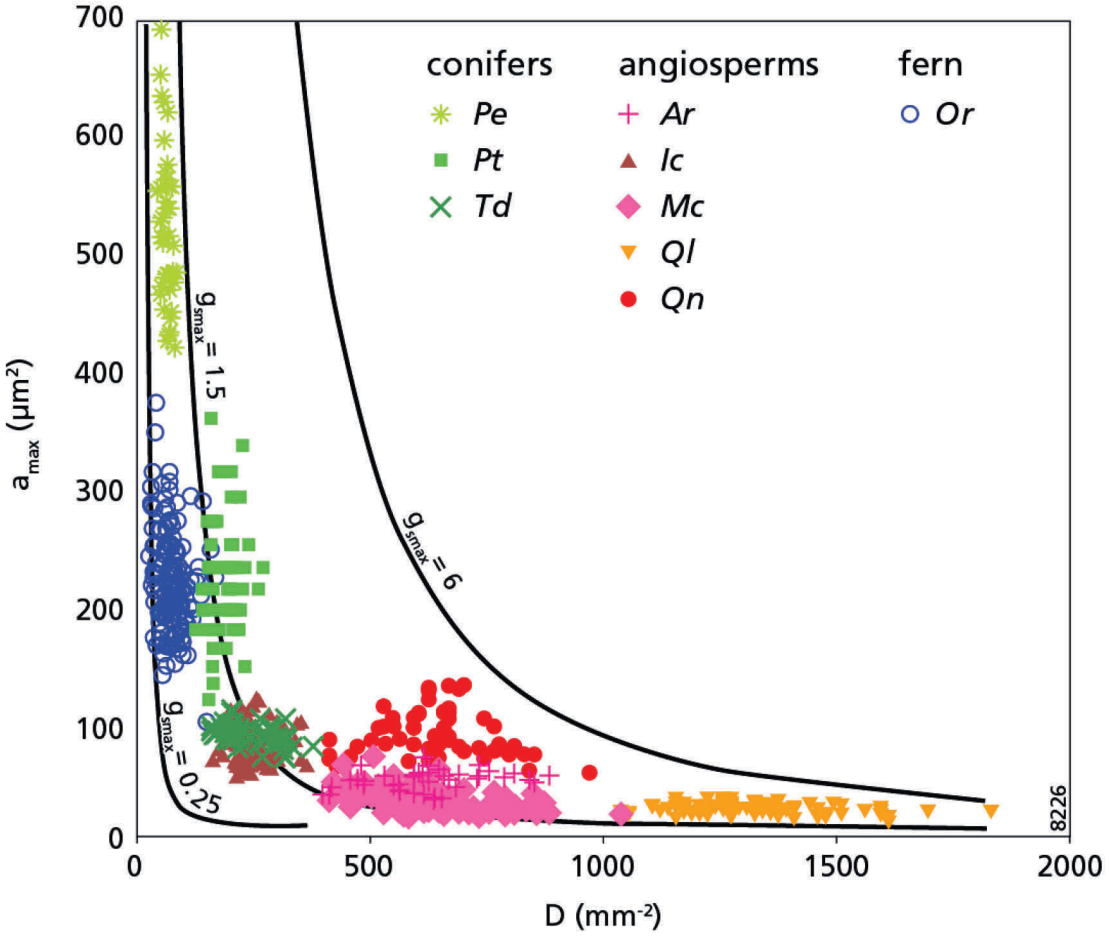

Figure 2.3 The measured stomatal density [D (mm^{-2})] and pore size [a_{max} (μm^2)]of nine common species in Florida (n = 667) (species names and abbreviations as in Table 2.1). The clusters depict a phenotypical range of D and a_{max} for each species under changing conditions of the past 150 y. Approximate lower limits are D = 20 mm^{-2} and a_{max} = 15 μm^2. Multiple combination of D and a_{max} can lead to the same g_{smax} value ($mol \cdot m^{-2} \cdot s^{-1}$), indicated by the black curved lines.

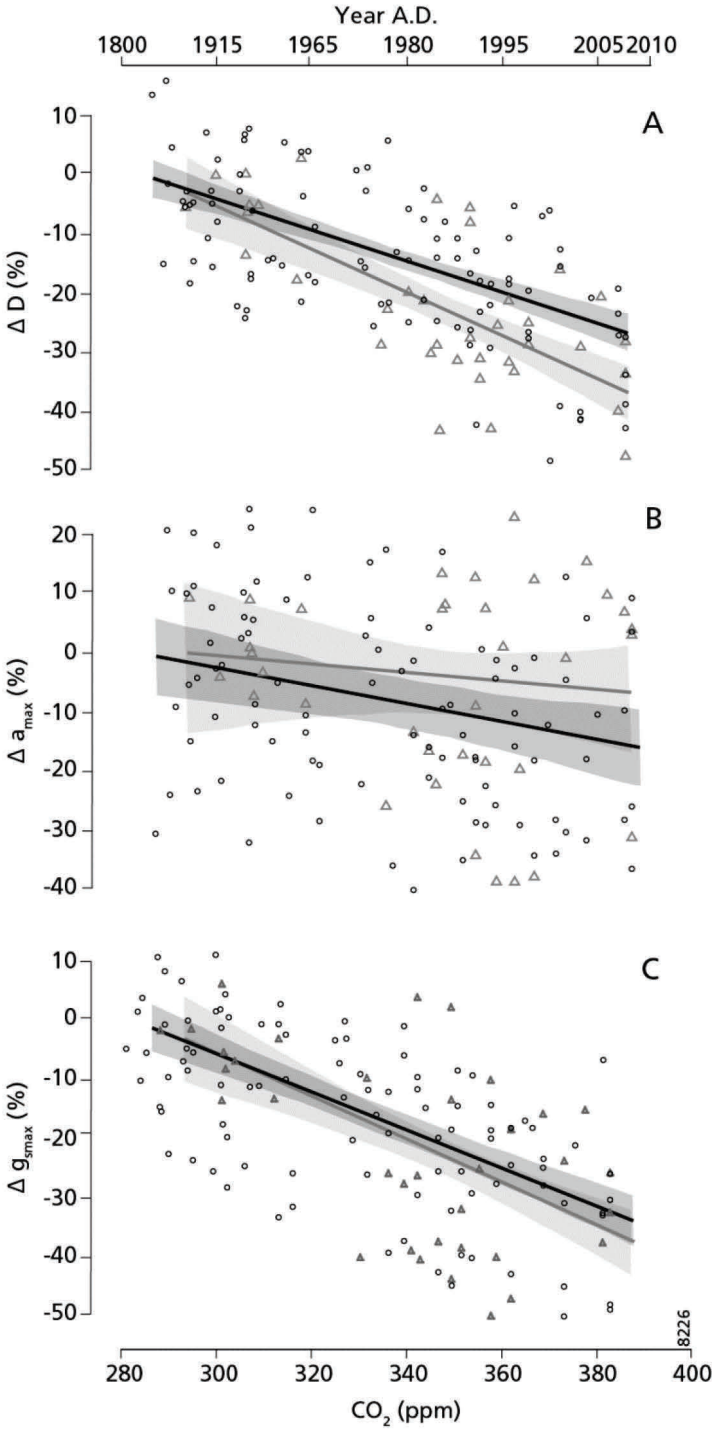

Figure 2.4 Relative sensitivity in *D* (A), a_{max} (B), and g_{smax} (C) of the grouped angiosperm species (black line, black dots) and coniferous species (gray line, gray triangles) over the sampled CO_2 increase since the industrial revolution. Dark and light shading depict the 95% confidence intervals for angiosperms and conifers, respectively. (SE, r^2, and *P* values are given in Table A6, in Appendix A). Only *D* is significantly different between angiosperms and conifers ($P < 0.001$).

Because it is hypothesized that the different leaf structures, in particular leaf vein density, of angiosperms and conifers (31) result in different epidermal structural responses to rising CO_2, we compared the general relative sensitivities of the two plant groups in our dataset. Results show that coniferous species seem to respond with a significantly stronger decrease in D (slope, −35% per 100 ppm) than angiosperms (slope, −27% per 100ppm) (Figure 2.4A and Table A6 in Appendix A). Conversely, angiosperms respond with an apparent but not significantly stronger decrease in a_{max} (slope, −15% per 100 ppm) compared with the conifers (slope, −7% per 100 ppm). Conifers also display a much larger range of variability, indicated by the broader confidence interval (Figure 2.4B). Despite these differences, a highly comparable overall decrease in g_{smax} to a rise of CO_2 from preindustrial to present in angiosperms (slope, −33% per 100 ppm) and conifers (slope,−37% per 100 ppm) emerges from this combination (Figure 2.4C). Summarizing, our data show that both angiosperms and conifers exhibit a similar response in g_{smax} to the anthropogenic rise in CO_2.

Discussion

The presented data reveal that the nine species from Florida reduce their g_{smax} in response to the industrial CO_2 rise via D and a_{max} adaptation within their phenotypic plasticity. This likely represents the plants' adaptation to increase *iWUE* by optimizing carbon gain to water loss (11, 37). We demonstrate that adaptation of g_{smax} is achieved by species-specific strategies to alter D and/or a_{max}. The overall decrease in g_{smax} is predominantly the result of a general and significant reduction of D in response to rising CO_2 in all species, whereas a_{max} seems to adapt to other environmental conditions as well, because no consistent relation with CO_2 was observed. However, the importance of including D as well as a_{max} in the reconstruction of g_{smax} is emphasized by the generally improved correlation of g_{smax} with CO_2, compared with D and a_{max} separately (Table 2.1). The observed change in a_{max} opposes the positive relation between pore size and CO_2 found over geological timescales (8). This discrepancy can be explained by considering that on the timescale studied here plants adapt within their phenotype and not genotype to reduce g_{smax}, which is most efficiently done by reducing rather than increasing pore size. This suggests that plants can and do adapt to changing conditions by fine-tuning D and a_{max} plastically to optimize their individual fitness.

Despite the consistent trend observed in g_{smax}, considerable variability characterizes the individual D and a_{max} data series, and consequently g_{smax}. This variability is likely related to climatic and site-specific environmental factors such as light, temperature, and water availability that affect D and a_{max} also (22, 24, 25). Even though the long-term mean temperature and precipitation in Florida have not changed over the past 150 y, strong interannual temperature and precipitation fluctuations (Figure 2.1) caused by the El Niño/Southern Oscillation (ENSO) and Atlantic Multidecadal Oscillation teleconnections (38, 39) may in part have caused D and a_{max} variability. Indeed, short-term changes in epidermis morphology in *Q. laurifolia* have been linked to ENSO-tied winter precipitation

(25). Together with D and a_{max} diversity throughout the canopy and even within the same leaf (40), these environmental factors produce substantial scatter in the data. Consequently, sampling on low temporal resolution might explain the lack of evidence for CO_2-induced *iWUE* adaptation as in herbarium studies covering 2 to 5 selected years only (41). The present study therefore emphasizes the necessity of sufficiently high-resolution as well as multidecadal data series to elucidate the long-term subtle response of g_{smax} to changing CO_2.

The large variation in reconstructed g_{smax} values reflect the difference in leaf vascular architecture, whereby the high vein density typical for angiosperms allows for high g_{smax} and the low vein density in ferns and conifers is reflected by low g_{smax} (31,42). The differences in the leaf hydraulic systems between angiosperms and conifers are also expressed in their position on the power law relation between D and a_{max}. Angiosperms reach high g_{smax} with numerous small stomata, and conifers reach lower g_{smax} with fewer large stomata (8). These findings can be placed against an evolutionary background, where ferns and conifers evolved in a higher-than-present CO_2 world, in which lower g_{smax} would be perfectly sufficient to maintain high photosynthesis. The late Cretaceous drop in CO_2 likely triggered the expansion of the leaf-vascular network in angiosperms (9), allowing them to attain higher photosynthesis rates than conifers and ferns but at the cost of high carbon and transpirational water loss (3). This water loss in angiosperms might be minimized as small stomata are faster to close than large stomata under desiccating conditions (43). Moreover, a consequence of the associated high water loss is the resulting evaporative cooling, which maintains an optimal leaf temperature (44). Our data thus show that species specific g_{smax} is determined in part by evolutionary adaptation to conditions in which they evolved.

When exposed to decadal variability the species studied adapt within the limits of their phenotypic plasticity, by adjusting D and a_{max}. Despite the large differences in D and a_{max} between species, even within the same genus they all exhibit highly comparable adaptation of g_{smax} to increasing CO_2. Comparing the general adaptation of the angiosperms and conifers as groups, however, a different strategy to reduce g_{smax} was observed, depending on their position on the power law curve. Although only the relative change in D between angiosperms and conifers is significantly different, the tendency towards an opposite response in D and a_{max} does illustrate that variable adaptations lead to the same reduction in g_{smax}. These results can be explained by the different position on the power law curve, whereby species reduce g_{smax} most efficiently by changing either D or a_{max} to get the steepest gradient in g_{smax} (Figure 2.3). Because the construction of an extended vascular network is coupled to high carbon costs (3, 42), it was hypothesized before that angiosperms reduce g_{smax} more than conifers and ferns. However, our data show a highly comparable sensitivity to the industrial CO_2 rise in all groups sampled and thereby demonstrate the underlying principle that plants generally optimize their leaf structure in response to rising CO_2, apparently irrespective of their leaf architecture.

Having discussed the responses and possible underlying mechanisms, the potential further development of g_{smax} under future increasing CO_2 can be evaluated. The *iWUE* responses measured in short-term growth experiments over below-present to present CO_2 levels are also found to be comparable in angiosperms, conifers, and ferns, but the trends diverge from present to elevated CO_2, where the response in conifers and ferns levels off (45). Our results of structural adaptation from~280 ppm to 387 ppm CO_2 does not bear any evidence for a diverging response between plant lineages. Whether any g_{smax} off-leveling will occur under continuing CO_2 enrichment, and at what CO_2 concentration this will happen, should be estimated by modeling exercises incorporating adaptation within the species specific phenotypic plasticity (37).

In conclusion, our results point to a common mechanism in C3 plants to reduce maximum stomatal conductance via adjustment of stomatal density and pore size within the limits of their phenotypic plasticity on a decadal timescale. As atmospheric carbon dioxide concentration is rising, plants can and do reduce water loss by reducing maximal stomatal conductance while maintaining carbon uptake (3, 31). Further decreases in stomatal conductance have been observed at CO_2 rising above present levels in FACE short-term experiments (21) and in fossil leaves over geological timescales (8). Both lines of evidence, however, fall beyond or below the timescales of the projected rate of continuing CO_2 increase, which is likely to surpass the time needed for adaptation via natural selection. Consequently, the adaptation within the phenotypic plasticity is likely to constrain epidermis structural adaptation in the near future when phenotypic response limits are reached (35, 37). Current increase in CO_2 and the coinciding reduction in plant transpiration already results in increased continental run-off (46), and climate models predict surface temperature increases arising from reduced evaporative cooling (6, 7). The mechanisms of optimization of carbon gain to water loss described here could be used to better estimate this physiological forcing for the past and future CO_2 but should be considered within the framework of species-specific phenotypic plasticity (37).

Materials and Methods

Sample Preparation and Analysis

The leaf fragments were treated in 4% sodium hypochlorite (NaClO2) at 40°C for several minutes up to 24 h, after which the stomata-bearing abaxial cuticle could be peeled off from the mesophyll, dyed with saffranine, and mounted in glycerine jelly. Because *Pinus* has an approximately equal amount of stomata on the abaxial as well as the adaxial surface, the entire cuticle was processed. Standardized, computer-aided analysis of the epidermal properties was performed on Leica Quantimet 500C/500+ and AnalySIS image analysis systems. Stomatal density (D; number of stomata·m^{-2}) was measured on 5–10 alveoles of each leaf sample and averaged. Because of different epidermis cell patterning, *Pinus* is measured with the stomatal rows running diagonally in the image. Pore length

(L; µm) is determined by averaging measurements of ~25 stomata for each sample. Data are available upon request.

Calculating g_{smax} to Water Vapor

To determine the stomatal conductance to water vapor g_{smax} (mol·m^{-2}·s^{-1}), the equation provided by Franks and Farquhar (17) is applied, using a two-way end correction accounting for the diffusion shells (8) (Eq. 1). Maximum pore surface area a_{max} (m^2) is defined as an ellipse and quantified as $\pi \cdot L^2/8$, with L being stomatal pore length (m). Stomatal pore depth l (m) is assumed to be equal to the guard cell width of the stomata when the guard cell is fully inflated (8). Quantification of l follows from the significant positive linear relations between pore length and guard cell width for each species, with exception of *P. taeda*, for which a constant value is taken (see Appendix A, Table A7). Values used for gas constants D and v are those for 25 °C. For the determination of the long-term relative sensitivities of the measured D and a_{max}, and consequent g_{smax}, the regressions are performed on values averaged per sampled year.

Statistical Analyses

The significance of the observed regressions presented here is tested in three steps, with P values of < 0.05 considered statistically significant. First, the significance of each regression plotted through the data series was tested. Second, using a Student t-test on the slopes of these regressions, it was determined whether the observed changes were significantly larger than 0. Finally, to test whether the average responses in D, a_{max}, and g_{smax} were significantly different between angiosperms and conifers, a t test (two samples assuming unequal variances) was performed on the pooled data of each group within the CO_2 interval of 360–387 ppm.

Acknowledgements

We thank H. van Konijnenburg-van Cittert, J. van der Burgh, M. Rietkerk, H. Visscher, and two reviewers for useful comments and discussion on this work; L. Bik for graphical support; K. Perkins of the University of Florida Herbarium for assistance in selecting samples; and Florida Park Service–District 4 for its overall support. This research was funded by the High Potential program of Utrecht University. This report is Netherlands Research School of Sedimentary Geology publication no.2011.01.01.

References

1. Cowan IR, Farquhar GD (1977) Stomatal function in relation to leaf metabolism and environment. Integration of Activity in the Higher Plants, ed Jennings DH (Cambridge Univ Press, Cambridge, UK), pp 471–505
2. Raven JA (2002) Selection pressures on stomatal evolution. New Phytol 153:371–386
3. Beerling DJ, Franks PJ (2010) Plant science: The hidden cost of transpiration. Nature 464:495–496
4. Bonan GB (2008) Forests and climate change: Forcings, feedbacks, and the climate benefits of forests. Science 320:1444–1449
5. Betts RA, et al. (2007) Projected increase in continental runoff due to plant responses to increasing carbon dioxide. Nature 448:1037–1041
6. Andrews T, Doutriaux-Boucher M, Boucher O, Forster PM (2011) A regional and global analysis of carbon dioxide physiological forcing and its impact on climate. Clim Dyn 36: 783–792.
7. Cao L, Bala G, Caldeira K, Nemani R, Ban-Weiss G (2010) Importance of carbon dioxide physiological forcing to future climate change. Proc Natl Acad Sci USA 107:9513–9518
8. Franks PJ, Beerling DJ (2009) Maximum leaf conductance driven by CO2 effects on stomatal size and density over geologic time. Proc Natl Acad Sci USA 106:10343–10347
9. Brodribb TJ, Feild TS (2010) Leaf hydraulic evolution led a surge in leaf photosynthetic capacity during early angiosperm diversification. Ecol Lett 13:175–183
10. Farquhar GD, Dubbe DR, Raschke K (1978) Gain of the feedback loop involving carbon dioxide and stomata: Theory and measurement. Plant Physiol 62:406–412
11. Katul G, Manzoni S, Palmroth S, Oren R (2010) A stomatal optimization theory to describe the effects of atmospheric CO2 on leaf photosynthesis and transpiration. Ann Bot (Lond) 105:431–442
12. Woodward FI (1987) Stomatal numbers are sensitive to increases in CO2 from preindustrial levels. Nature 327:617–618
13. Wagner F, et al. (1996) A natural experiment on plant acclimation: Lifetime stomatal frequency response of an individual tree to annual atmospheric CO2 increase. ProcNatl Acad Sci USA 93:11705–11708
14. Kürschner WM, van der Burgh J, Visscher H, Dilcher DL (1996) Oak leaves as biosensors of late neogene and early pleistocene paleoatmospheric CO_2 concentrations. MarMicropaleontol 27:299–312
15. Wagner F, Kouwenberg LLR, van Hoof TB, Visscher H (2004) Reproducibility of Holocene atmospheric CO_2 records based on stomatal frequency. Quat Sci Rev 23:1947–1954
16. Lake JA, Woodward FI, Quick WP (2002) Long-distance CO_2 signalling in plants. J Exp Bot 53:183–193
17. Franks PJ, Farquhar GD (2001) The effect of exogenous abscisic acid on stomatal development, stomatal mechanics, and leaf gas exchange in *Tradescantia virginiana*. Plant Physiol 125:935–942
18. Farquhar GD, Sharkey TD (1982) Stomatal conductance and photosynthesis. Annu Rev Plant Physiol 33:317–345
19. Long SP, Ainsworth EA, Rogers A, Ort DR (2004) Rising atmospheric carbon dioxide: Plants FACE the future. Annu Rev Plant Biol 55:591–628
20. Reid CD, et al. (2003) On the relationship between stomatal characters and atmospheric CO_2. Geophys Res Lett 30:1983–1986
21. Ainsworth EA, Rogers A (2007) The response of photosynthesis and stomatal conductance to rising CO_2 Mechanisms and environmental interactions. Plant Cell Environ 30:258–270
22. Royer DL (2001) Stomatal density and stomatal index as indicators of paleoatmospheric CO_2 concentration. Rev Palaeobot Palynol 114:1–28
23. Poole I, Kürschner WM (1999) Stomatal density and index: The practice. Fossil Plant and Spores: Modern Techniques, eds Jones TP, Rowe NP (Geological Society, London), pp 257–260
24. Franks PJ, Drake PL, Beerling DJ (2009) Plasticity in maximum stomatal conductance constrained by negative correlation between stomatal size and density: An analysis using Eucalyptus globulus. Plant Cell Environ 32:1737–1748

25. Wagner-Cremer F, Donders TH, Visscher H (2010) Drought stress signals in modern and subfossil Quercuslaurifolia (Fagaceae) leaves reflect winter precipitation in southern Florida tied to El Niño-Southern Oscillation activity. Am J Bot 97:753–759
26. Neftel A, et al. (1994) Trends: A compendium of data on global change. Available at: http://cdiac.ornl.gov/trends/co2/contents.htm. Accessed February, 2010
27. Keeling CD, Whorf TP (2003) Atmospheric CO_2 concentrations - Mauna Loa Observatory, Hawaii, 1958–2003. Available at: http://cdiac.ornl.gov/pns/pns_main.html. Accessed February, 2010
28. Wagner F, Dilcher DL, Visscher H (2005) Stomatal frequency responses in hardwood swamp vegetation from Florida during a 60-year continuous CO_2 increase. Am J Bot 92:690–695
29. Wagner F, Visscher H, Kürschner WM, Dilcher DL (2007) Influence of ontogeny and atmospheric CO_2 on stomata parameters of *Osmunda regalis*. Cour Forsch Inst Senckenberg 258:183–189
30. Donders TH, Wagner F, Van der Borg K, De Jong AFM, Visscher H (2004) A novel approach for developing high-resolution sub-fossil peat chronologies with 14C dating. Radiocarbon 46:455–464
31. Brodribb TJ, Holbrook NM, Zwieniecki MA, Palma B (2005) Leaf hydraulic capacity in ferns, conifers and angiosperms: Impacts on photosynthetic maxima. New Phytol 165:839–846
32. Franks PJ, Beerling DJ (2009) CO_2-forced evolution of plant gas exchange capacity and water-use efficiency over the Phanerozoic. Geobiology 7:227–236
33. Dilcher D (2000) Toward a new synthesis: Major evolutionary trends in the angiosperm fossil record. Proc Natl Acad Sci USA 97:7030–7036
34. Henry RJ (2005) Plant Diversity and Evolution: Genotypic and Phenotypic Variation in Higher Plants (Centre for Agricultural Bioscience International, Wallingford, UK), p332
35. Kürschner WM (1997) The anatomical diversity of recent and fossil leaves of the durmast oak (*Quercuspetraea Lieblein*/*Q. pseudocastanea Goeppert*): implications for their use as biosensors of palaeoatmospheric CO_2 levels. Rev Palaeobot Palynol 96:1–30
36. Garcia-Amorena I, Wagner F, van Hoof TB, Gómez Manzaneque F (2006) Stomatal responses in deciduous oaks from southern Europe to the anthropogenic atmosphericCO2 increase; refining the stomatal-based CO_2 proxy. Rev Palaeobot Palynol 141:303–312
37. de Boer HJ, et al. (2011) Climate forcing due to optimization of maximal leaf conductance in subtropical vegetation under rising CO2. Proc Natl Acad Sci USA 108:4041–4046.
38. Donders TH, Wagner F, Dilcher DL, Visscher H (2005) Mid- to late-Holocene El Nino-Southern Oscillation dynamics reflected in the subtropical terrestrial realm. Proc Natl Acad Sci USA 102:10904–10908
39. Curtis S (2008) The Atlantic Multidecadal Oscillation and extreme daily precipitation over the US and Mexico during the hurricane season. Clim Dyn 30:343–351
40. Poole I, Weyers JDB, Lawson T, Raven JA (1996) Variations in stomatal density and index: Implications for palaeoclimatic reconstructions. Plant Cell Environ 19:705–712
41. Miller-Rushing AJ, Primack RB, Templer PH, Rathbone S, Mukunda S (2009) Long-term relationships among atmospheric CO_2, stomata, and intrinsic water use efficiency in individual trees. Am J Bot 96:1779–1786
42. McKown AD, Cochard H, Sack L (2010) Decoding leaf hydraulics with a spatially explicit model: Principles of venation architecture and implications for its evolution. Am Nat 175:447–460
43. Hetherington AM, Woodward FI (2003) The role of stomata in sensing and driving environmental change. Nature 424:901–908
44. Upchurch DR, Mahan JR (1988) Maintenance of constant leaf temperature by plants II. experimental observations in cotton. Environ Exp Bot 28:359–366
45. Brodribb TJ, McAdam SAM, Jordan GJ, Feild TS (2009) Evolution of stomatal responsiveness to CO_2 and optimization of water-use efficiency among land plants. New Phytol 183:839–847
46. Gedney N, et al. (2006) Detection of a direct carbon dioxide effect in continental river runoff records. Nature 439:835–838.

Chapter 3.1

Climate forcing due to optimization of maximal leaf conductance in subtropical vegetation under rising CO_2

Published as De Boer, H. J., Lammertsma, E. I., Wagner-Cremer, F., Dilcher, D. L., Wassen, M. J. and Dekker, S. C.: Climate forcing due to optimization of maximal leaf conductance in subtropical vegetation under rising CO_2, Proc Natl Acad Sci USA (*PNAS*), 108(10), 4041–4046, 2011.

Abstract

Plant physiological adaptation to the global rise in atmospheric CO_2 concentration (CO_2) is identified as a crucial climatic forcing. To optimize their functioning under rising CO_2, plants reduce the diffusive stomatal conductance of their leaves (g_s) dynamically by closing their stomata and structurally by growing leaves with altered stomatal densities and pore sizes. The structural adaptations reduce maximal stomatal conductance (g_{smax}) and may constrain the dynamic responses of g_s. Here, we develop and validate models that simulate structural stomatal adaptations based on diffusion of CO_2 and water vapor through stomata, photosynthesis, and optimization of carbon gain under the constraint of a plant physiological cost of water loss. We hypothesize that the ongoing optimization of g_{smax} will eventually be constrained by species specific limits to phenotypic plasticity. Our model reproduces observed structural stomatal adaptations and predicts that adaptation will continue beyond double CO_2. Owing to their distinct stomatal dimensions, angiosperms are expected to reach their phenotypic response limits on average at 740 ppm, and conifers on average at 1250 ppm CO_2. Further, our simulations predict that doubling today's CO_2 will decrease the annual transpiration flux of subtropical vegetation in Florida by approximately 60 $W \cdot m^{-2}$. We conclude that plant adaptation to rising CO_2 is currently altering the freshwater cycle and climate, and will continue to do so throughout this century.

Introduction

Plants respond to the complex of environmental signals they perceive by plastic changes in their phenotype in order to increase individual fitness (1). The most apparent environmental change that induces phenotypic adaptations in plants is the global increase in atmospheric CO_2 concentration (CO_2) (2). In response to this rise in CO_2 plants reduce the diffusive stomatal conductance of their leaves [g_s (mol·m^{-2}·s^{-1})] to increase drought resistance (3) and reduce physiological costs associated with water transport (4). Plants can reduce g_s by dynamically closing their stomata within minutes (5, 6), and structurally within the life span of an individual by growing leaves with altered stomatal density [D (number of stomata·m^{-2})] and pore size at maximal stomatal opening [a_{max} (m^2)] (7, 8). Structural adaptations thereby reduce maximal stomatal conductance [g_{smax} (mol·m^{-2}·s^{-1})], which critically reduces actual g_s, especially when stomata are fully open during times with ample light and water (9).

Reduction of g_s via structural adaptation of g_{smax} has the potential to reduce transpiration fluxes. Plant responses to rising CO_2 may thereby lead to land surface warming in addition to changes in the hydrological cycle (10). This climatic effect is termed the physiological forcing of CO_2, which acts beside and independent of the radiative forcing of CO_2. Despite advances to quantify this physiological forcing with global climate models (11, 12), these models rely on semi-empirical relations to simulate g_s from environmental variables (13, 14). Alternative models have been proposed on the concept that stomatal adaptations optimize carbon gain under the constraint of a cost of water loss (15, 16). Because of their more mechanistic representation of stomatal responses, optimization models are potentially suitable to simulate canopy gas exchange under changing CO_2. However, optimization models implicitly assume that plants will continue to adapt g_s optimally to future rises in CO_2. Whether this assumption holds for the current rate of CO_2 increase is unknown, but structural stomatal responses might be constrained by limits to phenotypic plasticity (17, 18) and diffusion through stomatal pores (19).

To quantify the physiological forcing of CO_2 on past and future climate, two challenges must therefore be addressed. First we test if the observed structural adaptation of g_{smax} to rising CO_2 can be explained by optimization of carbon gain under the constraint of a cost of water loss. Second we predict at what level of CO_2 this structural adaptation may cease due to limits to phenotypic plasticity. Recent advances in stomatal modeling provide possibilities to tackle the first challenge, because the hypothesis that plants adapt g_{smax} structurally to rising CO_2 in order to optimize carbon gain with water loss can be tested mathematically (15, 16). However, limited experimental data is available for model validation because experiments are generally too short to measure structural stomatal adaptation in forests that take decades or longer to fully adapt to elevated CO_2 (20). A unique dataset provides measurements of structural adaptation of g_{smax} to the CO_2 rise of the past century in eight C3 canopy species from natural subtropical vegetation in Florida (see Table 3.1 for species names) (8). Because these species are representative for

vegetation in subtropical climates, the observations are crucial to validate models of stomatal adaptations for this climate zone.

The second challenge is more difficult to overcome because, ideally, species specific limits to structural stomatal adaptations should be observed in natural vegetation under rising CO_2. However, no historic analogue of the current high rate of CO_2 increase can be found in the 400-million year history of vascular plants (21, 22). The fossil record does show that CO_2 has been driving genetic adaptation that allowed plants to develop ranges of phenotypic plasticity to optimize functioning under changing CO_2 (22, 23). Despite these shifts in phenotype at geologic timescales, structural adaptation of g_{smax} was always constrained by interdependence of D and a_{max} in the form of a power law relationship (Figure 3.1A). Although D and a_{max} are not the only variables to determine g_{smax}, the constraint on their combined values does suggest a control on the range of g_{smax}, which is calculated as (23):

$$g_{s\max} = \frac{\frac{d_w}{v} \cdot D \cdot a_{\max}}{l + \frac{\pi}{2}\sqrt{a_{\max}/\pi}} \qquad (3.1)$$

where d_w ($m^2 \cdot s^{-1}$) is the diffusivity of water vapor and v ($m^3 \cdot mol^{-1}$) is the molar volume of air. The a_{max} is approximated from pore length [L (m)] on the premise that species studied here have ellipse-shaped stomatal apertures at a_{max} with width $W = L/2$. Pore depth l (m) is calculated from a species specific relation with guard cell width and pore length (8) (see Appendix B, Table B1). Note that g_s and g_{smax} are expressed as conductance to water vapor ($mol \cdot m^{-2} \cdot s^{-1}$). Additionally, D and a_{max} together express the percentage of leaf surface area allocated to fully opened stomatal pores as: $A_{\%} = 100 \cdot D \cdot a_{max}$. Figure 3.1A shows how combined values of D and a_{max} relate to values of equal g_{smax} and equal $A_{\%}$, which is distributed lognormally (Figure 3.1B).

The lognormal distribution of $A_{\%}$ allows for the estimation of species specific limits to structural adaptation of g_{smax}, because $A_{\%}$ is bounded on the lower side by a generic value of 0.6% independent of g_{smax}, defined here as $A_{\%low}$ (Figure 3.1B). While the species independent power law relationship between D and a_{max} is bound by $A_{\%low}$, each species uses a specific strategy to reduce g_{smax} linearly with $A_{\%}$ (Figure 3.1C). So, if a species were to decrease g_{smax} indefinitely, $A_{\%}$ would eventually surpass $A_{\%low}$ and beyond the range of historic observations. We therefore hypothesize that structural response limits are determined by consistent species specific strategies to reduce g_{smax} via adaptation of D and a_{max} along the linear relation between g_{smax} and $A_{\%}$, until $A_{\%low}$ is reached.

With a model of stomatal optimization and an empirical method to estimate response limits at hand, we may now quantify the physiological forcing of past and future CO_2 in a subtropical climate at decadal to centennial timescales. We first simulate how stomatal optimization reduces g_{smax} with rising CO_2 and validate these results against observations of eight C3 canopy species (8) that responded structurally to the CO_2 rise of the past

century. As we suggest that these adaptations may be constrained by limits to phenotypic plasticity, we estimate the upper stomatal response limit for each species in terms of CO_2. Finally, we use the stomatal optimization model with structural stomatal response limits to calculate the physiological forcing of CO_2 rising from pre-industrial (280 ppm) through present (385 ppm), and up to double present levels (770 ppm).

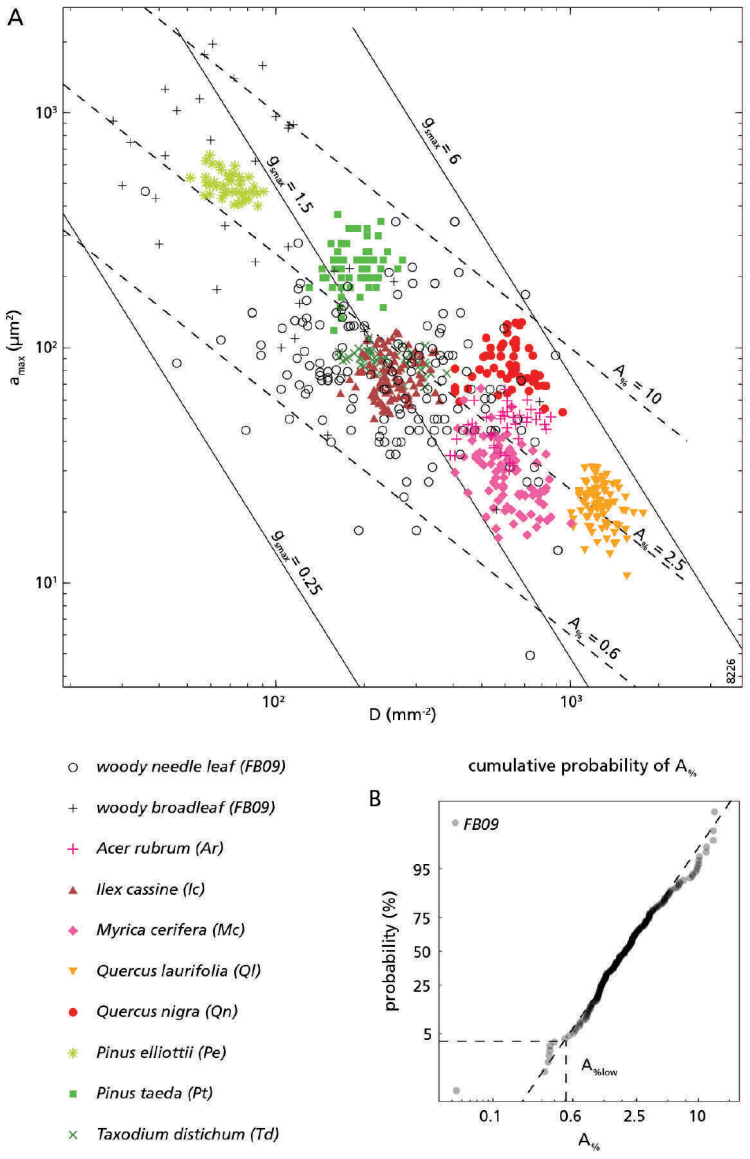

Figure 3.1 An overview of observed relationships between stomatal density (D), pore size at maximal stomatal opening (a_{max}), and the resulting maximal stomatal conductance (g_{smax}) and leaf surface area allocated to fully opened stomatal pores ($A_{\%}$). (A) Power law relationship between D and a_{max} are plotted together with lines of equal g_{smax} (solid lines) and $A_{\%}$ (dashed lines). See Equation (3.1) and Table B1 in Appendix B for calculations of g_{smax}. Note that logarithmic axes are used. (B) Cumulative probability of $A_{\%}$ for woody angiosperm and conifer species fitted to a lognormal distribution. The value of 0.6 indicates the estimated lower bound (5% probability) on $A_{\%}$ defined here as $A_{\%low}$. Note that a logarithmic x-axis is used →

Results

Our simulations of stomatal optimization are consistent with observations that report a 17-55% decrease in g_{smax} from pre-industrial to present CO_2 (Figure 3.2) (8). Our model simulates g_{smax} for all species within the variability of observed g_{smax} (Inset Figure 3.2) as a consequence of adaptations to the complex of environmental factors determining D and a_{max}, including CO_2 (24) (see Appendix B, Figure B1). Although not all variability in observed g_{smax} can be explained from adaptation to CO_2, the consistent decreases of g_{smax} observed at decadal to centennial timescales are accurately reproduced by our model. These results indicate that structural adaptations of g_{smax} to CO_2 rising from pre-industrial to present levels can be explained from optimization of carbon gain under the constraint of a cost of water loss.

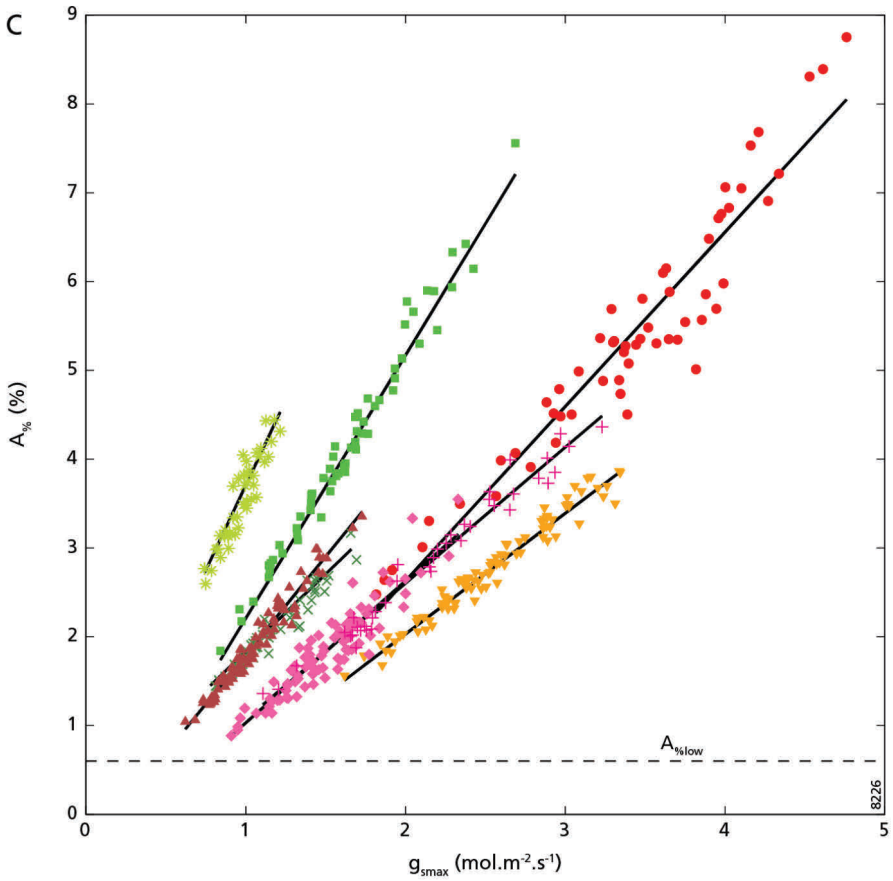

Figure 3.1 (continued) (C) Species specific strategies to adapt g_{smax} linearly with $A_{\%}$. The dashed line denotes $A_{\%low}$. Lines of linear least squares regressions are indicated per species and used to determine the intersect with $A_{\%low}$ to predict the lowest attainable g_{smax} for each species, defined as g_{low}. The r^2 values are: 0. 97 (Ar), 0.96 (Ic), 0.86 (Mc), 0.96 (Ql), 0.91 (Qn), 0.85 (Pe), 0.98 (Pt) and 0.94 (Td) with $p < 0.001$ for all. Data FB09 are from (23), others from (8). Species names and their abbreviations are defined in the legend.

Furthermore, our simulations show that g_{smax} continues to decrease with CO_2 rising beyond present values (Figure 3.2). Interpreting these model results, we find this ongoing decrease in g_{smax} unlikely because with the current rate of CO_2 increase, plants are likely to reach the limits of their phenotypic plasticity (17, 18, 25). We therefore predict structural response limits on the premise that the species specific adaptation strategies observed remain unchanged at elevated CO_2 and will eventually be limited by $A_{\%low}$ at the lowest attainable g_{smax}, defined here as g_{low} (Figure 3.1C). With our simulations of structural adaptation, we predict that values of g_{low} will be reached in a CO_2 range between 635 and 1465 ppm (Table 3.1). Consistent with observations of stomatal adaptations at evolutionary timescales (23), the angiosperms in our dataset (Ar, Ic, Mc, Ql and Qn) have notably lower response limits than conifers (Pe, Pt and Td) (740 and 1250 ppm CO_2 on average, respectively). This difference might be related to the distinct leaf vascular designs of angiosperms and conifers, which are intrinsically linked to the gas exchange capacity of their leaves (4). Angiosperms evolved towards densely veined leaves which require highly conductive leaf surfaces with many small stomata to maximize gas exchange under low CO_2 (26). Contrastingly, conifers have less conductive leaf surfaces with fewer and larger stomata, matching the lower water transport capacity of the simpler leaf vascular design suited for higher CO_2 (27).

Structural stomatal adaptations may potentially alter photosynthesis and canopy gas exchange because g_{smax} crucially constrains g_s, especially when assimilation rates reach their daily maximum and stomata are fully open. To determine how photosynthesis and leaf gas exchange is altered by structural stomatal adaptation, we perform three model ensemble simulations: one with dynamic adaptation superimposed on constant pre-industrial g_{smax} (GfixMod), one with structural and dynamic adaptation (GoptMod) and one with CO_2 response limits imposed at g_{low} (Table 3.1) (GlimMod), each of which consists of 8 species members.

Table 3.1 Species specific limits of the structural stomatal adaptation to rising CO_2, denoted by the lower limit on g_{smax} (defined as g_{low}) and CO_2 when mean g_{smax} reaches g_{low} (defined as CO_{2lim}).

Species names and abbreviations	g_{low} **(mol·m^{-2}·s^{-1})**	CO_{2lim} **(ppm)**
Angiosperm average	0.76	740
Acer rubrum (Ar)	0.69	830
Ilex cassine (Ic)	0.46	770
Myrica cerifera (Mc)	0.73	670
Quercus laurifolia (Ql)	0.95	635
Quercus nigra (Qn)	0.97	775
Conifer average	0.31	1250
Pinus elliottii (Pe)	0.19	1465
Pinus taeda (Pt)	0.46	1060
Taxodium distichum (Td)	0.29	1210

The differences in simulated g_s between GfixMod, and GoptMod and GlimMod ensemble averages show that structural adaptation of g_{smax} constrains daily average g_s (Figure 3.3A). From pre-industrial to present CO_2, daily average g_s decreases by 20% in the GlimMod and GoptMod ensembles and by 5% in the GfixMod ensemble. From present to double CO_2, g_s decreases by 40% in the GlimMod and GoptMod ensembles and by 10% in the GfixMod ensemble. Because transpiration (E) is controlled by g_s and humidity deficit in the lower atmosphere, E decreases in line with g_{smax} at increasing CO_2. Simulated E decreases with 1.0 mmol·m^{-2}·s^{-1} from pre-industrial to present, and with 1.8 mmol·m^{-2}·s^{-1} from present to double CO_2 in the GlimMod and GoptMod ensembles (Figure 3.3B). The GfixMod ensemble shows considerably less change in E with a decrease of 0.15 mmol·m^{-2}·s^{-1} from pre-industrial to present CO_2 and a decrease of 0.35 mmol·m^{-2}·s^{-1} from present to double CO_2. The change in E is less in the GfixMod simulations because only dynamic adaptation reduces g_s, while g_{smax} remains at its pre-industrial value in this model ensemble.

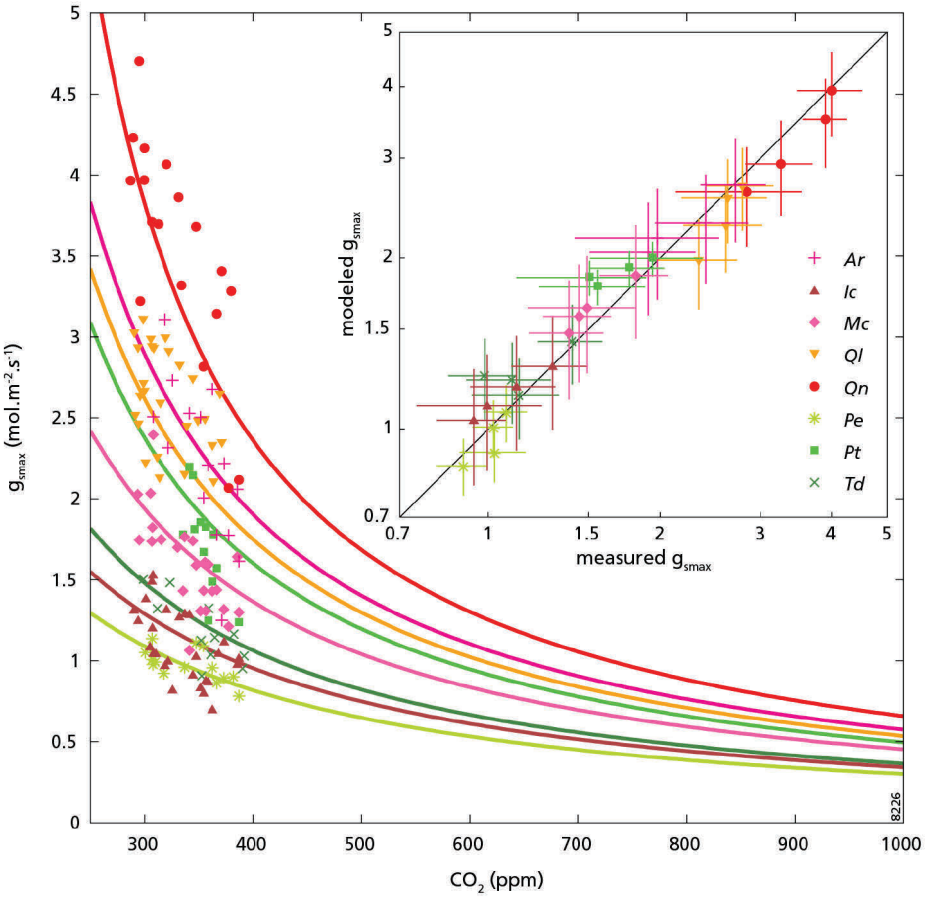

Figure 3.2 Modeled structural adaptations of g_{smax} to CO_2 for each species (solid colored lines), compared to measured g_{smax} averaged at each measured CO_2. Insert shows direct comparison between modeled and measured g_{smax} averaged over CO_2 quartiles of the data. Error bars indicate standard deviations of modeled (vertical) and measured (horizontal) g_{smax} in each quartile.

Contrasting the large differences in transpiration between the three ensemble runs, it is clear that they all show a similar increase in assimilation (*A*) from 9 µmol·m²·s⁻¹ at pre-industrial CO_2 to 15 µmol·m²·s⁻¹ at double CO_2 (Figure 3.3C). This indicates that g_{smax} does not strongly control *A*, but rather that *A* is controlled by CO_2 via changes in leaf interior CO_2 concentrations (C_i) (Figure 3.3C shows the ratio of internal to atmospheric CO_2 concentration, or C_i/C_a-ratio). The C_i therefore increases in line with CO_2 in the GfixMod ensemble and remains relatively constant over a wide range of CO_2 levels in the GoptMod and GlimMod ensembles. The latter response is commonly observed in C3 species and protects these plants from the adverse effects of photorespiration at low CO_2, while it increases the ratio of water loss versus carbon gain (termed water-use efficiency or *WUE*) with rising CO_2 (Figure 3.3D) (28). In addition to reduced leaf level transpiration, the changes in C_i/C_a-ratio and photosynthesis underline the advantage plants gain from adapting stomatal conductance in response to CO_2 (4).

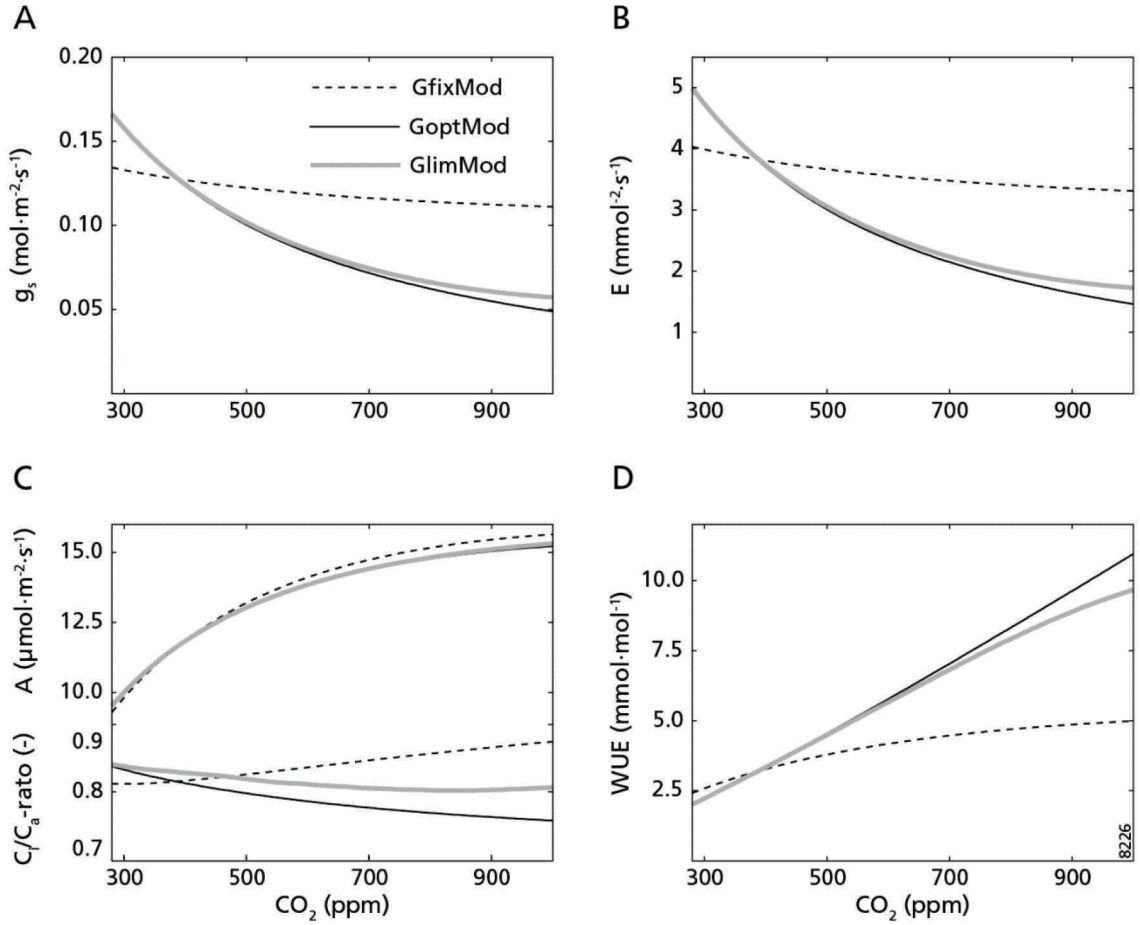

Figure 3.3 Overview of modeled daily average gas exchange at the leaf level for ensembles with dynamic stomatal adaptation only (GfixMod), with structural and dynamic adaptation (GoptMod) and with CO_2 response limits included (GlimMod). (A) Simulated stomatal conductance (g_s), (B) transpiration (*E*), (C) assimilation (*A*) and C_i/C_a-ratio at maximum photosynthesis, and (D) water use efficiency (WUE) expressed in mmol (CO_2)·mol $(H_2O)^{-1}$.

The strength of physiological forcing ultimately depends on the change of canopy transpiration (Δ*LE*) under rising CO_2. When stomatal adaptations occur at the canopy scale, reduced leaf level transpiration might reduce humidity in the lower atmosphere and in turn increase transpiration due to an increased humidity gradient. To determine how transpiration is altered by structural stomatal adaptation, we upscale our model to the canopy scale and include the feedback with moisture in the lower atmosphere. With this canopy scale model, we repeat the GfixMod, GoptMod and GlimMod ensembles and estimate physiological forcing of the CO_2 rise from pre-industrial to present levels and of doubling current CO_2.

The GoptMod and GlimMod ensembles both show a Δ*LE* of -30 W·m^{-2} due to the CO_2 rise from pre-industrial to present levels and a Δ*LE* of -60 W·m^{-2} if CO_2 doubles (Figure 3.4). The GfixMod ensemble includes only the effects of dynamic adaptation, so here Δ*LE* is just -15 W.m^{-2} from pre-industrial to double CO_2. The angiosperms in our dataset (Ar, Ic, Mc, Ql and Qn) reach their response limits between 635 and 830 ppm CO_2 (Table 3.1), so Δ*LE* is slightly less (5 W·m^{-2}) in the GlimMod compared to GoptMod ensemble at double CO_2. The conifers in our dataset (Pe, Pt and Td) reach their response limits at higher CO_2 (1250 ppm on average) and therefore show no difference in Δ*LE* between the GlimMod and GoptMod ensembles. These results suggest that structural stomatal adaptations exert a continuing physiological forcing on climate.

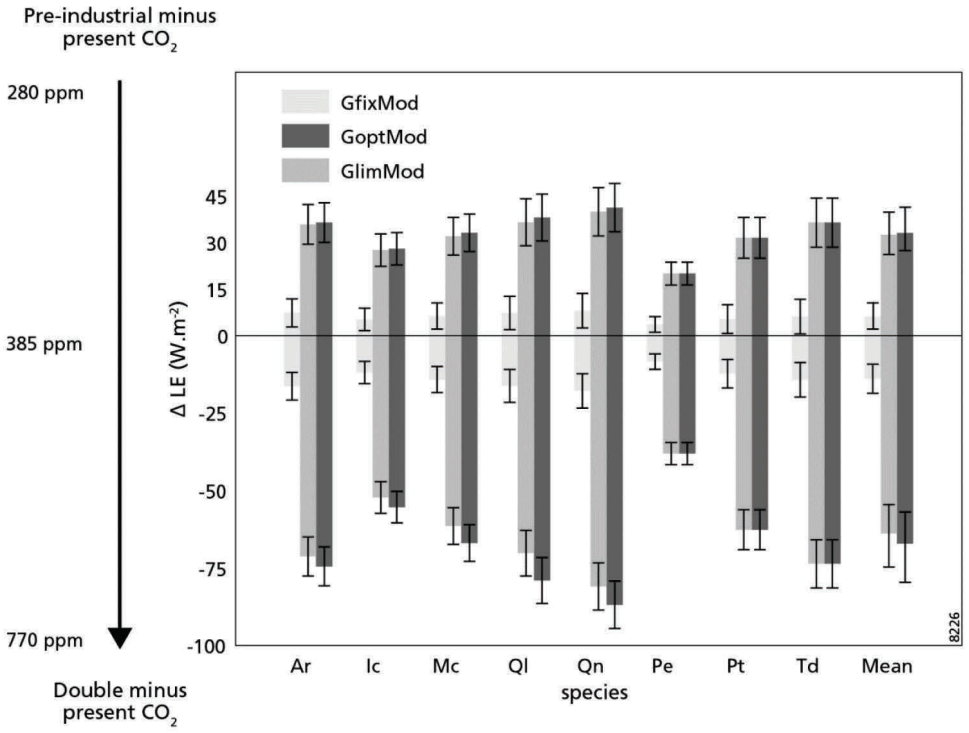

Figure 3.4 Changes in annual canopy transpiration [Δ*LE* (W·m^{-2})] between pre-industrial, present and double CO_2 for ensembles with dynamic stomatal adaptation only (GfixMod), with structural and dynamic adaptation (GoptMod) and with CO_2 response limits included (GlimMod). Error bars for individual species denote standard deviations in daily average transpiration for pre-industrial and double CO_2, error bars for mean values denote standard deviations between species averages.

Discussion

Our results suggest that structural adaptations of g_{smax} constrain the dynamic stomatal responses regulating g_s. These structural stomatal adaptations may thereby reduce the annual transpiration flux from natural subtropical vegetation in Florida under rising CO_2. Our hypothesis is supported by model simulations based on optimization of carbon gain under the constraint of a plant physiological cost of water loss that reproduce the observed adaptation of g_{smax} (which decreased with 17-55% from pre-industrial to present CO_2) (8). We further expect that plants will continue to adapt structurally until they reach the limits of their phenotypic plasticity. Because CO_2 is likely doubled by the end of this century (29) and response limits are generally reached around or above double present CO_2 levels, structural stomatal adaptation in subtropical vegetation may continue to amplify the climatic forcing of CO_2 throughout this century.

Our simulations with the stomatal optimization model predict that a doubling of present CO_2 will decrease the annual transpiration flux from subtropical vegetation in Florida by approximately 60 $W \cdot m^{-2}$. This decrease is considerable as the current annual evapotranspiration flux in Florida is approximately 120 $W \cdot m^{-2}$ and canopy transpiration contributes for approximately 50% to this regional-scale total (12, 30). Feedbacks at regional and continental scales could potentially compensate for reduced canopy transpiration and shift the fractional contribution away from transpiration (31). Accounting for these feedbacks and the contribution of transpiration to total surface latent heat flux, a comparable decrease in latent heat flux of 30 $W \cdot m^{-2}$ has been simulated over subtropical forests with the Hadley Centre global climate model (11, 32), which uses a semi-empirical stomatal response model (13). The finding that stomatal adaptations are currently reducing canopy transpiration is supported by independent empirical data from river runoff that reflect reduced continental scale evapotranspiration over the past century (33). We therefore conclude that plant adaptation to CO_2 is currently altering the hydrological cycle and climate and may continue to do so under further rising CO_2.

Despite this evidence for the climatic effects of stomatal adaptations, changes in transpiration could be compensated if forests respond to rising CO_2 by growing taller and denser and thus increase leaf area index (LAI) (34). However, in dense subtropical forests, self-shading and down regulation of photosynthetic capacity often limits this effect of CO_2 fertilization (35), so only forest-floor species are likely to benefit from rising CO_2 and these have little impact on canopy transpiration (36). Moreover, increased photosynthesis might also increase turnover rates, leading to a more dynamic forest with unchanged biomass and LAI (37). Simulations with a global vegetation model, which takes these considerations into account, indicate that in subtropical forests LAI increases by a maximum of 10% after a doubling of CO_2 (38). This increase in LAI can increase canopy transpiration by approximately 5%, which is not sufficient to compensate for reduced transpiration at the leaf level. Decreased transpiration therefore appears a robust response to increasing CO_2 in subtropical forests.

To estimate physiological forcing due to future CO_2 increase, it is essential to validate response limits to structural adaptation. We based estimates of response limits on the hypothesis that plant species adapt g_{smax} by altering D and a_{max} until they reach a generic value of $A_{\%low}$. Although the physiologic relevance of $A_{\%low}$ is not yet fully understood, it might represent a tradeoff between leaf interior CO_2 transport and the structural costs associated with the required leaf water transport system (4, 39). Since angiosperms and conifers have different leaf hydraulic systems (27), it could be argued that they also have different limits on $A_{\%}$ and that a generic $A_{\%low}$ overestimates phenotypic plasticity for either growth type (17, 40). However, our analysis does not show significant differences in the lower ranges of $A_{\%}$ between angiosperms and conifers (see Appendix B, Figure B2). Therefore we cannot reject the hypothesis that $A_{\%low}$ is a generic lower limit of $A_{\%}$ and thus the use of equal $A_{\%low}$ for angiosperms and conifers is considered appropriate. Response limits based on $A_{\%low}$ might therefore represent upper limits of ambient CO_2 to which the design of the water transport system of each species is optimized. Our prediction indicates that response limits are lower for angiosperms than conifers (on average 740 and 1250 ppm CO_2, respectively), roughly reflecting the ambient CO_2 under which these lineages evolved (41, 42).

Comparable differences in stomatal adaptation between angiosperms and conifers have been noted in free-air carbon enrichment (FACE) and greenhouse experiments under elevated CO_2 (28, 43). These studies indicate that angiosperms respond with a higher sensitivity in g_s to elevated CO_2 than conifers. Our results suggest that differences in CO_2 response could result from the plant physiological cost of water loss, represented by the Lagrangian multiplier (λ) (see Appendix B, Table B2) in the optimization procedure (15). According to the optimization hypothesis, angiosperm species with a low λ can resort to high values of g_{smax} to function under low CO_2, while conifer species with a high λ cannot. Conversely, a rise in CO_2 reverses this adaptation and therefore shows an (initial) stronger response in angiosperms than conifers. However, as conifers are expected to have higher response limits than angiosperms, they might continue to optimize g_{smax} at CO_2 levels when angiosperms have reached their limit of phenotypic plasticity.

Because CO_2 is currently rising at exceptional rates, plants face the challenge of increasing individual fitness with plastic responses in their phenotype. While modern plants have adapted their physiology to the historically low CO_2 by increasing the diffusive conductance of their leaves over the past million years (23), the current rise in CO_2 allows a reversal of this adaptation. This makes individual plants more productive and drought resistant but also has the climatic consequence of reduced transpiration and associated changes in surface energy balance and the hydrological cycle (10, 33). With CO_2 continuing to increase, it is crucial to estimate the global magnitude of this climatic forcing via plant physiological responses and the two-way coupling between vegetation and climate (44, 45). Furthermore, the ongoing rise in CO_2 might give competitive advantage to plant lineages that evolved under high CO_2 and thereby allow a shift of existing vegetation composition favoring plant lineages tied to an earlier time (25).

Materials and Methods

Model Equations

A biochemical model of photosynthesis (46) is used to simulate assimilation of CO_2 [(A (mol·m^{-2}·s^{-1})]:

$$A = \left(1 - \frac{\Gamma}{C_i}\right) \cdot \min\left(W_c, W_j\right) - R_d \qquad (3.2)$$

with

$$W_c = V_{c\max} \frac{C_i}{C_i + K_c\left(1 + \frac{p_0}{K_0}\right)} \qquad (3.3) \qquad \text{and} \qquad W_j = \tfrac{2}{9} J \frac{C_i}{C_i + \frac{7}{3}\Gamma} \qquad (3.4)$$

in which Γ (mol·mol^{-1}) is the CO_2 compensation point in absence of dark respiration R_d (mol·m^{-2}·s^{-1}), C_i (mol·mol^{-1}) is the intercellular CO_2 concentration, W_c and W_j (mol·m^{-2}·s^{-1}) are the Rusbisco and RuBP limited rates of carboxylation, V_{cmax} (mol·m^{-2}·s^{-1}) is the maximum carboxylation capacity, K_c (mol·mol^{-1}) and K_o (mol·mol^{-1}) are the Michaelis-Menten constants for carboxylation and oxygenation and p_o (mol·mol^{-1}) is the partial pressure of oxygen. The rate of electron transport [J (mol·m^{-2}·s^{-1})] depends on the photon flux density [Q (mol·m^{-2}·s^{-1})], the rate and maximum rate of electron transport (15) and temperature response of photosynthesis parameters (47). Furthermore, V_{cmax} and J_{max} exhibit down-regulation in response to rising CO_2 (22) (see Appendix B for details on parameter values).

Structural stomatal adaptations to changes in atmospheric CO_2 concentrations [CO_2 (mol·mol^{-1})] are simulated from optimization of carbon gain under the constraint of a plant physiological cost of water loss (15). The underlying assumption of this approach is that plants cannot transpire more water than they can transport from the soil, through their roots and stem up to their leaves (48). As maximum transpiration generally occurs during maximum photosynthesis, this model calculates an optimal g_{smax} [defined as g_{sopt} (mol·m^{-2}·s^{-1})] according to daily maximum photosynthesis and water availability at this time:

$$g_{sopt} = \frac{\sqrt{\frac{q(K+\Gamma)\left[CO_2(q-R_d) - (q\Gamma + KR_d)\right]}{(CO_2 + K - \lambda a w_d)\lambda a w_d}}(CO_2 + K - 2\lambda a w_d) + (q - R_d)CO_2 - (q\Gamma + KR_d) - q(K+\Gamma)a}{(CO_2 + K)^2} \qquad (3.5)$$

in which

$$q = \begin{cases} V_{c\max} & if \;\; W_c \le W_j \\ \frac{2}{9} J & if \;\; W_c > W_j \end{cases} \quad (3.6) \qquad \text{and} \qquad K = \begin{cases} K_c \left(1 + \frac{p_o}{K_o} \right) & if \;\; W_c \le W_j \\ \frac{7}{3} \Gamma & if \;\; W_c > W_j \end{cases} \quad (3.7)$$

and the Lagrangian multiplier [λ (mol·mol^{-1})] represents a species specific empirical constant for the cost of water loss (see Appendix B, Table B2), ω_d (mol·mol^{-1}) is the water vapor deficit calculated from relative and saturated atmospheric humidity [ω_{rel} (-) and ω_{sat} (mol·mol^{-1})] as $\omega_d = \omega_{sat}$ (1 - ω_{rel}) in which a (-) is the ratio between diffusivity of CO_2 and water vapor [d_c and d_w (m^2·s^{-1})]. Saturation value of water vapor and diffusivities of CO_2 and water vapor are calculated depending on ambient temperature (15, 49).

We obtain g_{smax} for every 5 ppm CO_2 interval from 280-2000 ppm from maximum g_{sopt} by prescribing an average diurnal cycle of environmental boundary conditions for the season when leaves are formed (March, April and May in Florida). Meteorological data are obtained from the AmeriFlux database (50) (see Appendix B, Figure B1). For each species, λ is calibrated on the highest CO_2 quartile of species specific g_{smax} observations.

Dynamic stomatal responses are simulated with a stomatal response model (51) superimposed on the model of structural adaptation. This model simulates dynamic adaption of g_s to environmental boundary conditions from changes in osmotic gradients in guard cells as a function of water availability and photosynthesis. Simulated actual g_s is the product of g_{smax} and the closure related to guard cell turgor (f_t [-]):

$$g_s = f_t \cdot g_{s\max} \quad (3.8) \qquad \text{with} \qquad f_t = \frac{\alpha - \gamma}{\alpha + K_g} \quad (3.9)$$

in which γ (-) is the hydroactive compensation point, K_g (-) is the Michaelis constant for the guard cell advantage [a (-)], which is calculated as a function of guard cell turgor related to water availability and photosynthesis (51).

To solve the model for leaf level gas exchange, we first obtain values for g_{smax} at each CO_2 level and then force the dynamic and structural adaptation models with a diurnal cycle of annual average environmental boundary conditions (Figure B1).

We upscale the leaf level simulations to canopy scale by considering photosynthesis at different heights in the canopy and the feedback between transpiration and moisture in the lower atmosphere. Differences in light conditions within the canopy are simulated from light interception. For this, we use a simple exponential light decay scheme (Beer's law) over 5 layers of equal LAI (52):

$$Q(L_c) = Q(0) e^{-kL_c} \quad (3.10)$$

where $Q(L_c)$ (mol·m^{-2}·s^{-1}) is the photosynthetically active radiation calculated from cumulative LAI [L_c (-)] above the considered location in the canopy, photosynthetically active radiation at the canopy top $Q(0)$, and the light extinction coefficient k (-). The feedback between transpiration and moisture in the lower atmosphere is included considering moisture redistribution in the planetary boundary layer (53).

To solve the model for canopy scale gas exchange over one year, the humidity of the upper atmosphere is iteratively calculated by forcing the model with an annual cycle of environmental boundary conditions (50) (Figure B1). Then, g_s and E are calculated for every CO_2 level in each layer of the canopy.

As A depends on the total leaf conductance [g_t (mol·m^{-2}·s^{-1})] but in turn controls g_s, C_i is expressed as a function of CO_2, A and g_t:

$$C_i = C_a - \frac{Aa}{g_t}, \qquad (3.11)$$

where

$$g_t^{-1} = g_{bl}^{-1} + g_s^{-1} + g_i^{-1}. \qquad (3.12)$$

The g_{bl} (mol·m^{-2}·s^{-1}) is the conductance of the leaf boundary layer (54) and g_i (mol·m^{-2}·s^{-1}) is the internal conductance, assumed here as $g_i = ½ \cdot g_s$ (39).

Acknowledgements

This research was partly funded by the High Potential project of Utrecht University. The manuscript was improved by comments from Henk Visscher, Brian Dermody, Max Rietkerk and two anonymous reviewers.

References

1. Trewavas A (2009) What is plant behaviour? *Plant, Cell & Environment* 32:606-616.
2. Hetherington AM, Woodward FI (2003) The role of stomata in sensing and driving environmental change. *Nature* 424:901-908.
3. Cowan IR, Farquhar GD (1977) Stomatal function in relation to leaf metabolism and environment. *Symp. Soc. Exp. Biol* 31:471-505.
4. Beerling DJ, Franks PJ (2010) Plant science: The hidden cost of transpiration. *Nature* 464:495-496.
5. Darwin F (1898) Observations on Stomata. [Abstract]. *Proceedings of the Royal Society of London* 63:413–417.
6. Farquhar GD, Sharkey TD (1982) Stomatal Conductance and Photosynthesis. *Annu. Rev. Plant. Physiol.* 33:317-345.
7. Royer DL (2001) Stomatal density and stomatal index as indicators of paleoatmospheric CO2 concentration. *Review of Palaeobotany and Palynology* 114:1-28.
8. Lammertsma EI, de Boer HJ, Dekker SC, Dilcher DL, Wagner-Cremer F (2010) Reduced stomatal conductance in Florida vegetation under anthropogenic CO2 increase. *Proc Natl Acad Sci USA* 108:4035–4040.
9. Wullschleger SD, Tschaplinski TJ, Norby RJ (2002) Plant water relations at elevated CO2 implications for water-limited environments. *Plant, Cell & Environment* 25:319-331.
10. Betts RA et al. (2007) Projected increase in continental runoff due to plant responses to increasing carbon dioxide. *Nature* 448:1037-1041.
11. Andrews T, Doutriaux-Boucher M, Boucher O, Forster PM (2011) A regional and global analysis of carbon dioxide physiological forcing and its impact on climate. *Clim Dyn* 36: 783–792.
12. Cao L, Bala G, Caldeira K, Nemani R, Ban-Weiss G (2010) Importance of carbon dioxide physiological forcing to future climate change. *Proc Natl Acad Sci USA* 107:9513-9518.
13. Ball JT, Woodrow IE, Berry A (1987) *Progress in Photosynthesis Research Vol. IV* (Martinus Nijhoff, Dordrecht).
14. Leuning R (1995) A critical appraisal of a combined stomatal-photosynthesis model for C3 plants. *Plant Cell Environ* 18:339-355.
15. Konrad W, Roth-Nebelsick A, Grein M (2008) Modelling of stomatal density response to atmospheric CO2. *Journal of Theoretical Biology* 253:638-658.
16. Katul G, Manzoni S, Palmroth S, Oren R (2010) A stomatal optimization theory to describe the effects of atmospheric CO2 on leaf photosynthesis and transpiration. *Ann Bot* 105:431-442.
17. Kürschner WM, Wagner F, Visscher EH, Visscher H (1997) Predicting the response of leaf stomatal frequency to a future CO2-enriched atmosphere: constraints from historical observations. *Geologische Rundschau* 86:512-517.
18. Ghalambor CK, McKay JK, Carroll SP, Reznick DN (2007) Adaptive versus non-adaptive phenotypic plasticity and the potential for contemporary adaptation in new environments. *Functional Ecology* 21:394-407.
19. Wynn JG (2003) Towards a physically based model of CO2-induced stomatal frequency response. *New Phytol* 157:394-398.
20. McMurtrie RE, Medlyn BE, Dewar RC (2001) Increased understanding of nutrient immobilization in soil organic matter is critical for predicting the carbon sink strength of forest ecosystems over the next 100 years. *Tree Physiol* 21:831-839.
21. Berner RA (2006) GEOCARBSULF: A combined model for Phanerozoic atmospheric O2 and CO2. *Geochimica et Cosmochimica Acta* 70:5653-5664.
22. Franks PJ, Beerling DJ (2009) CO2-forced evolution of plant gas exchange capacity and water-use efficiency over the Phanerozoic. *Geobiology* 7:227-236.
23. Franks PJ, Beerling DJ (2009) Maximum leaf conductance driven by CO2 effects on stomatal size and density over geologic time. *Proc Natl Acad Sci USA* 106:10343-10347.
24. Wagner-Cremer F, Donders TH, Visscher H (2010) Drought stress signals in modern and subfossil Quercus laurifolia (Fagaceae) leaves reflect winter precipitation in southern Florida tied to El Nino-Southern Oscillation activity. *Am. J. Bot.* 97:753-759.
25. Ward JK, Kelly JK (2004) Scaling up evolutionary responses to elevated CO2: lessons from Arabidopsis. *Ecology Letters* 7:427-440.

26. Brodribb TJ, Feild TS (2010) Leaf hydraulic evolution led a surge in leaf photosynthetic capacity during early angiosperm diversification. *Ecology Letters* 13:175-183.
27. Brodribb TJ, Holbrook NM, Zwieniecki MA, Palma B (2005) Leaf hydraulic capacity in ferns, conifers and angiosperms: impacts on photosynthetic maxima. *New Phytologist* 165:839-846.
28. Ainsworth EA, Rogers A (2007) The response of photosynthesis and stomatal conductance to rising CO2: mechanisms and environmental interactions. *Plant, Cell and Environment* 30:258-270.
29. IPCC (2007) Climate Change 2007: The Physical Science Basis. Contribution of Working Group I to the Fourth Assessment Report of the Intergovernmental Panel on Climate Change.
30. Douglas EM, Jacobs JM, Sumner DM, Ray RL (2009) A comparison of models for estimating potential evapotranspiration for Florida land cover types. *Journal of Hydrology* 373:366-376.
31. McNaughton K, Jarvis P (1991) Effects of spatial scale on stomatal control of transpiration. *Agricultural and Forest Meteorology* 54:279-302.
32. Boucher O, Jones A, Betts R (2009) Climate response to the physiological impact of carbon dioxide on plants in the Met Office Unified Model HadCM3. *Climate Dynamics* 32:237-249.
33. Gedney N et al. (2006) Detection of a direct carbon dioxide effect in continental river runoff records. *Nature* 439:835-838.
34. Norby RJ et al. (2005) Forest response to elevated CO2 is conserved across a broad range of productivity. *Proc Natl Acad Sci USA* 102:18052 -18056.
35. Millard P, Sommerkorn M, Grelet G (2007) Environmental change and carbon limitation in trees: a biochemical, ecophysiological and ecosystem appraisal. *New Phytol* 175:11-28.
36. Naumburg E, Ellsworth DS (2000) Photosynthetic sunfleck utilization potential of understory saplings growing under elevated CO2 in FACE. *Oecologia* 122:163-174.
37. Malhi Y et al. (2009) Exploring the likelihood and mechanism of a climate-change-induced dieback of the Amazon rainforest. *Proc Natl Acad Sci USA* 106:20610-20615.
38. Kergoat L et al. (2002) Impact of doubled CO2 on global-scale leaf area index and evapotranspiration: Conflicting stomatal conductance and LAI responses. *J. Geophys. Res.* 107(D24), 4808, 16 PP.
39. Warren CR (2008) Stand aside stomata, another actor deserves centre stage: the forgotten role of the internal conductance to CO2 transfer. *J. Exp. Bot* 59:1475-1487
40. Strand JA, Weisner SEB (2004) Phenotypic plasticity contrasting species-specific traits induced by identical environmental constraints. *New Phytol* 163:449-451.
41. Dilcher D (2000) Toward a new synthesis: Major evolutionary trends in the angiosperm fossil record. *Proc Natl Acad Sci USA* 97:7030-7036.
42. Henry RJ (2005) *Plant diversity and evolution: genotypic and phenotypic variation in higher plants* (CABI Publishing, Oxford, UK).
43. Brodribb TJ, McAdam SAM, Jordan GJ, Feild TS (2009) Evolution of stomatal responsiveness to CO2 and optimization of water-use efficiency among land plants. *New Phytologist* 183:839-847.
44. Kleidon A (2004) Optimized stomatal conductance of vegetated land surfaces and its effects on simulated productivity and climate. *Geophys. Res. Lett.* 31:4 PP.
45. Dekker SC et al. (2010) Biogeophysical feedbacks trigger shifts in the modelled vegetation-atmosphere system at multiple scales. *Biogeosciences* 7:1237-1245.
46. Farquhar GD, von Caemmerer S, Berry JA (2001) Models of Photosynthesis. *Plant Physiol.* 125:42-45.
47. Bernacchi CJ, Pimentel C, Long SP (2003) In vivo temperature response functions of parameters required to model RuBP-limited photosynthesis. *Plant, Cell & Environment* 26:1419-1430.
48. Baldocchi DD, Xu L (2007) What limits evaporation from Mediterranean oak woodlands - The supply of moisture in the soil, physiological control by plants or the demand by the atmosphere? *Advances in Water Resources* 30:2113-2122.
49. Nobel PS (1999) *Physicochemical and environmental plant physiology* Second edition. Academic Press, San Diego.

50. Powell TL et al. (2008) Carbon exchange of a mature, naturally regenerated pine forest in north Florida. *Global Change Biology* 14:2523-2538.
51. Buckley TN, Mott KA, Farquhar GD (2003) A hydromechanical and biochemical model of stomatal conductance. *Plant, Cell & Environment* 26:1767-1785.
52. Jogireddy VR, Cox PM, Huntingford C, Harding RJ, Mecardo L (2006) An improved description of canopy light interception for use in a GCM land-surface scheme: Calibration and testing against carbon fluxes at coniferous forest. Hadley Centre Technical note 63, The Hadley Centre, Exeter, UK.
53. McNaughton KG, Jarvis PG (1984) Using the Penman-Monteith equation predictively. *Agricultural Water Management* 8:263-278.
54. Vesala T (1998) On the Concept of Leaf Boundary Layer Resistance for Forced Convection. *Journal of Theoretical Biology* 194:91-100.

Chapter 3.2

Discussion about the stomatal control on transpiration

Letter published as Miglietta, F., Peressotti, A., Viola, R., Körner, C. and Amthor, J. S.: Stomatal Numbers, Leaf and Canopy Conductance, and the Control of Transpiration, Proc Natl Acad Sci USA (*PNAS*), 108(28), E275–E275, doi:10.1073/pnas.1105831108, 2011.

Response letter published as De Boer, H. J., Lammertsma, E. I., Wagner-Cremer, F., Dilcher, D. L., Wassen, M. J. and Dekker, S. C.: Reply to Miglietta Et Al.: Maximal Transpiration Controlled by Plants, Proc Natl Acad Sci USA (*PNAS*), 108(28), E276–E276, doi:10.1073/pnas.1107648108, 2011.

Stomatal Numbers, Leaf and Canopy Conductance, and the Control of Transpiration

De Boer et al. (1) concluded that doubled atmospheric CO_2 concentration ($[CO_2]$), by reducing both leaf stomatal density and conductance, would decrease modeled annual transpiration by approximately 60 W m^{-2} in Florida's subtropical vegetation. This remarkable result was accompanied by statements that current Floridian annual evapotranspiration (ET) is approximately 120 W m^{-2} and that transpiration is approximately 50% of current ET (i.e., ~60 W m^{-2}). (The remainder of ET is accounted for by evaporation from soil and interception water.) Because 60 minus 60 W m^{-2} equals 0 W m^{-2}, modeled transpiration in subtropical Florida would therefore cease with CO_2 doubling, implying significantly increased runoff at constant precipitation. This unlikely scenario may be related to (*i*) an unrealistically modeled effect of $[CO_2]$ on stomatal density and conductance and (*ii*) an exaggerated influence of reduced stomatal conductance on regional transpiration.

Actual stomatal density in more than half the plant species examined was insensitive to $[CO_2]$ on the time scale of the past 100 y (2). Moreover, comprehensive measurements made on plants grown for several years in subambient, ambient, and elevated $[CO_2]$ demonstrated little consequence of $[CO_2]$ on stomatal numbers (3), so we might reasonably assume that stomatal density will be little changed this century by $[CO_2]$ per se. However, even if stomatal density does decrease this century, that change would not scale to the level of regional transpiration as proposed by de Boer et al. (1).

Transpiration through higher-plant stomata is driven by atmospheric evaporative demand. For a given evaporative demand, actual transpiration is determined by soil water availability, leaf area and stomatal conductance, leaf- and canopyscale aerodynamic conductance, and overall canopy–atmosphere coupling (references in ref. 4). These factors tend to limit the control of transpiration by stomata. In addition, evaporative demand itself is inversely related to transpiration through regional scale feedbacks, which further limits the influence of stomata on transpiration (references in ref. 4). One illustrative result is that the response of native-forest canopy conductance to

a 150-ppm CO_2 increase might reduce annual transpiration only approximately 2% (4). Indeed, for annual crops and shortrotation tree plantations, which cover more than 11% of icefree global land area, increased [CO_2] might even increase transpiration because of more rapid leaf area development (5).

Despite a well documented effect of stomatal closure on transpiration by isolated leaves, stomatal conductance is expected to have only a modest degree of control over regional transpiration (4). Additionally, evidence that increasing [CO_2] per se reduces stomatal density, or canopy-scale stomatal conductance, is equivocal. We therefore advocate prudence in applying output from the model of de Boer et al. (1) to issues of regional transpiration or runoff. We also caution against an assumption that transpiration at the global scale is sensitive to a [CO_2]-induced decrease in stomatal conductance (with or without a reduction in stomatal density) and conclude that projecting effects of increasing [CO_2] on the hydrologic cycle must account for soil and canopy processes as well as atmospheric feedback mechanisms linking water supply to evaporative demand. In all this, an appropriate treatment of surface conductance is needed.

Franco Miglietta[a,b,1], Alessandro Peressotti[c], Roberto Viola[b], Christian Körner[d], and Jeffrey S. Amthor[e]

[a]Institute of Biometeorology, Consiglio Nazionale delle Ricerche, 50145 Florence, Italy; [b]FoxLab–Fondazione E. Mach, 38010 San Michele all'Adige, Italy; [c]Department of Agricultural and Environmental Sciences, Università di Udine, 33100 Udine, Italy; [d]Institute of Botany, University of Basel, CH-4056 Basel, Switzerland; and [e]Faculty of Agriculture, University of Sydney, Sydney 2006, Australia

[1]To whom correspondence should be addressed. E-mail: f.miglietta@ibimet.cnr.it.

Reply to Miglietta et al.: Maximal Transpiration Controlled by Plants

We thank Miglietta et al. (6) for their interest in our study (1). Their first and main point arises from the idea that plant transpiration (*T*) is driven by atmospheric demand, giving plants limited control over the water they lose. Miglietta et al. (6) add that stomatal density (*D*) will not change in response to increasing atmospheric CO_2 concentration ($[CO_2]$), so future changes in *T* are unlikely. This idea neglects plant physiology and is not supported by recent observations (7). Maximal *T* is limited by maximal stomatal conductance (g_{smax}) with stomata fully open. When atmospheric demand exceeds a plant's water transport capacity, stomata close in minutes. To long-term gradual $[CO_2]$ fluctuations, many perennial C3 plants adjust *D* and the size of fully opened stomata (a_{max}) to regulate g_{smax}. Concomitant *D* and a_{max} adjustments may therefore constrain *T* also at (multi)decadal time scales.

By using the measured responses of solely long-lived C3 plants to historical $[CO_2]$ increments (7), we developed a model for the optimization of g_{smax} under the constraint of a cost of water loss (1). This approach acknowledges that water loss is intrinsically linked to carbon uptake by diffusion through stomata. We stress that simulated changes in *T* are interpreted at canopy scales and not, as Miglietta et al. (6) imply, at regional scales. Our model was validated with measurements of *D* and a_{max} on 519 leaves from five angiosperm and three conifer species (7). All show a consistent decrease in g_{smax} (34% average) coeval with an approximately 100 ppm $[CO_2]$ increase. Crucial is that plants reduced g_{smax} by species-specific adaptations of both *D* and a_{max}. Changes in *D* alone cannot be related to g_{smax} without accounting for a_{max}.

The second point Miglietta et al. (6) raise is that, if plants respond to $[CO_2]$, a decrease in *T* results in limited change in evapotranspiration (*ET*) because additional evaporation (*E*) answers the demand from potential *ET*. Although regional feedbacks were not our focus, we calculate here that a decrease in *T* from 120 to 60 $W \cdot m^{-2}$ results in a 30 $W \cdot m^{-2}$ decrease in *ET*, assuming *T* accounts for 50% in *ET*. This compares with other results for densely forested (sub)tropical regions (8). To demonstrate the limited stomatal control on *ET*, Miglietta et al. (6) refer to a model that simulates little change in long-term runoff in a temperate forest under elevated $[CO_2]$ (4). As the referred model assumes that plants are not actively controlling *T*, we do not see how this proves their point. Moreover, the measurements on which this model was calibrated (9) show a 14% decrease in *T* under elevated $[CO_2]$, resulting in 10% less *ET*.

Changes in *T* occur in response to elevated $[CO_2]$ and are related to plant physiology aimed to optimize carbon gain with minimal water loss. Crucial and interesting at a regional scale are the feedbacks between atmosphere and land that may dampen or accelerate hydrological cycling in future climates. We therefore acknowledge the final statement of Miglietta et al. (6): "that projecting effects of increasing $[CO_2]$ on the hydrologic cycle must account for soil and canopy processes as well as atmospheric feedback."

References

1. de Boer HJ, et al. (2011) Climate forcing due to optimization of maximal leaf conductance in subtropical vegetation under rising CO2. Proc Natl Acad Sci USA 108: 4041–4046.
2. Royer DL (2001) Stomatal density and stomatal index as indicators of paleoatmospheric CO_2 concentration. Rev Palaeobot Palynol 114:1–28.
3. Reid CD, et al. (2003) On the relationship between stomatal characters and atmospheric CO_2. Geophys Res Lett 30:1983–1986.
4. Leuzinger S, Körner C (2010) Rainfall distribution is the main driver of runoff under future CO_2-concentration in a temperate deciduous forest. Glob Change Biol 16: 246–254.
5. Tricker PJ, et al. (2009) Water use of a bioenergy plantation increases in a future high CO_2 world. Biomass Bioenergy 33:200–208.
6. Miglietta F, Peressotti A, Viola R, Körner C, Amthor JS (2011) Stomatal numbers, leaf and canopy conductance, and the control of transpiration. Proc Natl Acad Sci USA 108: E275.
7. Lammertsma EI, et al. (2011) Global CO2 rise leads to reduced maximum stomatal conductance in Florida vegetation. Proc Natl Acad Sci USA 108:4035–4040.
8. Andrews T, Doutriaux-Boucher M, Boucher O, Forster PM (2011) A regional and global analysis of carbon dioxide physiological forcing and its impact on climate. Clim Dyn 36: 783–792.
9. Leuzinger S, Körner C (2007) Water savings in mature deciduous forest trees under elevated CO2. Glob Change Biol 13:2498–2508.

Chapter 4

Impact of the Atlantic warm pool on precipitation and temperature in Florida during North Atlantic cold spells

Published as *Donders, T. H., *Boer, H. J. de, Finsinger, W., Grimm, E. C., Dekker, S. C., Reichart, G.-J. and Wagner-Cremer, F.: Impact of the Atlantic Warm Pool on precipitation and temperature in Florida during North Atlantic cold spells, Climate Dynamics, 36(1-2), 109–118, doi:10.1007/s00382-009-0702-9, 2011.
*T. H. Donders and H. J. de Boer are joint lead authors

Abstract

Recurrent phases of increased pine at Lake Tulane, Florida have previously been related to strong stadials terminated by so-called Heinrich events. The climatic significance of these pine phases has been interpreted in different ways. Using a pollen–climate inference model, we quantified the climate changes and consistently found that mean summer precipitation (P_{JJA}) increased (0.5–0.9 mm/day) and mean November temperature increased (2.0–3.0°C) during pine phases coeval with Heinrich events and the Younger Dryas. Marine sea surface temperature records indicate that potential sources for these moisture and heat anomalies are in the Gulf of Mexico and the western tropical Atlantic. We explain this low-latitude warming by an increased Loop Current facilitated by persistence of the Atlantic Warm Pool during summer. This hypothesis is supported by a climate model sensitivity analysis. A positive heat anomaly in the Gulf of Mexico and equatorial Atlantic best approximates the pollen inferred climate reconstructions from Lake Tulane during the (stadials around) Heinrich events and the Younger Dryas.

Introduction

Paleoecological reconstructions spanning the past 60 ka (all ages cal BP) from Lake Tulane (subtropical central Florida, USA, Figure 4.1) revealed a series of sharp vegetation switches from open scrub-oak and prairie communities to pine dominated forests (Grimm et al. 1993, 2006). A recently improved age model (Grimm et al. 2006) shows that the pine phases (TP1–TP6) coincide with strong North Atlantic stadials that are terminated by massive iceberg discharges known as Heinrich events (H-events H1–H6) (Heinrich 1988; Bond et al. 1992, 1993). Pine phases at Lake Tulane were initially interpreted as indicative of wetter and cooler periods (Grimm et al. 1993), whereas the most recent interpretation considers them to represent wetter and warmer conditions in Florida (Grimm et al. 2006). The latter interpretation would involve a strong antiphase relationship between climate in Florida and the North Atlantic region, and strengthens the concept of low-latitude warming in response to North Atlantic surface freshening and subsequent reduction of the Atlantic Meridional overturning circulation (AMOC) (e.g. Stocker 1998; Rühlemann et al. 1999; Flower et al. 2004).

More evidence for the linkage between North Atlantic Cooling events and the AMOC comes from climate model simulations (e.g. Rahmstorf 1996; Ganopolski and Rahmstorf 2001; Flückiger et al. 2008). Proxy records of water mass reorganisation (e.g. Charles et al. 1996; Vidal et al. 1997; Rühlemann et al. 1999; McManus et al. 2004) also indicate abrupt reductions in northward heat transport during these time intervals. However, with regard to changes in low latitude Atlantic Sea surface temperatures (SSTs), model and proxy studies show less agreement. Although some combined climate model and proxy studies suggest a warming of low latitude Atlantic SSTs (e.g. Rühlemann et al. 2004; Menviel et al. 2008, Flückiger et al. 2008), the results of several other SST reconstructions are not uniform in sign and magnitude (Lea et al. 2003; Flower et al. 2004; Hill et al. 2006; Ziegler et al. 2008).

The size and northward expansion of the Atlantic Warm Pool (AWP) could hold the key to explaining the observed antiphase relationship between North Atlantic cooling and warming over Florida. The AWP is a region of surface waters warmer than 28.5°C and comprises the Gulf of Mexico (GoM), Caribbean Sea and the western tropical North Atlantic (Wang and Enfield 2001; Wang et al. 2006) during summer in the present day climate (Figure 4.1). In the present-day climate, the AWP reaches its northern most position in September. The size and northward extent of the AWP in summer determines the summer position of the Inter-Tropical Convergence Zone (ITCZ) and thereby affects precipitation and trade winds over the (sub)tropical North Atlantic region. Summer trade winds over the (sub)tropical North Atlantic partly drive the flow of warm surface waters from the Caribbean Sea through the GoM by the Loop Current (Johns et al. 2002).

To investigate the relation between low latitude SSTs and Florida climate, we provide an objective quantitative climate reconstruction from Lake Tulane based on newly developed pollen-climate inference models. We compare these results with available SST records from the (sub)tropical Atlantic section of the AMOC that are potential source areas for enhanced precipitation in Florida (Chen and Gerber 1992). The now fully layer-counted NGRIP Greenland ice core (Rasmussen et al. 2008; Svensson et al., 2008) provides an improved chronological framework, which allows better assessment of the correlation with South Florida. We use contrasting low-latitude Atlantic SST reconstructions as a basis for a series of climate model sensitivity experiments. Based on our model results, we discuss the mechanistic relation between low-latitude SST anomalies, specifically the role of Loop Current intensity, and land-surface temperature and precipitation changes in Florida during the periods with presumed AMOC reorganizations.

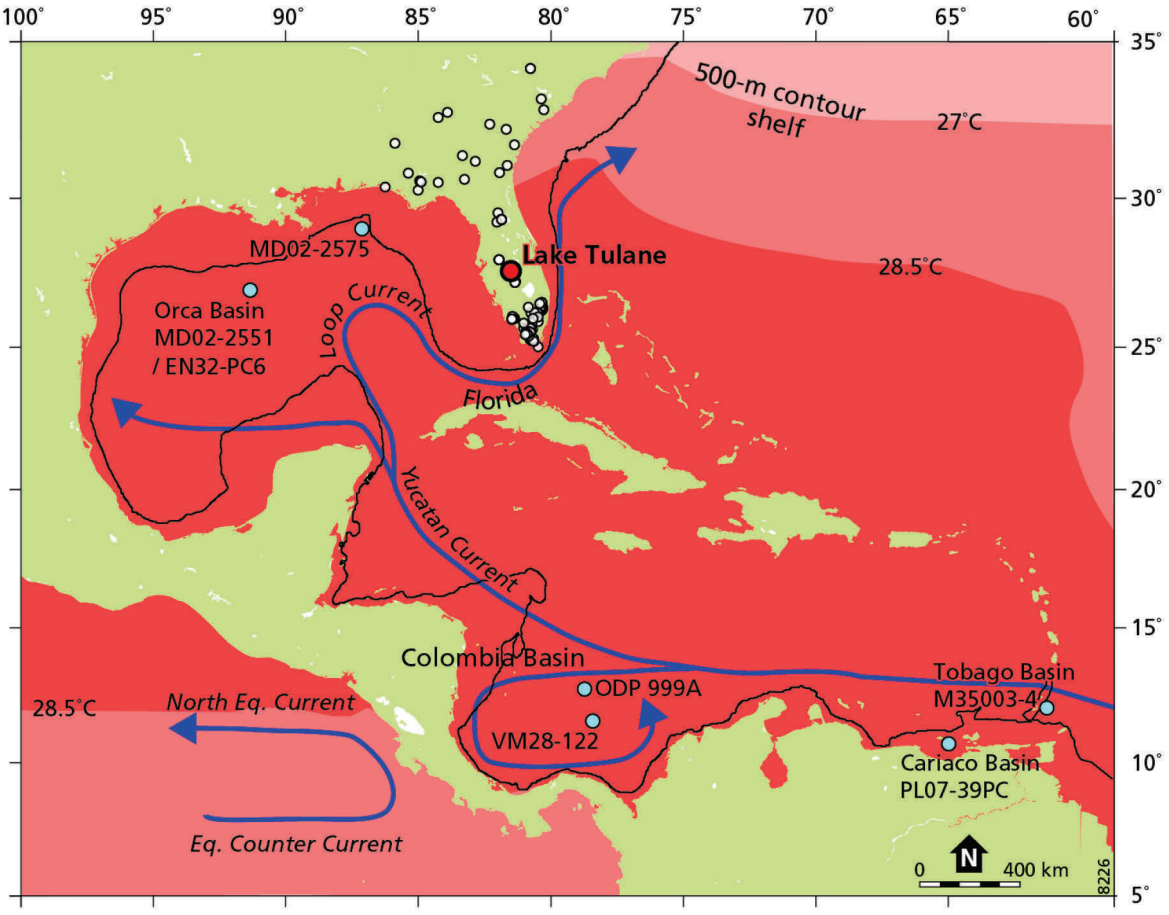

Figure 4.1 Location of Lake Tulane (red circle), surface sediment samples used in the calibration (empty circles), and marine sites (blue circles) discussed in the text. Arrows indicate approximate large-scale warm sea-surface circulation (Cherubin et al. 2005). Red contours indicate September SSTs. SSTs above 28.5°C indicate the extent of the Atlantic Warm Pool.

Environmental setting and data

Lake Tulane is one of numerous deep sinkhole lakes on the Lake Wales Ridge highland in south-central Florida (Figure 4.1), which locally rises to 55 m elevation. Unconsolidated sands cause the area to be excessively well drained with highly permeable soils. As a consequence, natural vegetation on the Lake Wales Ridge consists mainly of a mosaic of sand pine scrub and sandhill high pine communities. The first consists of scrub oak species (*Quercus myrtifolia*, *Q. inopina*, *Q. geminata*, *Q. chapmanii*), rosemary (*Ceratiola ericoides*), rusty lyonia (*Lyonia ferruginea*), and palmettos (*Serenoa repens* and *Sabal etonia*), with scattered sand pine (*Pinus clausa*) while the second is dominated by South Florida slash pine (*Pinus elliottii var. densa*), with wire grass (*Aristida stricta*) and scrub (*Quercus laevis*, *Carya floridana*) undergrowth (Abrahamson et al. 1984; Grimm et al. 2006). The vegetation mosaic depends largely on precipitation during the wet summer-growing season. The sandy soils and seasonal precipitation make the site sensitive to regional climate variations.

Our principal dataset consists of pollen counts on 191 samples taken from an 18-m long core collected at Lake Tulane (Grimm et al. 2006). To assess within and between site variability, we use pollen records from an earlier core collected at Lake Tulane (Grimm et al. 1993) and a record from Lake Annie 100 km south of Lake Tulane (Watts 1975; Appendix C1, Figure C3). A study by Willard et al. (2007) from Tampa Bay that shows significant dry/wet variations was assessed but was not used in the quantitative climate reconstruction because the catchment area and depositional setting of that site vary strongly through time, whereby changes in local vegetation disproportionately drive the results. All pollen percentages were calculated based on the taxonomical resolution of pollen counts from modern surface sediments (Whitmore et al. 2005).

Methods

Transfer-function development and climate reconstruction

In addition to the previous qualitative interpretations (Grimm et al. 1993, 2006) we use numerical methods to quantitatively reconstruct past climate changes based on the Lake Tulane pollen records. Regional pollen-based climate inference models were developed using an extensive compilation of (bio)climatic data (Whitmore et al. 2005) and pollen counts from surface sediment samples (Whitmore et al. 2005; Donders et al. 2005a). Our selection covers wide temperature and precipitation gradients (tropical to warm-temperate) across the SE USA (Figure 4.1; Appendix C1). In an attempt to increase the predictive power of the inference models (Table 4.1), we limited wide-ranging genera (e.g. *Carya*, *Quercus*, *Pinus*) to species with shorter environmental variables by excluding surface sediment samples from more temperate areas. The individual explanatory power of 36 (bio)climatic parameters was assessed using canonical correspondence analysis (CCA)(Supplemental material in Appendix C1). The ecologically and statistically most significant parameters, mean summer precipitation (P_{JJA}) and mean November

temperature (T_{NOV}), were tested and selected as predictands for the pollen-climate inference models (Table 4.1; Appendix C1). Inference models were derived by partial least squares (PLS) and weighted-averaging PLS (WA-PLS) with bootstrap cross-validated prediction errors. These methods have been used successfully for pollen-climate inferences (e.g. Finsinger et al. 2007) and are considered robust methods (Birks 2004), especially for predictions within the calibration range. To assess the reliability of the reconstruction and detect possible problematic intervals, a goodness-of-fit statistic was calculated for P_{JJA} and $T_{NOV.}$ For each variable the squared residual distance was calculated using a CCA with a single environmental variable, providing an estimate of the fit of the environmental variable with the calibration data.

Climate model sensitivity experiments

We performed climate model sensitivity experiments with the Earth-system model of intermediate complexity (EMIC) PUMA-2 (Fraedrich et al. 1998, 2005a, b) to investigate the sensitivity of the land-surface climate in Florida to SST anomalies in the (extra) tropical North Atlantic, Caribbean Sea, and GoM. PUMA-2 is a general circulation model (GCM) with relatively low computational demand, yet simulates an atmospheric response to SST forcing comparable to the more complex ECHAM4 (Romanova et al. 2006; Grosfeld et al. 2007, 2008). To represent details of the Florida region, the model was used in a T42 spectral triangular resolution with 10 vertical layers. We performed four climate model simulations: a last glacial maximum (LGM, 21 ka) reference (EMIC-LGM) with prescribed LGM boundary conditions for SSTs, solar insolation and atmospheric CO_2 concentrations (200 ppmv) and three climate sensitivity simulations with idealized SST anomalies (Table 4.2). In the sensitivity simulations, we altered only the prescribed SSTs to constrain potential source areas for the land-surface temperature and precipitation anomalies seen in Florida during H-events. Each simulation was run for 40-years and started from an atmosphere at rest. Because SSTs were prescribed, the model's spin-up time required at most 20 years. To reduce model noise, climatology is calculated as an average of the last 20 years of each simulation.

Table 4.1 Pollen-climate inference model performance for winter and summer precipitation (P_{DJF}, P_{JJA}, respectively), and November temperature (T_{NOV}).

	P_{DJF} (winter) (mm/season)	**P_{JJA} (summer) (mm/season)**	**T_{NOV} (°C)**
% variance	10.8	9.8	11.8
Model type	WA-PLS	PLS	WA-PLS
Gradient length	1.576	1.846	1.557
# Components	2	2	2
RMSEP	31.32	39.7	1.9
R2 boot	0.76	0.66	0.62
# Outliers removed	3	2	2
RMSEP % range	11.9	17.9	15.3

Monthly LGM SSTs and sea-ice boundary conditions were based on the GLAMAP dataset (Schäfer-Neth and Paul 2003), glacial ice cover, orography, sea level, and coastlines follow Peltier (1994), and LGM vegetation is based on Crowley (1995) and Martin (1998) (Appendix C, Figure C4). In the EMIC-H0 simulation (Figure 4.2A), SST boundary conditions were based on the assumption that, relative to LGM conditions, a decrease in northwards heat transport resulted in a zonal average SST cooling (of maximum 6°C) in the extra-tropical North Atlantic during the last H-event (after Bond et al. 1992, 1993). The EMIC-H1 simulation (Figure 4.2B) represented, besides North Atlantic cooling, increased low-latitude summer insolation resulting in a maximum 2°C zonal average warming of the equatorial surface waters (after Schmidt et al. 2004; Ziegler et al. 2008). The EMIC-H+ simulation (Figure 4.2C) additionally included increased zonal heat transport from the tropical East Atlantic, through the Caribbean Sea into the GoM, representing an intensification of the Loop Current. SSTs in EMIC-H+ simulation increased 1–2°C close to Florida (after Flower et al. 2004), relative to the LGM simulation (see Supplemental material in Appendix C2 for details on simulations).

Table 4.2 Description of the climate model simulations, SST boundary conditions and reference to the SST reconstruction on which the simulation is based.

Simulation	SST boundary conditions	Reference
EMIC-LGM	GLAMAP monthly	Schäfer-Neth and Paul, 2003
EMIC-H0	As EMIC-LGM with North-Atlantic cooling	Bond et al. 1992; 1993
EMIC-H1	As EMIC-H0 with increased low-latitude summer insolation	Schmidt et al. 2004 and Ziegler et al. 2008
EMIC-H+	As EMIC-H1 with Loop Current intensification	Flower et al. 2004

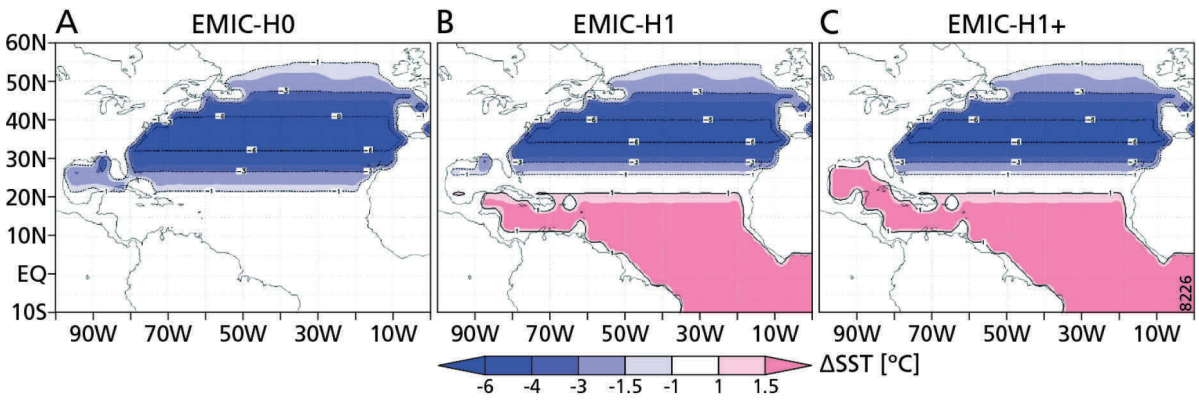

Figure 4.2 Boundary conditions for the EMIC-H0 (A), EMIC-H1 (B) and EMIC-H+ (C) climate sensitivity simulations, relative to those used in the EMIC-LGM control simulation.

Results

Pollen-inferred climate reconstruction

Inference model data show that during the TP1-TP6 phases, coeval with strong Greenland stadials, mean summer precipitation (P_{JJA}) increased by 0.5–0.9 mm/day, while November temperature (T_{NOV}) increased by 2.0–3.0°C (Figure 4.3). Reconstruction results from two independent datasets from Lake Tulane are highly consistent and offsets between records do not exceed the bootstrapped prediction errors (Table 4.1; Figure C3 in Appendix C1).

The Lake Tulane signals for 0–13 ka agree with the reconstruction from nearby Lake Annie (Appendix C1, Figure C3). Remarkable features at both sites are the consistently dry/cool conditions in the Allerød and warm/wet conditions during (part of) the Younger Dryas (YD). Increased wetness during the Middle Holocene is consistent with independent reconstructions from South Florida (Donders et al. 2005b). A coastal pollen record from Tampa Bay (Willard et al. 2007) partly confirms this result, showing wet conditions during H1 and a stepwise change during the YD that mirrors the changes seen in the Tulane 06 record, but not in the Tulane 93 and Lake Annie records. The length of the wet phase in the YD is therefore unclear. The middle Holocene temperature increase is remarkably high compared to the glacial-interglacial transition. Early Holocene vegetation stands out as an intermediate phase in the record (Grimm et al. 2006), with abundant *Quercus* and some *Ambrosia*, but low heath and intermediate *Pinus* abundance. In the calibration dataset, *Ambrosia* is generally more abundant in temperate areas due to forest clearance and land disturbance, which possibly skews the reconstruction to somewhat lower winter temperatures during the LGM and early Holocene. Figure C3 in Appendix C shows the goodness-of-fit with 90% percentile cutoff values. Only the lowest T_{NOV} reconstruction values between 21 and 20 ka BP are uncertain since the transfer model does not perform well in that interval. Our reconstruction data are reliable during the TP1-TP6 phases. Warming during these phases is also indicated qualitatively by lower *Ambrosia* abundances, because warm winters inhibit *Ambrosia* to germinate effectively (Bazzaz 1974).

Age uncertainties of the Lake Tulane record (Grimm et al. 2006) are larger than the NGRIP ice core record (Svensson et al. 2008), but in TP-0–2 do not exceed 1.5 ka, and only for TP-5 and 6 exceed the duration of the event. Especially for the pine phases TP1-3 we can confidently state that they correlate to Greenland Stadials (Figure 4.3) that include a Heinrich event, since the latter have been correlated independently to the Greenland ice cores (Stoner et al. 2000). The warm/wet TP2 and TP4 phases start well before and extend beyond H2 and H4, respectively. Despite uncertainties in both the Heinrich ages and the Lake Tulane chronology (see Stoner et al. 2000; Grimm et al. 2006), this long duration seems robust. Confining the duration of TP2 and TP4 events exactly to H2 and H4 would require an unrealistic threefold increase in sedimentation rate during the pine phases. See also Grimm et al. (2006) for a more extended discussion on the age uncertainties of the Lake Tulane record.

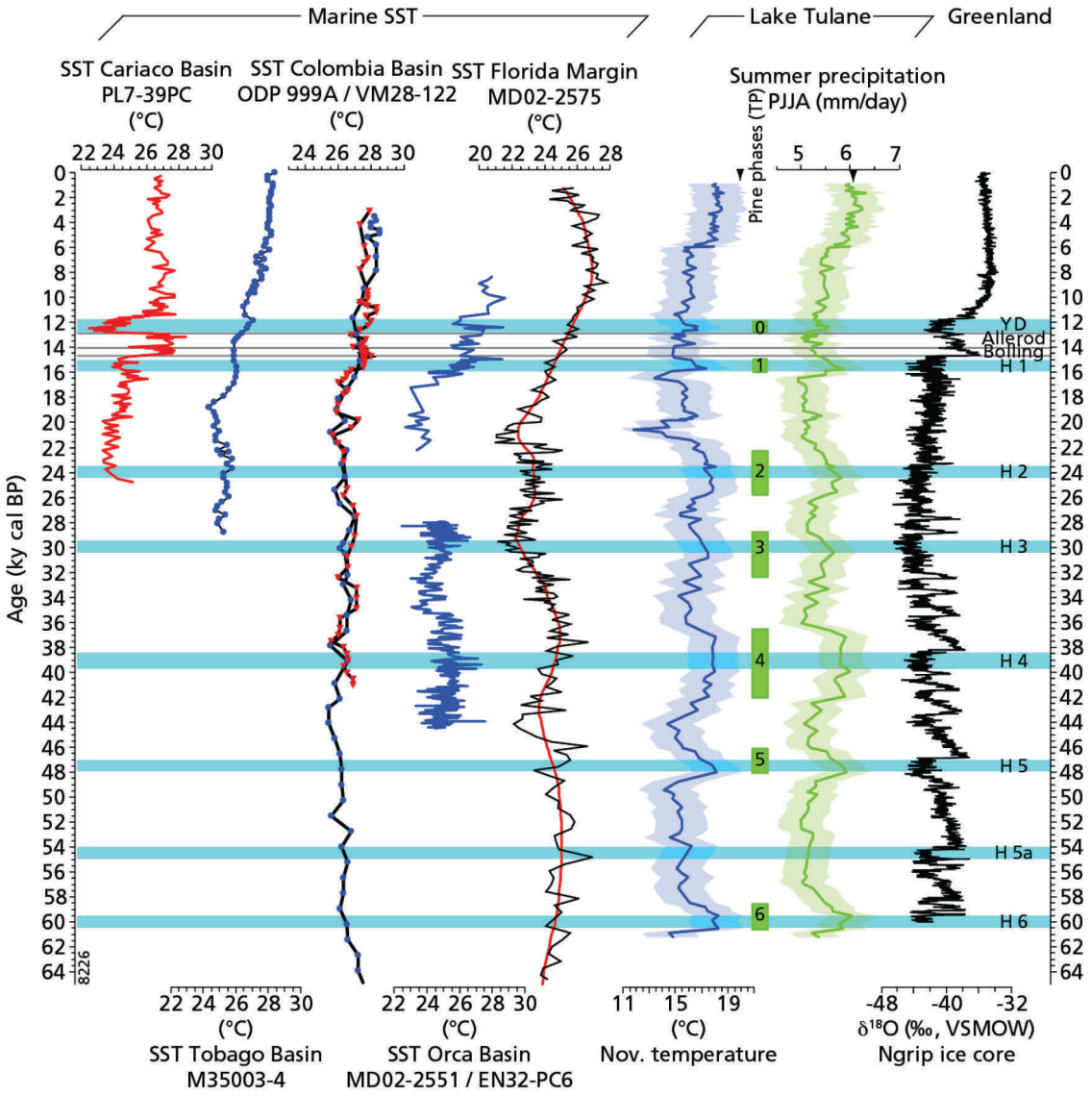

Figure 4.3 Paleoclimate reconstructions from Lake Tulane based on the pollen-climate inference models for the last 60 kyr. The Lake Tulane chronology is based on 55 AMS ^{14}C ages that were calibrated with the intcal04 (Reimer et al. 2004) for ages younger than 20,000 ^{14}C yr BP, and with the Fairbanks et al. (2005) calibration curve (based on paired AMS ^{14}C/U-series dating of corals) for ages 20,000–40,000 ^{14}C yr BP. Phases TP5 and TP6 are not independently dated but correlated to H5 and H6, analogous to the observed correlation of TP1–TP4 with H1–H4 (see Grimm et al. 2006 for more details). Arrows indicate present day climatic values at Lake Tulane. Data is compared to the regional marine SST records from the Cariaco Basin (Lea et al. 2003), Tobago Basin (Rühlemann et al. 1999), Colombia Basin (Schmidt et al. 2004), Orca Basin (Hill et al. 2006; Flower et al. 2004) and Florida Margin (Ziegler et al. 2008). Blue bars indicate maximum calendar age ranges of North Atlantic iceberg-rafted debris (IRD) deposition, following Stoner et al. (2000). Depending on the record used, the exact timing and duration of Heinrich events vary (Rashid et al. 2003). We consider the estimates based on correlation between paleomagnetic intensity measured in sediment records close to Greenland and cosmogenic isotopes fluxes measured in the GISP2 Greenland ice core record (Stoner et al. 2000) as most reliable, and use these for data comparison. Heinrich event ages, and hence the Lake Tulane record below TP4, have been updated to the new Greenland Ice Core Chronology 2005 (GICC05), which is based on layer counting of the NGRIP ice core back to 60 ka (Rasmussen et al. 2008; Svensson et al. 2008).

Climate sensitivity to Atlantic Ocean temperatures

Our climate model sensitivity experiments indicate that the climate in Florida is sensitive to changes in both low- and high-latitudinal (North) Atlantic SSTs. Figure 4.4 shows modeled land-surface temperature and precipitation (anomalies) for Florida (averaged over 75–88°W to 25–30°N). Summer precipitation varies strongly between experiments; while winter is consistently modeled as dry and summer as wet (Figures 4.4A and 4.4B), the EMIC-H+ simulation shows the strongest seasonality. All simulations produce a drier climate compared to the pollen-inferred reconstructions [P_{JJA} of 5– 6 mm/day based on pollen, and 1.4 (EMIC-LGM), 0.8 (EMIC-H0), 1.2 (EMIC-H1) and 1.7 mm/day (EMIC-H+) simulated] and peak precipitation is delayed by 1 month. Only the EMIC-H+ simulation explains the magnitude of the pollen-inferred P_{JJA} increase from LGM to H1. This increase in summer precipitation is related to a localized northward displacement of the intense precipitation associated with the ITCZ during summer (see Appendix C3, Figure C6).

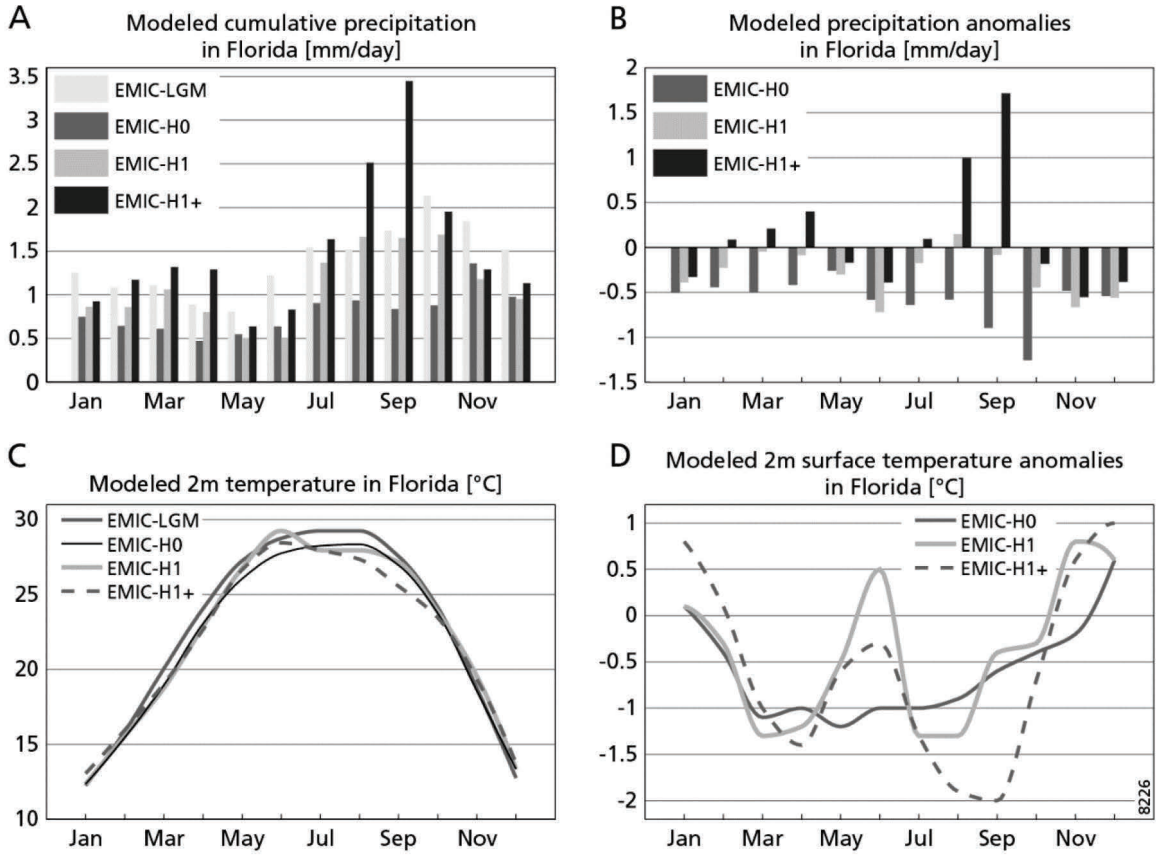

Figure 4.4 Simulated land surface temperature and precipitation for the Florida region. Simulated monthly precipitation (A) and precipitation anomalies relative to LGM simulation (B) are averaged over the larger Florida region (75-88°W to 25-30°N) including grid-cells over water. Simulated monthly land surface (2 m) temperature (C) and temperature anomalies relative to LGM simulation (D) are averaged over terrestrial grid-cells in the Florida region (75-88°W to 25-30°N).

Land-surface temperatures vary little between the experiments (Figures 4.4C and 4.4D). Compared to the EMIC-LGM simulation, all EMIC-H experiments show positive temperature anomalies at the onset of winter and are generally colder during spring, summer, and fall. The largest positive temperature anomaly (1°C) is simulated in the EMIC-H+ simulation for December. All simulations produce a warmer climate compared to the pollen-inferred reconstructions [T_{NOV} of 16-17°Cbased on pollen, and 18 (EMIC-LGM), 18 (EMIC-H0), 19 (EMIC-H1) and 19°C (EMIC-H+) simulated]. Relative to the EMIC-LGM simulation, the EMIC-H1 and EMIC-H+ simulations show a positive temperature anomaly in November (1°C), while the EMIC-H0 simulation shows little change. The results indicate that a warming of the equatorial Atlantic and the GoM is needed to explain the pollen-inferred increase in summer precipitation and November temperature during North-Atlantic cold spells.

Discussion

Source of heat and moisture anomalies

To explain the observed increases in precipitation and temperature in Florida, we hypothesize that the GoM warmed during North Atlantic colds spells and that this warming is potentially related to increased Loop Current (Hofmann and Worley 1986; Poore et al. 2004). Grimm et al. (2006) observed a general inverse correlation to Greenland stadials and the Lake Tulane pollen record, both on independent chronologies. With the quantitative temperature data from Lake Tulane and update to the fully layer-counted NGRIP chronology used in Figure 4.3, this conclusion is strengthened here. However, different SST records do not show a clear and unequivocal regional low-latitude warming (Figure 4.3).

At present, the Loop Current is controlled by an interplay between regional surface winds and water flow from the Caribbean Sea through the Yucatan Channel (Johns et al. 2002; Romanou et al. 2004; Cherubin et al. 2005). These studies indicate that a northerly ITCZ position during summer enhances the intrusion of the Loop Current because the associated (south)easterly trade winds enhance the northwestward advection of warm surface waters. Hodell et al. (1991) and Poore et al. (2004) indicate that during the Holocene the Loop Current was mainly controlled by the effect of summer insolation on ITCZ position. Nürnberg et al. (2008) reconstructed SSTs and sea surface salinities in the northeastern GoM (Florida margin) over the past 400 kyr. Their results reveal that Loop Current intrusion was modulated by the northward extend of the AWP and freshwater discharge from the Laurentide Ice Sheet. All these studies indicate a positive relation between a northerly ITCZ position and Loop Current intrusion. Observational evidence suggests that the ITCZ moved south during periods of North Atlantic cooling (Wang et al. 2005; Stott et al. 2002; Burns et al. 2003; Muller et al. 2008). These observations are supported by simulations with various climate models (Zhang and Delworth 2005; Stouffer et al. 2005). If the ITCZ was indeed displaced south over the western Atlantic

region, this would cause a decrease in summer trade winds and a reduction of the associated advection of warm surface waters through the GoM. However, based on the coincidence between our climate model simulations and pollen-based climate reconstructions, we infer that heat transport up to and through the GoM potentially increased, suggesting an increase in summer trade winds and a northerly position of the ITCZ over the region.

We explain this apparent contradiction by an increase in heat transport up to and through the GoM forced by increased summer trade winds driven by a steepened equator-pole temperature gradient during North Atlantic cold spells. Ziegler et al. (2008) indicate that summer expansion of the AWP into the GoM is generally insensitive to extra-tropical North Atlantic cooling. A persistent AWP, combined with a warm GoM should therefore allow for a northerly ITCZ position over the western tropical North Atlantic during boreal summer and could provide moisture and heat to Florida. The highest SST increase during H1 is seen in the central GoM (Flower et al. 2004) (Figures 4.1 and 4.3), which is directly influenced by the warm waters of the Loop Current (DeHaan and Sturges 2005). Koutavas et al. (2002) found evidence for decreased trade-winds with a lower equator-pole temperature gradient during LGM based on reduced upwelling offshore Peru. Conversely, increased equator-pole temperature gradient enhanced Hadley circulation during North Atlantic cold spells (Jain et al. 1999; Trenberth et al. 2000; Clement et al. 2004). The increase in Hadley circulation possibly led to an increase in easterly trade winds over the western equatorial North Atlantic in summer (Zhang and Delworth 2005), thereby enhancing Loop Current intrusion into the GoM and warming the surface waters around the Florida peninsula.

The observed increase of summer precipitation and November temperature in Florida could therefore represent an increase in summer trade winds and reflect the persistence of the AWP and increased Loop Current during North Atlantic cold spells (Nürnberg et al. 2008; Ziegler et al. 2008). It contrasts the presumed same-sign synchronicity of low and high latitude climates during the late glacial as observed in a planktic foraminiferal Mg/Ca record from the Cariaco Basin on the northern Venezuelan shelf (Lea et al. 2003). Analogous to well-known precipitation decrease at Cariaco during stadials (e.g. Haug et al. 2001; González et al. 2008), the SST cooling has been explained by invoking a mean southward migration of the ITCZ (Lea et al. 2003), which should reduce summer precipitation in Florida (e.g. Chen and Gerber 1992; Enfield et al. 2001). However, the Cariaco SST decrease during the YD is large (3-4°C) relative to other records from the AWP (Figure 4.3), and probably shows a winter upwelling signal in a restricted marine basin (Ziegler et al. 2008). Moreover, marine records from the western tropical Atlantic show SST increases (Tobago Basin), and terrestrial wet conditions with SST and sea surface salinity increases (offshore NE Brazil) during H1 and the YD (Rühlemann et al. 1999; Jennerjahn et al. 2004; Weldeab et al. 2006). These reconstructions are best explained by a more southward ITCZ position during stadial (boreal) winters. Farther north, reconstructed summer SSTs also show conflicting patterns. In the central GoM a clear warming during H1 is present (Flower et al. 2004), while summer SSTs from the

Florida margin (MD02-2575) do not show consistent warming during YD and H-events (Ziegler et al. 2008). However, the pre-Holocene long term temperature trends between MD02-2575 and Lake Tulane correspond remarkably well (Figure 4.3).

Ziegler et al. (2008) explain contrasting regional paleo-SST patterns by invoking a strongly seasonally biased climate response to North Atlantic cold events in the tropical Atlantic. Their GoM SST signal is controlled by boreal summer insolation that displaces the northern limit of the AWP, while it is relatively insensitive to the millennial-scale YD and H-events that primarily affect boreal winter conditions. Because our Lake Tulane record represents summer-precipitation changes, the variable duration of TP phases might be determined by summer insolation influencing the northern extent of the AWP. This hypothesis is supported by the results of our climate model sensitivity analysis, which indicates that the climate in Florida is relatively insensitive to extra-tropical North Atlantic cooling if the AWP is present. Rather, the clear warm/wet phases during H-events and YD result from heat flow from the AWP into the GoM by summer trade wind forcing.

Sensitivity of simulated land surface temperatures

Although variation in the simulated T_{NOV} anomalies in Florida among the EMIC-H0, EMIC-H1, and EMIC-H+ simulations is limited, their offset with the EMIC-LGM simulation is considerable. This contrast indicates that both extra-tropical North Atlantic cooling and low latitudinal Atlantic warming contribute to the temperature increase. Winter warming of Florida in the EMIC-H simulations relative to the EMIC-LGM simulation coincides with a decrease in winter precipitation in the region (Supplemental material in Appendix C3). The simulated T_{NOV} increase could therefore partly be explained by alterations in the surface energy balance related to a decrease in soil moisture and cloudiness (Wild and Ohmura 1999).

The absolute difference between our pollen-inferred and modeled November temperature could be caused by the constant solar forcing prescribed in our model simulations. Insolation changed considerably between the LGM and the last Heinrich event and has an important effect on tropical climate (Clement et al. 2004). Winter insolation decreased by approximately 30 W/m_2 and summer insolation increased by a similar value (Berger and Loutre 1991). Taking into account the decrease in winter insolation would potentially allow for a better match between the pollen-inferred and modeled November temperatures. This account however, would blur the results of the sensitivity analysis and was therefore omitted.

Conclusions

Increases in summer precipitation and November temperatures in Florida coincided with episodes of extreme cooling in the North Atlantic during Heinrich events and Younger Dryas, the latter of which may contain both a warm/wet and cold/dry subphase. These

reconstructed climate changes are best explained by a warming of the surface waters of the tropical Atlantic and the Gulf of Mexico. Surface waters in the Gulf of Mexico potentially warmed by an intensified Loop Current facilitated by a persistent Atlantic Warm Pool and increased easterly trade winds during summer. The inter-tropical convergence zone was generally displaced south of Florida during the glacial and its summer position was controlled by insolation changes and the extent of the Atlantic Warm Pool. These controls on the inter-tropical convergence zone may have influenced the duration of the lake Tulane pine phases which are associated with wet summer conditions.

Acknowledgments

We thank Jack Williams and Pat Bartlein for providing the modern climate dataset of our Florida surface samples. Oliver Heiri is thanked for his insightful advice on the statistical methods. We greatly appreciate the constructive comments from two reviewers and the editorial comments from Jean Claude Duplessy. Partial funding received from United States National Science Foundation grant ATM-9405145 and from the High Potential Program from Utrecht University.

References

Abrahamson WG, Johnson AF, Layne AN, Peroni PA (1984) Vegetation of the Archbold Biological Station, Florida: an example of the southern Lake Wales Ridge. Florida Sci 47:209-250

Bazzaz FA (1974) Ecophysiology of Ambrosia artemisiifolia: a successional dominant. Ecology 55:112-119. doi:10.2307/1934623

Berger A, Loutre MF (1991) Insolation Values for the Climate of the Last 10000000 Years. Quat Sci Rev 10:297–317

Birks HJB (2004) Quantitative palaeoenvironmental reconstructions from Holocene biological data. In: Mackay AW, Battarbee RW, Birks HJB, Oldfield F (eds) Global change in the Holocene. Arnold, London, pp 107–123

Bond G, Heinrich H, Broecker W, Labeyrie L, McManus J, Andrews J, Huon S, Jantschik R, Clasen S, Simet C, Tedesco K, Klas M, Bonani G, Ivy S (1992) Evidence for massive discharges of icebergs into the North Atlantic Ocean during the last glacial period. Nature 360:245–249

Bond G, Broecker W, Johnsen S, McManus J, Labeyrie L, Jouzel J, Bonani G (1993) Correlations between climate records from North Atlantic sediments and Greenland ice. Nature 365:143–147

Burns SJ, Fleitmann D, Matter A, Kramers J, Al-Subbary AA (2003) Indian ocean climate and an absolute chronology over Dansgaard/Oeschger events 9 to 13. Science 301:1365–1367

Charles CD, Lynch-Stieglitz J, Ninnemann US, Fairbanks RG (1996) Climate connections between the hemisphere revealed by deep sea sediment core ice core correlations. Earth Planet Sci Lett 142:19–27

Chen E, Gerber JF (1992) Climate. In: Myers RL, Ewel JJ (eds) Ecosystems of Florida. University of Central Florida Press, Orlando, pp 11–34

Cherubin LM, Sturges W, Chassignet EP (2005) Deep flow variability in the vicinity of the Yucatan Straits from a high-resolution numerical simulation. J Geophys Res 110:20

Clement AC, Hall A, Broccoli AJ (2004) The importance of precessional signals in the tropical climate. Clim Dyn 22:327– 341

Crowley TJ (1995) Ice-Age terrestrial carbon changes revisited. Global Biogeochem Cycles 9:377–389

DeHaan CJ, Sturges W (2005) Deep cyclonic circulation in the Gulf of Mexico. J Phys Oceanogr 35:1801–1812

Donders TH, Wagner F, Visscher H (2005a) Quantification strategies for human-induced and natural hydrological changes in southern Florida wetland vegetation. Quat Res 64:333–342

Donders TH, Wagner F, Dilcher DL, Visscher H (2005b) Mid-to late-Holocene El Niño—Southern Oscillation dynamics reflected in the subtropical terrestrial realm. Proc Natl Acad Sci USA 102:10904–10908

Enfield DB, Mestas-Nuñez AM, Trimble PJ (2001) The Atlantic multidecadal oscillation and its relation to rainfall and river flows in the continental US. Geophys Res Lett 28:2077–2080

Fairbanks RG, Mortlock RA, Chiu T-C, Cao L, Kaplan A, Guilderson TP, Fairbanks TW, Bloom AL, Grootes PM, Nadeau M-J (2005) Radiocarbon calibration curve spanning 0 to 50,000 years BP based on paired 230Th/234U/238U and 14C dates on pristine corals. Quat Sci Rev 24:1781–1796

Finsinger W, Heiri O, Valsecchi V, Tinner W, Lotter AF (2007) Modern pollen assemblages as climate indicators in southern Europe. Global Ecol Biogeogr 16:567–582

Flower BP, Hastings DW, Hill HW, Quinn TM (2004) Phasing of deglacial warming and Laurentide Ice Sheet meltwater in the Gulf of Mexico. Geology 32:560–597

Flückiger J, Knutti R, White JWC, Renssen H (2008) Modeled seasonality of glacial abrupt climate events. Clim Dyn 31:633– 645

Fraedrich K, Kirk E, Lunkeit F (1998) Portable University Model of the atmosphere. Deutsches Klimarechenzentrum, Tech. Rep. 16:37

Fraedrich K, Jansen H, Kirk E, Luksch U, Lunkeit F (2005a) The Planet Simulator: towards a user friendly model. Meteorol Z 14:299–304

Fraedrich K, Jansen H, Kirk E, Lunkeit F (2005b) The Planet Simulator: Green planet and desert world. Meteorol Z 14:305– 314

Ganopolski A, Rahmstorf S (2001) Simulation of rapid glacial climate changes in a coupled climate model. Nature 409:153–158
González C, Dupont LM, Mertens K, Wefer G (2008) Reconstructing marine productivity of the Cariaco Basin during marine isotope stages 3 and 4 using organic-walled dinoflagellate cysts. Paleoceanography 23:PA3215
Grimm EC, Jacobson GL Jr, Watts WA, Hansen BCS, Maasch KA (1993) A 50,000-year record of climate oscillations from Florida and its temporal correlation with the Heinrich events. Science 261:198–200
Grimm EC, Watts WA, Jacobson GLJ, Hansen BCS, Almquist HR, Dieffenbacher-Krall AC (2006) Evidence for warm wet Heinrich events in Florida. Quat Sci Rev 25:2197–2211
Grosfeld K, Lohmann G, Rimbu N, Fraedrich K, Lunkeit F (2007) Atmospheric multidecadal variations in the North Atlantic realm: proxy data, observations, and atmospheric circulation model studies. Clim Past 3:39–50
Grosfeld K, Lohmann G, Rimbu N (2008) The impact of Atlantic and Pacific Ocean sea surface temperature anomalies on the North Atlantic multidecadal variability. Tellus A 60:728–741
Haug GH, Hughen KA, Sigman DM, Peterson LC, Rohl U (2001) Southward migration of the intertropical convergence zone through the Holocene. Science 293:1304–1308
Heinrich H (1988) Origin and consequences of cyclic ice rafting in the northeast Atlantic Ocean during the past 130, 000 years. Quat Res 29:142–152
Hill HW, Flower BP, Quinn TM, Hollander DJ, Guilderson TP (2006) Laurentide ice sheet meltwater and abrupt climate change during the last glaciation. Paleoceanography 21:PA1006
Hodell DA, Curtis JH, Jones GA, Higueragundy A, Brenner M, Binford MW, Dorsey KT (1991) Reconstruction of Caribbean climate change over the past 10,500 years. Nature 352:790–793
Hofmann EE, Worley SJ (1986) An investigation of the circulation of the Gulf of Mexico. J Geophys Res 91:14221–14236
Jain S, Lall U, Mann ME (1999) Seasonality and interannual variations of northern hemisphere temperature: equator-to-pole gradient and ocean-land contrast. J Clim 12:1086–1100
Jennerjahn TC, Ittekkot V, Arz HW, Behling H, Patzold J, Wefer G (2004) Asynchronous terrestrial and marine signals of climate change during Heinrich events. Science 306:2236–2239
Johns WE, Townsend TL, Fratantoni DM, Wilson WD (2002) On the Atlantic inflow to the Caribbean Sea. Deep Sea Res I 49:211– 243
Koutavas A, Lynch-Stieglitz J, Marchitto TM Jr, Sachs JP (2002) El Niño-like pattern in ice age tropical Pacific sea surface temperatures. Science 297:226–230
Lea DW, Pak DK, Peterson LC, Hughen KA (2003) Synchroneity of tropical and high-latitude Atlantic temperatures over the last glacial termination. Science 301:1361–1364
Martin PH (1998) Land-surface characterization in climate models: biome-based parameter inference is not equivalent to local direct estimation. J Hydrol 212:287–303
McManus JF, Francois R, Gherardi JM, Keigwin LD, Brown-Leger S (2004) Collapse and rapid resumption of Atlantic meridional circulation linked to deglacial climate changes. Nature 428:834– 837
Menviel L, Timmermann A, Mouchet A, Timm O (2008) Meridional reorganizations of marine and terrestrial productivity during Heinrich events. Paleoceanography 23:PA1203
Muller J, Kylander M, Wust R, Weiss D, Martinezcortizas A, Legrande A, Jennerjahn T, Behling H, Anderson W, Jacobson G (2008) Possible evidence for wet Heinrich phases in tropical NE Australia: the Lynchs Crater deposit. Quat Sci Rev 27:468–475
Nürnberg D, Ziegler M, Karas C, Tiedemann R, Schmidt MW (2008) Interacting Loop Current variability and Mississippi River discharge over the past 400 kyr. Earth Planet Sci Lett 272:278–289
Peltier W (1994) Ice age paleotopography. Science 265:195–201
Poore RZ, Quinn TM, Verardo S (2004) Century-scale movement of the Atlantic intertropical convergence zone linked to solar variability. Geophys Res Lett 31:L12214
Rahmstorf S (1996) On the freshwater forcing and transport of the Atlantic thermohaline circulation. Clim Dyn 12:799–811

Rashid H, Hesse R, Piper DJW (2003) Evidence for an additional Heinrich event between H5 and H6 in the Labrador Sea. Paleoceanography 18:1077

Rasmussen SO, Seierstad IK, Andersen KK, Bigler M, Dahl-Jensen D, Johnsen SJ (2008) Synchronization of the NGRIP, GRIP, and GISP2 ice cores across MIS 2 and palaeoclimatic implications. Quat Sci Rev 27(1–2):18-28

Reimer PJ, Baillie MGL, Bard E, Bayliss A, Beck JW, Bertrand CJH, Blackwell PG, Buck CE, Burr GS, Cutler KB, Damon PE, Edwards RL, Fairbanks RG, Friedrich M, Guilderson TP, Hogg AG, Hughen KA, Kromer B, McCormac G, Manning S, Bronk-Ramsey C, Reimer RW, Remmele S, Southon JR, Stuiver M, Talamo S, Taylor FW, Van der Plicht J, Weyhenmeyer CE (2004) IntCal04 terrestrial radiocarbon age calibration, 0–26 cal kyr BP. Radiocarbon 46:1029–1058

Romanou A, Chassignet EP, Sturges W (2004) Gulf of Mexico circulation within a high-resolution numerical simulation of the North Atlantic Ocean. J Geophys Res Oceans 109:25

Romanova V, Lohmann G, Grosfeld K (2006) Effect of land albedo, CO2, orography, and oceanic heat transport on extreme climates. Clim Past 2:31–42

Rühlemann C, Mulitza S, Muller PJ, Wefer G, Zahn R (1999) Warming of the tropical Atlantic Ocean and slowdown of thermohaline circulation during the last deglaciation. Nature 402:511–514

Rühlemann C, Mulitza S, Lohmann G, Paul A, Prange M, Wefer G (2004) Intermediate depth warming in the tropical Atlantic related to weakened thermohaline circulation: Combining paleoclimate data and modeling results for the last deglaciation. Paleoceanography 19:1025

Schäfer-Neth C, Paul A (2003) The Atlantic Ocean at the last glacial maximum: objective mapping of the GLAMAP sea-surface conditions. In: Wefer G, Mulitza S, Ratmeyer V (eds) The South Atlantic in the late quaternary: reconstruction of material budgets and current systems. Springer, Berlin, pp 531–548

Schmidt MW, Spero HJ, Lea DW (2004) Links between salinity variation in the Caribbean and North Atlantic thermohaline circulation. Nature 428:160–163

Stocker TF (1998) Climate change: the seesaw effect. Science 282:61–62

Stoner JS, Channell JET, Hillaire-Marcel C, Kissel C (2000) Geomagnetic paleointensity and environmental record from Labrador Sea core MD95–2024: global marine sediment and ice core chronostratigraphy for the last 110 kyr. Earth Planet Sci Lett 183:161–177

Stott L, Poulsen C, Lund S, Thunell R (2002) Super ENSO and global climate oscillations at millennial time scales. Science 297:222– 226

Stouffer RJ et al (2005) Investigating the causes of the response of the thermohaline circulation to past and future climate change. J Clim 19(8):1365–1387

Svensson A, Andersen KK, Bigler M, Clausen HB, Dahl-Jensen D, Davies SM, Johnsen SJ, Muscheler R, Parrenin F, Rasmussen SO, Röthlisberger R, Seierstad I, Steffensen JP JP, Vinther BM (2008) A 60,000 year Greenland stratigraphic ice core chronology. Climate Past 4:47–57

Trenberth KE, Stepaniak DP, Caron JM (2000) The global monsoon as seen through the divergent atmospheric circulation. J Clim 13:3969–3993

Vidal L, Labeyrie L, Cortijo E, Arnold M, Duplessy JC, Michel E, Becque S, van Weering TCE (1997) Evidence for changes in the North Atlantic deep water linked to meltwater surges during the Heinrich events. Earth and Planet Sci Lett 146:13–27

Wang Y, Cheng H, Edwards RL, He Y, Kong X, An Z, Wu J, Kelly MJ, Dykoski CA, Li X (2005) The Holocene Asian monsoon: links to solar changes and North Atlantic climate. Science 308:854–857

Wang C, Enfield DB (2001) The tropical Western Hemisphere Warm Pool. Geophys Res Lett 28(8):1635–1638

Wang C, Enfield DB, Lee S, Landsea CW (2006) Influences of the Atlantic Warm Pool on Western Hemisphere summer rainfall and Atlantic hurricanes. J Clim 19(12):3011–3028

Watts WA (1975) A late Quaternary record of vegetation from Lake Annie, south-central Florida. Geology 3:344–346

Weldeab S, Schneider RR, Kölling M (2006) Deglacial sea surface temperature and salinity increase in the western tropical Atlantic in synchrony with high latitude climate instabilities. Earth Planet Sci Lett 241:699–706

Whitmore J, Gajewski K, Sawada M, Williams JW, Shuman B, Bartlein PJ, Minckley T, Viau AE, Webb TI, Shafer S, Anderson P, Brubaker L (2005) Modern pollen data from North America and Greenland for multi-scale palaeoenvironmental applications. Quat Sci Rev 24:1828–1848

Wild M, Ohmura A (1999) The role of clouds and the cloud-free atmosphere in the problem of underestimated absorption of solar radiation in GCM atmospheres. Phys Chem Earth 24:261–268

Willard DA, Bernhardt CE, Brooks GR, Cronin TM, Edgar T, Larson R (2007) Deglacial climate variability in central Florida, USA. J Palaeo 251(3–4):366–382

Zhang R, Delworth TL (2005) Simulated tropical response to a substantial weakening of the Atlantic thermohaline circulation. J Clim 18(12):1853–1860

Ziegler M, Nurnberg D, Karas C, Tiedemann R, Lourens LJ (2008) Persistent summer expansion of the Atlantic Warm Pool during glacial abrupt cold events. Nat Geosci 1:601–605

Chapter 5

A role for the Atlantic warm pool in altering the (sub)tropical hydrological cycle during millennial-scale glacial climate oscillations

Based on a discussion paper published as: de Boer HJ, Roche DM, Renssen H, Dekker SC, Two-signed feedback of cross-isthmus moisture transport on glacial overturning controlled by the Atlantic warm pool. 2011. Climate of the past discussions (7) 3859-3893

Abstract

The processes involved in rapid climate fluctuations that occurred at millennial timescales during the last glacial remain enigmatic. Central to these glacial climate fluctuations are changes in northward heat transport by the Atlantic Meridional Overturning Circulation (AMOC) linked to episodic decay of the Laurentide ice sheet. Feedbacks between the intensity of the AMOC and the (sub)tropical hydrological cycle have been proposed to amplify these climate fluctuations by changing the freshwater budget of the North Atlantic. However, the mechanisms involved are debated. We focused on a potential role of the Atlantic Warm Pool (AWP) in altering the easterly atmospheric moisture flow from the Atlantic across the Central American isthmus to the Pacific in relation to these glacial climate fluctuations. The AWP is defined by the 28.5°C Sea Surface Temperature (SST) isotherm and comprises the (sub)tropical Northwest Atlantic, Caribbean Sea and Gulf of Mexico during summer and fall in the present climate. At present, an inverse relation exists between the size of the AWP and the strength of the North Atlantic subtropical (Azores) high pressure system due to so-called Gill-type atmospheric response. Via this response, changes in AWP area initiate inverse changes in the easterly (moisture) flow over the Caribbean Sea and across the Central American isthmus. Our review of proxy-based SST reconstructions from the (sub)tropical North Atlantic region provided evidence for the existence of an AWP during the glacial but remained inconclusive about its spatial and temporal dynamics in relation to millennial-scale climate variability. From these data we developed hypotheses regarding potential glacial AWP dynamics that were explored using a combination of coupled and uncoupled ocean-atmosphere models. Our simulations of the glacial atmosphere indicated that variations in AWP expansion evoke inverse surface pressure changes in the Azores high pressure system and thereby alter the low-level atmospheric (moisture) flow across the Central American isthmus, resembling the present-day response. These results are discussed in relation to proxy-based evidence for changes in cross-isthmus moisture transport to indicate a potential role of the AWP in (de)stabilizing the glacial AMOC.

Introduction

Abrupt climate shifts occurred at millennial timescales during the last glacial due to variations in northward heat transport by the Atlantic Meridional Overturning Circulation (AMOC) (Alley et al., 1999). These millennial-scale climate fluctuations are termed Dansgaard-Oeschger (D-O) oscillations and appear organized in so-called Bond cycles (Bond et al., 1993; Dansgaard et al., 1993; Alley, 1998). Heinrich events occurred towards the end of Bond cycles during the coldest D-O stadials and are recognized by sediment depositions from massive iceberg surges from a decaying Laurentide ice sheet (Heinrich, 1988; Bond et al., 1992). Melting of these icebergs is identified as a key mechanism in disrupting northward heat transport by the density-driven Atlantic Meridional Overturning Circulation (AMOC) (Broecker, 1994; Rahmstorf, 1996). The resulting freshwater flux thereby limits the formation of North Atlantic deep water which disrupts the ocean circulation. Apart from ice sheet decay, also changes in the (sub)tropical hydrological cycle may affect the AMOC by altering the freshwater budget of the North Atlantic (Rahmstorf, 1996; Broecker, 2003). Changes in the atmospheric moisture flow from the Atlantic across the low-lying Central American isthmus towards the Pacific are especially relevant for the freshwater budget of the North Atlantic because this passageway is one of the few places where humid (sub)tropical air can escape the Atlantic basin at low altitudes (Zaucker and Broecker, 1992). Changes in cross-isthmus moisture transport may therefore constitute feedbacks with the glacial AMOC in relation to millennial-scale climate variability (Leduc et al., 2007; Lachniet et al., 2009).

A central feature of the (sub)tropical hydrological cycle is the belt with intense convective activity and precipitation organized around the Inter-Tropical Convergence Zone (ITCZ). Disruption of the AMOC induces cooling of the extratropical North Atlantic and a warming of the tropical and South Atlantic (Stocker, 1998) which displaces the ITCZ southwards (Broccoli et al., 2006; Peterson and Haug, 2006). A southerly position of the ITCZ during cold D-O stadials has been suggested to reduce cross-isthmus moisture transport due to the blocking effects of the Andes mountain ridge (Xu et al., 2005; Leduc et al., 2007). However, the planktonic $\delta^{18}O$ derived sea surface salinity reconstructions on which this inference was based (Schmidt et al., 2004; Leduc et al., 2007) remain problematic to reconcile with a displacement in the ITCZ alone (Prange et al., 2010; Richter and Xie, 2010). As an alternative explanation, Prange et al. (2010) proposed an analogue based on present-day moisture flow patterns related to the Niño/Southern Oscillation (ENSO).

Besides the high-latitudinal forcing on the ITCZ position and ENSO-like ocean-atmosphere dynamics, variations in (sub)tropical North Atlantic Sea Surface Temperatures (SSTs) may also influence the (sub)tropical hydrological cycle directly (Wang et al., 2006). Such a direct low-latitudinal imprint could be reflected by episodic pine pollen increases in a lake sediment record from Florida indicating warmer and wetter conditions during Heinrich events (Grimm et al., 2006; Donders et al., 2011). The apparent warming during these North Atlantic cold events may be explained by heat

retention in the low latitudes during periods of reduced AMOC (Rühlemann et al., 1999; Flower et al., 2004). Relative warmth is also reflected in proxy-based SST reconstructions from the Caribbean Sea and Gulf of Mexico, which show no consistent cooling imprints of millennial-scale cold events (Schmidt et al., 2004; Ziegler et al., 2008). The consistently warm SSTs in their record led Ziegler et al. (2008) to propose that the Atlantic Warm Pool (AWP) persisted to expand into the Gulf of Mexico during summer throughout the most of the last glacial.

The AWP is defined as a region of the Atlantic basin with SSTs above 28.5°C (Wang et al., 2006). This temperature is the approximate lower limit for starting deep atmospheric convection (Graham and Barnett, 1987; Johnson and Xie, 2010). The modern AWP expands from the (sub)tropical Northwest Atlantic into the Caribbean Sea and Gulf of Mexico during boreal summer and fall. Considerable variation in AWP expansion occurs at inter-annual and longer timescales due to ENSO variability, the Atlantic multi-decadal oscillation and global warming (Wang et al., 2008a). Such changes in AWP expansion may climatologically be relevant because they evoke inverse surface pressure changes in the North Atlantic subtropical high pressure system (termed the Azores High) via the so-called Gill-type atmospheric response (Gill, 1980; Wang et al., 2008b). This atmospheric response entails that heating associated with an anomalously large AWP reduces the easterly trade winds in the lower troposphere. Hence, an anomalously small AWP may strengthen the easterly trade winds. Changes in AWP expansion thereby affect the easterly low-level atmospheric moisture flow towards and across the Central American isthmus (Wang and Lee, 2007; Wang et al., 2008b). Based on these atmospheric responses, we put forward the hypothesis that variations in glacial AWP expansion may have altered atmospheric circulation patterns and associated moisture transport across the Central American isthmus in relation to millennial-scale climate variability.

Problematic for investigating this potential role of a glacial AWP are the uncertainties inherent to proxy data and the cold SST bias of coupled ocean-atmosphere models in the (sub)tropical North Atlantic region (Breugem et al., 2008; Misra et al., 2009). Our study therefore uses proxy-based evidence in combination with climate modelling to study the potential role of the AWP in the context of millennial-scale climate variability. To provide evidence for the existence of a glacial AWP and its potential spatial and temporal dynamics we first reviewed proxy-based SST reconstructions from the (sub)tropical North Atlantic region covering several Bond cycles. Second, we analyzed the present-day atmospheric response to variations in AWP area with a reanalysis of meteorological observations. We then performed simulations with coupled and uncoupled ocean-atmosphere models to analyze the sensitivity of the glacial atmosphere to potential variations in AWP expansion. Our model results are discussed in relation to proxy-based evidence on changes in cross-isthmus moisture transport.

Proxy evidence for glacial Atlantic warm pool dynamics

Proxy-based SST reconstructions from the (sub)tropical North Atlantic region covering the period between 60 and 11 thousand years ago (Marine isotope stages 2 and 3) were reviewed to provide evidence for the existence of a glacial AWP and its potential millennial-scale dynamics. The core locations and data series are indicated by the letters (i) through (o) and shown in Figures 5.1A and 5.1B, respectively. As a reference to the annual average SSTs that are typically reflected in planktonic Mg/Ca ratios (Anand et al., 2003), present-day annual average SSTs are plotted in Figure 5.1A. The 28.5°C September SST isotherms during years with small and large AWPs are indicated to show the variability in the spatial extent of the modern AWP. A small/large AWP is defined as being 33% smaller/larger than the average AWP in the months July through October (Wang et al., 2008b). Modern low-level (925 hPa) wind fields are shown by vectors to indicate the direction and strength of the easterly trade winds over the AWP and across the low-lying Central American isthmus.

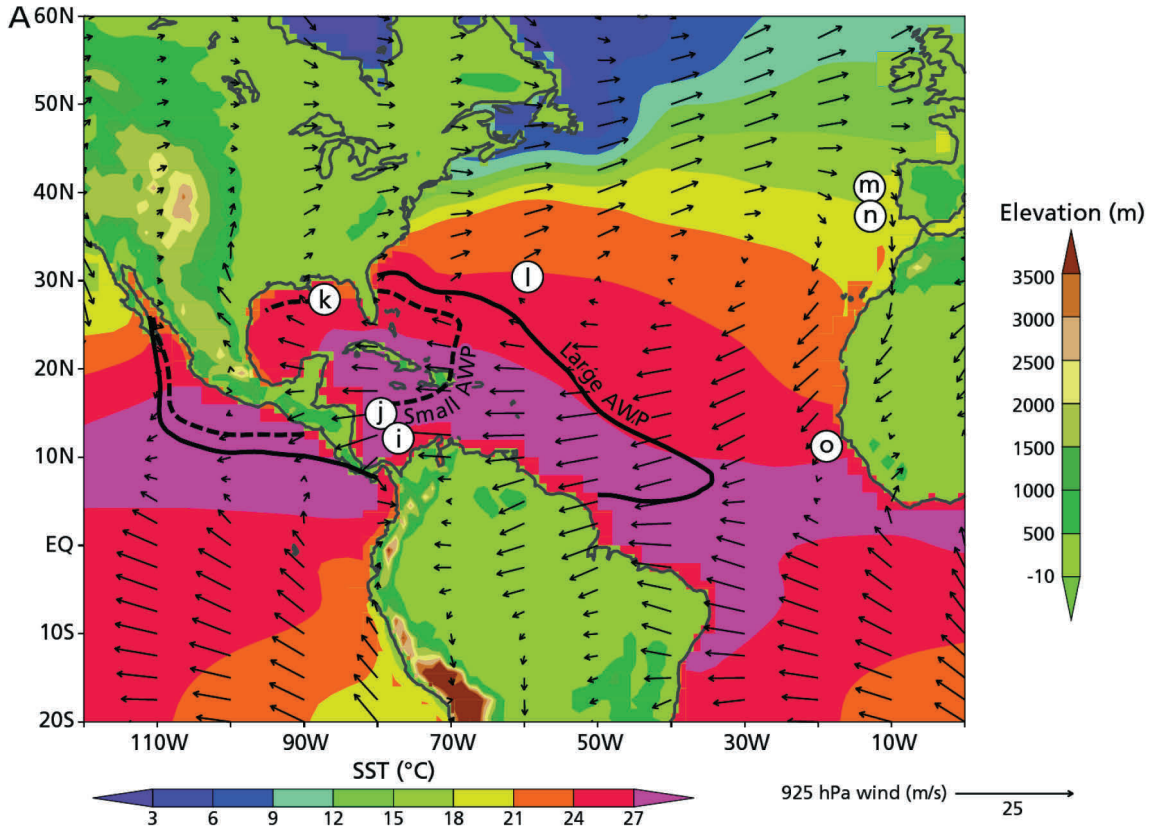

Figure 5.1 Overview of proxy-based SST reconstructions indicative of the spatial and temporal dynamics of a potential AWP during the last glacial. (A) Core locations of data series presented in panel B are indicated with the letters (i) through (o). Shading denotes the present-day annual average SSTs as a reference to the annual SSTs typically reflected by planktonic Mg/Ca-derived temperatures (Anand et al., 2003). The spatial extents of modern small and large AWPs are indicated by the dashed and solid black lines along the 28.5°C September isotherms, respectively. Vectors denote present-day average low-level wind speed and direction for the 925 hPa pressure level from the NCEP/NCAR reanalysis (Kalnay et al., 1996). →

Planktonic Mg/Ca-derived SST reconstructions from the Colombian basin in the Caribbean Sea (i, j) indicate a dominant control of summer insolation and glacial-interglacial variability and hint at a slight warming during Heinrich event 1 and the Younger Dryas (Schmidt et al., 2004). Compared to the present, SSTs in the Caribbean Sea were approximately 1˚C colder throughout the last glacial. A Mg/Ca-derived SST reconstruction from the northern edge of the modern AWP in the north-eastern Gulf of Mexico (k) also indicates a dominant control of summer insolation and glacial-interglacial variability (Nurnberg et al., 2008; Ziegler et al., 2008). Reconstructed SSTs in the Gulf of Mexico are comparable to the modern annual average. These SST records from the Caribbean Sea and Gulf of Mexico show no clear evidence of millennial-scale cooling, except for Heinrich event 3 which is documented in the Gulf of Mexico.

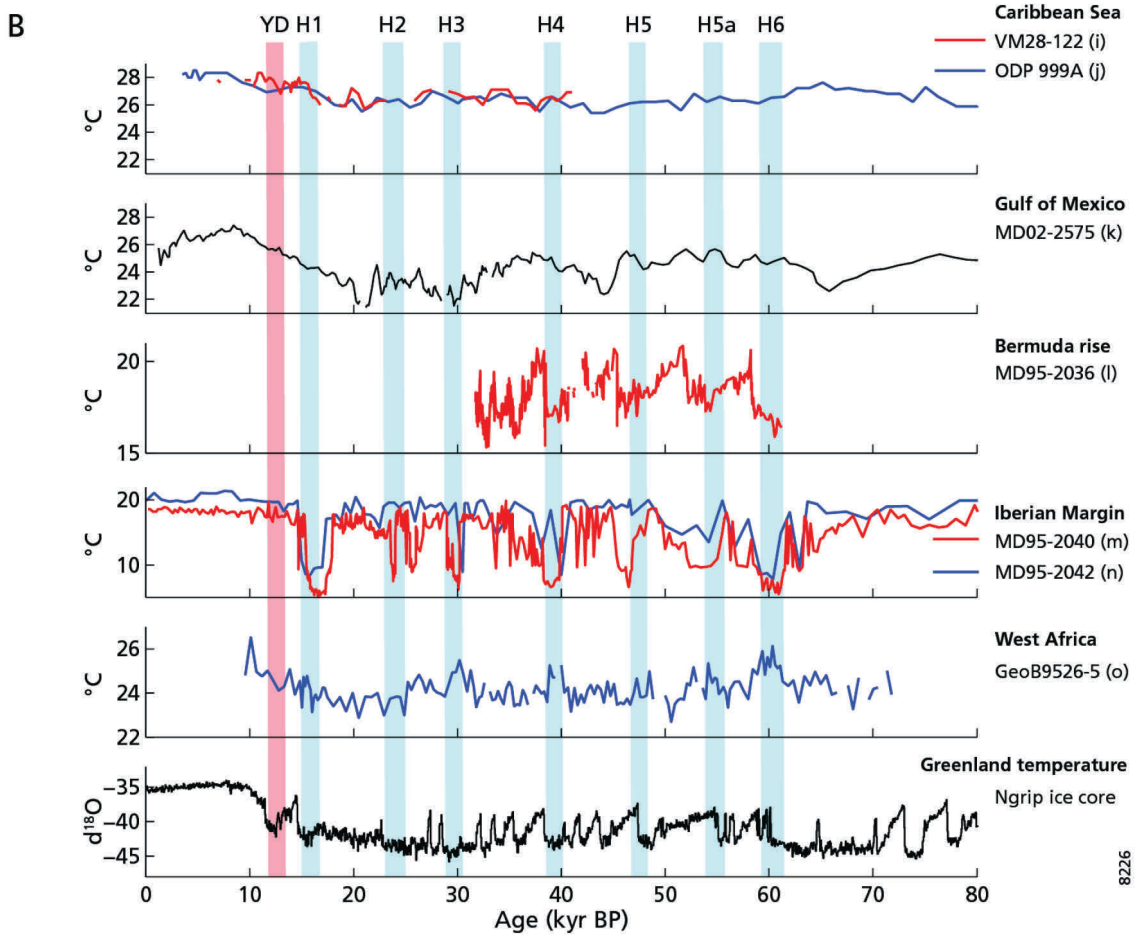

Figure 5.1 (continued) (B) Paleoclimate reconstructions shown from top to bottom: SSTs in the Caribbean Sea (i, j) (Schmidt et al., 2004), SSTs in the Gulf of Mexico (k) (Nurnberg et al., 2008; Ziegler et al., 2008), SSTs from the Bermuda rise (l) (Sachs and Lehman, 1999), SSTs from the Iberian margin (m, n) (Salgueiro et al., 2010) and SSTs off the coast of West Africa (o) (Zarriess et al., 2011) and, Greenland $\delta^{18}O$ values representative for Greenland temperatures (NGRIP-Members, 2004). Although the exact timing of Heinrich events varies depending on the records used (Rashid et al., 2003), coloured bars indicate maximum calendar age ranges of North Atlantic iceberg-rafted debris following Stoner et al. (2000). The blue bars indicate Heinrich events (H1-H6), the pink bar indicates the Younger Dryas (YD).

An alkenone-derived SST reconstruction from the Bermuda rise (l) reveals temperatures covarying with Greenland $\delta^{18}O$ ice core values (Sachs and Lehman, 1999; NGRIP-Members, 2004). These SSTs from the Bermuda rise are comparable to modern SSTs during the warm phases of D-O oscillations. Cooling of approximately 2-4˚C is observed during cold D-O phases and Heinrich events associated with a disrupted AMOC. These episodic cooling events are also imprinted with comparable magnitude in planktonic $\delta^{18}O$ SST reconstructions from the Iberian margin (m, n) (Salgueiro et al., 2010). In contrast, warming is observed in a Mg/Ca-derived SST reconstruction from the tropical Northeast Atlantic (o) during Heinrich events (Zarriess et al., 2011), reflecting the bi-polar Atlantic SST response to AMOC collapse.

This evidence suggests that warm waters remained in the Caribbean Sea and the Gulf of Mexico throughout most of the last glacial. The control of summer insolation in combination with glacial-interglacial variability most likely determined the summer expansion of the AWP in these basins. In contrast to the records from the Caribbean Sea and Gulf of Mexico, the SST reconstructions from the Bermuda rise and Iberian margin do reveal the imprint of millennial-scale cooling events. This could indicate that eastward expansion of the AWP beyond the Caribbean Sea and Gulf of Mexico was inhibited during millennial-scale cold events. However, the evidence of the spatial and temporal (seasonal) dynamics of the AWP in relation to millennial-scale glacial climate variability remains inconclusive. We therefore propose three potential responses of the AWP during the last glacial: (1) AWP evolution independent of extra-tropical North Atlantic temperatures, (2) reduced AWP expansion during millennial-scale cold events, and (3) persistent AWP expansion during millennial-scale cold events.

Methods

Our model approach was aimed at investigating the sensitivity of the glacial atmosphere to the three potential responses of the AWP in relation to millennial-scale climate variability. As a reference we also analyzed the present-day relation between the AWP and the (sub)tropical atmosphere using the NCEP/NCAR ERA-40 reanalysis of meteorological observations (Kalnay et al., 1996). The sensitivity of the glacial atmosphere to variations in AWP expansion was investigated with two model setups. First we simulated the glacial climate and its response to AMOC collapse by performing a classic 'water-hosing' experiment with the coupled ocean-atmosphere model LOVECLIM version 1.0 (Opsteegh et al., 1998; Goosse and Fichefet, 1999; Goosse et al., 2010). A freshwater forcing of 0.3 Sv (Sverdrup = 10^6 $m^3 \cdot s^{-1}$) was applied in the Labrador Sea for a duration of 200 years to evoke AMOC collapse. More details are provided in Roche et al. (2007, 2010). LOVECLIM was used here with three components activated: atmosphere (ECBilt), ocean (CLIO) and vegetation (VECODE). Experiments performed with LOVECLIM are named with the prefix “CLIO-” because we mainly focussed on its oceanic response. The CLIO-LGM simulation represented the climate of the Last Glacial Maximum (LGM) while the CLIO-OFF simulation represented the glacial climate with a disrupted AMOC.

Second, we performed six atmospheric sensitivity simulations with the atmospheric General Circulation Model (GCM) PUMA version 2 (Fraedrich et al., 2005). PUMA was used at a T42 horizontal resolution (approximately 2.8° latitude x 2.8° longitude) with 10 vertical layers. The rationale for using PUMA to simulate the atmospheric responses to variations in glacial AWP expansion is that ECBilt is a quasi-geostrophic model. PUMA is therefore more suited to simulate the (sub)tropical atmosphere while retaining computational efficiency compared to more detailed GCMs. A detailed validation of PUMA for the present climate is provided by Haberkorn et al. (2009). A comparison between the atmospheric responses of PUMA and the more detailed GCM ECHAM4 to variations in North Atlantic SSTs is provided by Grosfeld et al. (2007). Our PUMA simulations were forced using 50-year transient monthly fields of SSTs and sea ice cover obtained from the CLIO-LGM and CLIO-OFF simulations, while four simulations also included additional variations in AWP expansion. The atmospheric simulations were named "LGM" and "OFF" depending on the CLIO output used, with a superscript indicating the additional AWP dynamics included (Table 5.1). The LGM^N and OFF^N simulations thereby used CLIO output with no (^{N}) additional AWP dynamics. The LGM^S and OFF^S simulations used CLIO output with additional SST dynamics related to a present-day small (^{S}) AWP, while the LGM^L and OFF^L included additional SST dynamics related to a present-day large (^{L}) AWP. Average seasonal evolution of the AWP area in each experiment is shown in Figure 5.2A. Our simulations covered a range in AWP expansion from (almost) no AWP in the OFF^N simulation to the size of a modern large AWP of $9 \cdot 10^6$ km^2 in the LGM^L simulation. As a reference, the average modern AWP area during September is approximately $7.5 \cdot 10^6$ km^2. An overview of the average spatial extent of the AWP during September in each experiment is shown in Figure D1 in Appendix D. Average SST anomalies between the OFF^N and LGM^N experiments and the LGM^S and LGM^L experiments are shown in Figure 5.2B and 5.2C, respectively.

Table 5.1 Overview of the paleoclimate simulations and their boundary conditions. The LOVECLIM model resolved coupled ocean-atmosphere dynamics, PUMA-2 resolved atmosphere dynamics with prescribed surface ocean boundary conditions derived from the LOVECLIM simulations.

Simulation	Model	Boundary conditions
CLIO-LGM	LOVECLIM	Last glacial maximum (21 kyr BP) (Roche et al., 2007, 2010)
CLIO-OFF	LOVECLIM	Last glacial maximum (21 kyr BP) with 'freshwater hosing' in the North Atlantic (Roche et al., 2007, 2010)
LGM^N	PUMA-2	CLIO-LGM surface ocean and sea ice, no additional AWP
LGM^S	PUMA-2	As LGM^N, with dynamics related to a small AWP
LGM^L	PUMA-2	As LGM^N, with dynamics related to a large AWP
OFF^N	PUMA-2	CLIO-OFF surface ocean and sea ice, no additional AWP
OFF^S	PUMA-2	As OFF^N, with dynamics related to a small AWP
OFF^L	PUMA-2	As OFF^N, with dynamics related to a large AWP

The additional variations in AWP dynamics were included by replacing zonal SST gradients from CLIO in the (sub)tropical North Atlantic between 5°N and 30°N with modern zonal SST gradients observed during years with small and large AWPs. Our rationale for using SST gradients was that this approach retained the meridional Atlantic SST response of CLIO while allowing us to introduce zonal temperature gradients associated with modern seasonal AWP dynamics. Following the approach of Wang et al. (2008b) we considered (sub)tropical North Atlantic SST patterns associated with small or large AWPs. A small or large AWP was defined as being 33% smaller or larger than the

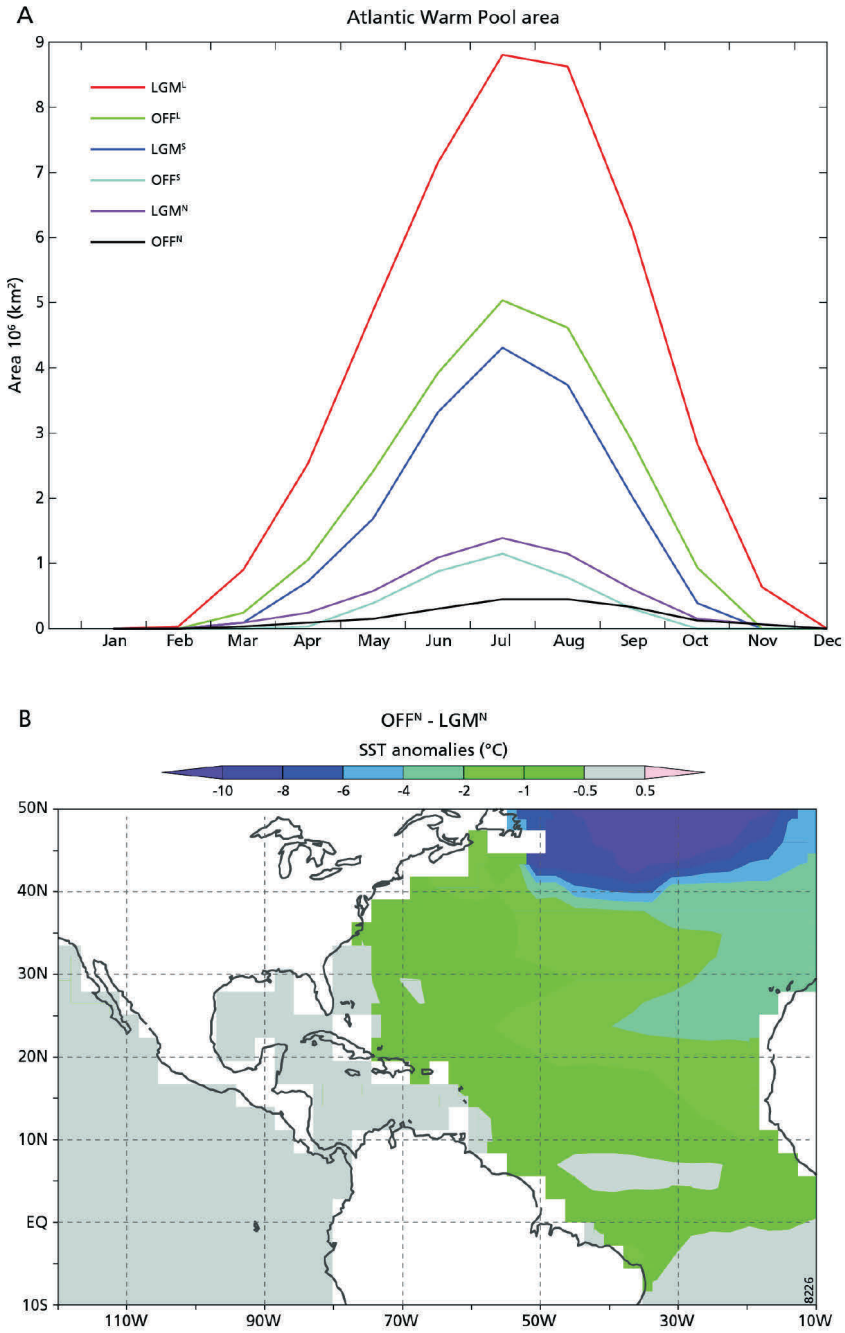

Figure 5.2 Overview of the SST boundary conditions used in the atmospheric sensitivity simulations. (A) Seasonal evolution of AWP area in all six atmospheric GCM simulations. (B) Annual average SST anomalies between the OFF^N and LGM^N simulations.→

average modern AWP in the months July through October, respectively. Modern SSTs were obtained from the HadISST dataset for the years 1949-2006 (Rayner et al., 2006). Accordingly, the years 1974, 1975, 1976, 1984, 1986 and 1992 had small AWPs and the years 1958, 1969, 1987, 1995, 1998, 2005 had large AWPs. These years were averaged to create one-year monthly composites representing small and large AWPs. From these composite years we calculated monthly zonal SST gradients relative to the zonal average monthly SSTs in the (sub)tropical Northeast Atlantic (eastward of 40˚W and between 5°N-30°N) in the small and large AWP composites. Similarly, we calculated the zonal average monthly SSTs in the (sub)tropical Northeast Atlantic from each CLIO simulation. By replacing these zonal SST gradients from the CLIO-LGM simulation with the gradients from the modern small and large AWP composites we obtained SST boundary conditions for the LGM^S and LGM^L simulations, respectively. Performing the same operation for the CLIO-OFF simulation output yielded the SST boundary conditions for the OFF^S and OFF^L simulations. As the CLIO-LGM simulation produced a warmer subtropical Northeast Atlantic than the CLIO-OFF simulation, replacing their respective zonal SST gradients with the same modern SST gradients resulted in differently sized AWPs. Hence, the LGM^S and OFF^L simulations have comparable AWP area (cf. Figure D1 in Appendix D).

In all atmospheric simulations with PUMA we applied constant LGM (21 thousand years BP) boundary conditions for solar insolation, ice-sheet cover and orography (Peltier, 1994). For atmospheric CO_2 concentrations we applied a value of 160 ppm to account for the combined radiative forcing of atmospheric CO_2 and CH_4. Each atmospheric simulation was spun-up by repeating the first simulation year 10 times to minimize the impact of initialization.

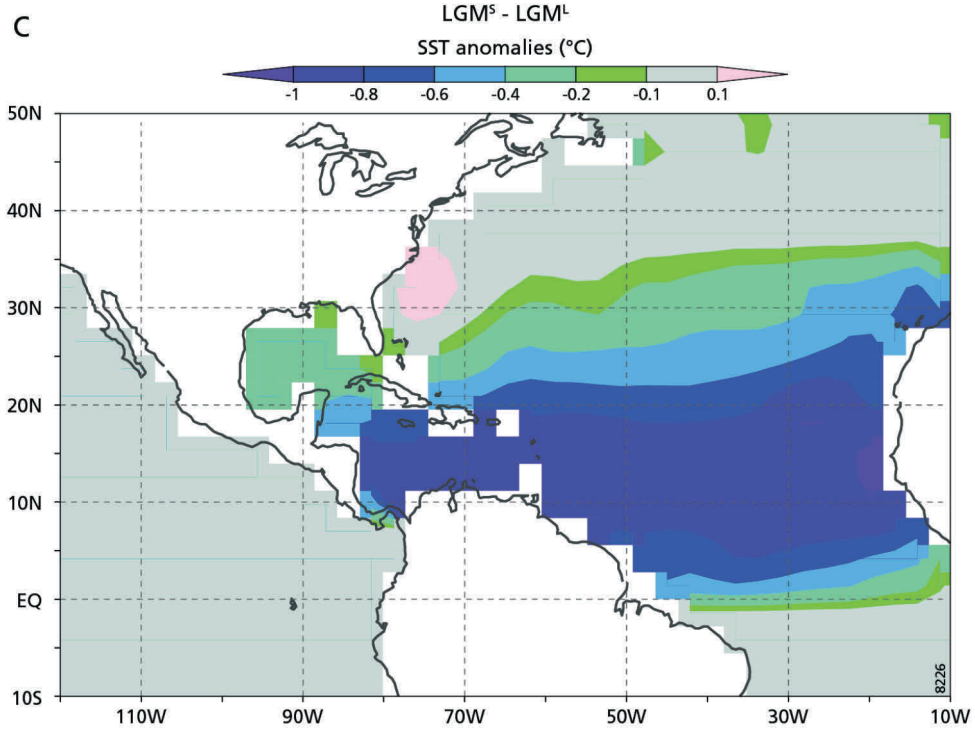

Figure 5.2 (continued) (C) Annual average SST anomalies between the LGM^S and LGM^L simulations.

Results

Modern atmosphere responses under variations in AWP area

The present-day link between changes in AWP area and the atmosphere was investigated with the NCEP/NCAR ERA-40 reanalysis of meteorological observations (Kalnay et al., 1996). From this reanalysis we compared composites of the years with anomalously small and large AWPs between 1949 and 2006. The annual average SST anomalies between years with small and large AWPs revealed a cooling of approximately 1˚C in the North Atlantic between 5-25˚N (Figure 5.3A). The Gill-type atmospheric response to this (sub)tropical cooling was reflected by an increase in sea level pressure in the centre of the Azores High by approximately 2 hPa and an westward expansion of this high pressure system over the Caribbean Sea and Gulf of Mexico (Figure 5.3B). This expansion of the Azores High strengthened the low-level easterly trade winds over the (sub)tropical North Atlantic and the Caribbean Sea with a maximum of 4 $m \cdot s^{-1}$, as shown for the 925 hPa level in Figure 5.3B. This pressure level represents a part of the lower troposphere that is most relevant for atmospheric moisture transport due to the high moisture content. The wind anomalies at this elevation are considerable compared to the annual average wind speeds with a maximum of 15 $m \cdot s^{-1}$ at the 925 hPa level (cf. Figure 5.1A). Strengthening of the easterly trade winds also enhanced the atmospheric moisture flow over the Caribbean Sea towards and across the Central American in the lower troposphere. This low-level moisture transport was calculated from specific humidity ($g \cdot kg^{-1}$) and wind speed ($m \cdot s^{-1}$) at the 925 hPa pressure level based on monthly average model output. We note that using monthly model output introduces only marginal errors comparable to the use of daily data (Richter and Xie, 2010). Low-level moisture transport anomalies revealed increases up to 20 $g \cdot kg^{-1} \cdot m \cdot s^{-1}$ near the Central American isthmus, as shown for 925 hPa level in Figure 5.3C. Such an increase in moisture transport is considerable compared to the moisture transport maximum near the isthmus of approximately 100 $g \cdot kg^{-1} \cdot m \cdot s^{-1}$ in the large AWP composite. This moisture transport maximum is shown for an atmospheric cross-section at 80˚W between 5-30˚N in Figure 5.3D.

A key feature in the atmospheric moisture transport over the Caribbean Sea and across the Central American isthmus is the Caribbean low-level jet. This low-level jet is formed by the intensification of the trade winds over the Caribbean Sea. Detailed discussions on this phenomenon and its relation with the AWP are presented by Wang and Lee (2007), Muñoz et al. (2008) and Cook and Vizy (2010). The core of the Caribbean low-level jet is visible in the atmospheric moisture transport maximum over the Caribbean Sea (Figure 5.3D). As a decrease in AWP area intensified the easterly low-level flow in this jet, moisture transport towards the isthmus was increased by approximately 20 $g \cdot kg^{-1} \cdot m \cdot s^{-1}$ in the small AWP composite (Figure 5.3E). These results suggest that in the present climate an inverse relation exists between AWP area and easterly low-level moisture flow over the Caribbean and across the Central American isthmus.

Glacial atmosphere responses to variations in AWP area

Our simulations of the glacial atmosphere with PUMA were analyzed for changes in sea level pressure, low-level wind speed and low-level moisture transport averaged between

the surface and the 700 hPa level. The atmospheric layers below 700 hPa are most relevant for analyzing moisture transport due to their high moisture content (Muñoz et al., 2008). Low-level moisture transport ($g \cdot kg^{-1} \cdot m \cdot s^{-1}$) was calculated from the modelled wind speed ($m \cdot s^{-1}$) and specific humidity ($g \cdot kg^{-1}$) at each pressure level based on monthly averaged model output. The LGM^N simulation resolved the low-level atmospheric flow around the Azores High, resulting in easterly winds up to 10 $m \cdot s^{-1}$ over the Caribbean Sea and towards the Central American isthmus (Figure 5.4A). Comparable to the NCEP/NCAR reanalysis, maxima in low-level moisture transport were simulated over the (sub)tropical Northwest Atlantic and the Caribbean Sea and reached approximately 80 $g \cdot kg^{-1} \cdot m \cdot s^{-1}$ near the Central American isthmus (Figure 5.4B).

The influence of changes in AWP expansion on the glacial atmosphere was analyzed with the anomalies between the LGM^S and LGM^L simulations. The anomalies between the OFF^S and OFF^L simulations were comparable and therefore not discussed separately. The key atmospheric response to the decrease in AWP expansion was an increase in sea level pressure in the Azores High of approximately 1 hPa extending over the (sub)tropical North Atlantic, Caribbean Sea and eastern North Pacific (Figure 5.4C). This pressure increase intensified the low-level winds over the Caribbean Sea with approximately 3 $m \cdot s^{-1}$. The wind speed increase also intensified the low-level moisture flow towards and across the isthmus with approximately 12 $g \cdot kg^{-1} \cdot m \cdot s^{-1}$ (Figure 5.4D). This atmospheric response to reduced AWP expansion was comparable to the present-day atmospheric response in the NCEP/NCAR reanalysis (cf. Figure 5.3C). These results suggest that also under glacial boundary conditions changes in AWP area lead to inverse changes in the easterly low-level flow towards and across the Central American isthmus.

Glacial atmosphere responses to variations in AWP area and high latitudinal cooling

To investigate the atmospheric response to reduced AWP expansion in relation to millennial-scale cold events we first analyzed anomalies between the OFF^N and LGM^N simulations. We note that the OFF^N and LGM^N simulations include cooling in both the extra-tropical and subtropical North Atlantic without additional AWP dynamics (Figure 5.2 and Figure D1 in Appendix D). The main atmospheric response to this North Atlantic cooling was an intensification of the easterly trade winds over the subtropical North Atlantic due to a localized increase in surface pressure in the Azores High (Figure 5.5A). Intensification of the easterly trade winds was simulated over the tropical Northwest Atlantic near the coast of South America. Little change in wind speed was simulated near the Central American isthmus while a drying of the atmosphere occurred over the northern part of the isthmus (not shown). As a result, a reduction in low-level moisture transport of approximately 4 $g \cdot kg^{-1} \cdot m \cdot s^{-1}$ was simulated over the northern part of the isthmus (Figure 5.5B). An increase in low-level moisture transport of approximately 2 $g \cdot kg^{-1} \cdot m \cdot s^{-1}$ was simulated over the southern part of the isthmus. Second, we analyzed anomalies between the OFF^S and LGM^L simulations that represent a more prominent decrease in AWP expansion compared to the OFF^N and LGM^N simulations but retain the same extra-tropical cooling (Figure D1, Appendix D). The surface pressure and low-level wind anomalies between the OFF^S and LGM^L simulations revealed a prominent (→ p.100)

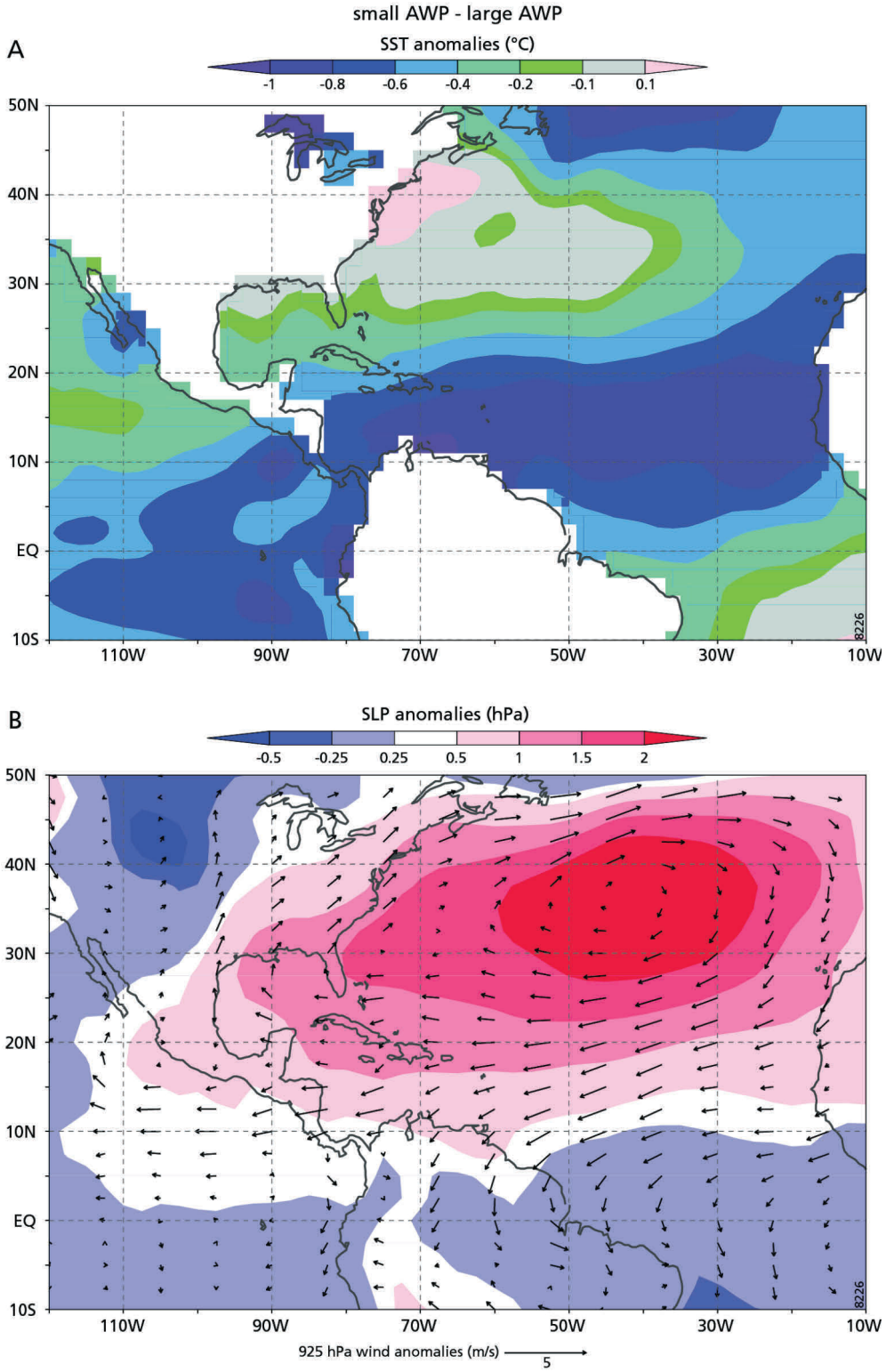

Figure 5.3 Present-day annual average atmospheric responses to changes in AWP expansion as resolved by the NCEP/NCAR reanalysis (Kalnay et al., 1996). (A) SST anomalies (˚C) between composite years with small and large AWPs. (B) Sea level pressure (SLP) anomalies (hPa) and low-level wind anomalies ($m \cdot s^{-1}$) at the 925 hPa pressure level between composite years with small and large AWPs. Vectors indicate the magnitude and direction of the change in wind speed. →

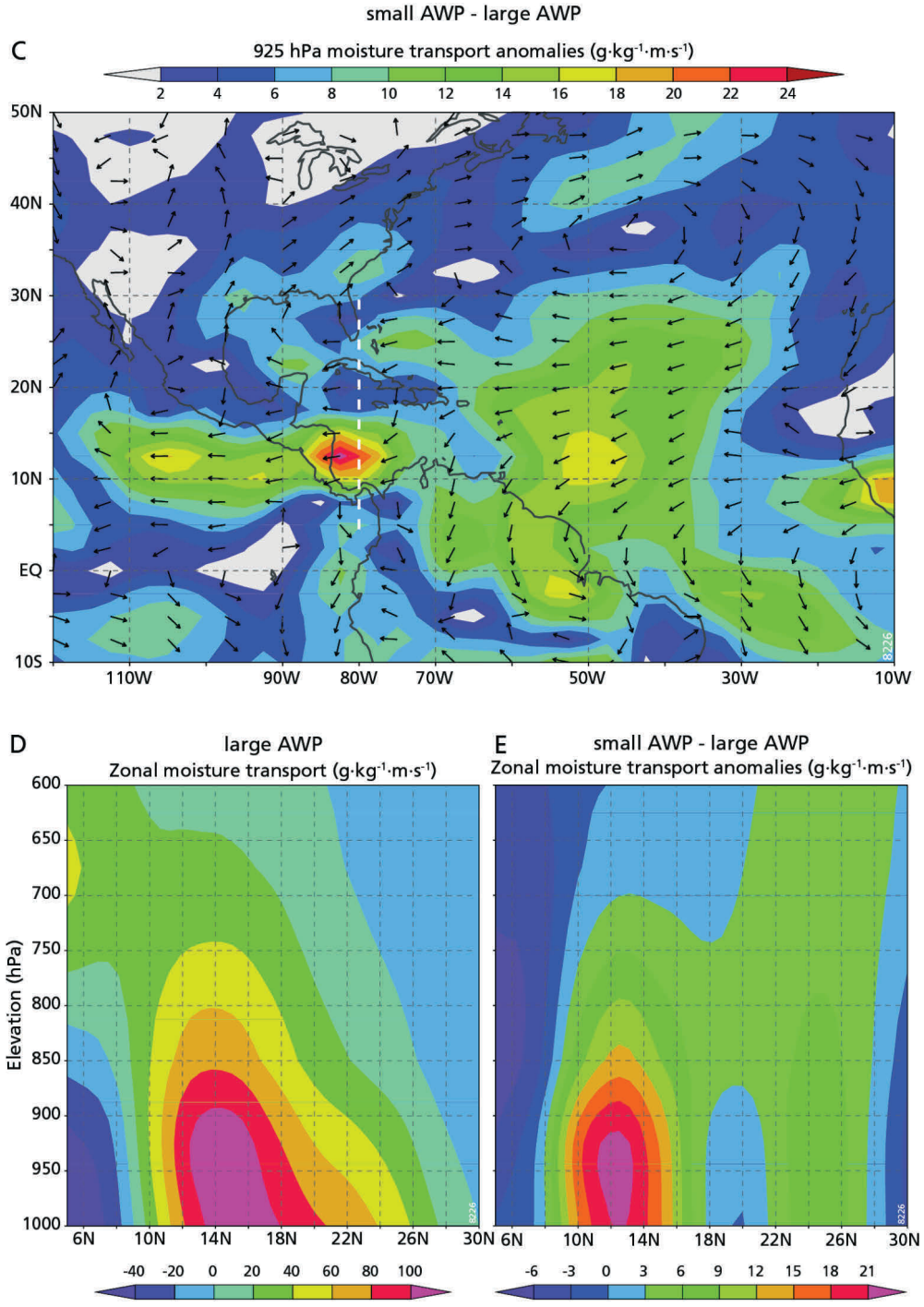

Figure 5.3 (continued) (C) Low-level moisture transport anomalies ($g \cdot kg^{-1} \cdot m \cdot s^{-1}$) at the 925 hPa pressure level between composite years with small and large AWPs. Shading indicates the magnitude of the change, vectors denote the direction of change. (D) Zonal atmospheric moisture transport ($g \cdot kg^{-1} \cdot m \cdot s^{-1}$) along a cross-section over the Caribbean Sea at 80˚W between 5˚N and 30˚N (shown by the white dashed line in panel C) in the large AWP composite. Note that positive values denote westward moisture transport. (E) Zonal atmospheric moisture transport ($g \cdot kg^{-1} \cdot m \cdot s^{-1}$) anomalies between the small and large AWP composites along a cross-section over the Caribbean Sea at 80˚W between 5˚N and 30˚N. Note that positive anomalies denote an increase in westward transport.

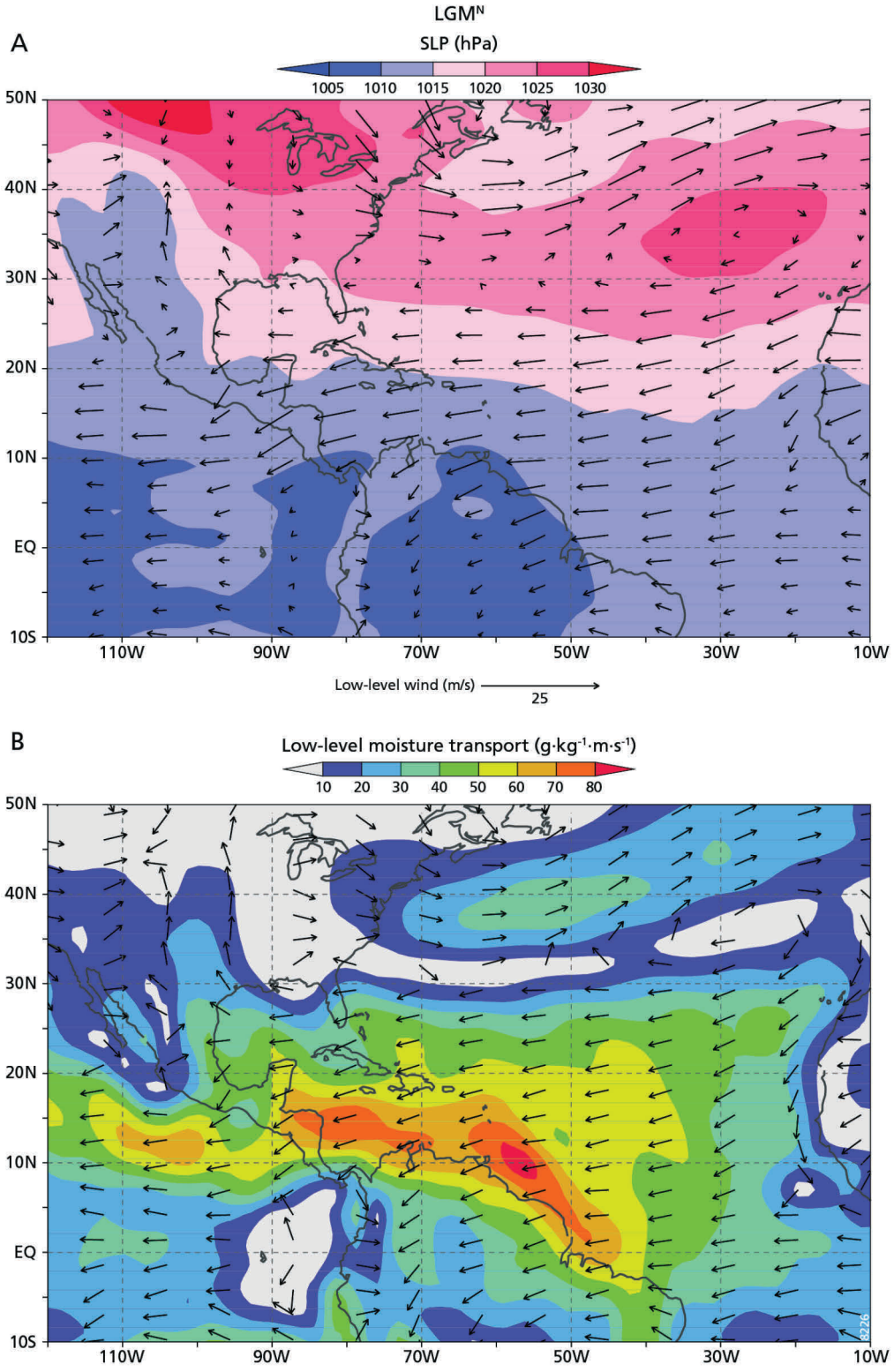

Figure 5.4 Simulated response of the glacial atmosphere to changes in AWP expansion. (A) Sea level pressure (SLP) and low-level wind averaged between the surface and the 700 hPa pressure level in the LGM^N simulation. Shading indicates the sea level pressure, vectors indicate the magnitude and direction of the wind speed. (B) Low-level moisture transport averaged between the surface and the 700 hPa pressure level in the LGM^N simulation. Shading indicates the magnitude of moisture transport, vectors denote the direction.→

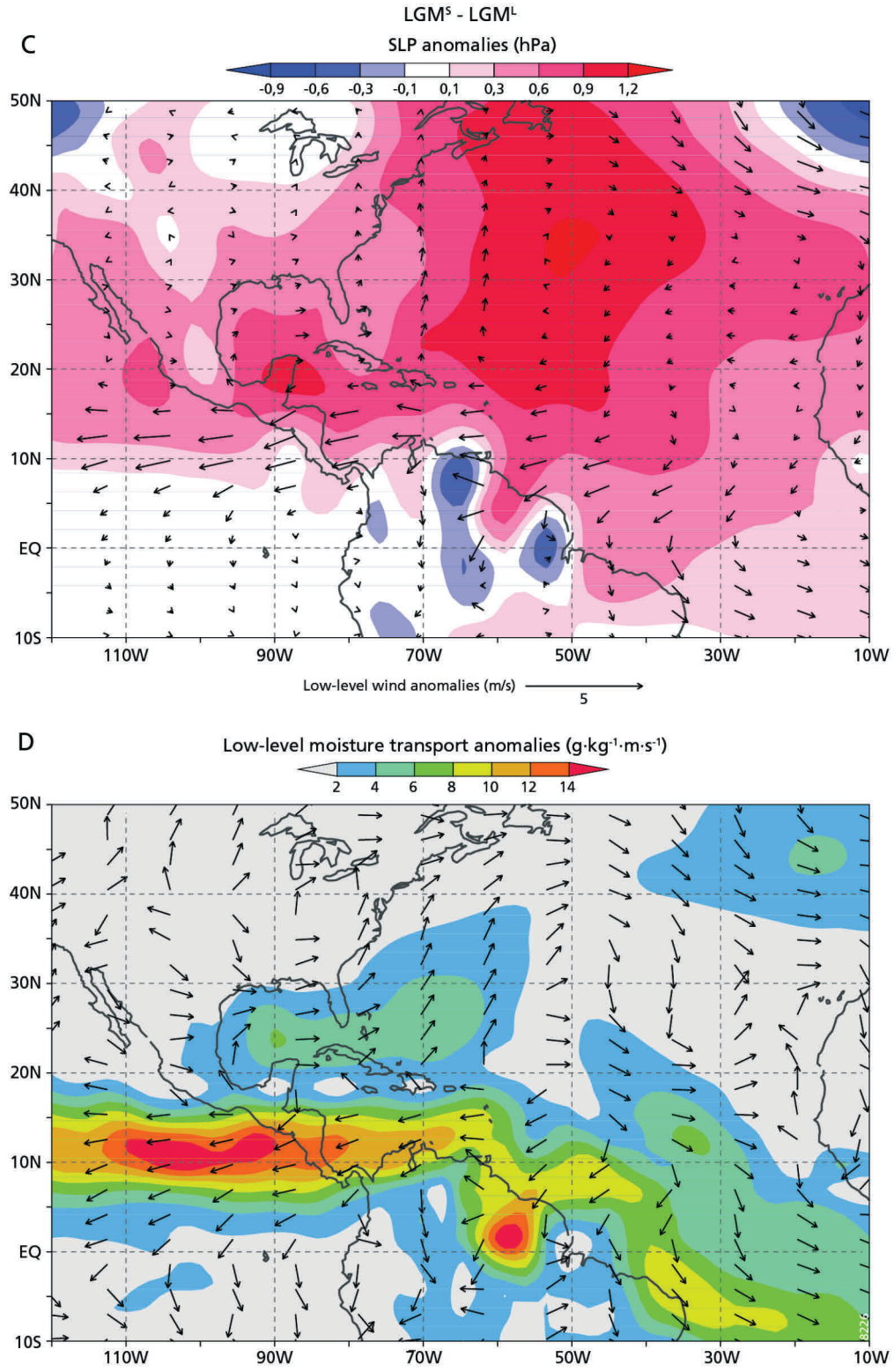

Figure 5.4 (continued) (C) Anomalous sea level pressure and low-level wind anomalies averaged between the surface and the 700 hPa pressure level between the LGM^S and LGM^L simulations. Shading indicates the pressure anomalies, vectors indicate the magnitude and direction of the wind speed anomalies. (D) Anomalous low-level moisture transport averaged between the surface and the 700 hPa pressure level between the LGM^S and LGM^L simulations. Shading indicates the magnitude of the change, vectors denote the direction of change.

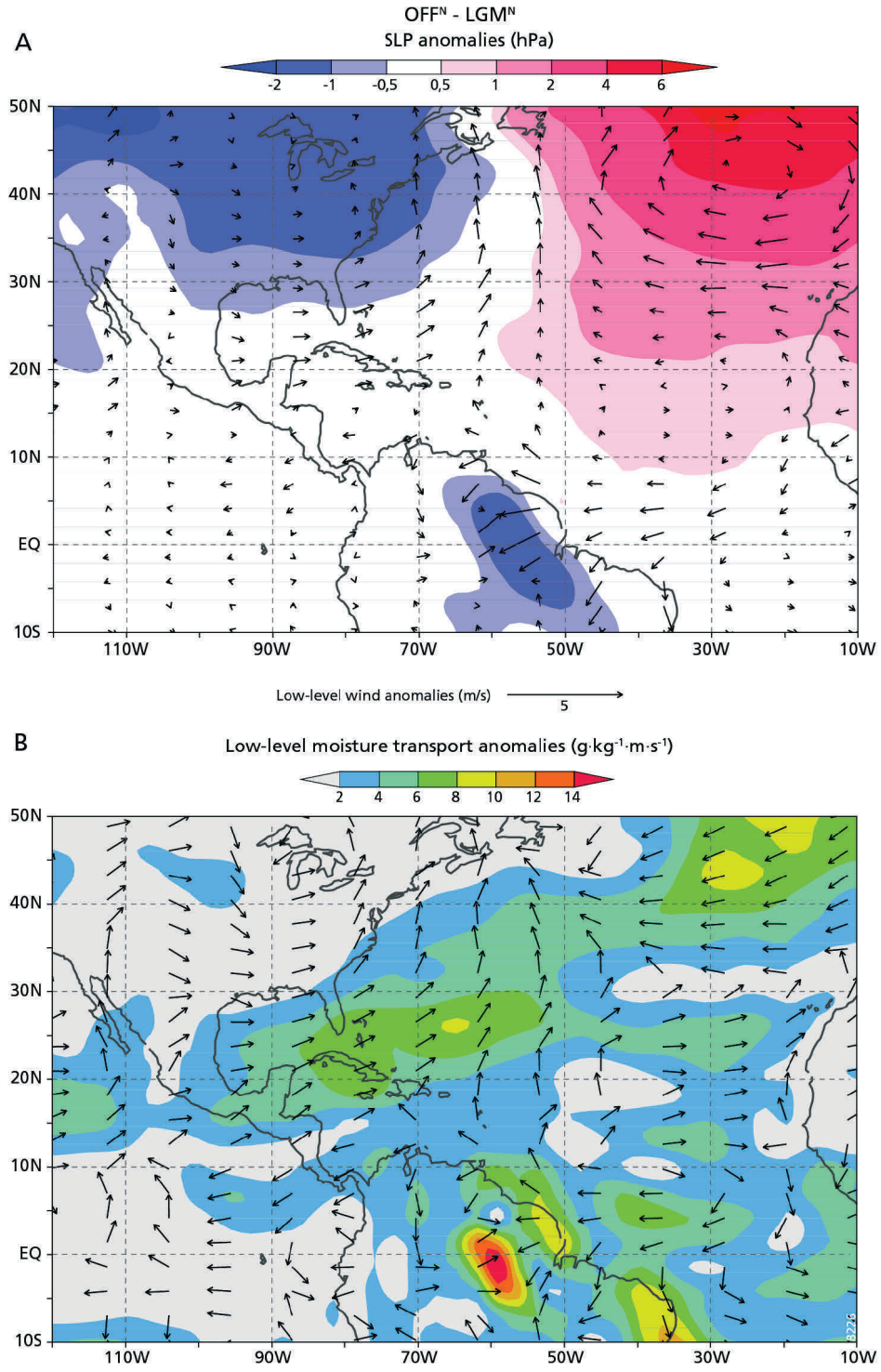

Figure 5.5 Simulated response of the glacial atmosphere to a reduction in AWP expansion under extra-tropical North Atlantic cooling. (A) Anomalous sea level pressure (SLP) and low-level wind anomalies averaged between the surface and the 700 hPa pressure level between the OFF^N and LGM^N simulations. Shading indicates the pressure anomalies, vectors indicate the magnitude and direction of the wind speed anomalies. (B) Anomalous low-level moisture transport averaged between the surface and the 700 hPa pressure level between the OFF^N and LGM^N simulations. Shading indicates the magnitude of the change, vectors denote the direction of change.→

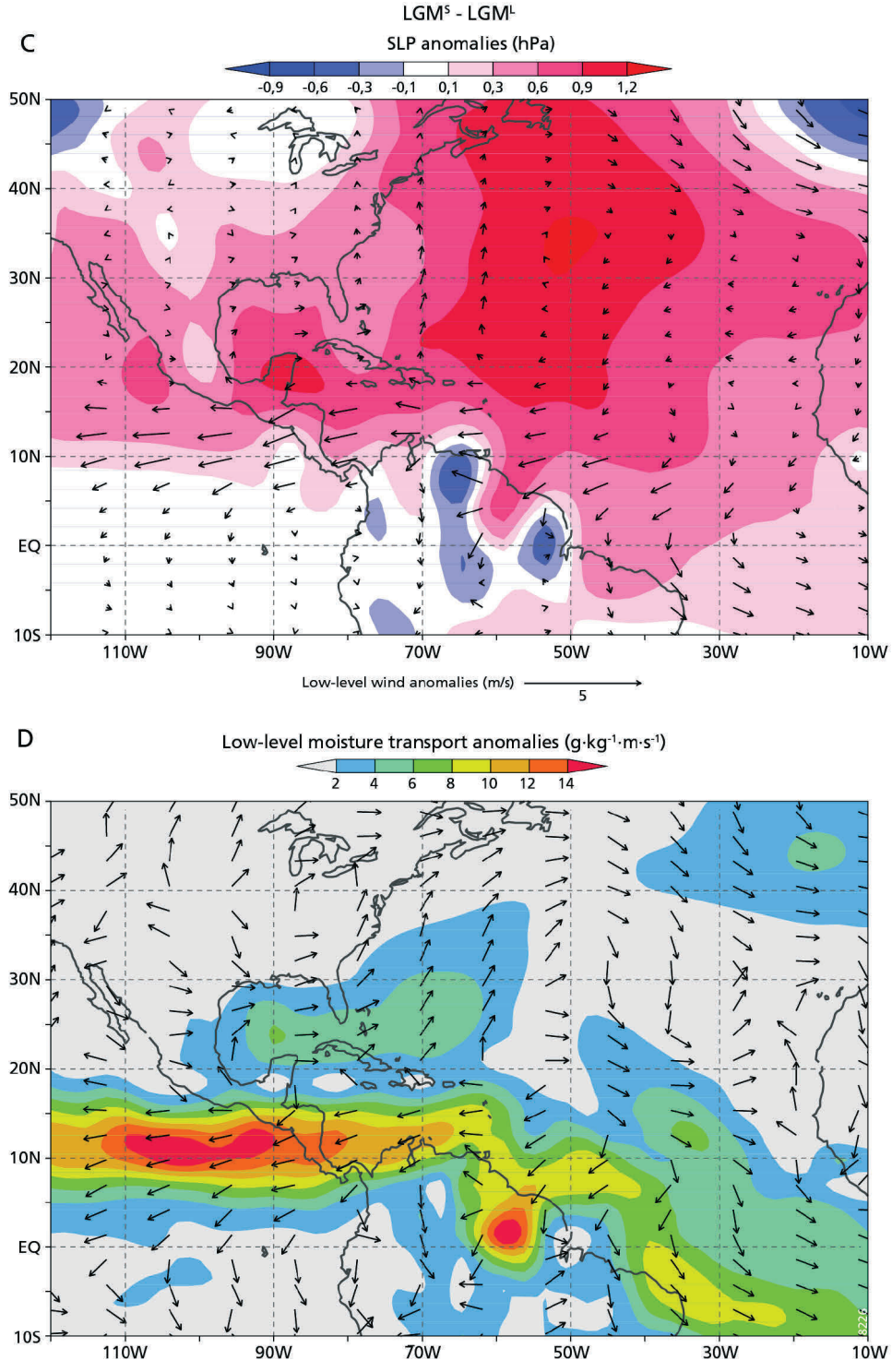

Figure 5.5 (continued) (C) Anomalous sea level pressure and low-level wind anomalies averaged between the surface and the 700 hPa pressure level between the OFF^S and LGM^L simulations. Shading indicates the pressure anomalies, vectors indicate the magnitude and direction of the wind speed anomalies. (D) Anomalous low-level moisture transport averaged between the surface and the 700 hPa pressure level between the OFF^S and LGM^L simulations. Shading indicates the magnitude of the change, vectors denote the direction of change.

(continued from page 93) westward expansion of the Azores High resulting in intensification of the easterly low-level flow over the Caribbean Sea by approximately 4 $m \cdot s^{-1}$ (Figure 5.5C). As a result, the low-level moisture flow towards and across the Central American isthmus increased by approximately 15 $g \cdot kg^{-1} \cdot m \cdot s^{-1}$ (Figure 5.5D).

To analyze the atmospheric response to extra-tropical North Atlantic cooling occurring besides a persistently expanding AWP during summer we analyzed anomalies between the OFF^{L} and LGM^{S} simulations. We note that these simulations have comparable AWP area because CLIO simulated cooling in the subtropical North Atlantic after AMOC shutdown (Figure 5.2B). The anomalies between the OFF^{L} and LGM^{S} simulations showed an increase in sea level pressure of approximately 4 hPa in the Azores High and a lowering of the sea level pressure over North America by approximately 1.5 hPa. As a result, the easterly low-level wind over the Caribbean Sea was reduced by approximately 2 $m \cdot s^{-1}$ (Figure 5.6A). Interestingly, the cooling of the extra-topical North Atlantic still resulted in a pressure increase of the Azores High. However, compared to the surface pressure anomalies between the OFF^{N} and LGM^{N} simulations, the pressure changes in the Azores High occurred further north and did not extend up to the Caribbean Sea. Low-level moisture flow towards and across the Central American isthmus was therefore reduced by a maximum of 10 $g \cdot kg^{-1} \cdot m \cdot s^{-1}$ (Figure 5.6B). These simulations suggest that although extra-tropical North Atlantic cooling has a prominent effect on the (sub)tropical atmosphere, changes in low-level moisture transport across the Central American isthmus are mainly controlled by the size and position of the AWP.

Discussion

Our simulations of the glacial atmosphere revealed an inverse relation between the size of the AWP and the strength of the easterly trade winds, resembling the Gill-type atmosphere response (Gill, 1980; Wang et al., 2008b). Due to this influence on wind speeds in the lower atmosphere, changes in AWP area resulted in inverse changes in low-level atmospheric moisture transport from the Atlantic across the Central American isthmus towards the Pacific. We found a similar response in the NCEP/NCAR reanalysis (Kalnay et al., 1996) and Wang et al. (2008b) also observe this response in the NCAR CAM3 model. This similarity suggests a common model response to AWP area changes. Our glacial simulations also revealed that the easterly moisture flow over the isthmus was reduced when high-latitudinal North Atlantic cooling occurred besides a persistently expanding AWP. These responses reveal the sensitivity of cross-isthmus moisture transport to temperature changes in the region of the (modern) AWP in addition to extra-tropical North Atlantic cooling. In contrast, typical 'water-hosing' experiments do not show consistent changes in cross-isthmus moisture transport between models (Richter and Xie., 2010). Considering that some coupled ocean-atmosphere models exhibit a cold SST bias in the region of the modern AWP (Breugem et al., 2008; Misra et al., 2009), we suggest that part of the inconsistency may be related to underestimation of low-latitude North Atlantic SST dynamics in simulations of the glacial climate.

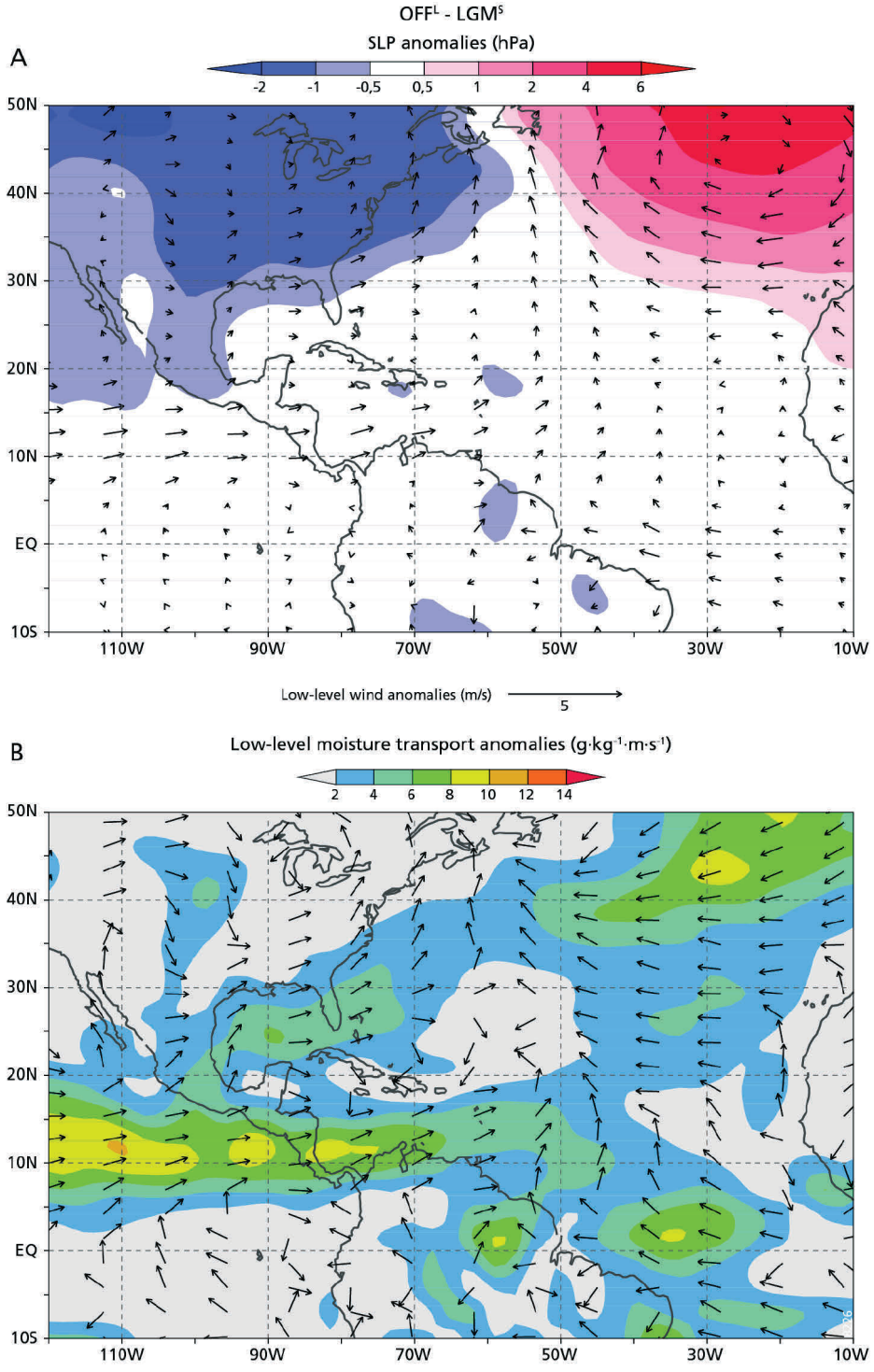

Figure 5.6 Simulated response of the glacial atmosphere to extra-tropical North Atlantic cooling besides a persistently expanding AWP. (A) Anomalous sea level pressure (SLP) and low-level wind anomalies averaged between the surface and the 700 hPa pressure level between the OFF^{L} and LGM^{S} simulations. Shading indicates the pressure anomalies, vectors indicate the magnitude and direction of the wind speed anomalies. (B) Anomalous low-level moisture transport averaged between the surface and the 700 hPa pressure level between the OFF^{L} and LGM^{S} simulations. Shading indicates the magnitude of the change, vectors denote the direction of change.

Correctly resolving the atmospheric moisture flux across the Central American isthmus is important to understand (glacial) climate dynamics because changes in cross-isthmus moisture transport play a role in (de)stabilizing the AMOC by altering the North Atlantic freshwater budget (Rahmstorf, 1996; Leduc et al., 2007). Estimates of present-day atmospheric moisture fluxes across the Central American isthmus are model dependent and range from 0.29 to 1.05 Sv (Richter and Xie, 2010). Although these fluxes may appear small in relation to the 17 Sv of (salt) water transported by the AMOC (Rahmstorf, 1996), estimates of the stability of the glacial AMOC suggest that an additional freshwater input of 0.05-0.1 Sv in the North Atlantic may be sufficient to induce AMOC collapse (Weber and Drijfhout, 2007). Considering the most conservative estimate of AMOC stability, a 10-35% decrease in cross-isthmus moisture transport may therefore be sufficient to destabilize the glacial AMOC. Alternatively, an increase in moisture transport makes the AMOC less vulnerable to other sources of freshwater, such as glacial meltwater. As our modelling results reveal changes in cross-isthmus moisture transport of similar magnitude, the AWP may have played a role in (de)stabilizing the glacial AMOC.

Our review of SST reconstructions from the (sub)tropical North Atlantic region provided evidence for the existence of an AWP in the Caribbean Sea and Gulf of Mexico during glacial summers (Ziegler et al., 2008). Although the question how far these warm (sub)tropical waters evolved beyond the Caribbean Sea and Gulf of Mexico remained unresolved, the cooling observed on the Bermuda rise and the Iberain margin suggested that AWP expansion was most likely inhibited after the disruption of the AMOC. A potential mechanism responsible for this subtropical cooling is the southward advection of anomalously cold North Atlantic surface waters via the Canary current following AMOC collapse (Zhao et al., 1995; Bard et al., 2000). The idea of reduced AWP expansion under AMOC collapse is supported by modern observations which indicate that anomalously small AWPs tend to develop when the extra-tropical North Atlantic is anomalously cold (Wang et al., 2008a). Alternatively, increased seasonality may have led to intense winter cooling during periods of AMOC collapse with less or no cooling during summer (Denton et al., 2005; Ziegler et al., 2008). In contrast to surface cooling during AMOC collapse, subsurface warming is documented in the North Atlantic at intermediate depths in relation to a weakening of the AMOC (Marcott et al., 2011). Marcott et al. (2011) propose that this subsurface warming may have triggered the Heinrich events by contributing to the decay of the Laurentide ice sheet. Sea surface warming is observed in the tropical Northeast Atlantic prior to and during Heinrich events (Zarriess et al., 2011) and provides a potential link with the hypothesis of low-latitude heat retention with a reduced AMOC (Rühlemann et al., 1999; Schmidt et al., 2004). This evidence suggests that the AWP persisted to expand prior to AMOC collapse but that its summer-time expansion was inhibited after AMOC collapse. Based on this SST response, our simulations suggest that cross-isthmus moisture transport decreased during the onset of Heinrich events, and increased during the later stages of Heinrich events. The decrease in freshwater export from the Atlantic basin during the initial stages of Heinrich events may thereby have contributed to AMOC collapse. The increase in freshwater export during the later stages of the Heinrich events may have acted to aid AMOC recovery from a disrupted state.

Reconstructions of sea surface salinities near the Central American isthmus may provide empirical evidence for changes in cross-isthmus moisture transport because they reflect precipitation and evaporation fluxes (Benway and Mix, 2004). When studying salinity changes observed on the Caribbean and Pacific sides of the isthmus during Heinrich events, Leduc et al. (2007) noted pronounced salinity increases on both sides of the isthmus. These salinity increases were interpreted to reflect a southward displacement of the ITCZ. Leduc et al. (2007) also noted that salinity increases were larger on the Pacific side of the isthmus than at the Atlantic side. Under the assumption that precipitation at the Pacific side of the isthmus consists of water evaporated in the Atlantic basin, Leduc et al. (2007) argued that cross-isthmus moisture transport was reduced during Heinrich events. This inferred decrease in freshwater export from the Atlantic basin was interpreted by Leduc et al. (2007) to constitute a destabilizing (positive) feedback with the AMOC during the Heinrich events. Whether these reconstructed changes in cross-isthmus moisture transport provide support for our model simulations depends on the timing of the reconstructed moisture transport changes in relation to the low-latitude SST responses. However, dating uncertainties complicate the inference of phase relations between the various components of the climate system during these rapid climate fluctuations (Ganopolski and Roche, 2009). Regardless of timing, the key insight obtained from the salinity records near the isthmus was that considerable changes in moisture fluxes occurred in relation to millennial-scale climate variability (Benway et al., 2006; Lachniet et al., 2009). In addition to ENSO-like ocean-atmospheric dynamics (Prange et al., 2010), our model results may explain these fluctuations in cross-isthmus moisture transport from changes in AWP expansion in relation to extra-tropical North Atlantic cooling.

The aim of our study was to test the sensitivity of the glacial atmosphere and the (sub)tropical hydrological cycle to variations in AWP expansion during millennial-scale climate fluctuations. It could be argued that higher resolution atmospheric models are required to resolve the atmospheric flow over the Caribbean Sea and across the Central American isthmus (Xu et al., 2005; Richter and Xie, 2010). However, the simulated responses of the glacial atmosphere to AWP variability were comparable to those simulated by higher resolution models (Wang, 2007; Wang and Lee, 2007; Wang et al., 2008b). Our results therefore rather emphasize the importance to constrain the spatial and temporal dynamics of the glacial AWP with additional empirical evidence and appropriate ocean models. Important for modelling the glacial AWP is to correctly resolve the warm SSTs in the (sub)tropical Northwest Atlantic, which remains problematic (Breugem et al., 2008; Misra et al., 2009). Eddy-resolving detail might be required to simulate the wind-driven currents through the Caribbean Sea (Johns et al., 2002) and the Loop Current in the Gulf of Mexico (Chang and Oey, 2011). Based on our simulations we conclude that the AWP may have played a role in altering the (sub)tropical hydrological cycle in relation to millennial-scale climate oscillations. Yet, additional work is required to resolve the spatial and temporal dynamics of the AWP to fully appreciate its role in constituting feedbacks in the (glacial) climate system.

Acknowledgements

We sincerely thank Maarten B. Eppinga, Guillaume Leduc, Gert-Jan Reichart, Martin Ziegler and two anonymous reviewers for their insightful comments on the manuscript. This research was funded by the High Potential project of Utrecht University.

References

Alley, R., Clark, P.U., Keigwin, L.D., Webb, R.S., Al, E., 1999. Making sense of millennial-scale climate change. In: Mechanisms of Global Climate Change at Millennial Time Scales. Geophysical Monograph (112), 385–394. American Geophysical Union.

Alley, R.B., 1998. Palaeoclimatology: Icing the North Atlantic. Nature 392, 335–337.

Anand, P., Elderfield, H., Conte, M.H., 2003. Calibration of Mg/Ca thermometry in planktonic foraminifera from a sediment trap time series. Paleoceanography 18, 15 PP.

Bard, E., Rostek, F., Turon, J.-L., Gendreau, S., 2000. Hydrological Impact of Heinrich Events in the Subtropical Northeast Atlantic. Science 289, 1321–1324.

Benway, H., Mix, A.C., 2004. Oxygen isotopes, upper-ocean salinity, and precipitation sources in the eastern tropical Pacific. Earth and Planetary Science Letters 224, 493–507.

Benway, H., Mix, A.C., Haley, B.A., Klinkhammer, G.P., 2006. Eastern Pacific Warm Pool paleosalinity and climate variability: 0–30 kyr. Paleoceanography 21, 11 PP.

Bond, G., Broecker, W., Johnsen, S., McManus, J., Labeyrie, L., Jouzel, J., Bonani, G., Ivy, S., 1993. Correlations between climate records from North Atlantic sediments and Greenland ice. Nature 365, 143–147.

Bond, G., Heinrich, H., Broecker, W., Labeyrie, L., McManus, J., Andrews, J., Huon, S., Jantschik, R., Clasen, S., Simet, C., Tedesco, K., Klas, M., Bonani, G., Ivy, S., 1992. Evidence for massive discharges of icebergs into the North Atlantic ocean during the last glacial period. Nature 360, 245–249.

Breugem, W.-P., Chang, P., Jang, C.J., Mignot, J., Hazeleger, W., 2008. Barrier layers and tropical Atlantic SST biases in coupled GCMs. Tellus A 60, 885–897.

Broccoli, A.J., Dahl, K.A., Stouffer, R.J., 2006. Response of the ITCZ to Northern Hemisphere cooling. Geophys. Res. Lett. 33, 4 PP.

Broecker, W.S., 1994. Massive iceberg discharges as triggers for global climate change. Nature 372, 421–424.

Broecker, W.S., 2003. Does the Trigger for Abrupt Climate Change Reside in the Ocean or in the Atmosphere? Science 300, 1519 –1522.

Chang, Y.-L., Oey, L.-Y., 2011. Loop Current Cycle: Coupled Response of the Loop Current with Deep Flows. Journal of Physical Oceanography 41, 458–471.

Cook, K.H., Vizy, E.K., 2010. Hydrodynamics of the Caribbean Low-Level Jet and Its Relationship to Precipitation. J. Climate 23, 1477–1494.

Dansgaard, W., Johnsen, S.J., Clausen, H.B., Dahl-Jensen, D., Gundestrup, N.S., Hammer, C.U., Hvidberg, C.S., Steffensen, J.P., Sveinbjornsdottir, A.E., Jouzel, J., Bond, G., 1993. Evidence for general instability of past climate from a 250-kyr ice-core record. Nature 364, 218–220.

Denton, G.H., Alley, R.B., Comer, G.C., Broecker, W.S., 2005. The role of seasonality in abrupt climate change. Quaternary Science Reviews 24, 1159–1182.

Donders, T.H., Boer, H.J. de, Finsinger, W., Grimm, E.C., Dekker, S.C., Reichart, G.-J., Wagner-Cremer, F., 2011. Impact of the Atlantic Warm Pool on precipitation and temperature in Florida during North Atlantic cold spells. Clim Dyn 36, 109–118.

Flower, B.P., Hastings, D.W., Hill, H.W., Quinn, T.M., 2004. Phasing of deglacial warming and Laurentide Ice Sheet meltwater in the Gulf of Mexico. Geology 32, 597 –600.

Fraedrich, Jansen, H., Kirk, E., Luksch, U., Lunkeit, F., 2005. The Planet Simulator: Towards a user friendly model. Meteorologische Zeitschrift 299–304(6).

Ganopolski, A., Roche, D.M., 2009. On the nature of lead–lag relationships during glacial–interglacial climate transitions. Quaternary Science Reviews 28, 3361–3378.

Gill, A.E., 1980. Some simple solutions for heat-induced tropical circulation. Quarterly Journal of the Royal Meteorological Society 106, 447–462.

Goosse, H., Brovkin, V., Fichefet, T., Haarsma, R., Huybrechts, P., Jongma, J., Mouchet, A., Selten, F., Barriat, P.-Y., Campin, J.-M., Deleersnijder, E., Driesschaert, E., Goelzer, H., Janssens, I., Loutre, M.-F., Morales Maqueda, M.A., Opsteegh, T., Mathieu, P.-P., Munhoven, G., Pettersson, E.J., Renssen, H., Roche, D.M., Schaeffer, M., Tartinville, B., Timmermann, A., Weber, S.L., 2010. Description of the Earth system model of intermediate complexity LOVECLIM version 1.2. Geoscientific Model Development Discussions 3, 309–390.

Goosse, H., Fichefet, T., 1999. Importance of ice-ocean interactions for the global ocean circulation: A model study. J. Geophys. Res. 104, PP. 23,337–23,355.
Graham, N.E., Barnett, T.P., 1987. Sea Surface Temperature, Surface Wind Divergence, and Convection over Tropical Oceans. Science 238, 657–659.
Grimm, E.C., Watts, W.A., Jacobson Jr., G.L., Hansen, B.C.S., Almquist, H.R., Dieffenbacher-Krall, A.C., 2006. Evidence for warm wet Heinrich events in Florida. Quaternary Science Reviews 25, 2197–2211.
Grosfeld, K., Lohmann, G., Rimbu, N., Fraedrich, K., Lunkeit, F., 2007. Atmospheric multidecadal variations in the North Atlantic realm: proxy data, observations, and atmospheric circulation model studies. Clim. Past 3, 39–50.
Haberkorn, K., Sielmann, F., Lunkeit, F., Kirk, E., Schneidereit, A., Fraedrich, K., 2009. Planet Simulator Climate. Meteorologisches Institut, Universität Hamburg.
Heinrich, H., 1988. Origin and consequences of cyclic ice rafting in the Northeast Atlantic Ocean during the past 130,000 years. Quaternary Research 29, 142–152.
Johns, W.E., Townsend, T.L., Fratantoni, D.M., Wilson, W.D., 2002. On the Atlantic inflow to the Caribbean Sea. Deep Sea Research Part I: Oceanographic Research Papers 49, 211–243.
Johnson, N.C., Xie, S.-P., 2010. Changes in the sea surface temperature threshold for tropical convection. Nature Geosci 3, 842–845.
Kalnay, E., Kanamitsu, M., Kistler, R., Collins, W., Deaven, D., Gandin, L., Iredell, M., Saha, S., White, G., Woollen, J., Zhu, Y., Chelliah, M., Ebisuzaki, W., Higgins, W., Janowiak, J., Mo, K.C., Ropelewski, C., Wang, J., Leetmaa, A., Reynolds, R., Jenne, R., Joseph, D., 1996. The NCEP/NCAR 40-year reanalysis project. Bulletin of the American Meteorological Society 77, 437–471.
Lachniet, M.S., Johnson, L., Asmerom, Y., Burns, S.J., Polyak, V., Patterson, W.P., Burt, L., Azouz, A., 2009. Late Quaternary moisture export across Central America and to Greenland: evidence for tropical rainfall variability from Costa Rican stalagmites. Quaternary Science Reviews 28, 3348–3360.
Leduc, G., Vidal, L., Tachikawa, K., Rostek, F., Sonzogni, C., Beaufort, L., Bard, E., 2007. Moisture transport across Central America as a positive feedback on abrupt climatic changes. Nature 445, 908–911.
Marcott, S.A., Clark, P.U., Padman, L., Klinkhammer, G.P., Springer, S.R., Liu, Z., Otto-Bliesner, B.L., Carlson, A.E., Ungerer, A., Padman, J., He, F., Cheng, J., Schmittner, A., 2011. Ice-shelf collapse from subsurface warming as a trigger for Heinrich events. PNAS 108(33) 13415-13419
Misra, V., Chan, S., Wu, R., Chassignet, E., 2009. Air-sea interaction over the Atlantic warm pool in the NCEP CFS. Geophys. Res. Lett. 36, 6 PP.
Muñoz, E., Busalacchi, A.J., Nigam, S., Ruiz-Barradas, A., 2008. Winter and Summer Structure of the Caribbean Low-Level Jet. J. Climate 21, 1260–1276.
NGRIP-Members, 2004. High-resolution record of Northern Hemisphere climate extending into the last interglacial period. Nature 431, 147–151.
Nurnberg, D., Ziegler, M., Karas, C., Tiedemann, R., Schmidt, M., 2008. Interacting Loop Current variability and Mississippi River discharge over the past 400 kyr. Earth and Planetary Science Letters 272, 278–289.
Opsteegh, J.D., Haarsma, R.J., Selten, F.M., Kattenberg, A., 1998. ECBILT: a dynamic alternative to mixed boundary conditions in ocean models. Tellus A 50, 348–367.
Peltier, W.R., 1994. Ice Age Paleotopography. Science 265, 195 –201.
Peterson, L.C., Haug, G.H., 2006. Variability in the mean latitude of the Atlantic Intertropical Convergence Zone as recorded by riverine input of sediments to the Cariaco Basin (Venezuela). Palaeogeography, Palaeoclimatology, Palaeoecology 234, 97–113.
Prange, M., Steph, S., Schulz, M., Keigwin, L.D., 2010. Inferring moisture transport across Central America: Can modern analogs of climate variability help reconcile paleosalinity records? Quaternary Science Reviews 29, 1317–1321.
Rahmstorf, S., 1996. On the freshwater forcing and transport of the Atlantic thermohaline circulation. Clim Dyn 12, 799–811.

Rashid, H., Hesse, R., Piper, D.J.W., 2003. Evidence for an additional Heinrich event between H5 and H6 in the Labrador Sea. Paleoceanography 18, 1077–1092.
Rayner, N.A., Brohan, P., Parker, D.E., Folland, C.K., Kennedy, J.J., Vanicek, M., Ansell, T.J., Tett, S.F.B., 2006. Improved Analyses of Changes and Uncertainties in Sea Surface Temperature Measured In Situ since the Mid-Nineteenth Century: The HadSST2 Dataset. J. Climate 19, 446–469.
Richter, I., Xie, S.-P., 2010. Moisture transport from the Atlantic to the Pacific basin and its response to North Atlantic cooling and global warming. Clim Dyn 35, 551–566.
Roche, D.M., Dokken, T.M., Goosse, H., Renssen, H., Weber, S.L., 2007. Climate of the Last Glacial Maximum: sensitivity studies and model-data comparison with the LOVECLIM coupled model. Clim. Past 3, 205–224.
Roche, D.M., Wiersma, A.P., Renssen, H., 2010. A systematic study of the impact of freshwater pulses with respect to different geographical locations. Clim Dyn 34, 997–1013.
Rühlemann, C., Mulitza, S., Muller, P.J., Wefer, G., Zahn, R., 1999. Warming of the tropical Atlantic Ocean and slowdown of thermohaline circulation during the last deglaciation. Nature 402, 511–514.
Sachs, J.P., Lehman, S.J., 1999. Subtropical North Atlantic Temperatures 60,000 to 30,000 Years Ago. Science 286, 756–759.
Salgueiro, E., Voelker, A.H.L., de Abreu, L., Abrantes, F., Meggers, H., Wefer, G., 2010. Temperature and productivity changes off the western Iberian margin during the last 150 ky. Quaternary Science Reviews 29, 680–695.
Schmidt, M.W., Spero, H.J., Lea, D.W., 2004. Links between salinity variation in the Caribbean and North Atlantic thermohaline circulation. Nature 428, 160–163.
Stocker, T.F., 1998. The Seesaw Effect. Science 282, 61–62.
Stoner, J.S., Channell, J.E.T., Hillaire-Marcel, C., Kissel, C., 2000. Geomagnetic paleointensity and environmental record from Labrador Sea core MD95-2024: global marine sediment and ice core chronostratigraphy for the last 110 kyr. Earth and Planetary Science Letters 183, 161–177.
Wang, C., 2007. Variability of the Caribbean Low-Level Jet and its relations to climate. Clim Dyn 29, 411–422.
Wang, C., Enfield, D.B., Lee, S., Landsea, C.W., 2006. Influences of the Atlantic Warm Pool on Western Hemisphere Summer Rainfall and Atlantic Hurricanes. J. Climate 19, 3011–3028.
Wang, C., Lee, S., 2007. Atlantic warm pool, Caribbean low-level jet, and their potential impact on Atlantic hurricanes. Geophys. Res. Lett. 34, 5 PP.
Wang, C., Lee, S.-K., Enfield, D.B., 2008a. Atlantic Warm Pool acting as a link between Atlantic Multidecadal Oscillation and Atlantic tropical cyclone activity. Geochem. Geophys. Geosyst. 9, 16 PP.
Wang, C., Lee, S.-K., Enfield, D.B., 2008b. Climate Response to Anomalously Large and Small Atlantic Warm Pools during the Summer. J. Climate 21, 2437–2450.
Weber, S. L. and Drijfhout, S. S., 2007. Stability of the Atlantic Meridional Overturning Circulation in the Last Glacial Maximum climate, Geophys. Res. Lett., 34, 5 PP.
Xu, H., Xie, S.-P., Wang, Y., Small, R.J., 2005. Effects of Central American Mountains on the Eastern Pacific Winter ITCZ and Moisture Transport. J. Climate 18, 3856–3873.
Zarriess, M., Johnstone, H., Prange, M., Steph, S., Groeneveld, J., Mulitza, S., Mackensen, A., 2011. Bipolar seesaw in the northeastern tropical Atlantic during Heinrich stadials. Geophys. Res. Lett. 38, 6 PP.
Zaucker, F., Broecker, W.S., 1992. The Influence of Atmospheric Moisture Transport on the Fresh Water Balance of the Atlantic Drainage Basin: General Circulation Model Simulations and Observations. J. Geophys. Res. 97, PP. 2765–2773.
Zhao, M., Beveridge, N.A.S., Shackleton, N.J., Sarnthein, M., Eglinton, G., 1995. Molecular stratigraphy of cores off northwest Africa: Sea surface temperature history over the last 80 Ka. Paleoceanography 10, PP. 661–675.
Ziegler, M., Nurnberg, D., Karas, C., Tiedemann, R., Lourens, L.J., 2008. Persistent summer expansion of the Atlantic Warm Pool during glacial abrupt cold events. Nature Geosci 1, 601–605.

Chapter 6

A critical transition in leaf evolution sparked the Cretaceous angiosperm revolution

Hugo Jan de Boer, Maarten B. Eppinga, Martin J. Wassen and Stefan C. Dekker
(Manuscript is under review with *Nature Communications*)

Abstract

The revolutionary rise of broad-leaved (flowering) angiosperm plant species during the Cretaceous initiated a global ecological transformation towards modern biodiversity. The mechanism that sparked this sudden angiosperm success remained unrevealed. Falling atmospheric CO_2 concentrations likely drove angiosperm leaf evolution towards higher stomatal conductance and more reticulated venation during this period. We found that angiosperm evolution sparked after the leaf interior (post-venous) transport path length for water was reduced beyond the leaf interior transport path length for CO_2 at a critical leaf vein density of 3-8 mm·mm^{-2}. Our data and modelling approaches suggest that surpassing this critical vein density initiated a critical transition in leaf evolution that triggered evolving angiosperms to increase their gas exchange capacity by developing leaves with more and smaller stomata. The subsequent rise in carbon uptake enabled evolving angiosperms to invest in expanding their water transport system. We propose that these adaptations sparked the angiosperm rise to global ecological dominance.

Introduction

Almost 90% of present-day terrestrial plant biodiversity consists of flowering (angiosperm) species[1]. The ecological success of angiosperms did not grow gradually, rather, they appeared so suddenly in the fossil record of the Cretaceous period (between 145 and 66 million years ago) that Charles Darwin feared it challenged his ideas on gradual evolution[2,3]. Evidence is now emerging that ancestral angiosperms existed in low evaporative niches during the Early Cretaceous[4,5] prior to the period of their rapid diversification in the Mid Cretaceous[6]. During the Late Cretaceous, evolving angiosperms spread poleward[7] and gained ecological dominance in most of our planet's ecosystems by replacing needle-leaved (gymnosperm) conifer tree species in the upper canopy[8] (Figure 6.1A). Previous explanations for this angiosperm radiation[1] include coevolution with insects[9] and positive environmental feedbacks[10]. Recent insights suggest that the evolution towards more reticulated leaf venation[11,12] was linked to the escalation of angiosperm leaf gas exchange capacity during this floral regime shift[13,14]. The resulting rise in productivity likely enabled evolving angiosperms to outcompete conifers in the upper canopy[15]. However, the underlying mechanism which sparked the angiosperm revolution remains unexplained.

Falling atmospheric CO_2 concentrations (C_a) prior to the angiosperm radiation[16] (Figure 6.1B) put evolutionary pressure on terrestrial C3 plants[17] because carbon uptake for photosynthesis is intrinsically linked to transpirative water loss through the stomatal pores on their leaf surfaces[18]. Natural selection may therefore have favoured those species with most plastic stomatal traits[19,20] capable of optimising photosynthesis with minimal transpiration[17,21]. As a result, falling C_a drove leaf evolution towards higher maximal stomatal conductance (g_{smax})[22]. The physical properties of stomatal gas exchange are principally governed by diffusion and adhere to Stefan's diameter law[23]. Stefan's law states that the rate of evaporation relative to the evaporative surface area increases with a diminishing pore size. As leaf surface area is finite, the evolution towards higher g_{smax} was therefore linked to a reduction in the pore size of fully opened stomata and an increase in stomatal density (D_s)[22] (Figure 6.1C). The development of leaves with more conductive surfaces also required expansion of the leaf's water transport system to prevent desiccation[24]. This adaptation is revealed in the geologic record by rising angiosperm leaf vein density (D_v)[13,14] (Figure 6.1D). The sudden competitive success of angiosperms in the (dryer) upper canopy may therefore have been initiated by a new-found ability to increase g_{smax} with more and smaller stomata combined with an ability to answer the additional hydraulic demand by increasing D_v. However, to benefit from such highly conductive leaves in terms of additional growth and reproduction, the required additional carbon investments in water transport tissue should have been paid off by a larger increase in carbon gain[12].

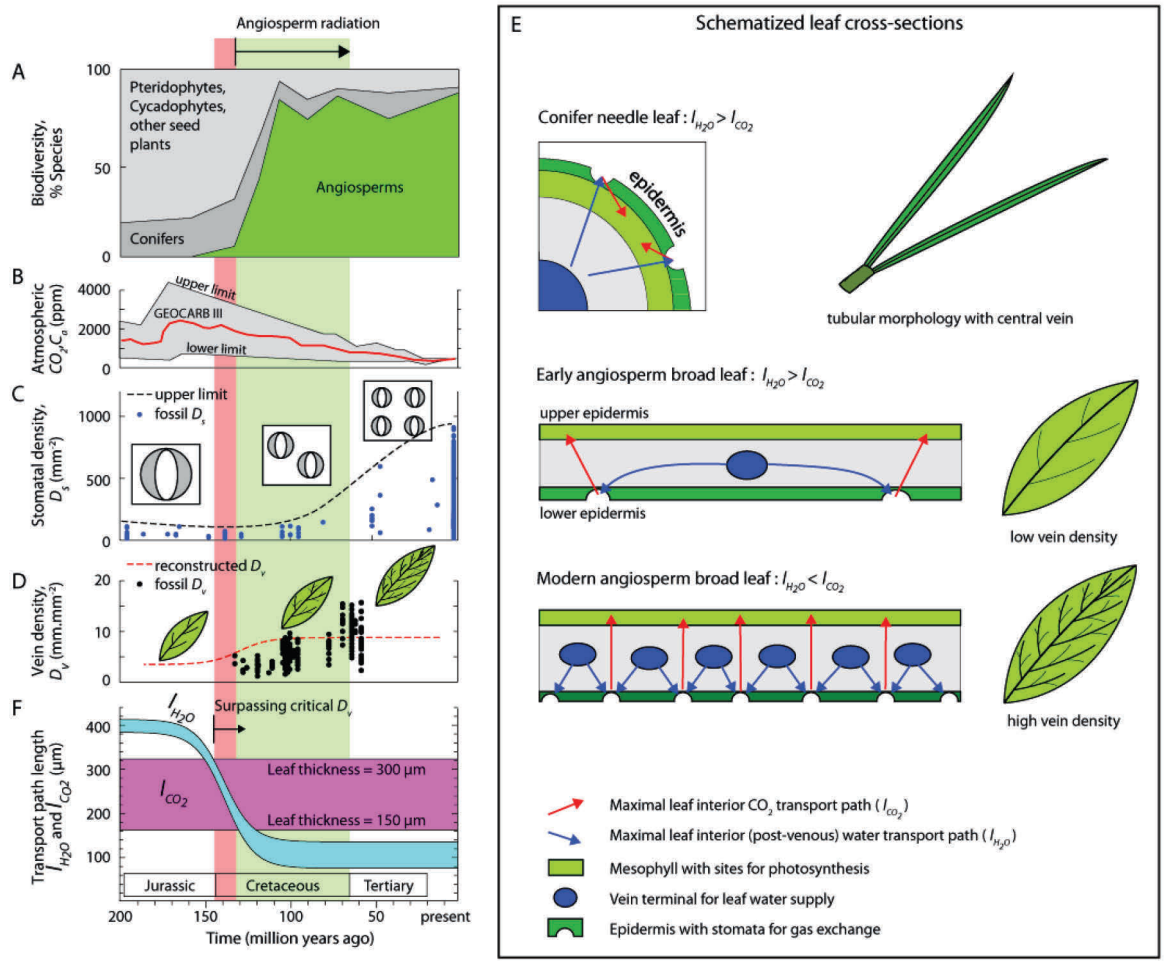

Figure 6.1 The angiosperm evolution sparked when the maximum leaf interior transport distance for water vapour (l_{H2O}) became shorter than the maximum leaf interior transport distance for CO_2 (l_{CO2}) at a critical leaf vein density (D_v) of 3-8 mm·mm^{-2}. (A) The angiosperm radiation occurred at the expense of pteridophytes (horsetails, ferns) and cycadophytes (cycades) living near the forest floor and conifers dominating the upper canopy[1,6–8]. (B) Reconstructed atmospheric CO_2 concentrations (C_a) from the GEOCARB III model[16]. (C) Falling C_a required rising maximal stomatal conductance (g_{smax}) via decreasing pore size and rising stomatal density (D_s)[17,22]. (D) Rising angiosperm D_v obtained from fossil leaves[14] and age-calibrated ancestral state analyses[13]. The sigmoid curve is based on the equation: $D_v = 3.3 + 5.3 / (1+e^{-(Time - 130)/-8.7})$ following Brodribb et al.[13] (E) Schematized cross-sections of a conifer needle leaf (top) with l_{H2O} longer than l_{CO2}, an early hypostomatous angiosperm broad leaf (middle) with low D_v and l_{H2O} longer than l_{CO2}, and a modern hypostomatous angiosperm broad leaf (bottom) with high D_v and l_{H2O} shorter than l_{CO2}. (F) Changes in angiosperm l_{H2O} and l_{CO2}, as calculated from reconstructed angiosperm D_v, as shown in Figure 6.1E. These results reveal that surpassing the critical D_v (at which l_{H2O} became shorter than l_{CO2}) occurred at the onset of angiosperm the radiation.

Results

Based on a combination of data and modelling approaches we propose and substantiate a novel mechanism to explain why evolving angiosperms could suddenly afford to expand their water transport system and increase productivity during the Cretaceous, and why conifers could not. This proposed mechanism is based on the consequences of morphological differences between planar shaped hypostomatous (angiosperm) broad leaves and tubular shaped (conifer) needle leaves for the leaf interior transport path lengths of CO_2 and water (Figure 6.1E). The leaf interior transport paths for CO_2 and water start/end at the same stomatal pores but end/start in the chloroplasts and leaf vein endings, respectively[25,26]. It is relevant to consider the different lengths of these transport paths because they may influence the transport of CO_2 and water vapour in the leaf interior. Importantly, diffusion around individual stomata inside the leaf is a 3-dimensional process whereby the driving concentration gradients are altered both by the length of the diffusion path and by the size of the stomatal pore[26]. We used schematized leaf morphologies of broad-leaved angiosperms and needle-leaved conifers to calculate the maximum leaf interior (post-venous) transport path length for water (l_{H2O}) and the maximum leaf interior transport path length for CO_2 (l_{CO2}). The calculation of these leaf interior transport distances is presented in section E1 of Appendix E. Our analysis revealed a fundamental difference between angiosperms and conifers. In the schematized needle leaf, l_{H2O} is always longer than l_{CO2} due to the central-veined and tubular morphology. In the schematized broad-leaf with D_v in the range observed in leaves of Early Cretaceous angiosperms[13,14] the l_{H2O} is also longer than l_{CO2}. However, when leaf venation increases beyond a critical density of 3-8 $mm \cdot mm^{-2}$ l_{H2O} becomes shorter than l_{CO2} (Figure E1, in Appendix E). Following the reconstructed evolution in angiosperm leaf venation[13], l_{H2O} became shorter than l_{CO2} right at the onset of the Cretaceous angiosperm radiation (Figure 6.1F).

We hypothesize that surpassing this critical D_v gave evolving angiosperms a competitive advantage over conifers when falling C_a required rising g_{smax} via increases in D_s and decreases in stomatal pore size. Key to the proposed mechanism is that, due to the 3-dimensional character of diffusion around individual stomata inside the leaf, differences in l_{CO2} and l_{H2O} will alter the trade-off between CO_2 transport and water vapour transport through the leaf interior. The proposed mechanism is illustrated for the diffusive fluxes of two conceptual substances (J_X, J_Y) with equal diffusivity (assumed unity) driven by an equal concentration difference (also assumed unity) over different radial distances (l_X and l_Y) from a single hemispherical pore with variable radius (r_a) (Figure 6.2A). The first implication shown by this example is that the diffusive flux is highest of that substance which diffuses over the shortest radial distance. The second implication is that a change in pore radius has the largest effect on the flux of that substance which diffuses over the shortest radial distance. Interpreting this example for leaf-interior fluxes of CO_2 and water vapour around individual stomata inside the leaf first of all suggests that the highest carbon return from water loss can be achieved when l_{H2O} is longer than l_{CO2}. This situation would resemble the diffusion distances in the schematized conifer and early

angiosperm leaf morphologies (cf. Figure 6.1E). Second, the example suggests that when l_{H2O} is shorter than l_{CO2}, as in the schematized modern angiosperm leaf morphology, a decrease in pore size may lead to a larger decrease in leaf interior water vapour transport than in CO_2 transport. Our hypothesis entails that when angiosperms surpassed the critical D_v they could increase leaf interior carbon transport relative to leaf interior water vapour transport by developing leaves with more and smaller stomatal pores. Such a change in stomatal properties will also have affected the gas exchange with the atmosphere. Surpassing the critical D_v may therefore have allowed evolving angiosperms to benefit more from the implications of Stefan's law by developing leaves with more and smaller stomata.

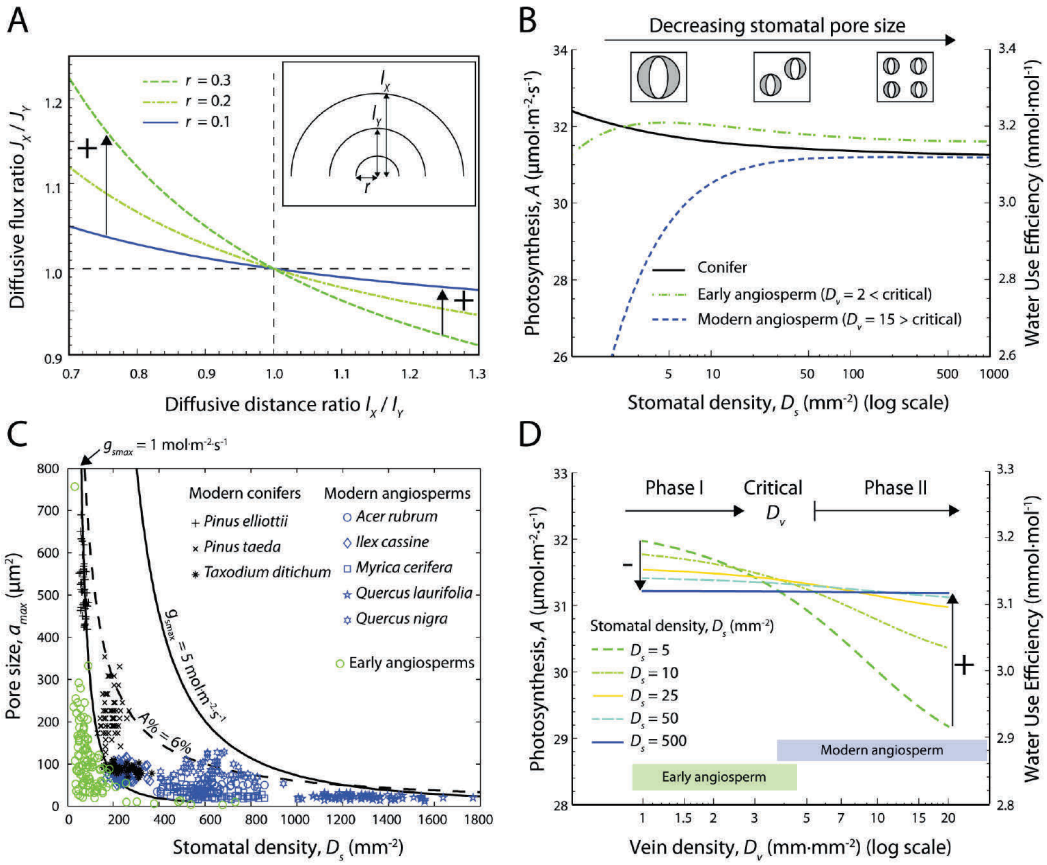

Figure 6.2 Surpassing the critical leaf vein density (D_v) provided evolving angiosperms with a carbon uptake advantage under falling atmospheric CO_2 concentrations (C_a). (A) Theoretical relation between diffusive fluxes of substances *X* and *Y* (J_x and J_y) relative to their respective radial diffusion distances (l_x and l_y) from a single hemispherical pore with variable radius r_a. This example is based on Eq. 6.6 in the Methods section[36]. (B) Simulated changes in maximum photosynthesis (A) with equal water loss for the conifer, and the early and modern angiosperm leaf morphologies as a function of stomatal density (D_s). Changes in D_s are associated with inverse changes in stomatal pore size to answer the constant water loss specified to the model. Water Use Efficiency (WUE) is indicated on the second y-axis. (C) Relation between D_s and the pore size of fully opened stomata (a_{max}) observed in modern angiosperms (blue symbols) and modern conifers (black symbols) from Florida[28] and extant relatives of early angiosperms (green symbols)[5]. Lines of equal maximal stomatal conductance (g_{smax}) and leaf surface area allocated to fully opened stomatal pores ($A_{\%}$) are indicated. (D) Angiosperms experienced a shift from falling (Phase I) to rising (Phase II) photosynthesis with equal water loss by increasing D_s after surpassing the critical D_v. WUE is indicated on the second y-axis. Ranges of D_v observed in early and modern angiosperms[14] are indicated.

We investigated the proposed mechanism with an analytical model of leaf gas exchange which coupled the diffusion pathways of CO_2 and water vapour between the atmosphere and the stomata to their respective diffusion pathways in the leaf interior. A graphical representation of our model approach is shown in Figure E2, in Appendix E2. We thereby considered the schematized morphologies of needle-leaved conifers and broad-leaved angiosperms, as shown in Figure 6.1E. To reveal the potential consequences of changes in stomatal pore size, D_s, and D_v on leaf gas exchange, we solved the model for maximum photosynthetic carbon returns from equal transpirative water loss. This approach linked changes in D_s to (inverse) changes in stomatal pore size to yield equal transpirative water loss in a constant evaporative environment. We then calculated how these changes in D_s and stomatal pore size altered photosynthesis relative to the (constant) amount of water loss. This analysis was based on the premise that the maximum water transport capacity of the whole plant constrains the maximum transpiration rate[27], which determines maximum photosynthesis and productivity in a specific evaporative environment[18].

Our model showed that the early angiosperm and conifer leaf morphologies allow for relatively high photosynthesis with equal water loss due to the relatively short distance for CO_2 transport and the relatively large distance for water transport inside the leaf (Figure 6.2B). A rise in D_s combined with a decrease in pore size led to diminishing carbon returns with equal water loss for these leaf morphologies. In contrast, the angiosperm leaf morphology with D_v beyond the critical density appeared relatively inefficient with low D_s but it may increase photosynthesis with equal water loss by developing leaves with higher D_s and smaller pores. As evolution will likely have favoured those individuals that achieve highest carbon returns from water loss, we may find evidence for the proposed mechanism in observations of D_s and stomatal pore sizes on the leaves of conifers, early angiosperms and modern angiosperms. We therefore compared observations of these stomatal properties of modern conifers and angiosperms from the mid to upper canopy of subtropical forests in Florida[28] with observations on extant relatives of Early Cretaceous angiosperms[5] (Figure 6.2C). Statistical comparisons are shown in Table E1 in Appendix E3. These data showed that modern angiosperms develop leaves with most and smallest stomata of the three groups. The differences in these stomatal properties also showed that the modern angiosperms profit most from the implications of Stefan's law and reach highest g_{smax} within the constraint of available leaf surface area. This effect of Stefan's law is illustrated by the solid and dashed lines in Figure 6.2C indicating g_{smax} and the percentage of leaf surface area allocated to fully opened stomatal pores ($A_{\%}$), respectively. These lines show that highest g_{smax} within the constraint of $A_{\%}$ may only be reached by developing leaves with many small stomata. Additional evaluation of the modelled relation between stomatal properties, leaf interior transport distances and leaf interior conductances is presented in Appendix E4.

The proposed ability of angiosperms that surpassed the critical D_v to profit from developing leaves with more and smaller stomata provides a mechanism to explain the revolutionary escalation of angiosperm leaf gas exchange during the Cretaceous. In accordance with fossil evidence[14] the mechanism entails that angiosperm evolution

occurred in two phases with the first phase linked to D_v rising up to the critical density, and a second phase during which their gas exchange capacity escalated. During the first evolutionary phase, our model revealed that decreasing pore size combined with rising D_s led to diminishing photosynthesis with equal water loss (Figure 6.2D). Our model revealed that when the critical D_v was surpassed evolving angiosperms could increase photosynthesis with equal water loss by developing leaves with more and smaller stomata. Surpassing the critical D_v may thereby have initiated the second phase in angiosperm evolution during which their leaf gas exchange capacity escalated[14].

Discussion

An important concept for the interpretation of these results is the idea that water loss presents a cost to plants. As a result, stomatal adaptations are aimed at the optimisation of carbon gain with minimal water loss[29,30] depending on environmental conditions[31]. This optimisation hypothesis may explain short-term stomatal opening and closing responses and the adaptation of g_{smax} at longer timescales[21,32]. Based on our results we propose to expand the concept of optimal gas exchange to describe the adjustments of stomatal pore size and D_s in relation to morphological adaptations in leaf evolution. As shown by observations in Figure 6.2C and indicated by the arrows in Figure 6.3A, our

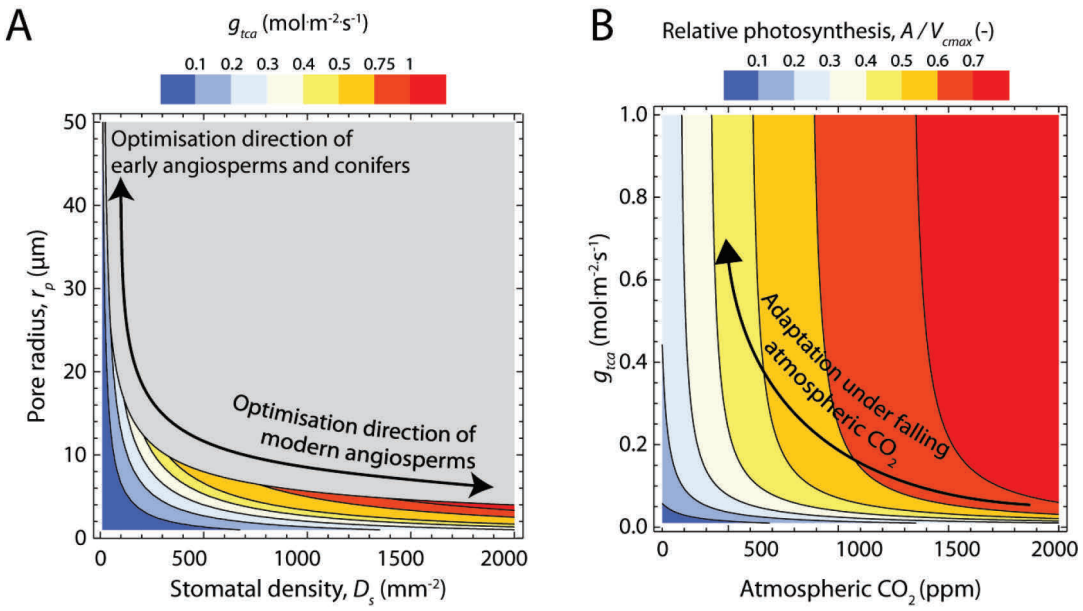

Figure 6.3 Proposed directions of stomatal optimisation in relation to stomatal adaptations required under falling atmospheric CO_2 concentrations (C_a) to prevent carbon 'starvation'. (A) Relations between stomatal density (D_s), stomatal pore radius (r_p) and total leaf conductance to CO_2 (g_{tc}). The proposed directions of stomatal optimisation by conifers, early angiosperms and modern angiosperms are indicated. Values of g_{tc} that require more than 10% of the leaf surface to be allocated to fully opened stomatal pores (the $A_{\%}$) are shaded gray. Highest g_{tc} can only be achieved within this constraint of $A_{\%}$ by developing leaves with high D_s and small r_p. (B) Falling C_a required a rise in g_{tc} to keep up photosynthesis. Maximum photosynthesis is scaled relative to maximum carboxylation rate (V_{cmax}) as changes in V_{cmax} likely occurred at geological timescales[17].

hypothesis entails that conifers and early angiosperms optimise their gas exchange by developing leaves with low D_s and large stomatal pores. In contrast, angiosperms that surpassed the critical D_v may optimise towards high D_s and small pores. Only angiosperms that have surpassed the critical D_v may therefore optimise their leaf gas exchange with stomatal adaptations in the direction that permit highest gas exchange within the constraint of $A_{\%}$. The resulting relation between pore size, D_s and the total leaf conductance to CO_2 (g_{tc}) in relation to the constraint posed by $A_{\%}$ is shown for the angiosperm leaf morphology in Figure 6.3A.

To interpret crossing of the critical D_v as a critical transition in angiosperm leaf evolution, we argue that falling C_a during the Cretaceous required plants to increase g_{tc} to prevent carbon 'starvation'[17] (Figure 6.3B). Due to the implications of Stefan's diameter law and the limited space on the leaf surface, higher g_{tc} can only be reached by developing leaves with more and smaller stomatal pores. As apparent in the fossil record[22], the Cretaceous C_a decline therefore required terrestrial plants to develop leaves with more and smaller stomata. An additional evolutionary development towards more reticulated leaf venation may have minimized the required carbon investment in water transport tissue[11,12] and facilitated a gradual rise in angiosperm leaf venation towards the critical D_v. Our results indicate that surpassing the critical D_v may have suddenly allowed evolving angiosperms to profit more from the implications of Stefan's law by developing leaves with more and smaller stomata, and higher g_{smax}. The subsequent rise in leaf gas exchange and carbon uptake could have allowed evolving angiosperms to invest in expanding their water transport system which enabled them to offset the transpirational demand of the upper canopy. This critical transition[33] in angiosperm leaf evolution is shown conceptually in Figure 6.4. Our results also suggest that conifers could not benefit similarly from developing leaves with more and smaller stomata due to the implications of their tubular leaf morphology. Consequently, the rise in angiosperm leaf gas exchange[14,15] may explain their sudden competitive success over conifers and explain their rapid speciation in dryer niches associated with the upper canopy[34]. These results imply that surpassing the critical D_v provided a tipping point in leaf evolution that sparked the Cretaceous angiosperms revolution at the expense of conifers.

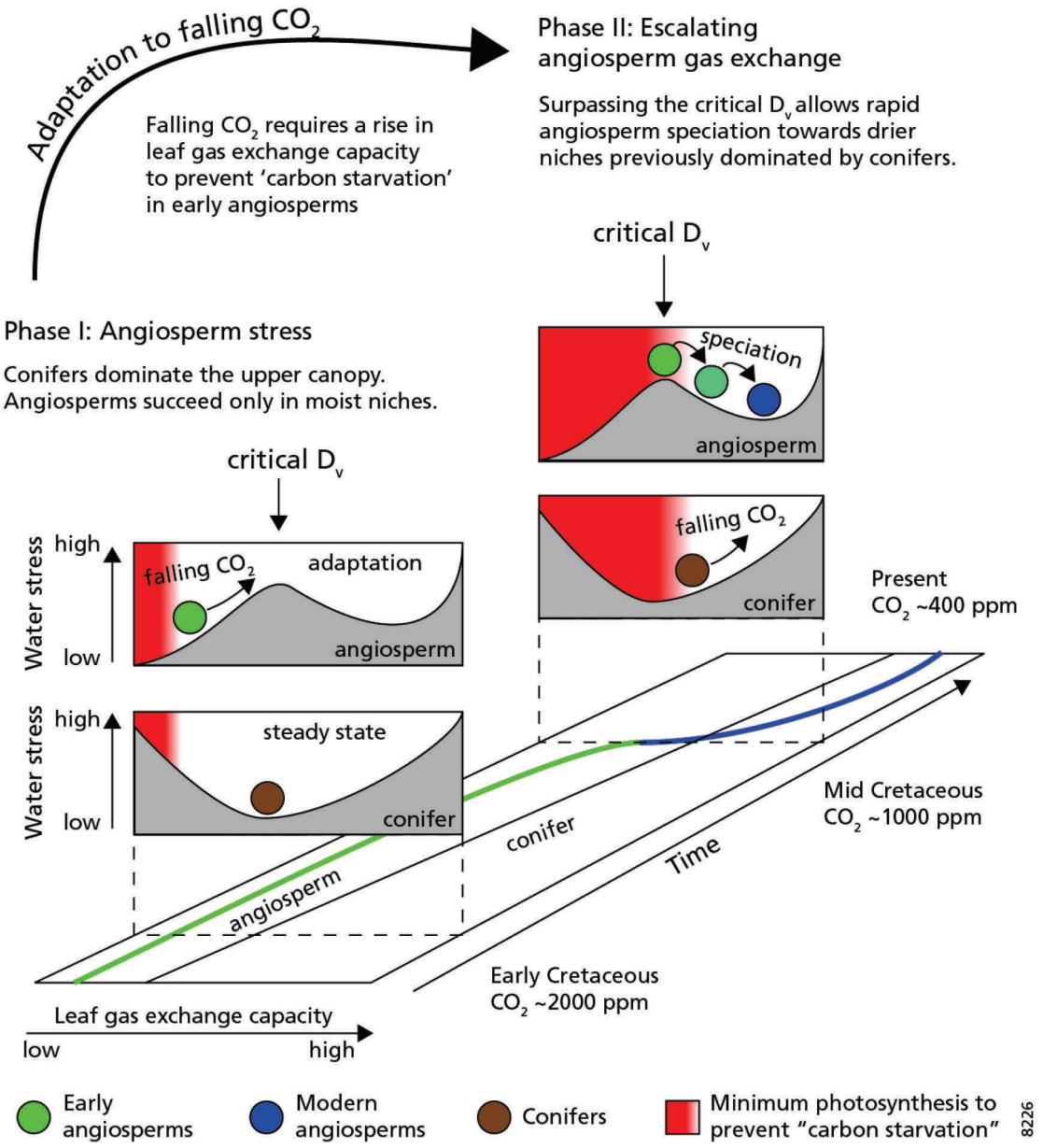

Figure 6.4 Overview of how surpassing the critical leaf vein density (D_v) may have resulted in a critical transition[33] in angiosperm leaf evolution. Evolution towards more reticulated leaf venation by angiosperms was likely driven by the need to limit the (carbon) cost associated with water transport[11,12] in order to prevent carbon starvation under the Cretaceous CO_2 decline[16]. This first phase in angiosperm evolution is indicated by the green ball being driven to the top of the hill-shaped water stress surface. Surpassing the critical D_v enabled evolving angiosperms to increase carbon returns from water loss by developing leaves with more and smaller stomata. This development likely enabled evolving angiosperms to reduce water stress and permit their functioning in dryer environments, such as the upper canopy. A similar carbon uptake advantage did not occur for conifers owing to their tubular leaf morphology. The resulting competitive advantage of evolving angiosperms over conifers may explain their competitive success and rapid speciation during the Cretaceous CO_2 decline[1,6–8].

METHODS

Stomatal size, density and conductance relations

The maximal stomatal conductance to water vapour (g_{smax}) and CO_2 (g_{cmax}) (both with the unit mol·m^{-2}·s^{-1}) were calculated from stomatal properties as[22]:

$$g_{s\max} = \frac{\frac{D_{H_2O}}{v} D_s a_{\max}}{p_d + \frac{\pi}{2}\sqrt{a_{\max}/\pi}} \quad \text{and} \quad g_{c\max} = g_{s\max}\frac{D_{CO_2}}{D_{H_2O}} \qquad (6.1, 6.2)$$

where D_{H2O} and D_{CO2} (m^2·s^{-1}) are the diffusivities of water vapour and CO_2, respectively, v (m^3·mol^{-1}) is the molar volume of air, D_s is the stomatal density (m^{-2}), a_{max} is the stomatal pore size with fully inflated guard cells (m^2) and p_d (m) is the pore depth. The a_{max} was calculated from measurements of pore length assuming stomata are ellipse shaped with pore width equal to half the pore length[28]. The p_d was calculated from species specific relations with guard cell width for the modern conifers and angiosperms from Florida[21,28] and based on measurements for the extant relatives of Early Cretaceous angiosperms[5]. When g_{smax} was calculated to indicate the scaling with D_s and a_{max} (as shown in Figure 6.2C) the species average relation between guard cell width and p_d for the modern conifers and angiosperms was used[21]. The percentage of the leaf surface area occupied by fully opened stomatal pores ($A_{\%}$) was calculated as:

$$A_{\%} = D_s \cdot a_{\max} \cdot 100 \cdot \qquad (6.3)$$

Model rationale

We developed an analytical model of leaf gas exchange which simulated the diffusion of CO_2 and water vapour between the leaf boundary layer and the sites of carboxylation (for CO_2) and the leaf vein endings (for water vapour). Our model expands on descriptions of stomatal gas exchange which calculate g_{smax} from stomatal geometries[35] by also considering the diffusion of CO_2 and water vapour in the leaf interior (Figure E2, in Appendix E). We thereby explicitly accounted for the 3-dimensional character of diffusion around individual stomata inside the leaf[26] using an analytical solution of diffusion in a hemisphere[36]. Our model was applied to the basic schematized leaf morphologies representing the fundamental geometric differences between hypostomatous (angiosperm) broad leaves and tubular shaped (conifer) needle leaves. A more elaborate explanation of the model assumptions is given in Appendix E5.

Stomatal gas exchange

To solve the equations for leaf gas exchange in our analytical model we simplified equations (6.1) and (6.2) by assuming that stomata had circular shapes with radius (r_p) and p_d equal to ½ r_p:

$$g_{s\max} = \frac{\frac{D_{H_2O}}{v} D_s \pi \cdot r_p{}^2}{\frac{1}{2} r_p + \frac{\pi}{2} \sqrt{\pi \cdot r_p{}^2 / \pi}} = \frac{2 \frac{D_{H_2O}}{v} D_s \pi \cdot r_p}{1 + \pi} \quad \text{and} \quad g_{c\max} = g_{s\max} \frac{D_{CO_2}}{D_{H_2O}}. \quad (6.4, 6.5)$$

We are aware that stomata are sometimes ellipse or dumbbell shaped[37] which could potentially alter the g_{smax} related to a specific pore size. Still, the diffusion through stomata remains governed by Stefan's law yielding a similar relation between pore size, D_s and g_{smax}[23,35]. Our results are therefore not fundamentally altered by this assumption.

Leaf interior diffusion

We simulated leaf interior transport of CO_2 and water vapour around individual stomata by using the analytical solution of 3-dimensional spherical diffusion[36]. This solution describes the 3-dimensional diffusive flux J (mol·s^{-1}) of a substance with diffusivity D (m^2·s^{-1}) from a single (hemi)spherical pore with radius r_a (m) over a radial distance l (m) driven by a concentration difference between the pore interior C_1 (mol·mol^{-1}) and the concentration C_2 (mol·mol^{-1}) at radial distance l:

$$J = 2\pi \frac{r_a \cdot l}{l - r_a} \frac{D}{v} \left(C_2 - C_1\right). \quad (6.6)$$

The basic results of this equation were presented in Figure 6.2A to indicate the scaling of diffusive fluxes of two comparable substances over different distances around a single hemispherical pore of variable size.

The 3-dimensional solution for the conductance g_{3D} (mol·s^{-1}) over a radial distance (l) from a single hemispherical pore with radius r_a may then be written as:

$$g_{3D} = 2\pi \frac{r_a \cdot l}{l - r_a} \frac{D}{v}. \quad (6.7)$$

Prior modelling results[26] have indicated that the concentration gradients around the end of the stomatal pore in the leaf interior take the form of a hemisphere with a radius approximately equal to r_p. Expanding on these results, we assumed that the CO_2 and water vapour concentrations at the end of the stomatal pore equalled the concentrations at the start/end of their respective leaf interior diffusion pathways. Hereby we note that the "end correction" term to account for these spherical diffusion shells around individual stomata was applied to both sides of the stomatal pore in Eqs. 6.4 & 6.5[38]. Hence, we extended the analytical solution of g_{3D} to represent multiple stomata expressed per unit leaf surface area to simulate the leaf interior conductance of CO_2 (g_{ic} (mol·m^{-2}·s^{-1})) between the end of the stomatal pore and the mesophyll as:

$$g_{ic} = 2\pi \cdot D_s \frac{r_p \cdot l_{CO2}}{l_{CO2} - r_p} \frac{D_{CO_2}}{\eta v} \frac{\theta}{\tau} \quad (6.8)$$

where l_{CO2} (m) represent the maximum radial diffusion distance for CO_2 between each stomatal pore and the sites of carboxylation, η (-) accounts for part of the leaf interior CO_2 transport occurring through the mesophyll cells[26], and θ (-) and τ (-) denote the porosity and tortuosity of the leaf interior assumed to be ½ and π/2, respectively. Our calculation of l_{CO2} and the estimation of the parameter η are presented in Appendix E1 and Appendix E4, respectively.

Similar to the calculation of g_{ic}, we calculated the leaf interior (post-venous) conductance of water vapour g_{iw} (mol·m^{-2}·s^{-1}) over the maximum distance between the leaf vein endings and the stomatal pore l_{H2O} (m) as:

$$g_{iw} = 2\pi D_s \frac{r_p \cdot l_{H2O}}{l_{H2O} - r_p} \frac{D_{H_2O}}{v} \frac{\theta}{\tau}. \quad (6.9)$$

Our calculation of l_{H2O} is presented in Appendix E1.

Linking leaf interior and stomatal gas exchange

Assuming conservation of mass, the transport pathway between the atmosphere and the end of the stomatal pore was coupled to the transport pathway between the end of the stomatal pore and the sites of carboxylation (for CO_2) and vein endings (for water vapour). This allowed us to express the stomatal conductance and leaf interior conductance as a series of resistances which may be summed up to a single total conductance to CO_2 (g_{tc} (mol·m^{-2}·s^{-1})):

$$g_{tc}^{-1} = \left(f_d g_{c\max}\right)^{-1} + g_{ic}^{-1} \quad (6.10)$$

and a total conductance to water (g_{tw} (mol·m^{-2}·s^{-1})):

$$g_{tw}^{-1} = \left(f_d g_{s\max}\right)^{-1} + g_{iw}^{-1}. \quad (6.11)$$

in which f_d (-) was a constant compensating for the difference between the geometric maximal stomatal conductance and the actual stomatal conductance during periods of maximum photosynthesis. Although such a simple correction factor neglects the variety in mechanisms that may alter this ratio, we assumed f_d to be ½ representing plants

functioning at a leaf water potential (ψ_l) initiating a 50% reduction in actual stomatal conductance[39].

The CO_2 transport from the atmosphere to the sites of carboxylation $A_{0\text{-}2}$ (mol·m^{-2}·s^{-1}) was then calculated as:

$$A_{0-2} = g_{tc}(C_{0c} - C_{2c}) \quad (6.12)$$

and water vapour transport from the leaf vein endings to the atmosphere $E_{2\text{-}0}$ (mol·m^{-2}·s^{-1}) was calculated as:

$$E_{2-0} = g_{tw}(C_{2w} - C_{0w}) \quad (6.13)$$

The C_{0c} (mol·mol^{-1}) and C_{2c} (mol·mol^{-1}) represented the atmospheric CO_2 concentration and the CO_2 concentration at the sites of carboxylation, respectively. The C_{2w} (mol·mol^{-1}) and C_{0w} (mol·mol^{-1}) represented the leaf vein ending and atmospheric water vapour concentrations, respectively. The water vapour concentration in the leaf vein ending was assumed saturated and a constant temperature of 25˚C was assumed throughout the leaf. Further we neglected the leaf boundary layer resistance to both CO_2 and water vapour to allow testing our hypothesis on the effect of stomatal adaptations on leaf gas exchange. We note that by assuming conservation of mass, the concentrations of CO_2 and water vapour at the end of the stomatal pore in the leaf interior (C_{1c} and C_{1w}, respectively) were not required in the calculations. An evaluation of our model with empirical evidence on leaf gas exchange is presented in Appendix E4.

Photosynthesis

Photosynthesis was simulated using the model of Farquhar et al.[40] to obtain a second expression for $A_{0\text{-}2}$:

$$A_{0-2} = \frac{(C_{2c} - c_p)a_1}{a_2 - C_{2c}} \quad (6.14)$$

where c_p is the CO_2 compensation point (mol·mol^{-1}) and the a_1 (mol·m^{-2}·s^{-1}) and a_2 (mol·mol^{-1}) are determined by whether photosynthesis is limited by light or by Rubisco. As we assume maximum photosynthesis rates (light saturation), a_1 equals the maximum carboxylation capacity V_{cmax} (mol·m^{-2}·s^{-1}) and $a_2 = K_c(1+C_{oa}/K_o)$. Here, K_c (mol·mol^{-1}) and K_o (mol·mol^{-1}) are the Michaelis constants for CO_2 fixation and oxygen inhibition, respectively. The C_{oa} (mol·mol^{-1}) is the oxygen concentration in the air. For values of these parameters and their temperature dependencies we followed Katul et al.[30]. A constant V_{cmax} value of 59 mol·m^{-2}·s^{-1} was assumed at a temperature of 25˚C to represent the maximum carboxylation rate. We note that up and down regulation of V_{cmax} likely occurred in response to changes in C_a[17] and that altered oxygen levels may have affected photosynthesis during the Cretaceous[41,42]. Yet, we assumed constant photosynthesis

parameters to allow testing our hypothesis on the effect of stomatal adaptations on leaf gas exchange.

Solving the equations

The equations were solved with Wolfram Mathematica version 7. To obtain the results presented in Figures 6.2B and 6.2D, a fixed maximum transpiration rate of 10 mmol·m^{-2}·s^{-1} was expressed in terms of g_{tw} assuming a constant atmospheric demand related to a relative humidity of 80% with temperature of 25˚C. As both g_{tw} and g_{tc} are functions of the variables D_s and r_p (Eqs. 6.10 & 6.11), we expressed g_{tw} in terms of those D_s and r_p required to answer the specified maximum transpiration rate $E_{2\text{-}0}$ (Eq. 6.13). The resulting photosynthetic carbon returns were obtained by solving the two expressions for $A_{0\text{-}2}$ with the CO_2 concentration at the sites of carboxylation (Eqs. 6.12 & 6.14) assuming C_a of 1000 ppm. Photosynthesis could then be expressed as a function of D_s and, for the angiosperm leaf morphology, D_v. We note that solving our model for higher constant transpiration rates yielded higher values of g_{tw} (Eq. 6.11) which, via the underlying changes in D_s and r_p, yielded higher g_{tc} (Eq. 6.10) which resulted in higher photosynthetic carbon returns for all leaf morphologies.

Acknowledgments

We would like to thank David Dilcher, Emmy Lammertsma, Max Rietkerk and Rike Wagner-Cremer for commenting on the manuscript. This work was funded by the High Potential program of Utrecht University.

References

1. Crepet, W. L. & Niklas, K. J. Darwin's second 'abominable mystery': Why are there so many angiosperm species? *Am J Bot* 96, 366 –381 (2009).
2. Darwin, C. *The origin of species by means of natural selection, or the preservation of favoured races in the struggle for life*. (John Murray: London, UK, 1872).
3. Friedman, W. E. The meaning of Darwin's 'abominable mystery'. *Am. J. Bot.* 96, 5–21 (2009).
4. Feild, T. S., Arens, N. C., Doyle, J. A., Dawson, T. E. & Donoghue, M. J. Dark and disturbed: a new image of early angiosperm ecology. *Paleobiology* 30, 82–107 (2004).
5. Feild, T. S. *et al.* Fossil evidence for low gas exchange capacities for Early Cretaceous angiosperm leaves. *Paleobiology* 37, 195–213 (2011).
6. Lidgard, S. & Crane, P. R. Quantitative analyses of the early angiosperm radiation. *Nature* 331, 344–346 (1988).
7. Crane, P. R. & Lidgard, S. Angiosperm Diversification and Paleolatitudinal Gradients in Cretaceous Floristic Diversity. *Science* 246, 675 –678 (1989).
8. Bond, W. The tortoise and the hare: Ecology of angiosperm dominance and gymnosperm persistence. *Biol J Linn Soc* 36, 227–249 (1989).
9. Dilcher, D. Toward a new synthesis: Major evolutionary trends in the angiosperm fossil record. *Proc Natl Acad Sci USA* 97, 7030–7036 (2000).
10. Berendse, F. & Scheffer, M. The angiosperm radiation revisited, an ecological explanation for Darwin's 'abominable mystery'. *Ecology Letters* 12, 865–872 (2009).
11. McKown, A. D., Cochard, H. & Sack, L. Decoding Leaf Hydraulics with a Spatially Explicit Model: Principles of Venation Architecture and Implications for Its Evolution. *Am Nat* 175, 447–460 (2010).
12. Blonder, B., Violle, C., Bentley, L. P. & Enquist, B. J. Venation networks and the origin of the leaf economics spectrum. *Ecology Letters* 14, 91–100 (2011).
13. Brodribb, T. J. & Feild, T. S. Leaf hydraulic evolution led a surge in leaf photosynthetic capacity during early angiosperm diversification. *Ecol. Lett.* 13, 175–183 (2010).
14. Feild, T. S. *et al.* Fossil evidence for Cretaceous escalation in angiosperm leaf vein evolution. *Proc Natl Acad Sci USA* 108, 8363–8366 (2011).
15. Brodribb, T. J., Holbrook, N. M., Zwieniecki, M. A. & Palma, B. Leaf hydraulic capacity in ferns, conifers and angiosperms: impacts on photosynthetic maxima. *New Phytol* 165, 839–846 (2005).
16. Berner, R. A. & Kothavala, Z. Geocarb III: A Revised Model of Atmospheric CO2 over Phanerozoic Time. *Am J Sci* 301, 182–204 (2001).
17. Franks, P. J. & Beerling, D. J. CO2-forced evolution of plant gas exchange capacity and water-use efficiency over the Phanerozoic. *Geobiology* 7, 227–236 (2009).
18. Brodribb, T. J., Feild, T. S. & Jordan, G. J. Leaf Maximum Photosynthetic Rate and Venation Are Linked by Hydraulics. *Plan Physiol* 144, 1890 –1898 (2007).
19. Brodribb, T. J. & McAdam, S. A. M. Passive Origins of Stomatal Control in Vascular Plants. *Science* 331, 582 –585 (2011).
20. McAdam, S. A. M. & Brodribb, T. J. Stomatal innovation and the rise of seed plants. *Ecology Letters* 15, 1–8 (2012).
21. de Boer, H. J. *et al.* Climate forcing due to optimization of maximal leaf conductance in subtropical vegetation under rising CO2. *Proc Natl Acad Sci USA* 108, 4041 –4046 (2011).
22. Franks, P. J. & Beerling, D. J. Maximum leaf conductance driven by CO2 effects on stomatal size and density over geologic time. *Proc Natl Acad Sci USA* 106, 10343–10347 (2009).
23. Stefan, J. Ueber die Verdampfung aus einem kreisförmig oder elliptisch begrenzten Becken. *Annalen der Physik* 253, 550–560 (1882).
24. Beerling, D. J. & Franks, P. J. Plant science: The hidden cost of transpiration. *Nature* 464, 495–496 (2010).
25. Sack, L. & Holbrook, N. M. Leaf Hydraulics. *Annu Rev Plant Boil* 57, 361–381 (2006).
26. Parkhurst, D. F. Tansley Review No. 65. Diffusion of CO2 and Other Gases Inside Leaves. *New Phytol* 126, 449–479 (1994).

27. Tyree, M. T. & Sperry, J. S. Do Woody Plants Operate Near the Point of Catastrophic Xylem Dysfunction Caused by Dynamic Water Stress? *Plant Physiol* 88, 574–580 (1988). Answers from a Model.
28. Lammertsma, E. I. *et al.* Global CO2 rise leads to reduced maximum stomatal conductance in Florida vegetation. *Proc Natl Acad Sci USA* 108, 4035 –4040 (2011).
29. Mäkelä, A., Berninger, F. & Hari, P. Optimal Control of Gas Exchange during Drought: Theoretical Analysis. *Ann Bot* 77, 461 –468 (1996).
30. Katul, G., Manzoni, S., Palmroth, S. & Oren, R. A stomatal optimization theory to describe the effects of atmospheric CO2 on leaf photosynthesis and transpiration. *Ann Bot* 105, 431–442 (2010).
31. Manzoni, S. *et al.* Optimizing stomatal conductance for maximum carbon gain under water stress: a meta-analysis across plant functional types and climates. *Funct Ecol* 25, 456–467 (2011).
32. Roth-Nebelsick, A., Grein, M., Utescher, T. & Konrad, W. Stomatal pore length change in leaves of Eotrigonobalanus furcinervis (Fagaceae) from the Late Eocene to the Latest Oligocene and its impact on gas exchange and CO2 reconstruction. *Review of Palaeobotany and Palynology* 174, 106–112 (2012).
33. Scheffer, M., Carpenter, S., Foley, J. A., Folke, C. & Walker, B. Catastrophic shifts in ecosystems. *Nature* 413, 591–596 (2001).
34. Tilman, D. Niche tradeoffs, neutrality, and community structure: A stochastic theory of resource competition, invasion, and community assembly. *Proc Natl Acad Sci USA* 101, 10854 –10861 (2004).
35. Parlange, J.-Y. & Waggoner, P. E. Stomatal Dimensions and Resistance to Diffusion. *Plant Physiol* 46, 337–342 (1970).
36. Crank, J. *The mathematics of diffusion.* (Oxford □: Clarendon Press: 1979).
37. Franks, P. J. & Farquhar, G. D. The Mechanical Diversity of Stomata and Its Significance in Gas-Exchange Control. *Plant Physiol.* 143, 78–87 (2007).
38. Franks, P. J. & Farquhar, G. D. The Effect of Exogenous Abscisic Acid on Stomatal Development, Stomatal Mechanics, and Leaf Gas Exchange in Tradescantia virginiana. *Plan Physiol* 125, 935 –942 (2001).
39. Brodribb, T. J. & Holbrook, N. M. Stomatal Closure During Leaf Dehydration, Correlation with Other Leaf Physiological Traits. *Plant Physiol.* 132, 2166–2173 (2003).
40. Farquhar, G. D., Caemmerer, S. & Berry, J. A. A biochemical model of photosynthetic CO2 assimilation in leaves of C3 species. *Planta* 149, 78–90 (1980).
41. Beerling, D. J. Modelling Palaeophotosynthesis: Late Cretaceous to Present. *Philosophical Transactions: Biological Sciences* 346, 421–432 (1994).
42. Berner, R. A. GEOCARBSULF: A combined model for Phanerozoic atmospheric O2 and CO2. *Geochimica et Cosmochimica Acta* 70, 5653–5664 (2006).

Appendix A

Supplemental material for Chapter 2

Tables and Captions

Table A1 Sample selection and species growth specifics

Species	Growth type	Canopy layer	Hydrological preference	No. of samples: Sub-fossil	No. of samples: Collected	CO_2 range (ppm)
Acer rubrum	BD	Upper	Cosmopolitan	23	17	308-387
Ilex cassine	BE	Middle	Moist/wet	39	49	290-387
Myrica cerifera	BE	Middle	Cosmopolitan	48	40	294-387
Osmunda regalis	BD	Lower	Moist	65	83	307-387
Pinus elliottii	NE	Upper	Moist	-	41	300-387
Pinus taeda	NE	Upper	Cosmopolitan	59	3	335-387
Quercus laurifolia	BD	Upper	Moist/wet	89	-	290-371
Quercus nigra	BD	Upper	Cosmopolitan	-	57	287-387
Taxodium distichum	ND	Upper	Wet	21	33	294-387

The *Acer rubrum*, *Ilex cassine*, *Myrica cerifera*, *Osmunda regalis*, and *Pinus taeda* subfossil material is extracted from a peat core taken in 1998 A.D. in a hardwood swamp forest near Gainesville, FL (Alligator Crossing: 29°39'35"N, 82°15'14"W) (1). Subfossil leaf fragments of *Taxodium distichum* and *Quercus laurifolia* are extracted from two peat cores taken in 1998 A.D. and 2002 A.D., respectively, in a cypress swamp forest of the Fakahatchee Strand Preserve State Park (25°95'N, 81°49'W) (2). For all cores age models are constructed with an accuracy of 2–5 y (1, 2). The herbarium samples, obtained from the University of Florida and State Park Headquarters District 4 herbaria, have been collected during the 19th and 20th century from various sites across Florida. Only leaves picked between August and January have been selected to ensure that leaves were fully developed. Self-collected material is available from 1998 A.D. onward. Details of the nine analyzed species, the origin and amount of samples, and the CO_2 range covered by the samples are given in Table A1. BD, broadleaved deciduous; BE, broad-leaved evergreen; NE, needle-leaved evergreen; ND, needle-leaved deciduous; —, no material analyzed.

1. Wagner F, Dilcher DL, Visscher H (2005) Stomatal frequency responses in hardwood-swamp vegetation from Florida during a 60-year continuous CO2 increase. Am J Bot 92:690–695.
2. Donders TH, Wagner F, Van der Borg K, De Jong AFM, Visscher H (2004) A novel approach for developing high-resolution sub-fossil peat chronologies with 14C dating. Radiocarbon 46: 455–464.

Table A2 Linear regressions of maximum stomatal conductance g_{smax} (mol·m^{-2}·s^{-1}) with CO_2 (ppm)

Species	**Function**	**CV (RMSE) (%)**	r^2	P
Acer rubrum	g_{smax} = -0.013·[CO_2]+6.77	14	0.45	0.01*
Ilex cassine	g_{smax} = -0.004·[CO_2]+2.59	14	0.36	0.002*
Myrica cerifera	g_{smax} = -0.006·[CO_2]+3.72	11	0.49	<0.001*
Osmunda regalis	g_{smax} = -0.003·[CO_2]+1.51	20	0.24	0.01*
Pinus elliottii	g_{smax} = -0.002·[CO_2]+1.66	8	0.36	0.02*
Pinus taeda	g_{smax} = -0.016·[CO_2]+7.41	9	0.54	0.006*
Quercus laurifolia	g_{smax} = -0.005·[CO_2]+4.31	12	0.21	0.03*
Quercus nigra	g_{smax} = -0.016·[CO_2]+8.65	10	0.61	<0.001*
Taxodium distichum	g_{smax} = -0.005·[CO_2]+2.93	10	0.58	0.006*

For easier interspecies comparison, the range of variability is normalized and presented as the variability coefficient of the root mean squared errors CV(RMSE), in %.

*All statistically significant regressions ($P < 0.05$) also have significantly different slopes.

Table A3 Stomatal density D (number of stomata ·mm^{-2}) with pore size a_{max} (µm^2)

Species	**Function**	r^2	P
Acer rubrum	a_{max} = 0.019·[D]+34.6	0.07	0.09
	log10 a_{max} = 0.278·[log10 D] + 0.9	0.08	0.08
Ilex cassine	a_{max} = 0.017·[D]+72.6	0.002	0.69
	log10 a_{max} = 0.063·[log10 D] + 1.7	0.002	0.66
Myrica cerifera	a_{max} = -0.041·[D]+55.9	0.25	<0.001*
	log10 a_{max} = -0.852·[log10 D] + 3.8	0.27	<0.001*
Osmunda regalis	a_{max} = -0.391·[D]+246.9	0.06	0.004*
	log10 a_{max} = -0.161·[log10 D] + 2.6	0.07	0.001*
Pinus elliottii	a_{max} = -3.101·[D]+736.3	0.20	0.003*
	log10 a_{max} = -0.406·[log10 D] + 3.5	0.20	0.003*
Pinus taeda	a_{max} = 0.171·[D]+186.1	0.01	0.42
	log10 a_{max} = 0.197·[log10 D] + 1.9	0.02	0.29
Quercus laurifolia	a_{max} = -0.008·[D]+31.5	0.06	0.02*
	log10 a_{max} = -0.475·[log10 D] + 2.8	0.06	0.02*
Quercus nigra	a_{max} = -0.017·[D]+97.2	0.01	0.45
	log10 a_{max} = -0.065·[log10 D] + 2.1	0.003	0.68
Taxodium distichum	a_{max} = -0.075·[D]+106.5	0.20	<0.001*
	log10 a_{max} = -0.207·[log10 D] + 2.4	0.20	<0.001*
Angiosperms	a_{max} = -0.049·[D]+ 84.1	0.42	<0.001*
	log10 a_{max} = -0.724·[log10 D] + 3.6	0.51	<0.001*
Conifers	a_{max} = -1.995·[D]+ 598.9	0.72	<0.001*
	log10 a_{max} = -1.162·[log10 D] + 4.8	0.72	<0.001*
Complete dataset	log10 a_{max} = -0.853·[log10 D] + 4.0	0.79	<0.001*

For each species studied the linear as well as the log-linear relation between D and a_{max} are given. Accompanying coefficients of determination (r^2) and probability (P) are also given. *Statistical significance for the regression. Although a negative power law relation between stomatal density and size is generally known, comparison between the linear and logarithmic relations shows that our data series of individual species do not follow this power relation. From these results weak and unidirectional relations are apparent, and only negative relations are statistically significant (*M. cerifera*, *O. regalis*, *P. elliottii*, *Q. laurifolia*, and *T. distichum*). However, the pooled angiosperm and conifer data series, as well as the complete dataset, are best described by a log-transformed linear regression.

Table A4 Linear regressions of stomatal density *D* (number of stomata ·mm^{-2}) with CO_2 (ppm)

Species	Function	CV(RMSE) (%)	r^2	*P*
Acer rubrum	$D = -2.23 \cdot [CO_2] + 1398$	13	0.30	0.05*
Ilex cassine	$D = -0.77 \cdot [CO_2] + 509$	11	0.39	0.001*
Myrica cerifera	$D = -2.39 \cdot [CO_2] + 1446$	12	0.40	0.002*
Osmunda regalis	$D = -0.33 \cdot [CO_2] + 194$	22	0.09	0.15
Pinus elliottii	$D = -0.19 \cdot [CO_2] + 134$	7	0.55	0.002*
Pinus taeda	$D = -1.14 \cdot [CO_2] + 591$	6	0.56	0.005*
Quercus laurifolia	$D = -1.21 \cdot [CO_2] + 1650$	12	0.13	0.09
Quercus nigra	$D = -2.08 \cdot [CO_2] + 1316$	8	0.44	0.002*
Taxodium distichum	$D = -1.08 \cdot [CO_2] + 613$	12	0.52	0.01*

For easier interspecies comparison, the range of variability is normalized and presented as the variability coefficient of the root mean squared errors CV(RMSE), in %.
*All statistically significant regressions ($P < 0.05$) also have significantly different slopes.

Table A5 Linear regressions of pore size a_{max} (μm^2) with CO_2 (ppm)

Species	Function	CV(RMSE) (%)	r^2	*P*
Acer rubrum	$a_{max} = -0.156 \cdot [CO_2] + 101$	5%	0.40	0.02*
Ilex cassine	$a_{max} = -0.108 \cdot [CO_2] + 116$	9%	0.04	0.35
Myrica cerifera	$a_{max} = 0.005 \cdot [CO_2] + 29$	3%	<0.001	0.94
Osmunda regalis	$a_{max} = -0.8 \cdot [CO_2] + 497$	7%	0.31	0.004*
Pinus elliottii	$a_{max} = 0.607 \cdot [CO_2] + 310$	4%	0.15	0.17
Pinus taeda	$a_{max} = -1.016 \cdot [CO_2] + 579$	5%	0.25	0.10
Quercus laurifolia	$a_{max} = -0.032 \cdot [CO_2] + 32$	9%	0.07	0.21
Quercus nigra	$a_{max} = -0.209 \cdot [CO_2] + 156$	7%	0.18	0.08
Taxodium distichum	$a_{max} = 0.051 \cdot [CO_2] + 71$	3%	0.06	0.46

For easier interspecies comparison, the range of variability is normalized and presented as the variability coefficient of the root mean squared errors CV(RMSE), in %.
*All statistically significant regressions ($P < 0.05$) also have significantly different slopes.

Table A6 Relative sensitivities in g_{smax}, D and a_{max} of angiosperms and conifers to CO_2 (ppm) increase

Species	Slope (% ppm^{-1})	SE (% ppm^{-1})	r^2	P
Angiosperm				
g_{smax}	-0.33	0.04	0.35	<0.01*
D	-0.28	0.03	0.41	<0.01*†
a_{max}	-0.15	0.06	0.06	0.02*
Conifers				
g_{smax}	-0.37	0.09	0.33	<0.01*
D	-0.35	0.06	0.49	<0.01*†
a_{max}	-0.07	0.11	0.01	0.53

Intercept = 100% at CO_2 280 ppm, with slope, SE, r^2, and P of linear regressions. *Statistically significant for the regression to CO_2, and slope significantly different from 0 ($P < 0.05$). †Change in D between angiosperms and conifers is significantly different.

Table A7 Pore length/ guard cell width linear relations

Species	Mean C_w (µm)	σ (µm)	n	Linear regression	r^2
Acer rubrum	6.79	0.94	36	C_w =0.36·[L]+2.90	0.49
Ilex cassine	10.26	1.33	27	C_w =0.28·[L] +6.19	0.57
Myrica cerifera	7.84	1.10	25	C_w =0.41·[L] +3.57	0.62
Pinus elliottii	16.24	2.22	28	C_w =0.27·[L] +6.66	0.62
Pinus taeda	11.51	1.22	33	C_w= 11.5 µm	
Quercus laurifolia	6.72	0.77	22	C_w =0.27·[L] +4.57	0.49
Quercus nigra	7.29	1.21	27	C_w =0.26·[L] +3.55	0.56
Taxodium distichum	9.79	1.57	20	C_w =0.55·[L] +1.52	0.72

Species-specific relations between pore length (L) and guard cell width (C_w) are used to derive pore depth (l), based on the assumption that l is equal to C_w (1). The standard deviation (σ) and number of measurements (n) are indicated, alongside the linear regressions and r^2 values. Species-specific regressions between C_w and L are highly significant (P < 0.001), with exception of *P. taeda*. We therefore derive l from these species-specific regressions, except for *P. taeda*, for which a constant value is applied. The species-specific regressions are used to calculate g_{smax} for each species.

1. Franks PJ, Beerling DJ (2009) Maximum leaf conductance driven by CO2 effects on stomatal size and density over geologic time. Proc Natl Acad Sci USA 106:10343–10347.

Appendix B

Supplemental material for Chapter 3.1

Table B1 Species specific relations between pore length and guard cell width

Species names and abbreviations	Mean C_w (µm)	σ (µm)	n	Linear regression	r^2
Acer rubrum (Ar)	6.79	0.94	36	C_w =0.36**L*+2.90	0.49*
Ilex cassine (Ic)	10.26	1.33	27	C_w =0.28* *L* +6.19	0.57*
Myrica cerifera (Mc)	7.84	1.10	25	C_w =0.41* *L* +3.57	0.62*
Pinus elliottii (Pe)	16.24	2.22	28	C_w =0.27* *L* +6.66	0.62*
Pinus taeda (Pt)	11.51	1.22	33	C_w= 11.5 µm	
Quercus laurifolia (Ql)	6.72	0.77	22	C_w =0.27* *L* +4.57	0.49*
Quercus nigra (Qn)	7.29	1.21	27	C_w =0.26* *L* +3.55	0.56*
Taxodium distichum (Td)	9.79	1.57	20	C_w =0.55* *L* +1.52	0.72*

Species specific relations between pore length (*L*) and guard cell width (C_w) are used to derive pore depth (*l*), based on the assumption that *l* is equal to C_w (1). The standard deviation (σ) and number of measurements (n) are indicated, alongside the linear regressions and r^2 values. Species specific regressions between C_w and *L* are highly significant (P < 0.0001, indicated by *) with exception of *P. taeda*. We therefore derive *l* from these species specific regressions, except for *P. taeda* for which a constant value is applied. The average slope of these regressions is used to calculate lines of equal g_{smax} in Figure 4.1A.

Table B2 Species-specific model parameters

Species	λ	LAI (11, 12)	V_{cmax25}	J_{max25}	R_{d25}	derived from	M_a*	Reference
Ar	72	5.5	75.0	94	1.1	Foliar N		(13)
Ic	134	5.5	55.5	79.2	0.8	Foliar N	127(15)	(14)
Mc	99	5.5	62.5	89.1	0.9	Foliar N	101(35)	(14)
Pe	244	2	60.9	86.9	0.9	Foliar N		(14)
Pt	87	2	47.0	77.1	0.7	A/C_i curves		(5)
Ql	62	5.5	54.0	77.0	0.8	Foliar N	102(34)	(15)
Qn	58	5.5	64.8	92.4	1.0	Foliar N	96(10)	(15)
Td	55	3	30.0	49.2	0.5	A/C_i curves		(5)

Species specific model parameters. Lagrangian multiplier [λ (µmol·mol^{-1})], leaf area index [*LAI* (-)] and photosynthesis parameters V_{cmax25}, J_{max25} and R_{d25} (µmol·m^{-2}·s^{-1}) and how photosynthesis parameters are derived. If photosynthesis parameters are based on foliar nitrogen (N) concentrations on a leaf mass base, measurements of leaf mass with area [M_a (g·m^{-2})] and their standard deviations are indicated. LAI values for conifers (8, 9) are doubled in the model to account for their amphistomatic leaves.

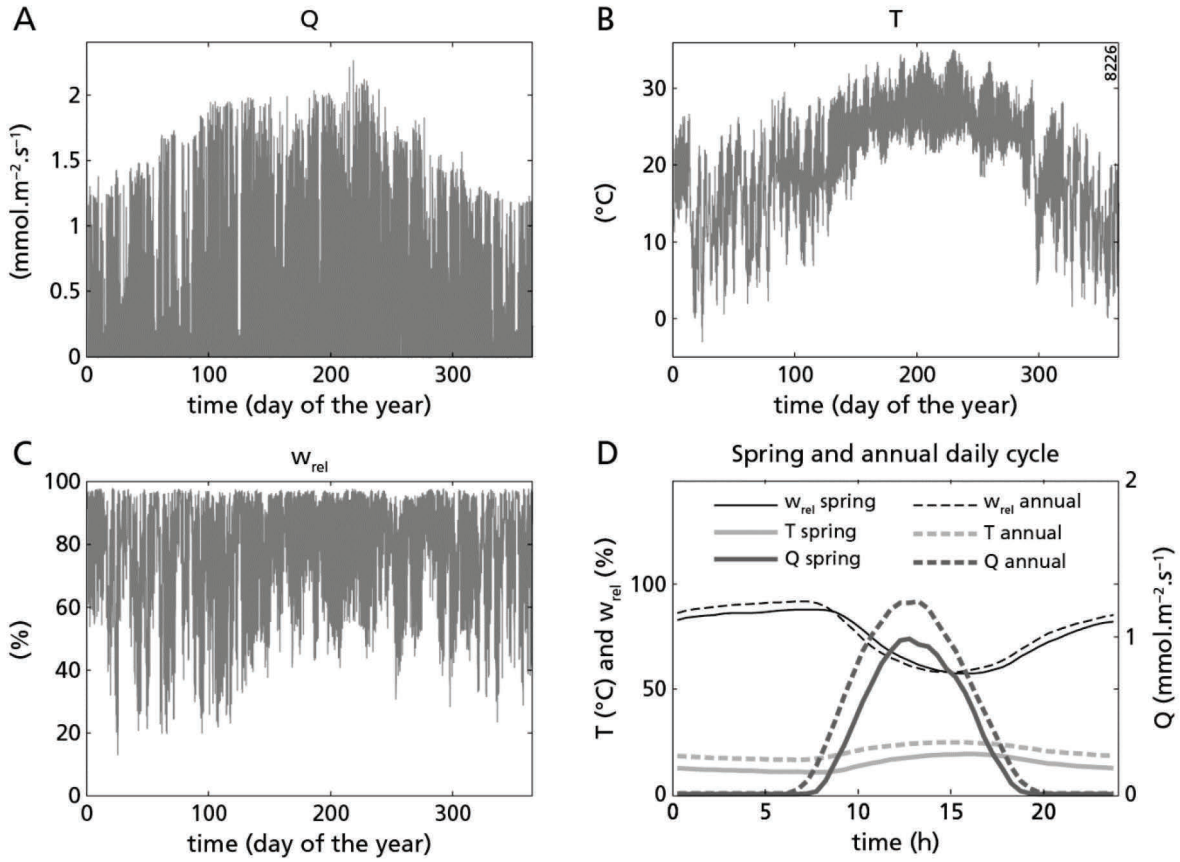

Figure B1 Environmental boundary conditions used to force the stomatal adaptation models. Annual cycles of climatic boundary conditions of photosynthetic active radiation [Q (mmol·m^{-2}·s^{-1})] (A), ambient air temperature [T (°C)] (B), and relative humidity [w_{rel} (%)] (C) measured over a pine flatwoods ecosystem near Gainesville, FL, during the year 2003 (10, 11). (D) Average diurnal cycles for Q, T, and w_{rel} during leaf development (March, April, and May) are prescribed to the optimization models to determine g_{smax}. Annual average diurnal cycles of these boundary conditions are prescribed to calculate gas exchange at the leaf level. A complete annual cycle of these boundary conditions is prescribed to calculate changes in annual canopy transpiration.

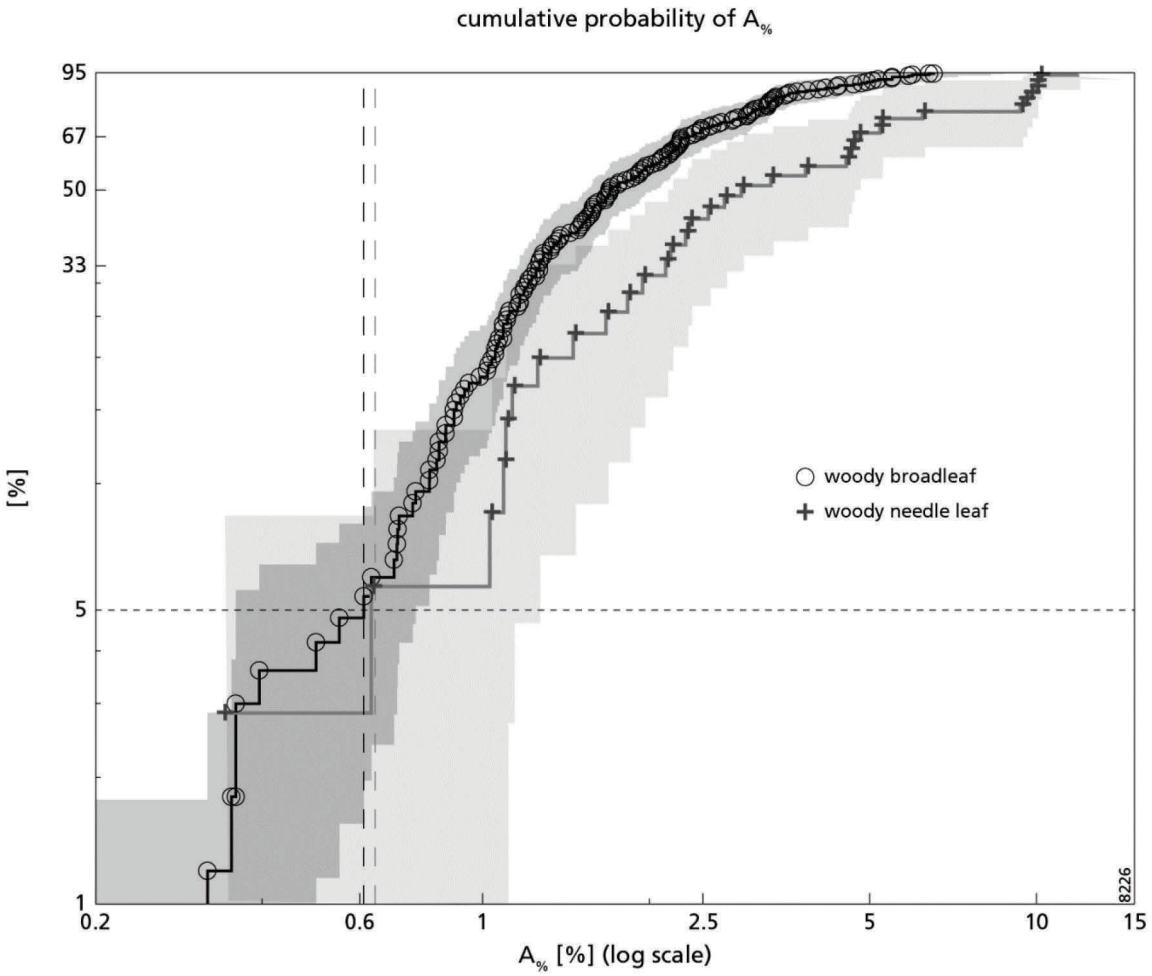

Figure B2 Empirical cumulative probability of $A_{\%}$ for woody broadleaf and woody needle leaf species. Data are from Franks and Beerling (12). Circles and crosses denote data points; connecting lines denote the fit of the empirical distribution. The 95% confidence level of each distribution is indicated by shading. Dashed lines denote the lower 5% limit of $A_{\%}$. On average, stomata occupy less space on leaves of woody broadleaf species than on leaves (needles) of woody needle leaf species. However, the 5% lower limit of $A_{\%}$ (defined as $A_{\%low}$) for both distributions cannot be distinguished. Note that a logarithmic x axis is used.

Supplementary methods

The biochemical model of photosynthesis (1) requires three species-specific photosynthesis parameters (at 25 °C) to be known: maximum carboxylation capacity [V_{cmax25} (mol·m^{-2}·s^{-1})], maximum rate of electron transport [J_{max25} (mol·m^{-2}·s^{-1})] and mitochondrial respiration rate R_{d25} (mol·m^{-2}·s^{-1}) (Table B2). For *Pinus taeda* (Pt) and *Taxodium distichum* (Td), we derived these values from published *A/Ci* curves (2) and the empirical relation among V_{cmax25}, J_{max25}, and R_{d25} (3, 4):

$$J_{\max 25} = \left(29.1 + 1.64 \cdot 10^{6} \cdot V_{c\max 25}\right) \cdot 10^{-6} \qquad \text{(B.1)}$$

and

$$R_{d25} = 0.015 \cdot V_{c\max 25} \quad \text{(B.2)}$$

For the other species *[Acer rubrum* (Ar), *Ilex cassine* (Ic), *Myrica cerifera* (Mc), *Quercus laurifolia* (Ql), *Quercus nigra* (Qn), *Pinus elliottii* (Pe), and *Pinus taeda* (Pt)], we derived V_{cmax25} and J_{max25} from foliar nitrogen content (5) and R_{d25} from Eq. B.2:

$$V_{c\max 25} = 6.25 \cdot V_{cr} M_A N_m P_R \cdot 10^{-6} \quad \text{(B.3)}$$

where 6.25 is the ratio of weight of Rubisco to the weight of nitrogen in Rubisco ($g \cdot g^{-1}$), V_{cr} is the specific activity of Rubisco at 25 °C [20.7 ($\mu mol \cdot g^{-1} \cdot s^{-1}$)], M_A is the leaf mass ($g \cdot m^{-2}$), N_m is leaf nitrogen content per leaf dry mass ($g \cdot g^{-1}$) and P_R (-) is the fraction of nitrogen allocated to Rubisco, estimated at 0.15, and:

$$J_{\max 25} = 8.06 \cdot J_{mc} M_A N_m P_B \cdot 10^{-6} \quad \text{(B.4)}$$

where 8.06 is the minimal nitrogen investment in cytochrome bioenergetics [µmol of cytochrome·(g of N)$^{-1}$], the potential rate of photosynthetic electron transport per unit cytochrome (J_{MC}) is estimated at 156 µmol electrons·(µmol of cytochrome·s)$^{-1}$ at 25 °C and P_B (g of N in cytochrome) is the fraction of N allocated to RuBP estimated at 0.035.

Down-regulation of the photosynthesis parameters V_{cmax25} and J_{max25} in response to rising CO_2 (6, 7) is simulated with an exponential decay function:

$$V_{c\max 25}(CO_2) = V_{c\max 25}(385) \cdot e^{-\kappa(CO_2 - 385)} \quad \text{(B.5)}$$

and

$$J_{\max 25}(CO_2) = J_{\max 25}(385) \cdot e^{-\kappa(CO_2 - 385)} \quad \text{(B.6)}$$

where $V_{cmax25}(385)$ and $J_{max25}(385)$ represent the photosynthesis parameters V_{cmax25} and J_{max25} at their present day values (Table B2) and κ is a decay constant for the CO_2 response of V_{cmax25} and J_{max25}. A value of $2 \cdot 10^{-4} \cdot ppm^{-1}$ is chosen for κ to match estimated down-regulation of photosynthesis parameters at geological timescales (7). Furthermore, species specific values of leaf area index [LAI (-)] are derived from literature (Table B2) (8, 9).

References

1. Farquhar GD, von Caemmerer S, Berry JA (2001) Models of photosynthesis. Plant Physiol 125:42–45.
2. Ellsworth DS, et al. (2004) Photosynthesis, carboxylation and leaf nitrogen responses of 16 species to elevated pCO2 across four free-air CO2 enrichment experiments in forest, grassland and desert. Glob Change Biol 10:2121–2138.
3. Wullschleger SD (1993) Biochemical limitations to carbon assimilation in C3 plants–a retrospective analysis of the A/CI curves from 109 species. J Exp Bot 44:907–920.
4. Baldocchi DD, Wilson KB (2001) Modeling CO2 and water vapor exchange of a temperate broadleaved forest across hourly to decadal time scales. Ecol Modell 142:155–184.
5. Niinemets Ü, Tenhunen JD (1997) A model separating leaf structural and physiological effects on carbon gain along light gradients for the shade-tolerant species Acer saccharum. Plant Cell Environ 20:845–866.
6. Ainsworth EA, Rogers A (2007) The response of photosynthesis and stomatal conductance to rising [CO2]: Mechanisms and environmental interactions. Plant Cell Environ 30:258–270.
7. Franks PJ, Beerling DJ (2009) CO(2)-forced evolution of plant gas exchange capacity and water-use efficiency over the Phanerozoic. Geobiology 7:227–236.
8. Vose JM, et al. (1995) Vertical leaf area distribution, light transmittance, and application of the Beer-Lambert Law in four mature hardwood stands in the southern Appalachians. Can J For Res 25:1036–1043.
9. Liu S, Riekerk H, Gholz H (1997) Leaf litterfall, leaf area index, and radiation transmittance in cypress wetlands and slash pine plantations in north-central Florida. Wetlands Ecol Manage 4:257–271.
10. Clark KL, Gholz HL, Castro MS (2004) Carbon dynamics along a chronosequence of slash pine plantations in North Florida. Ecological Applications 14:1154–1171.
11. Powell TL, et al. (2008) Carbon exchange of a mature, naturally regenerated pine forest in north Florida. Glob Change Biol 14:2523–2538.
12. Franks PJ, Beerling DJ (2009) Maximum leaf conductance driven by CO2 effects on stomatal size and density over geologic time. Proc Natl Acad Sci USA 106:10343–10347.
13. Williams M, et al. (1996) Modelling the soil-plant-atmosphere continuum in a Quercus & Acer stand at Harvard Forest: The regulation of stomatal conductance by light, nitrogen and soil/plant hydraulic properties. Plant Cell Environ 19:911–927.
14. Saha AK, Sternberg LDSLO, Miralles-Wilhelm F (2009) Linking water sources with foliar nutrient status in upland plant communities in the Everglades National Park, USA. Ecohydrology 2:42–54.
15. Moorhead KK, McArthur J (1996) Spatial and temporal patterns of nutrient concentrations in foliage of riparian species. Am Midl Nat 136:29–41.

Appendix C

Supplemental material for Chapter 4

C1 Pollen-climate inference model

To determine the length of the compositional gradient, a detrended correpondence analysis (DCA)(as implemented in CANOCO version 4.5 (Ter Braak and Šmilauer 2002)) was carried out using square-root transformed pollen percentage data. Following recommendations of Ter Braak and Prentice (1988), the relatively long gradient (3.03 standard deviation (SD) units) merits use of unimodal methods for the numerical analyses. We therefore used canonical correspondence analysis (CCA) to explore the relation between fossil pollen assemblages and the (bio)climatic variables taken from Whitmore et al. (2005). The percentage explained variance was determined for each (bio)climatic variable by constraining a CCA with a single variable of interest, after which significance was tested with a Monte-Carlo method using 999 iterations. A CCA with forward selection was used to select a subset of significant variables. The variable with the highest explanatory power was tested for significance and, when significant, included. The next variable that explains most of the remaining variance was then selected and tested, and the procedure repeated until $P > 0.05$. The subset of variables thus selected (T_{FEB}, T_{MAY}, T_{NOV}, T_{DEC}, T_{MAX}, P_{total}, P_{DJF}, P_{JJA}, P_{MAM}, and P_{SON}) were considered to be potentially suitable for pollen-inferred climate reconstructions. Although P_{DJF} had the highest explanatory power of this subset, it is ecologically not very relevant for the Lake Tulane site since winter precipitation is not retained for the growing season in the highly permeable soils (Grimm et al. 2006). Hence, summer precipitation (P_{JJA}), which is the main wet season throughout the year in Florida, was considered as the most relevant parameter for vegetation at Lake Tulane. In addition to P_{JJA}, also T_{NOV} was selected as it explained, amongst all temperature variables, most variance and is a relevant, cold-season, limiting factor for (sub)tropical plant growth.

Despite significant inverse correlation between November temperature and summer precipitation (Table C1), CCA with variance partitioning shows that the explanatory power of T_{NOV} independent of the P_{JJA} is 9%, and the explained variance shared between both variables is only 2.8% (both variables together explain 18.8%). In contrast, summer and winter precipitation have very little independent explanatory power and share 8.1% of the total variance (both variables together 12.6%). This is further reason not to use a separate inference model for P_{DJF}. The gradient length of each individually selected environmental variable was estimated using detrended CCA (DCCA). Transfer functions were developed using the partial-least-squares (PLS) and the weighted averaging PLS (WA-PLS) methods as implemented in the C^2 program version 1.5 (Juggins, 2003). With gradient lengths < 1.5 SD units, the linear-model based PLS method generally performs better than the unimodal-model based WA-PLS method. However, since gradient lengths are just above 1.5 SD units (Table C1), we made model choice dependent on r^2_{boot}, lowest

root mean square error of prediction (RMSEP), and the number of outliers. Model components were added until a RMSEP reduction of < 5% with respect to the simplest one-component model was reached (Birks, 1998). Analysis of the variance (CCA with fossil samples added as passive samples) in all the data confirms that the fossil samples cluster within the spread of the calibration samples (Figure C2).

Table C1 Explanatory power of (bio)climatic variables on the pollen composition of surface sediment samples. ***P ≤ 0.001, **P ≤ 0.01

	% variance (CCA)	% variance (CCA, variance partitioning)		Gradient length
Variable	**Marginal**	**Conditional**	**Covariable**	**DCCA**
Temperature				
Tann	11.3***			
Tjan	11.6***			
Tfeb	11.6***			
Tmar	11.5***			
Tapr	11.1***			
Tmay	9.9***			
Tjun	6.1***			
Tjul	5.2***			
Taug	7.9***			
Tsep	9.8***			
Toct	11.3***			
T_{NOV}	11.8***	9***	P_{JJA}	1.557
Tdec	11.7***			
Tmax	11.3***			
Tmin	11.6***			
Precipitation				
Ptotal	9***			
P_{DJF}	10.8***	2.8***	P_{JJA}	1.576
Pspring	7.6***			
P_{JJA}	9.8***	1.7**	P_{DJF}	1.846
Paut	12.7***			
Pjan	10.4***			
Pfeb	11.7***			
Pmar	11.5***			
Papr	6.8***			
Pmay	12.2***			
Pjun	11.7***			
Pjul	4.5***			
Paug	7.7***			
Psep	11.3***			
Poct	12.7***			
Pnov	9.7***			
Pdec	9.8***			
Geography				
Long	9.4***			
Lat	11.2***			
Elev	6.4***			
PotEvap	11.7***			
Site type	3.9***			
All canonical axes	51.7			

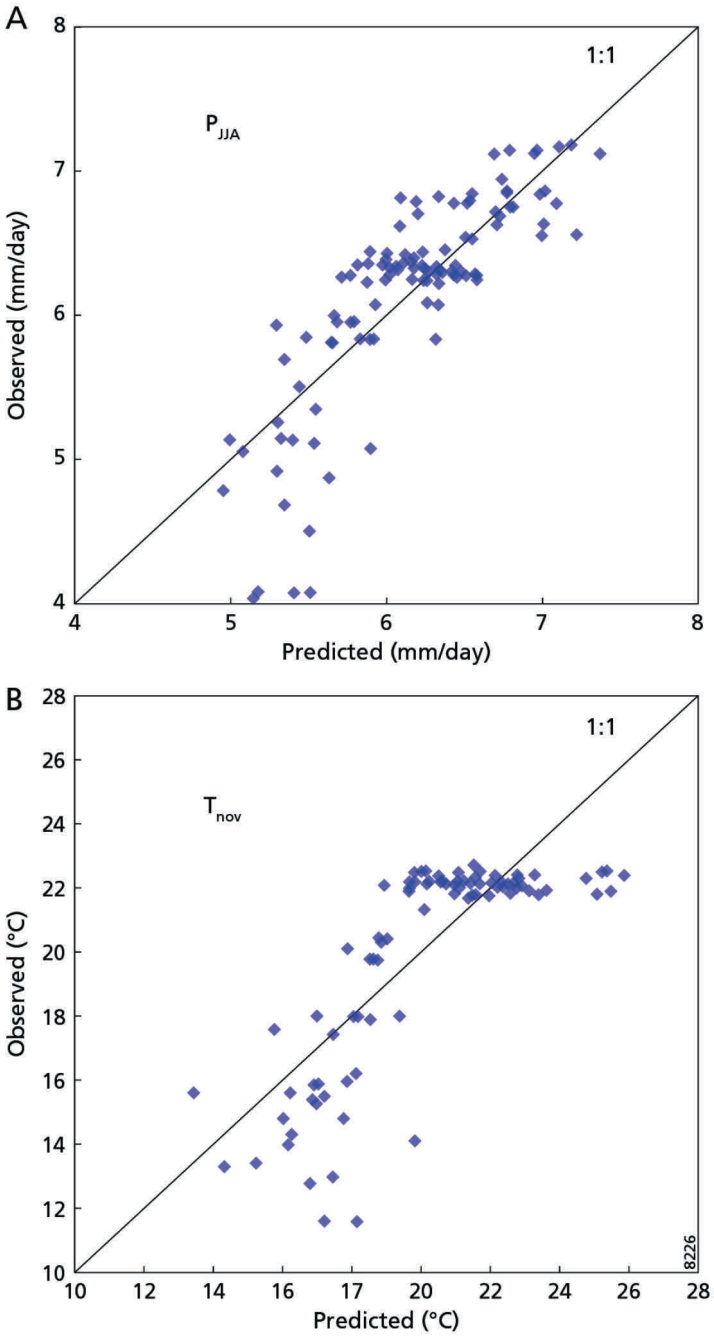

Figure C1 P_{JJA} and T_{NOV} as predicted by the inference models versus observed values. Following recommendations by Racca and Prairie (2004), the residuals are examined as a function of the model predictions (see also Table 4.1 in Chapter 4).

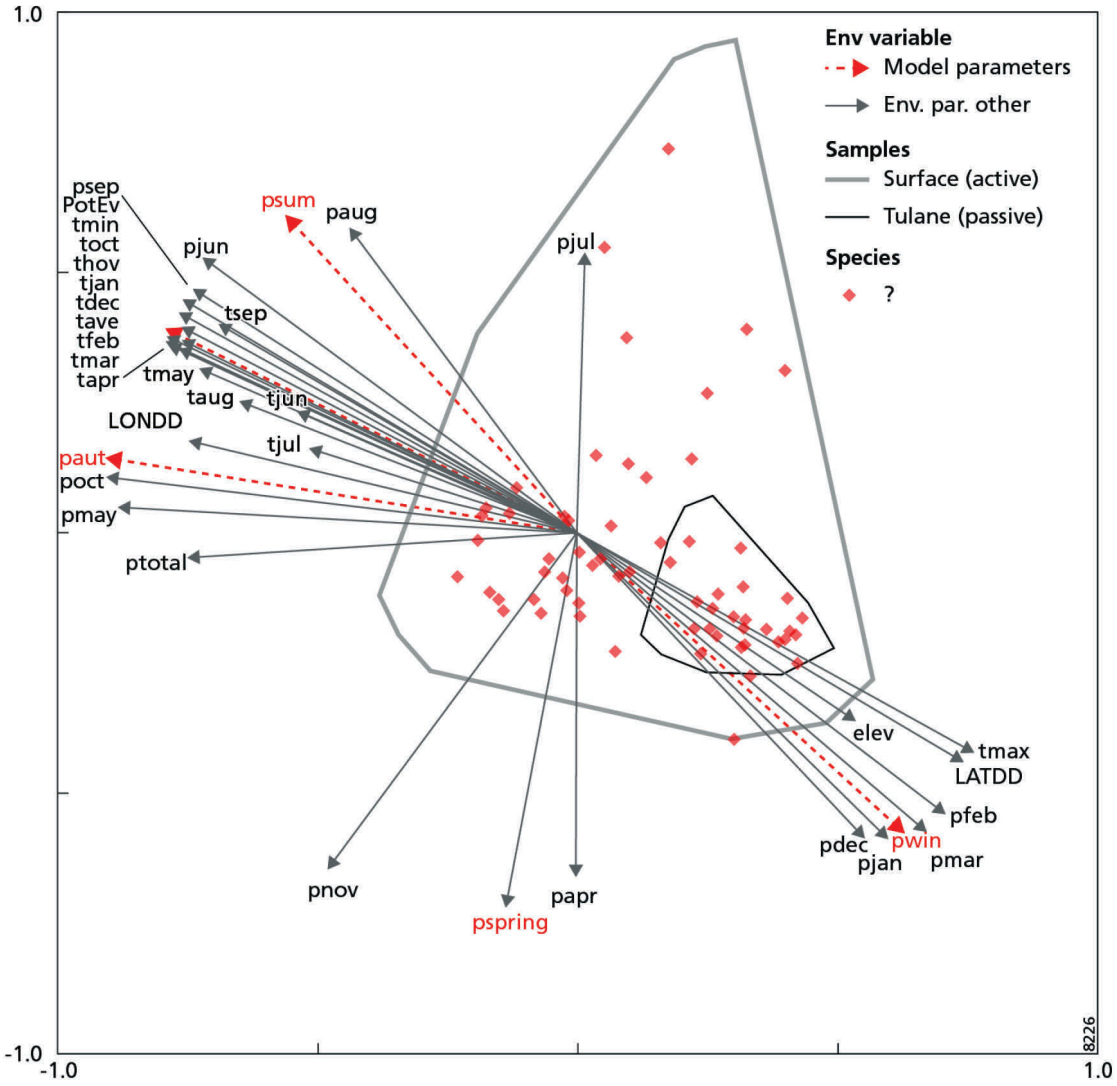

Figure C2 CCA of Lake Tulane and modern reference samples, and (bio)climatic variables.

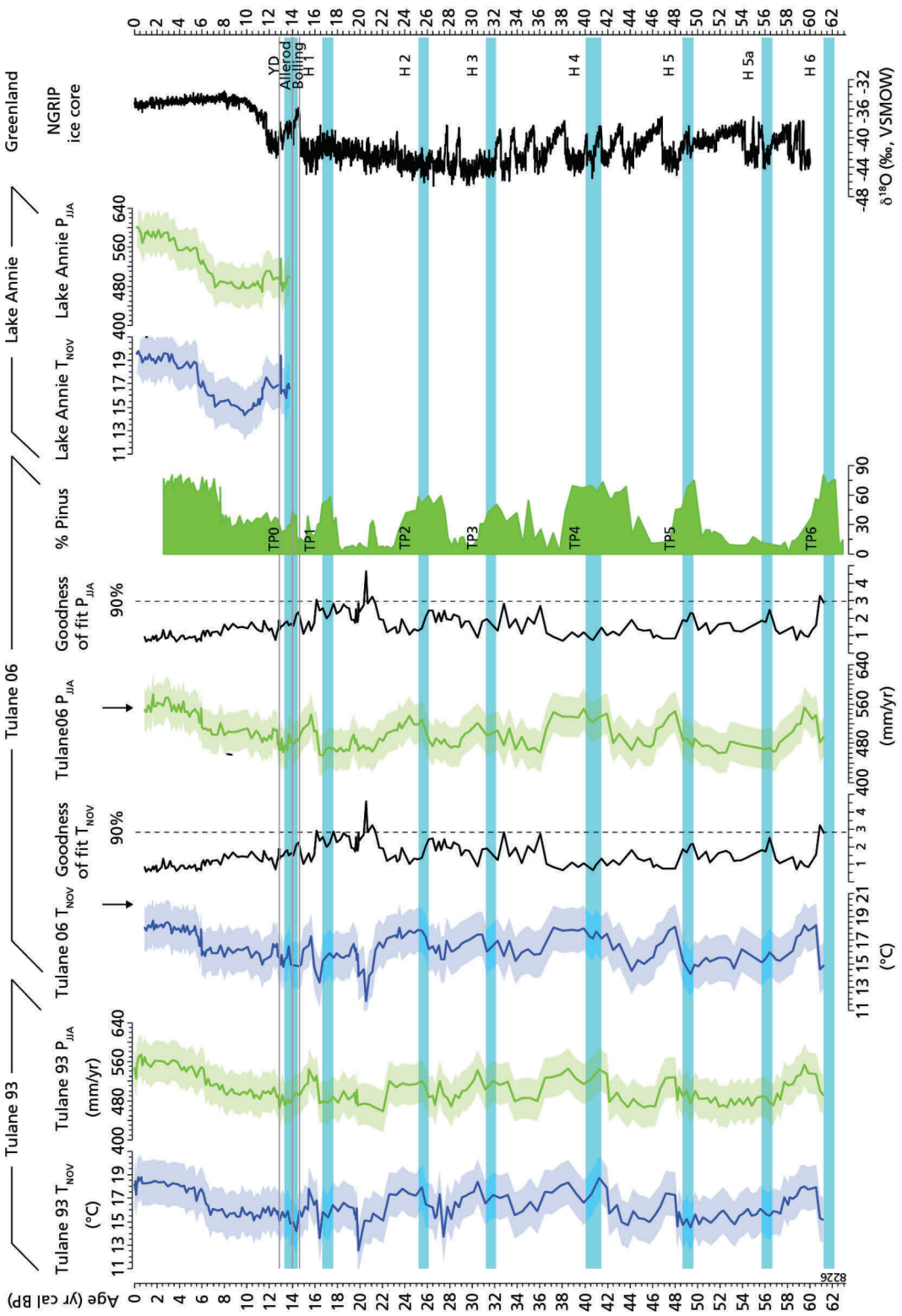

Figure C3 Reconstruction results and comparison between the independent Tulane 93 (Grimm et al. 1993), Tulane 06 (Grimm et al. 2006) and Lake Annie records used to assess the reproducibility of the paleoclimatic signals. Tulane 93 has been transferred to the Tulane 06 age scale by wiggle matching the pine percentage curves (see Grimm et al. 2006)

C2 Construction of climate model boundary conditions

In the following section we will discuss how the climate model SST boundary conditions (as shown in Figure 4.2 in the main text of Chapter 4) were constructed. The SST anomalies were calculated relative to boundary conditions of the EMIC-LGM control simulation (Figure C4). The EMIC-LGM SSTs were derived from Schäfer-Neth and Paul (2003).

First, the distribution of the zonal average of Atlantic SSTs during the LGM (Schäfer-Neth and Paul, 2003) was approximated with Equation C.1 (see also Figure C5A):

$$T(lat) = f_p + \frac{T_{\max}}{1 + C_1 \cdot \left| C_3 (lat - lat_{T\max}) \right|^{C_2}} \qquad \text{(C.1)}$$

in which *T(lat)* are the zonally averaged SSTs at a latitude (-90 <*lat*> 90), f_p is the mean freezing point of the seawater (-1.85°C) and T_{max} is the maximum temperature of 23°C at latitude lat_{Tmax} = 0°N. The scaling parameters C_1, C_2 and C_3 were set to the values presented in Table C2. Secondly, the approximation of the zonal average LGM SST distribution was reshaped by changing the scaling parameters to meet the assumptions and conditions of the EMIC-H0 and EMIC-H1 SST distributions. Finally, the absolute EMIC-H0 and EMIC-H1 SST boundary conditions were calculated by adding the zonal SST anomalies to the Atlantic SSTs (in the region 85°S–85°N) (Figures 4.2A and 4.2B in Chapter 4).

The EMIC-H+ simulation represent the hypothesis that an increased Loop Current warmed the Gulf of Mexico. To incorporate this warming, an east-west temperature gradient was imposed on the SSTs in the Gulf of Mexico at the area from 15-30°N to 80-98° equal to the south-north temperature gradient on the Atlantic at the latitudes from 8-22°N in the EMIC-H1 simulation. This results in a warming of 1-2°C of the GoM relative to LGM conditions (Figure 4.2C in Chapter 4).

Table C2 Scaling parameters to approximate the zonal average of Atlantic SSTs with Equation S1

Simulation	C1	C1	C3	T_{max} (°C)	Lat_{Tmax} (°N)
EMIC-LGM	60	8	0.0145	23	0
EMIC-H0	65.225	7	0.0145	23	-3
EMIC-H1 & H+	65.225	7	0.0145	25	-3

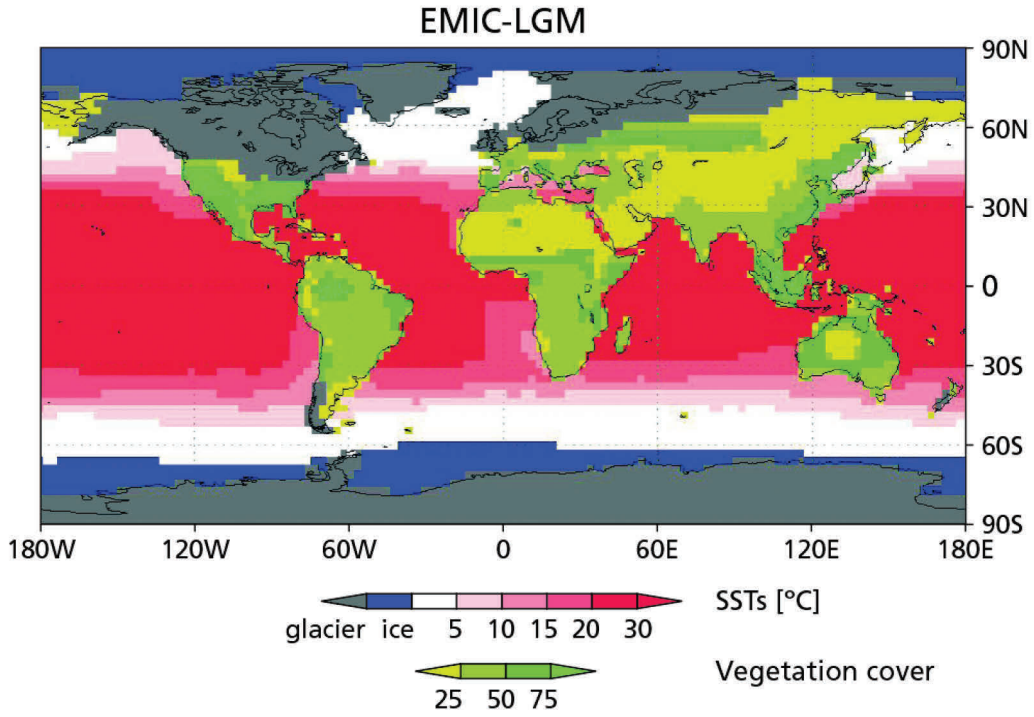

Figure C4. Boundary conditions for the EMIC-LGM control simulation. SSTs are derived from Schäfer-Neth and Paul (2003), glacial ice cover, orography, sea level, and coastlines follow Peltier (1993), and LGM vegetation is based on Crowley (1995) and Martin (1998)

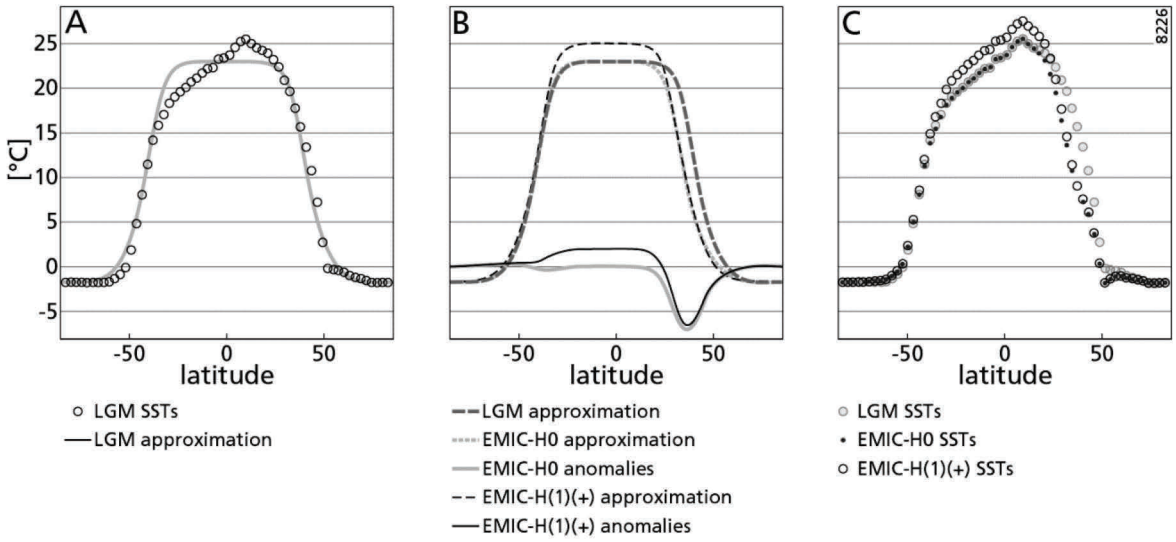

Figure C5 Approximation of the zonal average of Atlantic SSTs during the LGM (Schäfer-Neth and Paul 2003) (A) and construction of the anomalous climate model SST boundary conditions (B and C). We assume a maximum 6°C cooling of the extra-tropical North-Atlantic (EMIC-H0, EMIC-H1 and EMIC-H+) and a maximum 2°C warming of the tropical North-Atlantic (EMIC-H1 and EMIC-H+)(panel B) relative to the EMIC-LGM boundary conditions. Absolute SSTs for the experiments are calculated by adding anomalies to LGM SSTs (panel C).

C3 Climate model results

In the following section we present maps of simulated effects of SST anomalies in the (extra)tropical Atlantic on precipitation and temperature (Figures C6 and C7). The intense precipitation associated with the ITCZ is resolved over Brazil and Venezuela in the LGM simulation (Figure C6A). Cooling of the extra-tropical North Atlantic induces a southward displacement of the ITCZ in the EMIC-H0 simulation (Figure C6B). An additional equatorial warming in the EMIC-H1 simulation leads to an intensification of tropical summer precipitation and forces the ITCZ position north over the Caribbean Sea, without leading to precipitation increases over Florida (Figure C6C). An additional warming in the Gulf of Mexico in the EMIC-H+ simulation allows more intense precipitation to reach Florida and the Gulf Coast during summer (Figure C6D).

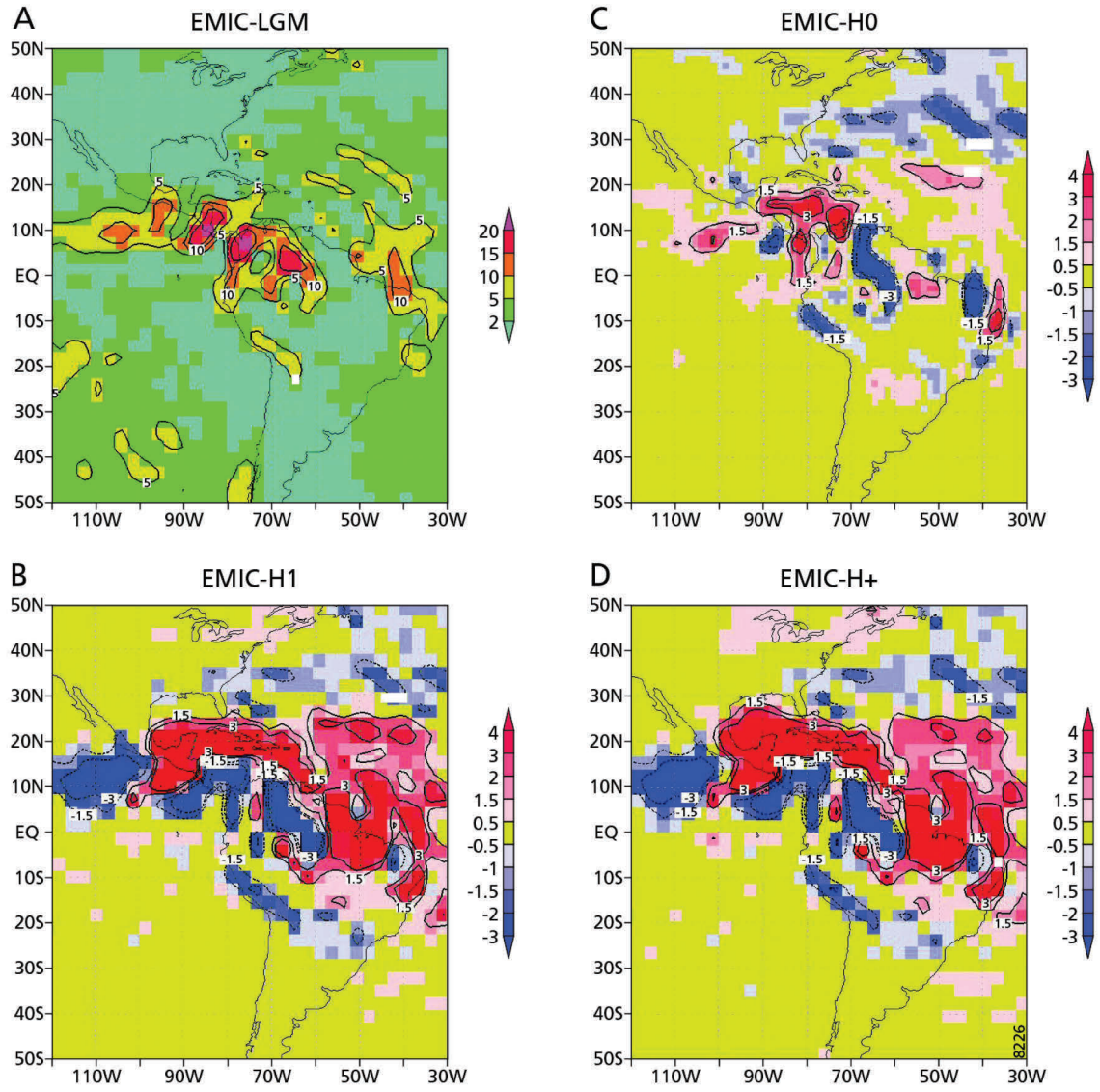

Figure C6 Results of the modelled precipitation (anomalies). All values are in [mm/day]. Simulated summer (JJA) precipitation anomalies (panels B,C and D) are calculated relative to the EMIC-LGM simulation (panel A).

The effects of the idealized warming patterns on November temperatures are more complex. Glacial conditions are calculated over North-America in the EMIC-LGM simulation, except for the Gulf Coast where November temperatures remain above 15°C (Figure C7A). Tropical conditions (25-30°C) are calculated over inland South-America. Cooling of the extra-tropical North Atlantic leads to a warming over North-America, but shows localized cooling over South-America in the EMIC-H0 simulation (Figure C7B). Additional equatorial warming leads to a localized warming over North-America and pronounced local cooling and warming over South-America in the EMIC-H1 simulation (Figure C7C). Additional warming in the Gulf of Mexico leads to localized warming over the Gulf Coast and more pronounced local cooling and warming over South-America in the EMIC-H+ simulation (Figure C7D).

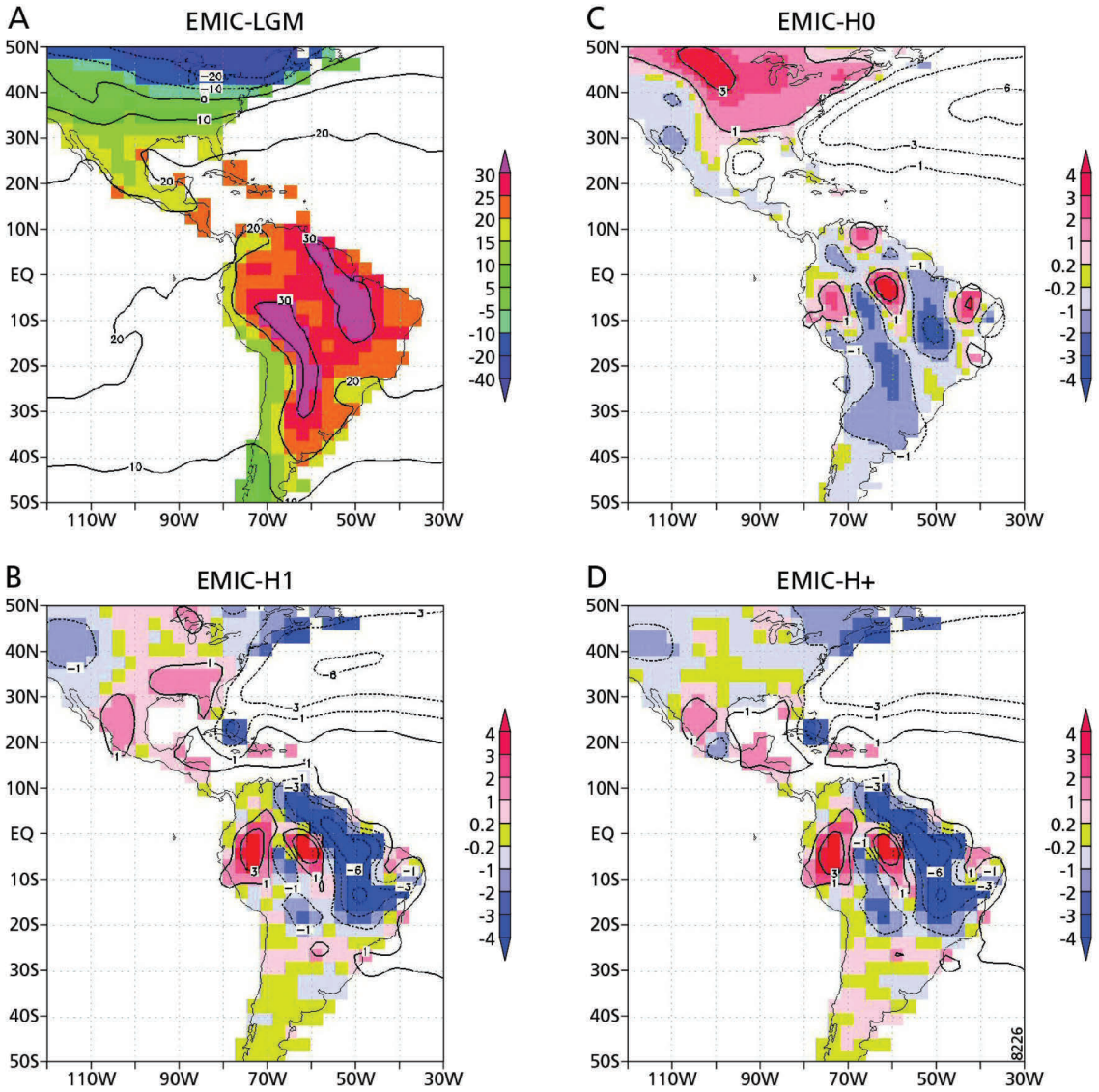

Figure C7 Results of the modelled November 2m temperature (anomalies). All values are in (°C). Simulated T_{NOV} anomalies (panels B,C and D) are calculated relative to the EMIC-LGM simulation (panel A). Land temperatures are calculated by the model, SSTs are prescribed.

References

Crowley TJ (1995) Ice-Age Terrestrial Carbon Changes Revisited. Global Biogeochem Cycles 9:377-389

Grimm EC, Jacobson Jr. GL, Watts WA, Hansen BCS, Maasch KA (1993) A 50,000-year record of climate oscillations from Florida and its temporal correlation with the Heinrich events. Science 261:198-200

Grimm EC, Watts WA, Jacobson GLJ, Hansen BCS, Almquist HR, Dieffenbacher-Krall AC (2006) Evidence for warm wet Heinrich events in Florida. Quaternary Science Reviews 25:2197–2211

Juggins S (2003) C² Software for ecological and palaeoecological data analysis and visualisation. University of Newcastle, Newcastle upon Tyne

Martin PH (1998) Land-surface characterization in climate models : biome-based parameter inference is not equivalent to local direct estimation. J Hydrol 212:287-303

Peltier W (1994) Ice age paleotopography. Science 265:195-201

Racca JMJ, Prairie YT (2004) Apparent and real bias in numerical transfer functions in palaeolimnology. Journal of Paleolimnology 31:117-124

Schäfer-Neth C, Paul A (2003) The Atlantic Ocean at the last glacial maximum: Objective mapping of the GLAMAP sea-surface conditions. In: Wefer G, Mulitza S, Ratmeyer V (eds) The South Atlantic in the Late Quaternary: Reconstruction of Material Budgets and Current Systems. Springer, Berlin, p 531-548

Ter Braak CJF, Prentice IC (1988) A theory of gradient analysis. Advances in Ecological Research 18:271-317

Ter Braak CJF, Smilauer P (2002) CANOCO reference manual and CanoDraw for Windows user's guide: software for canonical community ordination (version 4.5), Vol. Microcomputer Power, Ithaca, New York

Whitmore J, Gajewski K, Sawada M, Williams JW, Shuman B, Bartlein PJ, Minckley T, Viau AE, Webb TI, Shafer S, Anderson P, Brubaker L (2005) Modern pollen data from North America and Greenland for multi-scale palaeoenvironmental applications. Quaternary Science Reviews 24:1828-1848

Appendix D

Supplemental material for Chapter 5

Sea Surface Temperature (SST) boundary conditions

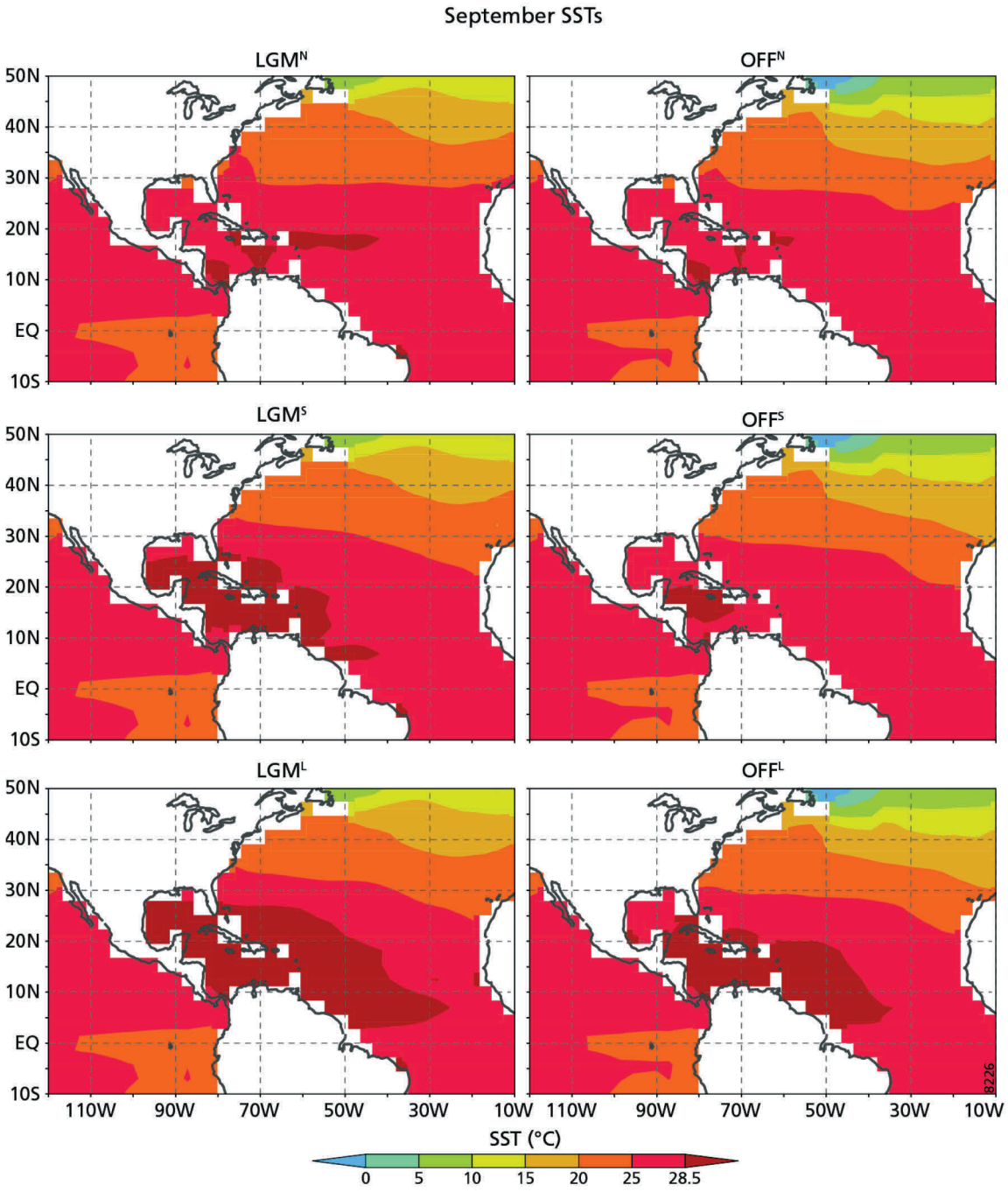

Figure D1 Overview average September SSTs (˚C) in the six atmospheric sensitivity simulations. SSTs above 28.5˚C are shaded pink to denote expansion of the AWP in each experiment.

Appendix E

Supplemental material for Chapter 6

E1 Calculation of the leaf interior transport distances

Central to our model were the geometrically schematized hypostomatous (angiosperm) broad leaves and tubular shaped (conifer) needle leaves, as shown in Figure 6.1E. Based on these schematizations we calculated the maximum leaf interior transport path length for CO_2 (l_{CO2} (m)) and the maximum leaf interior (post-venous) transport path length for water vapour (l_{H2O} (m)). The l_{H2O} was calculated following Brodribb et al.[13,18]:

$$l_{H2O} = \tau\sqrt{x_w^2 + y_w^2} \qquad \text{(E.1)}$$

in which the tortuosity, or curvature, of the diffusion pathway (τ (-)) was assumed $\pi/2$. For broad leaves, the leaf internal water transport distances parallel (x_w (m)) and perpendicular (y_w (m)) to the plane of the leaf were calculated:

$$x_W = \frac{V_d \cdot 10^{-3}}{D_v} \quad \text{and} \quad y_W = \tfrac{1}{3} T_l \,. \qquad \text{(E.2, E.3)}$$

In which V_d (-) has been empirically derived at a value of 0.65[13,18] and accounts for the hierarchical pattern of leaf venation in angiosperm broad leaves rather than a fully geometric pattern for which an value of 1 would be appropriate. The D_v ($m \cdot m^{-2}$) is the leaf vein density. The T_l (m) is the leaf thickness. Our approximation of y_w relative to T_l was motivated by our schematization of the broad-leaf morphology with veins lying amidst the upper and lower epidermis while accounting for the thickness of the cuticle and leaf veins.

As needle leaves are assumed to have a tubular shape we approximated x_w from half the distance between neighbouring stomata and an approximate vein to needle thickness ratio (ϕ_{VN} (-)), which is assumed to be 1/3 to allow comparison with the angiosperm results:

$$x_W = \sqrt{\frac{1}{2D_s}} \quad \text{and} \quad y_W = \Phi_{VN} \,. \qquad \text{(E.4, E.5)}$$

The l_{CO2} was calculated for the schematized broad leaf morphology from the leaf interior CO_2 transport distances parallel (x_c (m)) and perpendicular (y_c (m)) to the plane of the leaf:

$$l_{CO2} = \tau\sqrt{x_c^2 + y_c^2} \qquad \text{(E.6)}$$

In which:

$$x_C = \sqrt{\frac{1}{2D_s}} \qquad \text{and} \qquad y_C = \tfrac{2}{3}T_l\,. \qquad \text{(E.7, E.8)}$$

Our approximation of y_c relative to T_l was motivated by our schematization of the angiosperm broad leaf while accounting for the thickness of photosynthetically active mesophyll and the cuticle, resulting in the ratio $y_c = 2{\cdot}y_w$.

For the schematized needle leaf morphology, the l_{CO2} was calculated assuming the sites of carboxylation are located near the cuticle so that:

$$l_{CO2} = \tau\sqrt{\frac{1}{2D_s}} \qquad \text{(E.9, E.10)}$$

For the model results presented, equal and typical T_l and R_n of 200 µm were assumed to allow comparison between the results for broad leaf and needle leaf morphologies. A sensitivity analysis of the parameters used to calculate l_{H2O} and l_{CO2} is presented in the following.

The D_v and D_s values for which l_{H2O} equals l_{CO2} as a function of T_l for the broad leaf morphology are indicated in Figure E1. With D_s in the range observed for basal and early angiosperms[5] (approximately 30-700 mm^{-2}) and assuming an estimated early angiosperm leaf thickness between 150 and 300µm[13,18], l_{H2O} was reduced beyond l_{CO2} at a critical D_v between approximately 3-8 $mm{\cdot}mm^{-2}$. The results for the conifer needle leaf morphology are fundamentally different because l_{H2O} always exceeds l_{CO2} regardless of D_s and ϕ_{VN}.

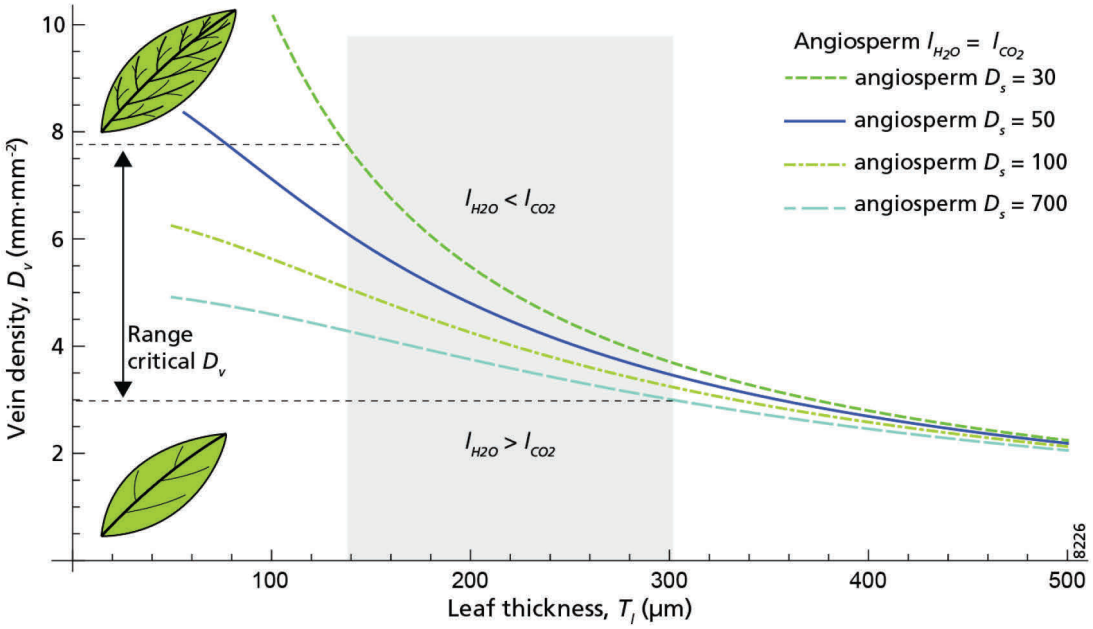

Figure E1 Calculation of the critical D_v for which I_{H2O} equalled I_{CO2} in the schematized angiosperm broad leaf. Calculations are based on a range of D_s observed in extant relatives of Early Cretaceous angiosperms[5] of 30-700 mm^{-2} and assuming a typical leaf thickness between 150 and 300µm[13,18]. Crossing of the critical D_v thereby occurred at a value of approximately 3-8 mm·mm^{-2} as indicated with the dashed lines.

E2 Graphical representation of our model approach

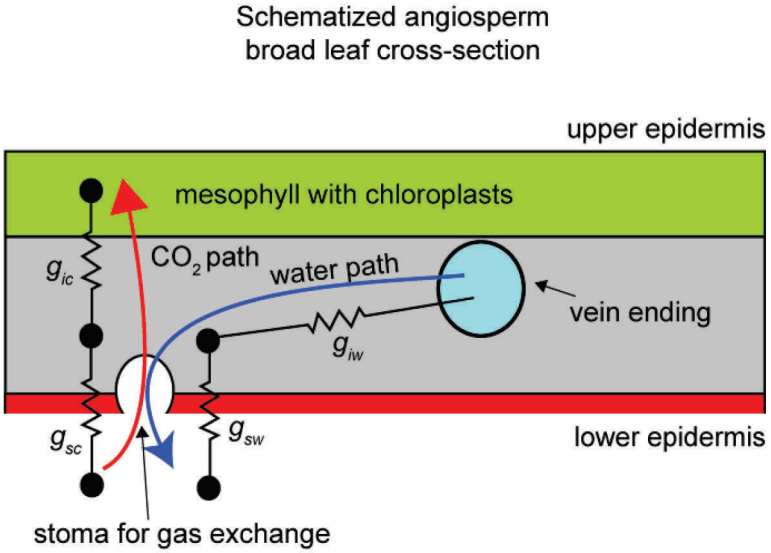

Figure E2 Graphical representation of stomatal gas exchange and leaf interior transport of CO_2 and water vapour in a schematized (angiosperm) broad leaf. The model differentiates between leaf interior conductance to CO_2 (g_{ic}) and leaf interior (post-venous) conductance to water vapour (g_{iw}) while the stomatal conductance to CO_2 (g_{sc}) is equal to stomatal conductance to water vapour (g_{sw}), when accounting for different diffusivities of CO_2 and water vapour.

E3 Statistical comparison of stomatal properties

The measurements of D_s and a_{max} on modern (1850 AD to present) subtropical mid and upper canopy species from Florida[28] and extant relatives of Early Cretaceous angiosperms[5] revealed that highest g_{smax} is achieved by those species that develop leaves with most and smallest stomata (Table E1 and Figure 6.2C in Chapter 6). A similar relation between D_s, a_{max} and g_{smax} is observed in fossil leaves over the last 400 million years[22]. A theory to explain why plants develop leaves with more and smaller stomata to reach higher g_{smax} is referred to as Stefan's diameter law[23] which also applies to stomatal gas exchange[35,43].

The statistics shown in Table E1 also revealed that both the modern angiosperm and conifer species do not exceed a similar $A_{\%}$ of approximately 6%, as shown by the 95th percentile of $A_{\%}$. An explanation why $A_{\%}$ values rarely exceed ~6% is that guard cells surrounding the stomata are held in place by several cuticle cells important for leaf development and stomatal opening/closing responses[37]. Another explanation is that at larger $A_{\%}$ interferences between neighboring stomata may reduce diffusion from individual stomata[44]. The shared consequence of these explanations is that many small stomata are required to reach highest g_{smax} within the limited space available on the leaf surface.

Table E1 Statistics on stomatal properties of modern mid to upper canopy conifer and angiosperm species from Florida[28] and extant relatives of Early Cretaceous angiosperms[5] as shown in Figure 6.2C. Species are grouped as conifers, early angiosperms and modern angiosperms. Group averages and standard deviations are indicated. Pair-wise Mann-Whitney U-tests were used, followed by a Bonferroni correction (unless indicated otherwise) to compare group means.

	Conifer (n=157, n_{95}=16)	**Early angiosperm** (n=114, n_{95}=12)	**Modern angiosperm** (n=357, n_{95}=36)	Statistics **Conifer** versus **Early angiosperm**	Statistics **Conifer** versus **Modern angiosperm**	Statistics **Early angiosperm** versus **Modern angiosperm**
g_{smax} (mol·m^{-2}·s^{-1})	1.30 (0.41)	0.40 (0.19)	2.02 (0.91)	U=4199 (p< 0.001)	U=2379 (p< 0.001)	U=1121 (p< 0.001)
D_s (mm^{-2})	174 (74)	116 (117)	689 (380)	U=3906 (p< 0.001)	U=2531 (p< 0.001)	U=10791 (p< 0.001)
a_{max} (µm^2)	252 (174)	108 (93)	50 (29)	U=187 (p< 0.001)	U=19496 (p< 0.001)	U=1453 (p< 0.001)
$A_{\%}$ (%)	3.3 (1.2)	0.8 (0.5)	2.8 (1.4)	U=87 (p< 0.001)	U=14592 (p< 0.001)	U=127 (p< 0.001)
95th percentile of A% (%)	5.7 (0.7)	1.8 (0.5)	6.2 (1.0)	U=0 (p< 0.001)	U=216 (p=0.15)$^+$	U=0 (p< 0.001)

$^+$No Bonferroni correction was used to increase the power of the test.

E4 Parameter estimation and model evaluation

The goal of our model was to investigate how changes in l_{CO2} and l_{H2O} may have affected the evolution of stomatal dimensions in angiosperms and conifers. The key results of our model emerge from the resulting changes in photosynthesis and transpirative water loss. In the following section we will evaluate these results and thereby focus on general relations observed amongst multiple species.

Before we could evaluate our model with empirical data, the parameter η (in Eq. 6.8) needed to be estimated to account for the additional limitation of CO2 diffusion through the mesophyll cells. Due to the complexity of the diffusion pathway of CO2 though intercellular airspaces, cell walls and cell interiors, it is difficult to individually measure the ratio of diffusion in the gaseous and aqueous phases[26,45]. We therefore estimated η by comparing our model with the data reviewed by Warren[46] on combined measurements of stomatal conductance to CO_2 (g_{sc} (mol·m^{-2}·s^{-1})) and g_{ic} on 53 species under ambient CO_2 of 360-400 ppm. We thereby assumed measured g_{sc} to be comparable to the term $f_d \cdot g_{cmax}$ in our model. Our model was solved for the broad leaf and needle leaf morphologies assuming an average $A_{\%}$ of 3% (cf. Table E1) and D_s ranging from 5 to 2000 mm^{-2}. In our model both g_{cmax} and g_{ic} were functions of the stomatal properties D_s and a_{max}, whereby the slope of the relation between g_{cmax} and g_{ic} was determined by the parameter η (Figure E3A). In our model, the parameter η accounted for a reduction of the diffusivity of CO_2 inside the leaf, which may be related to part of the diffusion of CO_2 occurring in the liquid phase. From the data of Warren[46] we estimated η in the range of 1.5 to 6 with an average value of 3, which was used in our analyses. As the constants τ, θ and ϕ_{VN} have the same effect as η in our model, we note that our estimation of η should be considered with regard to these other constants.

We evaluated the modelled association between leaf water transport and photosynthesis using previously published data on maximum photosynthesis in relation to leaf morphology and the length of the post-venous hydraulic pathway[18]. This post-venous hydraulic pathway was assumed comparable to the term l_{H2O} in our model. These data from Brodribb et al.[18] reveal that photosynthesis increases with reducing the l_{H2O} (Figure E3B). This relation was evaluated by solving our model for maximum photosynthesis with D_s ranging from 5 to 2000 mm^{-2} linked to a fixed $A_{\%}$ at a approximately average value of 3% and present C_a of 380 µmol·m^{-2}·s^{-1}. As our model assumed that the leaf vein endings are always saturated, any transpirative flux could theoretically be answered regardless of leaf venation. In reality, leaf water transport and venation are linked because desiccation of leaves occurs when water loss exceeds the water transport capacity of a leaf[18]. To allow comparison with the observational evidence we included the empirical relation between D_v and stomatal conductance to water vapour (g_M (mol·m^{-2}·s^{-1})) obtained from leaf gas exchange measurements by Feild et al.[5] for extant relatives of Early Cretaceous angiosperms:

$$g_M = Dv \cdot 0.0361 \qquad \text{(E.11)}$$

By assuming that g_M equaled the term $f_d \cdot g_{smax}$ in our model, we could explore the modelled effects of variations in leaf morphology, leaf venation and stomatal dimensions on photosynthesis rates and l_{H2O}. For both the angiosperm broadleaf and the conifer needle leaf morphology the generic relation between l_{H2O} and photosynthesis is reproduced by our model (Figure E3B).

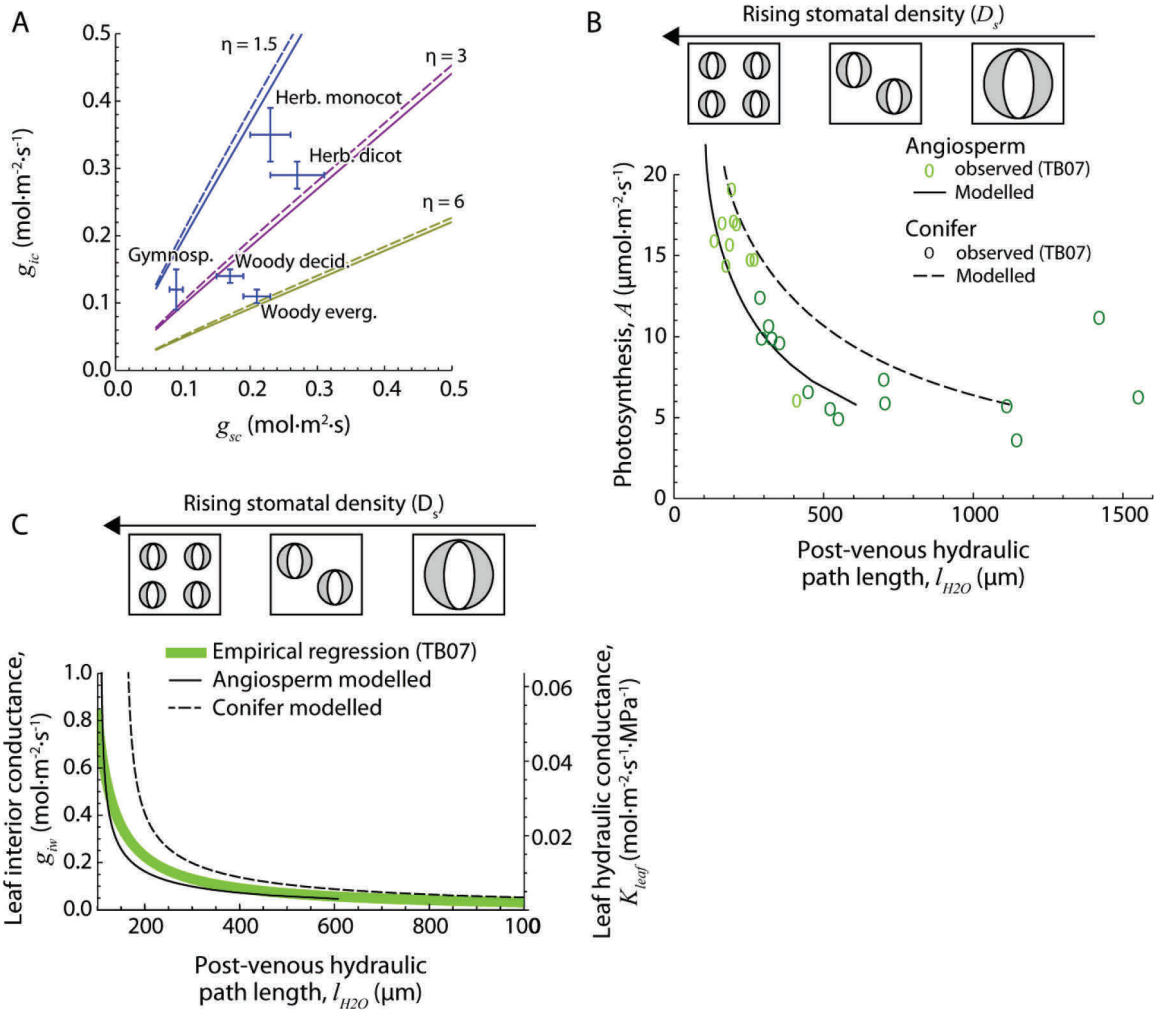

Figure E3 Model evaluation with available empirical data. (A) modelled and observed[46] relationship between leaf interior conductance to CO_2 (g_{ic} (mol·m^{-2}·s^{-1})) and stomatal conductance to CO_2 (g_{sc} (mol·m^{-2}·s^{-1})) resulting from changes in stomatal density (D_s) within the constraint of a constant $A_{\%}$. Solid lines denote model results for the (angiosperm) broad leaf morphology, dashed lines denote model results for the (conifer) needle leaf morphology. Different values of η yield different slopes in the relationship between g_{sc} and g_{ic}. (B) Observed[18] and modelled relationship between l_{H2O} and maximum photosynthesis rates for angiosperms and conifers. (E) Observed[18] relationship between l_{H2O} and leaf hydraulic conductance (K_{leaf} (mol·m^{-2}·s^{-1}·KPa^{-1})) and modelled relation between l_{H2O} and total leaf conductance to water transport (g_{tw} (mol·m^{-2}·s^{-1})) for the angiosperm and conifer leaf designs. The thick green line indicates an empirical regression (r^2 = 0.95) based on measurements of 43 species including bryophytes, lycopods, ferns, angiosperms and conifers, presented by Brodribb et al.[18].

The measurements presented by Brodribb et al.[18] of whole leaf hydraulic conductivity (K_{leaf} (mol·m^{-2}·s^{-1}·MPa^{-1})) in relation to l_{H2O} were very useful to evaluate the relation between g_{iw} and l_{H2O} in our model. These measurements reveal a log-linear relationship between l_{H2O} and K_{leaf} (Figure E3C). As our model considered the conductance of the post-venous transport path of water vapour and not the hydraulic conductance of the whole leaf as measured by Brodribb et al.[18], a direct comparison between model and data was not possible. Yet, the scaling of K_{leaf} with l_{H2O} was similar to the scaling between g_{iw} and l_{H2O} when we solved our model with D_s ranging from 5 to 2000 mm^{-2} and $A_{\%}$ of 3%.

E5 Model assumptions

Our model accounted for the leaf-interior transport pathways by considering the 3-dimensional character of diffusion around an individual stoma following an analytical solution of diffusion in a (hemi)sphere[36]. Yet, diffusion around a single stoma inside the leaf may not be fully 3-dimensional due to interference with concentration gradients generated by neighbouring stomata[26]. Numerical modelling results indicate that this interference is minimal near the stoma and increases deeper inside the mesophyll[26,47]. We therefore argued that it is important to consider the 3-dimensional character of diffusion around individual stomata in the leaf interior. Another key assumption of our model was that we described the diffusion of CO_2 and water vapour inside the leaf as occurring through and homogenous porous medium. In reality, CO_2 moves first through the intercellular airspaces[26] and then through the mesophyll cells[45]. Water moves in the opposite direction and flows as a liquid from the leaf vein endings and through the mesophyll cell walls before it evaporates somewhere inside the leaf[25]. Although models of stomatal gas exchange typically assume that evaporation occurs on the boundary of the substomatal cavity[25], experimental evidence suggest that evaporation occurs throughout the mesophyll[48] or deep inside the mesophyll[49]. Although the exact location of evaporation remains to be determined[25] and will likely depend on the water status of a leaf, we considered the longest leaf interior transport pathways in our model. It could be argued that average transport lengths would be more representative, yet we refrained from this approach because it yielded comparable results and complicated our calculations. As an alternative to our analytical approach, 3-dimensional numerical models could have been used to solve leaf interior gas transport[45,47,50]. However, a drawback of such numerical approaches is their limited flexibility required to explore the implications of variations in leaf morphology and stomatal adaptations on the efficiency at which water is exchanged for CO_2.

References

43. Brown, H. T. & Escombe, F. Static Diffusion of Gases and Liquids in Relation to the Assimilation of Carbon and Translocation in Plants. [Abstract]. Proceedings of the Royal Society of London 67, 124–128 (1900).
44. Ting, I. P. & Loomis, W. E. Diffusion Through Stomates. American Journal of Botany 50, 866–872 (1963).

45. Tholen, D. & Zhu, X.-G. The Mechanistic Basis of Internal Conductance: A Theoretical Analysis of Mesophyll Cell Photosynthesis and CO2 Diffusion. Plan Physiol 156, 90–105 (2011).
46. Warren, C. R. Stand aside stomata, another actor deserves centre stage: the forgotten role of the internal conductance to CO2 transfer. J Exp Bot 59, 1475–1487 (2008).
47. Parkhurst, D. F. A three-dimensional model for CO2 uptake by continuously distributed mesophyll in leaves. J Theor Biol 67, 471–488 (1977).
48. Nonami, H. & Schulze, E.-D. Cell water potential, osmotic potential, and turgor in the epidermis and mesophyll of transpiring leaves. Planta 177, 35–46 (1989).
49. Farquhar, G. D. & Raschke, K. On the Resistance to Transpiration of the Sites of Evaporation within the Leaf. Plant Physiol 61, 1000–1005 (1978).
50. Roth-Nebelsick, A. Computer-based Studies of Diffusion through Stomata of Different Architecture. Ann Bot 100, 23–32 (2007).

Summary

The continuous recycling of water is essential to our planet's ability to support life as we know it. The physical properties of water in its liquid, solid and gaseous phases allow for the redistribution of energy in the oceans and atmosphere keeping climate conditions in a life-sustaining range. At the scale of individual organisms, water and energy are also essential for the biochemical reactions required for life to develop. Especially plant life is an important part of the global energy and water cycles because it captures light from the sun and exchanges carbon dioxide (CO_2) for water vapor and oxygen by photosynthesis. The terrestrial biosphere may affect the water and carbon cycles because plants actively control the rate at which they lose water to the atmosphere by closing the microscopically small pores that cover the surfaces of their leaves (the cuticle). These pores are called stomata (Greek for *mouths*) and allow plants to take up CO_2 from the atmosphere and limit their water loss through the cuticle. Interactions between the biosphere and climate system may change with plastic and genetic adaptations in individual plants or the plant community. By adjusting water use and altering carbon sequestration, these plant responses may act to amplify or counteract climatic changes via feedbacks with the water and carbon cycles. As plants are an interactive component in the complex climate system, they can also be used to indicate climatic changes. Fossilized plant remains can therefore be used as so-called paleoecological proxy evidence to infer changes of the climate prior to the start of instrumental measurements.

In this thesis we focused on this dual role plants play in the climate system by altering and documenting changes in the water and carbon cycles. Our aim was to gain understanding about interactions between the various components of the climate system during time periods with relatively rapid fluctuations in the water and carbon cycles. The main study site was the Florida peninsula and its surrounding ocean basins. This region is ecologically and climatologically interesting because it is situated on the boundary between the humid tropics and the subtropics. The close proximity to the Atlantic Ocean and Gulf of Mexico makes that changes in ocean circulation responsible for global climate fluctuations are documented by the Florida plant community. Due to the moist climate, (sub)fossil plant remains are stored in peat deposits and lake sediments that allowed us to study ecosystem responses to past climate changes. In the Florida region we investigated three coupling pathways that interlink the water and carbon cycles within the climate system: (1) land-atmosphere coupling reflected by changes in leaf gas exchange of plants responding to changes in atmospheric CO_2 concentrations, (2) ocean-atmosphere-land coupling reflected by changes in plant community in response to rapid climate fluctuations that occurred during the last glacial period, and (3) ocean-atmosphere-ocean coupling between the Atlantic and Pacific basins as a potential feedback with rapid climate fluctuations that occurred during the last glacial. The coupling between these climate system components was investigated using proxy data and numerical models. Models thereby helped to explore mechanisms and sharpen hypotheses to explain proxy-based observations.

Our results underlined that the terrestrial biosphere links the global water and carbon cycles and that stabilizing (negative) and destabilizing (positive) feedbacks emerge within the climate system at various spatial and temporal scales. In chapter 2 we presented measurements of the stomatal density and pore sizes of fully opened stomata on the leaves of nine common species from Florida. These leaves were stored in terrestrial organic sediments and in herbaria over the last 150 years and subsequently span a CO_2 range between approximately 280 and 390 parts per million (ppm). The species studied include angiosperms, conifers and a fern. With these data we calculated the maximal stomatal conductance *(g_{smax})* of the studied leaves, which is a generic measure for the upper limit of their stomatal gas exchange capacity. Our results revealed a 34% (±12%) reduction in g_{smax} expressed per 100 ppm CO_2 increase. This response is comparable among the conifers and angiosperm species. We did observe differences in species-specific g_{smax} values, whereby the angiosperms sampled attained highest g_{smax} by developing leaves with numerous small stomata and the conifers and fern attained lower g_{smax} with fewer and larger stomata. These differences in stomatal properties were explained from different evolutionary backgrounds of angiosperms, conifers and ferns.

Adaptive responses in the diffusive properties of stomata under rising atmospheric CO_2 concentrations may affect transpiration and change the surface energy balance. In chapter 3.1 we therefore investigated the changes in transpiration that may result from changes in g_{smax}, as shown in chapter 2. Hereto we first explored a mechanism potentially underlying the observed stomatal responses. It was hypothesized that the observed adaptations of g_{smax} were aimed at optimizing photosynthesis with minimal transpiration in response to rising atmospheric CO_2 concentrations. The optimization hypothesis entails that carbon gained by photosynthesis is maximized under the constraint of water lost to transpiration. This principle stools on the idea that, even when water is ample, water loss presents a cost to plants. We used a stomatal optimization model to investigate if the observed changes in g_{smax} can be explained by optimization at decadal and longer timescales. The optimization model reproduced the observed changes in g_{smax} under the anthropogenic CO_2 rise and thereby provided support for our hypothesis. A potential unrealistic result of the optimization model is the prediction that g_{smax} will continue to decrease under rising atmospheric CO_2 without considering the potential constraints posed by the phenotypic plasticity of individual plants. We therefore estimated ranges in phenotypic plasticity based on observations at geological timescales. Our optimization model revealed that a doubling of present atmospheric CO_2 concentrations may reduce annual transpiration fluxes from the Florida species by approximately 50%. These results sparked a debate about the stomatal control on transpiration and the potential feedbacks with the hydrological cycle, as presented in chapter 3.2. The key point of discussion involved the scaling between leaf-level responses and the effects on transpiration at larger spatial scales. We see that these processes may mitigate the stomatal control on transpiration, however, we also note that plants eventually determine the maximum rates of transpiration by their dynamic stomatal responses. Changes in g_{smax} may thereby crucially constrain the maximum transpiration rates of individual leaves.

Plant responses to environmental changes may also be used to infer climate changes that occurred prior to the start of instrumental measurements. In chapter 4 we have shown that rapid climatic fluctuations that occurred at millennial timescales during the last glacial period (between approximately 114 and 11.7 thousand years ago) were documented in a pollen record from Lake Tulane in Florida. These community level responses reflected changes in the (sub)tropical hydrological cycle related to a disruption of northward heat transport by the Atlantic Meridional Overturning Circulation (AMOC). Using a pollen–climate inference model, we quantified the climate changes and consistently found precipitation and temperature increases during pine phases coeval with Heinrich events. These results were at odds with cooling that occurred in the extra-tropical North Atlantic region due to a disruption of the AMOC. The warming that was reflected in sea surface temperature reconstructions from the Gulf of Mexico and the western tropical Atlantic suggested a potential link with the heat and moisture anomalies observed in Florida. With climate model simulations we found that these low-latitude sea surface temperature anomalies could explain the precipitation and temperature increases reflected in Florida. This result supported proxy-based evidence of a persistent Atlantic Warm Pool (AWP) during summer throughout the glacial. The Atlantic warm pool is defined by the 28.5°C sea surface temperature isotherm and comprises the (sub)tropical Northwest Atlantic, Caribbean Sea and Gulf of Mexico during summer and fall in the present climate. These results provided novel evidence about changes in the (sub)tropical hydrological cycle during times of rapid glacial climate fluctuations.

In chapter 5 we further explored the potential role of the AWP in altering the (sub)tropical hydrological cycle in relation to the millennial-scale glacial climate fluctuations. Here, our focus was on the potential feedbacks between the (sub)tropical hydrological cycle and the intensity of the AMOC via changes in the freshwater budget of the North Atlantic. As the AMOC is driven by the density difference between the surface water and the deep water in the North Atlantic, changes in the Atlantic freshwater budget may alter the AMOC. At present, an inverse relation exists between the size of the AWP and strength of the Azores high pressure system due to so-called Gill-type atmospheric response. Via this response, changes in AWP area initiate inverse changes in the amount of atmospheric moisture transported out of the Atlantic basin, across the Central American isthmus and towards the Pacific. Based on a review of sea surface temperature reconstructions we developed hypotheses regarding potential AWP dynamics in relation to millennial-scale glacial climate fluctuations. These hypotheses were explored using a combination of coupled and uncoupled ocean-atmosphere models. Our simulations of the glacial atmosphere indicated that variations in AWP expansion evoke inverse surface pressure changes in the Azores High and thereby alter the low-level atmospheric (moisture) flow across the Central American isthmus, resembling the present-day response. These results were discussed in relation to proxy based evidence for changes in cross-isthmus moisture transport. Although our results remain inconclusive about the spatial and temporal dynamics of the glacial AWP, they imply a potential role for changes in the (sub)tropical hydrological cycle in destabilizing the AMOC during millennial-scale glacial climate fluctuations.

In chapter 6 we explored the Cretaceous period which took place in the deep past of the Earth's history between 146 and 66 million years ago. During this period, evolving (flowering) angiosperm plant species experienced a period of rapid evolution while atmospheric CO_2 concentrations declined. Prior to the Cretaceous period, coniferous species dominated the upper canopy in most forested ecosystems. The revolutionary rise of angiosperms during the Cretaceous thereby initiated an evolutionary development towards modern biodiversity. To explain the sudden evolutionary success of angiosperms during the Cretaceous we presented a novel hypothesis involving morphological differences between planar-shaped (broad) leaves and tubular shaped (needle) leaves. Central to our hypothesis is that the evolutionary development to more densely veined leaves allowed early angiosperms to surpass an evolutionary “tipping point” once the leaf interior (post-venous) transport path length for water was reduced beyond the leaf interior transport path length for CO_2. We proposed that surpassing this "tipping point" suddenly rewarded evolving angiosperms with rising photosynthetic carbon returns from equal transpirative water loss by developing leaves with more and smaller stomata. The resulting carbon uptake advantage may have offered evolving angiosperms a sudden competitive advantage over conifers under the falling CO_2 concentrations of the Cretaceous. The proposed mechanism entails that only broad-leaved angiosperms that surpassed the critical leaf vein density could optimize gas exchange by developing leaves with more and smaller stomata. This adaptation was required to increase leaf gas exchange capacity within the constraint of leaf surface area available for stomatal pores. The resulting global rise of angiosperms may have had implications for carbon sequestration and water cycling due to their unprecedented leaf gas exchange capacities.

The results presented in this thesis have shown novel aspects regarding the interactions between the terrestrial biosphere and the climate system via changes in the water and carbon cycles. We presented new ideas on how plants may optimize their leaf gas exchange under changes in atmospheric CO_2 concentrations. These ideas provide new insights for the consequences of continued anthropogenic CO_2 emissions on the climate system. Besides that the enhanced greenhouse effect may alter the climate by global warming and intensification of the freshwater cycle, the biosphere will also be directly influenced by elevated atmospheric CO_2 concentrations. The question how the combined effects of climate change and carbon 'fertilization' will alter interspecies competition and the interaction between the biosphere and atmosphere remains a topic of ongoing research. Also we have shown that plant responses may be used as proxy evidence to infer climate changes that occurred in the past. Our results imply that uncertainties are introduced in the (quantitative) interpretation of plant responses in terms of climate variables due to the ability of plants to adapt their phenotypes and genotypes to environmental changes. Moreover, stomatal responses may not only reflect changes in environmental conditions such as atmospheric CO_2 concentrations and water availability, they could also be indicative of evolutionary advances in the plants water transport system. We therefore argue that climatic interpretation of paleoecological proxy-evidence should be embedded in multi-disciplinary approaches including climate modeling.

Samenvatting

Water is essentieel voor het leven op aarde. Allereerst speelt water een centrale rol in de biochemische processen die het ontstaan van leven mogelijk maken. Daarnaast is de waterkringloop een belangrijk onderdeel van het klimaatsysteem. De waterkringloop speelt namelijk een rol bij de verdeling van de warmte van de zon in de atmosfeer en oceanen, waardoor het klimaat op aarde relatief stabiel blijft. Dit proefschrift omvat onderzoek naar de interacties tussen de waterkringloop en het klimaat en behandelt daarbij in detail de rol die planten daarin spelen. Deze aandacht voor planten is belangrijk omdat zij een dynamische rol spelen in de kringlopen van water en koolstof en zo invloed uitoefenen op het klimaat. Planten benutten namelijk de energie van zonlicht en zetten hiermee door middel van fotosynthese koolstofdioxide (CO_2) en water om in zuurstof en suiker. De opname van CO_2 uit de atmosfeer gaat via microscopisch kleine huidmondjes in het relatief ondoorlatende oppervlak van bladeren. Doordat CO_2- en watermoleculen ongeveer even groot zijn, gaat de opname van CO_2 onvermijdelijk gepaard met het verlies van water via deze huidmondjes. Bijna al het water dat een plant opneemt bij de wortels verlaat daarom het blad weer via de huidmondjes. Deze stroming van water door de plant speelt een belangrijke rol bij het transport van voedingsstoffen en hormonen. Echter, wanneer onvoldoende water beschikbaar is bestaat het gevaar dat een plant uitdroogt. Planten hebben daarom de mogelijkheid dit waterverlies te beperken door hun huidmondjes te sluiten. Het sluiten van huidmondjes duurt enkele minuten en biedt directe bescherming tegen uitdroging, maar deze aanpassing beperkt ook de CO_2-opname en daardoor de groei. Planten kunnen hun gasuitwisseling ook reguleren door, op langere tijdschalen, het aantal en de grootte van de huidmondjes structureel aan te passen. Dit gebeurt bijvoorbeeld wanneer de CO_2 concentratie in de atmosfeer stijgt zodat planten met minder waterverlies toch voldoende CO_2 kunnen 'inademen'. Bij een veranderend klimaat kunnen deze dynamische eigenschappen van planten voor terugkoppelingen in het klimaatsysteem zorgen doordat ze de water- en koolstofkringlopen beïnvloeden. Omdat plantensoorten onderling verschillen in hun eigenschappen en de mate waarin ze deze kunnen aanpassen, kan klimaatverandering ook leiden tot veranderingen in de samenstelling van de plantengemeenschap. Fossiele plantenresten, zoals pollen en bladeren, kunnen daarom dienen als indicator (proxy) van klimaatveranderingen die zich in het verleden hebben voorgedaan. De interpretatie van deze paleoecologische proxy geeft vervolgens inzicht in de dynamiek van het klimaat over langere tijdschalen.

Dit proefschrift onderzoekt de rol die planten in het klimaatsysteem spelen door de water- en koolstofkringlopen te beïnvloeden. Daarnaast worden paleoecologische proxies gebruikt om klimaatveranderingen in het verleden te reconstrueren. Het doel van dit onderzoek is om inzicht te krijgen in de interacties tussen de verschillende componenten van het klimaatsysteem tijdens perioden met relatief snelle veranderingen in de kringlopen van water en koolstof. Het onderzoeksgebied omvat hoofdzakelijk het schiereiland van Florida en de omringende oceaanbekkens. Deze regio is bijzonder interessant voor klimaatonderzoek omdat, ten eerste, het relatief vochtige klimaat ervoor

zorgt dat plantenresten niet worden afgebroken, maar bewaard blijven op de bodem van moerassen en meertjes. Florida herbergt daardoor een schat aan informatie over het klimaat in het verleden. Ten tweede zorgt de nabijheid van de Atlantische Oceaan en de Golf van Mexico ervoor dat veranderingen in oceaanstromingen, die in het verre verleden voor sterke klimaatsfluctuaties hebben gezorgd, worden gedocumenteerd in paleo-ecologische proxies. De analyse van het fossiele plantenmateriaal uit Florida geeft daardoor inzicht in de dynamiek van het klimaatsysteem op grotere schaalniveaus. Het onderzoek van dit proefschrift richt zich op drie belangrijke koppelingen tussen een aantal centrale componenten van het klimaatsysteem:
(1) de koppeling tussen het land en de atmosfeer. Hierbij onderzoeken we hoe de gasuitwisseling van planten is veranderd door de aanpassing van planten aan de stijgende CO_2-concentratie in de atmosfeer,
(2) de koppeling tussen de zee en het land tijdens snelle klimaatschommelingen in de laatste ijstijd, en
(3) de koppeling tussen de Atlantische en Stille Oceaan door verandering in de atmosferische circulatie tijdens deze snelle klimaatschommelingen.
De koppelingen tussen deze componenten van het klimaatsysteem worden onderzocht met een combinatie van voornamelijk paleoecologische proxy data en computermodellen. De computermodellen helpen om mechanismen te onderzoeken die niet direct zichtbaar zijn in de proxy data, maar wel een rol spelen bij de koppelingen in het klimaatsysteem.

De resultaten van dit onderzoek benadrukken de rol die planten spelen in de wisselwerkingen tussen de kringlopen van water en koolstof. Daarnaast laten we zien dat stabiliserende (negatieve) en destabiliserende (positieve) terugkoppelingen kunnen ontstaan door wisselwerking tussen verschillende componenten van het klimaatsysteem, waarbij de watercyclus een belangrijke rol speelt. In hoofdstuk 2 presenteren we metingen van het aantal en de grootte van huidmondjes op de bladeren van negen veel voorkomende plantensoorten uit Florida. Deze bladeren zijn afkomstig uit veenbodems en herbaria in Florida en geven een beeld van de aanpassing van huidmondjes aan de CO_2-concentratie in de atmosfeer die sind 1850 is gestegen van ongeveer 280 tot 390 parts per million (ppm). De onderzochte soorten zijn vijf loofbomen, drie naaldbomen en één varen. Met de metingen van de grootte en aantallen van de huidmondjes hebben we de maximale doorlatendheid van de bladeren (g_{smax}) voor de uitwisseling van CO_2 en waterdamp berekend. De g_{smax} gaat uit van een maximale opening van de huidmondjes en is een algemene maat voor de bovengrens van de gasuitwisseling van bladeren. Onze resultaten laten zien dat, gemiddeld voor alle soorten, de g_{smax} afneemt met 34% (±12%) per 100 ppm CO_2-toename. Verder valt het op dat alle soorten de waarde van hun g_{smax} in gelijke mate aanpassen. Wel zien we duidelijke verschillen in de grootte en de aantallen van de huidmondjes van de naaldbomen en de loofbomen. De loofbomen hebben bladeren met veel kleine huidmondjes en een hoge g_{smax}. Dit in tegenstelling tot de naaldbomen die juist weinig grote huidmondjes en een lagere g_{smax} hebben. Onze hypothese is dat deze verschillen in eigenschappen van huidmondjes te maken hebben met het verschil in watertransportsysteem van loofbomen en naaldbomen.

Hoewel het reeds bekend was dat planten hun huidmondjes aanpassen aan veranderende CO_2-concentraties, was de reden hiervoor nog onduidelijk. Ook onbekend was welke gevolgen deze aanpassing zou kunnen hebben voor de wisselwerking tussen planten en de atmosfeer, aangezien het vochtgehalte in de atmosfeer zal worden beïnvloed door een veranderende transpiratie. In hoofdstuk 3.1 presenteren we daarom een onderzoek naar welk mechanisme de waargenomen aanpassing van huidmondjes aan de stijgende CO_2-concentratie zou kunnen verklaren en welke gevolgen deze aanpassing heeft voor de transpiratie van planten. We onderzochten de hypothese dat de aanpassing van g_{smax} is gericht op het optimaliseren van fotosynthese met minimale transpiratie. Het principe achter deze hypothese is dat planten de baten van CO_2-opname voor fotosynthese afwegen tegen de daarmee samenhangende kosten die gemoeid gaan met het waterverlies door transpiratie. Dit principe zou in het algemeen kunnen gelden omdat het transport van water door de plant altijd kosten met zich meebrengt. Zelfs wanneer er voldoende water beschikbaar is, moet een plant namelijk investeringen doen om een uitgebreid watertransportsysteem te onderhouden. Om deze hypothese te testen gebruikten we een rekenmodel dat de aanpassing van de grootte en de aantallen van de huidmondjes beschrijft op tijdschalen van tientallen jaren en langer. Dit model beschrijft de waargenomen aanpassing van g_{smax} bij de stijgende CO_2-concentraties over de laatste 150 jaar goed. Een mogelijk onrealistisch resultaat is echter de modelvoorspelling dat g_{smax} zal blijven dalen bij een verdere stijging van de CO_2-concentratie. Hierbij wordt geen rekening gehouden met de mogelijke limieten van de plasticiteit van planten om g_{smax} blijvend te veranderen. Zelfs wanneer we rekening houden met een mogelijke limiet van deze plasticiteit, laat ons model zien dat een verdubbeling van de huidige CO_2-concentratie voor een 50% afname van de transpiratie van de onderzochte plantensoorten in Florida kan zorgen. Deze resultaten waren aanleiding voor een discussie over de invloed die planten hebben op hun waterverlies. Deze discussie, die bestaat uit een ingezonden brief van Franco Miglietta en collega's naar het tijdschrift waar onze studie is gepubliceerd en onze reactie daarop, is terug te lezen in hoofdstuk 3.2. Het belangrijkste discussiepunt is de invloed van de opschaling van veranderingen in transpiratie op bladniveau naar de schaal van complete bossen. We zijn het eens met de opmerking van Franco Miglietta dat op grotere schaalniveaus de invloed van huidmondjes op transpiratie vermindert. Maar we stellen echter ook dat planten wel degelijk controle hebben op het waterverlies door enerzijds hun huidmondjes te sluiten en anderzijds de aantallen en grootte van hun huidmondjes aan te passen.

Deze aanpassingen van planten en veranderingen in de soortensamenstelling kunnen ook worden gebruikt om inzicht te krijgen in klimaatveranderingen die zich in het verre verleden hebben afgespeeld. In hoofdstuk 4 gebruikten we stuifmeelkorrels om inzicht te krijgen in veranderingen in de soortensamenstelling van de plantengemeenschap van Florida tijdens de laatste ijstijd. Deze koude klimaatperiode speelde zich af tussen 114 en 11.7 duizend jaar geleden. De gebruikte pollen zijn afkomstig uit een sedimentkern van de bodem van een meertje in Florida en weerspiegelen sterke veranderingen in de plantengemeenschap die samen lijken te hangen met perioden dat het warmtetransport met de warme golfstroom was verstoord. Het stilvallen van de warme golfstroom is al

eerder aangetoond en lijkt te maken te hebben met het smelten van de ijskap die tijdens de laatste ijstijd over een groot deel van Noord Amerika en Canada lag. Het hierbij vrijgekomen (zoete) smeltwater verstoorde het grootschalige stromingspatroon in de Atlantische Oceaan en het warmtetransport met de warme golfstroom. In zulke perioden met een verstoorde warme golfstroom zien we een toename van plantensoorten in Florida die goed gedijen in een warm en vochtig klimaat. Deze resultaten lijken in eerste instantie tegenstrijdig met andere klimaatsreconstructies, die aangeven dat tijdens deze perioden juist een sterke afkoeling plaatsvond van de Noord-Atlantische Oceaan. In tegenstelling tot deze afkoeling in het noorden zijn er echter ook aanwijzingen dat de Golf van Mexico en Caribische Zee juist opwarmden. Om te onderzoeken of deze opwarming mogelijk de oorzaak zou kunnen zijn van de veranderingen in de plantengemeenschap in Florida deden we simulaties met een klimaatmodel. Deze modelresultaten geven aan dat opwarming van de Golf van Mexico en de Caribische Zee inderdaad verantwoordelijk zou kunnen zijn voor een toename van de neerslag en de temperatuur in Florida.

In hoofdstuk 5 onderzochten we in meer detail hoe de temperatuur van de Golf van Mexico en de Caribische Zee invloed uitoefent op de hydrologische cyclus in deze regio. We keken daarbij vooral naar terugkoppelingen tussen veranderingen in de hydrologische cyclus in deze regio en de intensiteit van het warmtetransport van de warme golfstroom. Zulke terugkoppelingen kunnen ontstaan omdat de noordwaarts gerichte warme golfstroom wordt aangedreven door het dichtheidsverschil tussen het oppervlaktewater en het diepe zeewater in de regio van Groenland. Wanneer het relatief warme en zoute oppervlaktewater vanuit de (sub)tropen richting de noordelijke Atlantische Oceaan stroomt, koelt het af en wordt het zwaarder. Uiteindelijk zinkt dit zoute en koude water naar de oceaanbodem waar het via de bodem weer zuidwaards stroomt. Omdat zowel de temperatuur als het zoutgehalte van invloed zijn op deze stroming wordt de gehele cyclus aangeduid als de thermohaliene circulatie. In hoofdstuk 4 hebben we al laten zien dat veranderingen in de warme golfstroom invloed kunnen hebben op de hydrologische cyclus in de regio van Florida. Omgekeerd heeft de hydrologische cyclus ook invloed op het zoutgehalte van de Atlantische Oceaan, waardoor een terugkoppeling met de warme golfstroom kan ontstaan. Deze terugkoppeling ontstaat omdat er een verband is tussen de temperatuur van de (sub)tropische Atlantische Oceaan en de luchtdruk in de regio van de Azoren. De luchtdruk in de regio van dit zogenaamde Azorenhoog wordt lager wanneer de (sub)tropische Atlantische Oceaan opwarmt, en omgekeerd wordt de luchtdruk in deze regio hoger bij een afkoeling van het zeewater. Dit Azorenhoog is bijzonder van belang voor het klimaatsysteem, omdat de oostelijke passaatwinden die rond dit hogedrukgebied waaien een rol spelen bij het atmosferische vochttransport vanuit het Atlantische bekken, over Centraal Amerika, richting de Stille Oceaan. Een opwarming van de (sub)tropische Atlantische Oceaan kan daardoor zorgen voor een verzwakking van de passaatwinden en een afname van het atmosferische vochttransport uit het Atlantische bekken. Een afname van de hoeveelheid zoetwater dat met de passaatwinden mee uit het Atlantische bekken verdwijnt zorgt voor een daling van het zoutgehalte van de Atlantische Oceaan, en daarmee voor een verzwakking van de thermohaliene circulatie.

Het onderzoek in hoofdstuk 5 richt zich op de vraag in hoeverre veranderingen in atmosferische circulatie rond het Azorenhoog een rol zouden kunnen hebben gespeeld bij de verstoringen van de warme golfstroom tijdens de laatste ijstijd. Om dit mechanisme te onderzoeken voerden we eerst een literatuuronderzoek uit naar reeds gepubliceerde reconstructies van de zeewatertemperatuur in de regio. Hieruit blijkt dat, ondanks grote temperatuursveranderingen in de noordelijke Atlantische Oceaan, het water in de (sub)tropen relatief warm bleef. Sommige reconstructies laten zelfs een opwarming in de (sub)tropen zien ten tijde van het stilvallen van de warme golfstroom. Op basis van deze gegevens hebben we modelsimulaties gedaan met verschillende klimaatmodellen, waarin we onderzochten hoe de luchtstroming rond het Azorenhoog reageert op veranderingen in de warme golfstroom in combinatie met temperatuursveranderingen in de (sub)tropische Atlantische Oceaan. Onze simulaties lieten zien dat de luchtdruk in het Azorenhoog ook in de laatste ijstijd bijzonder gevoelig was voor temperatuurveranderingen in de (sub)tropische Atlantische Oceaan. Kleine temperatuursveranderingen in de (sub)tropische Atlantische Oceaan, de Caribische Zee en de Golf van Mexico hadden daarbij grote invloed op de kracht van de passaatwinden en het atmosferische vochttransport vanuit het Atlantische bekken naar de Stille Oceaan. Hoewel er nog onzekerheid bestaat over de dynamiek van de zeewatertemperatuur in deze regio, geven onze resultaten wel aan dat terugkoppelingen tussen de hydrologische cyclus in de (sub)tropische regio en de thermohaliene kunnen bijdragen aan fluctuaties in de warme golfstroom.

In hoofdstuk 6 gaan we nog aanzienlijk verder terug in de tijd, namelijk naar een geologisch tijdperk tussen ongeveer 146 tot 66 miljoen jaar geleden dat het Krijt wordt genoemd. In deze periode maakten bloemplanten (Angiospermae) een bijzonder snelle evolutionaire opmars ten koste van de daarvoor dominante coniferen (Gymnospermae). Ook daalde de CO_2-concentratie in de atmosfeer van meer dan 2000 ppm tot ongeveer 750-1000 ppm. Ondanks het belang van deze evolutionaire ontwikkeling voor de huidige wereldwijde soortensamenstelling is nog altijd onbekend wat ten grondslag lag aan de snelle evolutie van de bloemplanten. In het laatste hoofdstuk van dit proefschrift postuleren we een nieuwe hypothese die zou kunnen verklaren waarom juist de bloemplanten profiteerden van de dalende CO_2-concentraties tijdens het Krijt. Belangrijk voor onze hypothese is het morfologische verschil tussen de platte bladeren van bloemplanten en de naaldvormige bladeren van coniferen. De bladeren van bloemplanten hebben over het algemeen de huidmondjes aan de onderzijde en een vertakte nervenstructuur. Aangezien de fotosynthese plaatsvindt aan de bovenkant van deze bladeren moet CO_2 vanuit de huidmondjes via diffusie door de gehele dikte van het blad bewegen voordat de plant het kan opnemen. Water stroomt tot de eindpunten van de nerven en beweegt dan, deels als gas, door de open structuur van het blad richting de huidmondjes. Afhankelijk van hoe vertakt de nervenstructuur van bladeren is, kan de transportafstand van CO_2 langer of korter zijn dan de transportafstand van water door het blad. Omdat de naalden van coniferen geen vertakte nervatuur hebben, maar juist een centraal gelegen nerf, is de transportafstand van CO_2 door hun bladeren korter dan de transportafstand voor water.

Aan de hand van eerder gepubliceerde metingen aan het vatensysteem van fossiele bloemplanten laten wij zien dat hun evolutionaire opmars begon met de ontwikkeling van een steeds meer vertakte nervatuur. Het begin van deze snelle evolutionaire opmars van bloemplanten viel daarbij precies samen met het moment dat de transportafstand voor water korter werd dan voor CO_2. Met behulp van een plantenfysiologisch model laten wij zien dat dit evolutionaire 'kantelpunt' het de bloemplanten mogelijk maakte te profiteren van de ontwikkeling van bladeren met meer en kleinere huidmondjes. Zoals we in de hoofdstukken 2 en 3 reeds lieten zien was deze aanpassing noodzakelijk om een hogere gasuitwisseling te bereiken. Aangezien een aanpassing naar een hogere gasuitwisseling noodzakelijk was om te kunnen overleven in een wereld met dalende CO_2-concentraties, stellen wij dat bloemplanten met platte bladeren en een sterk vertakte nervatuur tijdens het Krijt een evolutionair voordeel kregen ten opzichte van coniferen met naaldvormige bladeren. De snelle evolutionaire opmars van bloemplanten had echter niet alleen gevolgen voor de wereldwijde vegetatiesamenstelling. Doordat de bladeren van bloemplanten een hogere gasuitwisseling bereikten en hun wortels de verwering van de bodem versnelden, zorgde deze evolutionaire sprong ook voor grote veranderingen in de wereldwijde kringlopen van water en koolstof.

De resultaten van dit proefschrift laten zien dat planten een belangrijke rol spelen in de water- en koolstofkringloop en daardoor een dynamisch onderdeel zijn van het klimaatsysteem. Het belang van deze kennis is tweeledig. Allereerst zorgen de aanpassingen van planten aan hun omgeving voor een wisselwerking met het klimaat. Daarnaast kunnen de aanpassingen van planten ook benut worden als indicator van klimaatveranderingen die in het verleden hebben plaatsgevonden. Dit onderzoek heeft daardoor nieuwe inzichten opgeleverd in de rol die planten spelen bij wisselwerking tussen stijgende CO_2-concentraties in de atmosfeer en het klimaatsysteem. De belangrijkste conclusie is dat een stijgende CO_2-concentratie, naast het versterken van het broeikaseffect, ook een directe invloed heeft op de water- en koolstofkringloop doordat planten hun gasuitwisseling aanpassen. Het is echter nog onduidelijk hoe deze aanpassing zich zal voortzetten in de toekomst en welke gevolgen deze heeft voor de wisselwerking tussen de biosfeer en de atmosfeer op regionale en grotere schaalniveaus. Onze resultaten suggereren ook dat bij de interpretatie van paleoecologische proxies rekening gehouden dient te worden met mogelijke plastische en evolutionaire aanpassingen van planten aan veranderende milieuomstandigheden. Wij stellen daarom dat de klimatologische interpretatie van paleoecologische proxies moet worden ingebed in een multidisciplinaire aanpak waarbij het onderzoek naar plantenfysiologische processen en klimaatdynamiek een belangrijke rol spelen.

Dankwoord

Het belangrijkste dat ik tijdens mijn promotieonderzoek heb geleerd is dat mensen in je naaste omgeving enorm waardevol zijn. Alle collega's en vrienden die mij de afgelopen vier jaar hebben gesteund wil ik daarvoor dan ook hartelijk bedanken. Op de eerste plaats bedank ik Stefan, mijn co-promotor, voor zijn dagelijkse begeleiding. Ik denk dat een AIO zich geen betere begeleider kan wensen. Je wist altijd tijd vrij te maken voor overleg of het kritisch becommentariëren van een nieuw manuscript. Daarnaast kon ik ook nog altijd bij je aankloppen voor een praatje over wielrennen, het weer, of zomaar wat. Ook wil ik Martin, mijn promotor, in het bijzonder bedanken voor zijn begeleiding van mijn onderzoek. Jouw originele inzichten en scherpe opmerkingen bij de ecologische aspecten van het onderzoek hebben in belangrijke mate bijgedragen aan de resultaten.

Naast mijn directe begeleiders ben ik nog een aantal mensen zeer dankbaar voor hun prettige samenwerking en inspirerende ideeën. Allereerst Emmy, onze samenwerking aan de huidmondjes maakt een belangrijk deel uit van dit proefschrift. Ik wil je daarom enorm bedanken voor jouw inzet bij het verzamelen van de data en het schrijven van de artikelen. Daarnaast stel ik het enorm op prijs dat je paranimf wilde zijn bij mijn promotie. Ook wil ik Brian, collega en (oud) kamergenoot, hartelijk bedanken voor de leuke en inspirerende samenwerking die we hebben gehad. Verder wil ik ook mijn collega en (oud)kamergenoot Maarten bedanken. De gesprekjes bij de koffieautomaat hielpen altijd enorm om mijn gedachten weer op een rijtje te krijgen. Er zijn uiteraard nog meer (oud)collega's van de vakgroep Milieuwetenschappen die ervoor hebben gezorgd dat ik elke dag weer met veel plezier naar de universiteit ging: Pieter, Max, Mara, Mart, Koen, Jiefei, Ineke, Angie, Dagmar, Jerry, Karin, Floris, Margien, Aat, Paul, Hester, Wilma, Arnoud en Arnaut. De goede sfeer die bij ons op de vakgroep heerst wordt gemaakt door jullie allemaal. Hartelijk dank daarvoor! Daarnaast ben ik nog mijn dank verschuldigd aan de directe collega's binnen het HiPo project: Rike, Gert-Jan, Els en Timme. Hartelijk dank voor jullie prettige samenwerking en de leuke tijd die we hebben gehad bij het veldwerk in Florida! Ook wil ik Margot en Ton van de afdeling (Carto)grafische Vormgeving hartelijk bedanken voor het opmaken van de figuren in dit proefschrift.

Ook buiten de directe omgeving van de universiteit zijn er natuurlijk mensen zonder wie deze promotie niet gelukt was. Joost, samen met Emmy paranimf, hartelijk dank voor jouw bijdrage aan de promotie en de relativerende gesprekken die we hadden over onderzoeksperikelen. Hoewel onderzoek focus vergt, vergt focus ook ontspanning en afleiding. Voor mij kwam deze afleiding vaak in de vorm van (wind)surfen of wielrennen. Ik wil daarom mijn surf- en fietsmaatjes, Hans, Martin, Frank, Marc, Tijmen, Bram, Henk, Matthijs en iedereen die ik nog vergeten ben hartelijk danken voor hun gezelschap.

Ten slotte gaat mijn allergrootste dank en waardering uit naar Margje. Jij wist als geen ander hoe ik me voelde en hoe je me op kon beuren wanneer het soms een beetje tegenzat. Margje, heel erg bedankt voor jouw liefde en geduld.

Curriculum Vitae

Hugo de Boer was born on the 3th of December 1981. He grew up in Purmerend, a little town near Amsterdam, where he went to primary school and high school (VWO). In 2002 he moved to Utrecht to study Environmental Sciences at Utrecht University. During his BSc he also participated in the Erasmus Programme to study at the Technical University of Denmark (DTU). He received his BSc degree in 2006 and continued his studies at Utrecht University with a Master in Sustainable Development. Within the specialization track Global Change and Ecosystems he wrote two theses that were supervised by Dr. Stefan Dekker. In his first thesis he performed and analyzed simulations with a global climate model that was coupled to a global vegetation model. His second thesis used the same model setup to analyze the climatic imprint of cold Heinrich events in Florida during the last ice age. He obtained his MSc degree *cum laude* in 2008. In the same year he started his PhD research under supervision of Prof. Martin Wassen and Dr. Stefan Dekker with the Environmental Sciences group at Utrecht University. The results of this research are presented in this dissertation. From August 2012 onwards, Hugo continues his work with the Environmental Sciences group in Utrecht. Also he received an Endeavour Award to conduct a 6 month Postdoc in Australia, starting November 2012. Here he will collaborate with Prof. Erik Veneklaas from the University of Western Australia and Prof. Graham Farquhar from the Australian National University to continue his research on stomatal adaptations.